PROCEEDINGS

OF THE

THIRD JOINT MEETING

OF THE

UJNR PANEL ON EARTHQUAKE PREDICTION TECHNOLOGY

TSUKUBA, JAPAN

SEPTEMBER 20-22, 1982

Panel Chairmen:

David P. Hill
U.S. Geological Survey
Menlo Park, California 94025
U.S.A.

Keiji Nishimura
Geographical Survey Institute
Ibaraki-Ken 305
Japan

U.S. Geological Survey

Open-File Report 83-174

TABLE OF CONTENTS

EARTHQUAKE PREDICTION RESEARCH IN SOUTHERN CALIFORNIA

James H. Dieterich
U. S. Geological Survey
Menlo Park, California

Detailed trenching studies indicate that the mean recurrence time for great earthquakes ($M \geq 8$) on the southern section of the San Andreas fault is 136 ± 40 years, and geodetic data suggest a similar value for the north-central section of this major transform fault. The last great earthquakes on the San Andreas fault occurred 125 years ago in southern California (the 1857 Fort Tejon earthquake) and only 86 years ago in north-central California (the 1906 San Francisco earthquake). On this basis most scientists anticipate that the next $M \geq 8$ San Andreas earthquake will occur in southern California sometime in the next several decades, and accordingly we are focusing much of our research on earthquake prediction in the southern California region.

At this stage, our work in earthquake prediction is basically a research program involving both government and university scientists. Nevertheless, in an effort to prepare for the eventual implementation of an operational earthquake prediction program, we have initiated periodic reviews of all data collected under the research program. The objectives of these reviews are to 1) maintain a uniform servailance of the various types of data being collected such that "obvious" precursors to the next major earthquake are not overlooked, and 2) provide an on-going evaluation of the quality and usefullness of the data being collected as a basis for future decisions on the design of an operational prediction

program. The review of data in southern California has been carried out during semi-annual meetings held at California Institute of Technology of the principal investigators of projects funded under the U. S. Geological Survey's Earthquake Prediction Program. This year, we initiated a series of similar meetings in Menlo Park for projects gathering data in northern and central California.

EARTHQUAKE PRECURSORS DETECTED BY ROUTINE OBSERVATION OF JAPAN METEOROLOGICAL AGENCY

The Japan Meteorological Agency

1. Introduction

The Japan Meteorological Agency (J.M.A.) takes the responsibility of watching the occurrence of all earthquakes greater than magnitudes 3 in and near Japanese Islands, of determining the focal parameters (origin time, hypocenter and magnitude) of these earthquakes, and of publishing the obtained data. These data, we believe, are the fundamental material for seismology, especially for the research of earthquake prediction in Japan.

In order to perform the above mentioned responsibility, J.M.A. has set up seismological observation network all over the Japanese Islands as shown in Fig. 1 The response curves of seismometers in Fig. 1 are shown in Fig. 2.

To shorten the time to determine focal parameters, J.M.A. is now establishing a real time or semi-real time data processing system. Seismograms recorded at seismological stations are telemetered on real time basis to local centers where records are pre-processed by a mini-computer. The pre-processed digital seismograms are transmitted to Tokyo Center through a national meteorological data transmitting system, and are processed with high accuracy by a large computer in J.M.A..

In addition to the above mentioned responsibility, J.M.A. also takes another grave responsibility of making short-term prediction of the great shallow earthquke in the Tokai area along the Suruga trough expected in the near future. For the purpose to predict the earthquake, real time and continuous watch system has been set up with a very dense network of various instruments in the Tokai area Telemetering systems of bore-hole dilatation strainmeters in the Tokai area and a telemetering array system of ocean bottom seismographs off the Tokai area are the important part of the watch system. Data recorded by other instruments of not only J.M.A. but also other organizations such as the Geographical Survey Institute (GSI), the National Research Center for Disaster Prevention (NRCDP), the Geological Survey of Japan, the Nagoya University and Tokyo University are also telemetered to the Center of J.M.A. which is staffed 24 hours a day and 7 days a week with five experts.

The southern Kanto area which includes the metropolitan area are also assigned as an intensified observation area as well as the Tokai area. J.M.A. has set up also telemetering systems of bore-hole dilatation strainmeters in the

sensitivity and low sensitivity records, respectively. Scale of sensitivity are given in the figures.

In Fig.6 , at 20 45 and 22 05 hours, two clear step-like contraction changes on the high sensitivity record at Yokaichiba are recognized.

Even on the low sensitivity record the corresponding step-like contraction changes can be clearly recognized. Coseismic step-like contraction changes at Yokaichiba are clearly recognized. Coseismic step-like changes are also recognized on other strainmeters at neighboring sites where no precursory strain changes cannot be recognized as shown in Fig. 6.

3. Conclusion

In this report, the precursors which appeared in dilatational strainmeters are mainly presented. On the other hand, foreshocks can also be one of very effective precursors for the prediction of earthquakes.

Foreshocks activity, however, are very low in some cases and considerably high in other cases, according to regions where main shocks take places. Even in regions where foreshock activity is expected to be very low, there are possibilities that sufficiently high sensitivity seismological observation can detect micro or ultra micro foreshocks.

In such regions, however, strain changes discussed in this paper can be very effective precursors for the prediction of earthquakes.

Other kind of precursors, such as, changes on records of other crustal observation such as extensometers and tiltmeters, geomagnetic and geoelectric observation, geochemical observation, and ground water level measurements may also be effective in some cases.

Needless to say, that in the regions where high foreshock activities can be expected, the detection of foreshocks combined with precursors such as changes on the records of dilatational strainmeters and the above mentioned various kinds of observations and measurements may be very effective for the prediction of earthquakes.

At present, except the Tokai and the southern Kanto areas, observation of strainmeters are not made by J.M.A.. So that effective precursors of the 1982 Off -Urakawa earthquake on 21st March (M: 7.1) could not be detected with the exceptions of several micro-foreshocks. However, data of precursors before earthquakes are certainly accumulating, and the prediction of earthquakes smaller than the Tokai earthquake whose prediction most of Japanese seismologist are aiming at, may not an unrealistic dream in future.

southern Kanto area. J.M.A. is also going to set up a telemetering system of ocean bottom seismographs south-east off Boso-Peninsula.
The telemetering watch system of earthquakes in the Tokai and the southern Kanto area is shown in Fig. 3.
In this paper, earthquake precursors detected by the above-mentioned various kinds of routine observations of J.M.A. are reported.

2. Earthquake Precursors Detected by J.M.A. Watch System

As reported in the last UJNR conference held in the USA, the Near Izu-Oshima earthquake (M:7.0) on Jan. 14, 1978 was preceded by rather remarkable precursors such as foreshock activities and strain changes, and J.M.A. issued an earthquake information which could be regarded as a kind of warning, one and a half hours before the earthquake.
Many other earthquakes are preceded by noticeable precursors, mainly of strain changes. These are listed in Table 1.

Here, remarkable precursors before the earthquake off Ibaraki Pref. in the Kanto area on July 23rd are described in detail.
Fig. 4 shows the distribution of epicenters of foreshocks, the main shock and aftershocks located by the routine observation of J.M.A.. All epicenters of foreshocks are concentrated near the epicenter of the main shock, as usually seen in other cases. The epicenters of aftershocks immediately after the main shock are roughly distributed along the WNW-ESE direction ; which suggests the strike of the fault plane. On the other hand, epicenters of aftershocks which occurred several days after the main shock were distributed along the NEN-SWS direction conjugate to the above mentioned direction.
Fig. 5 shows the seismic activities observed by the routine observation of J.M.A. before and after the earthquake. The observed foreshock activity began at 18 00 hours of 21st of July, then on 22nd the seismic activity became slightly higher including 2 felt shocks, on 23rd activity became still higher including 3 felt shocks. Among them, the largest shock (M: 5.5) is the one of 02 32 hours. In the afternoon of 23rd, there were a couple of hours of calm period. Then three hours before the occurrence of the main shock, began foreshocks activity, including one felt shock.

Fig. 6 shows records of the dilatational strainmeters on 23rd and 24th of July at Yokaichiba. The top and bottom figures of each record show the high

Table 1.

PRECURSORY STRAIN CHANGES AND RELATED EARTHQUAKES

No.	Date	Epicenter	Lat.	Long.	Dep.	M	Remarks
1	1976 6 16 07 36	Eastern Yamanashi	35 30	139 00	20	5.5	Several strain steps at Sizuoka during Apr to Jun. Max. : 4 x 10^{-8}
2	1977 6 (last decade	E off Chiba(Swarm)	35 27 (Max. event)	140 32	40	5.0	Several strain steps at Katsuura Max. 2 x 10^{-8}
3	1976 7 26 22 02	Ise bay	34 49	136 48	40	4.1	Strain steps at Irako on Jul 20 (0.3 x 10^{-6}) and
	31 09 50	Near Irako	(unknown)				on Jul 26 (0.15 x 10^{-6})
4	1977 11 6 00 31	Western Kanagawa	35 12	139 08	10	3.9	Strain step at Ajiro on Nov. 5 (2 x 10^{-8})
5	1978 1 14 12 24	Near Izu-Oshima	34 46	139 15	0	7.0	Strain step at Ajiro 1977 Jul , at Irozaki on Dec. 4, at Ajiro on Dec. 20 and at Irozaki on Jan. 10, 1978.
6	1978 8 30 18 27	Central Izu Pen.	34 43	139 02	0	3.5	Strain step at Irozaki on Aug. 28.
7	1978 10 13 17 50	Near Choshi	35 49	140 53	30	4.4	Strain change at Choshi on Oct. 11 and at Katsuura on Oct. 11.
8	1978 11 23 10 43	Central Izu Pen.	34 46	139 01	00	4.9	Strain change at Irozaki on Oct. 5, 30 and Nov. 5.
9	1980 6 29 16 20	E off Izu Pen.	34 55	139 14	10	6.7	Strain changes at Ajiro on May 18 and Jun. 14.
10	1981 3 22 17 04	Southern Chubu	35 19	138 19	30	4.4	Strain step at Fuji on Mar. 20.
11	1981 5 4 10 44	Sagami bay (Swarm)	35 12	139 15	0	3.1	Strain step at Hadano on May 4.
12	1981 6 22 08 10	E coast of Kanto	35 49	140 21	50	3.2	Strain change at Yokaichiba 04h30m - 07h30m.
13	1981 9 2 18 24	E off Kanto	35 48	141 08	40	5.8	Strain step at Yokaichiba on Aug. 28.
14	1982 1 13 11 49	On the lower Tone river	35 55	140 30	50	4.1	Strain step at Yokaichiba on Jan. 12.
15	1982 3 10	E coast of Izu Pen (micro earthquake swarm)					Strain step at Ajiro on Mar. 10.
16	1982 7 23 23 23	Off Ibaraki	36 15	141 55	10	7.0	Strain changes at Hino 17h 45m, at Yokaichiba 20h 45m and 22h 4m on Jul. 23.
17	1982 8 12 13 33	Near Izu Oshima	34 54	139 32	40	5.7	Strain changes at Yugawara on Aug. 2, at Miura on Aug. 8 and 11, and at Kamogawa on Aug. 12.

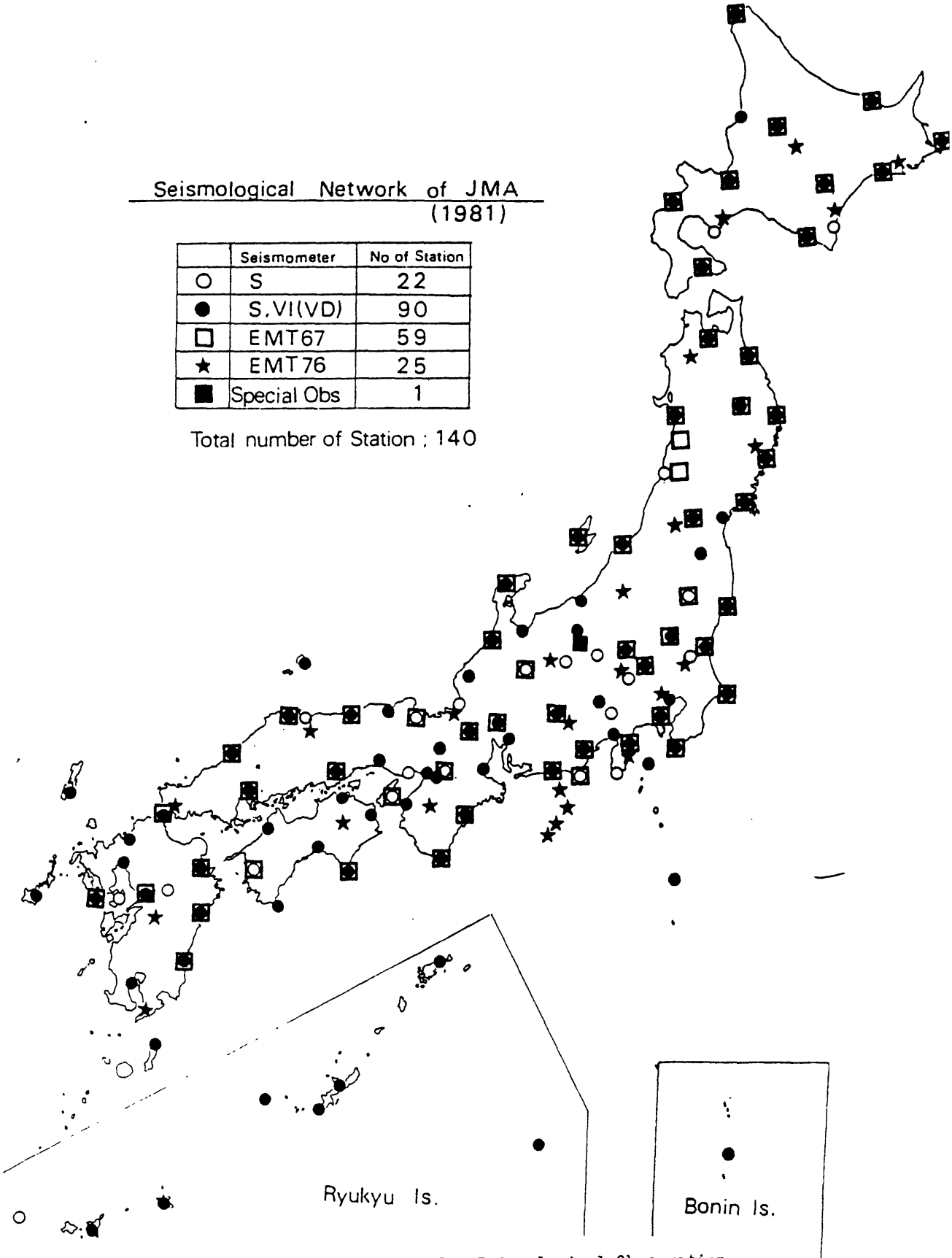

Fig. 1 Network For Seismological Observation

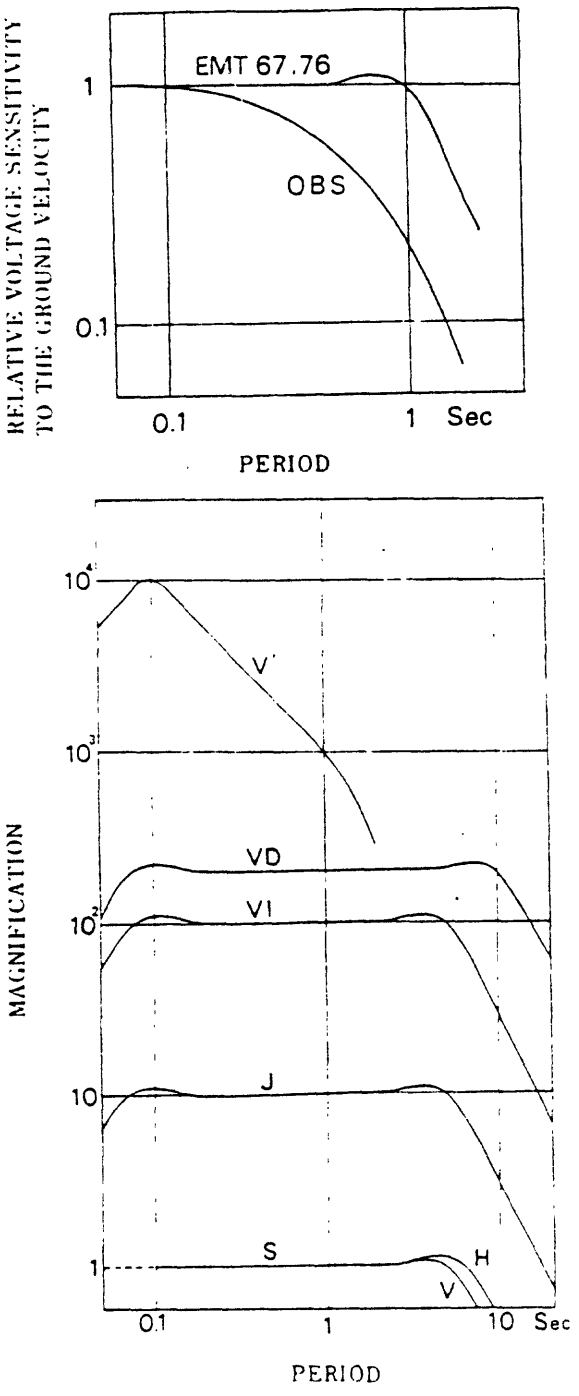

Fig. 2

Magnification Curves for Standard Classes of Seismometers

Fig. 3

Permanent Earthquake Surveillance System in the Tokai District

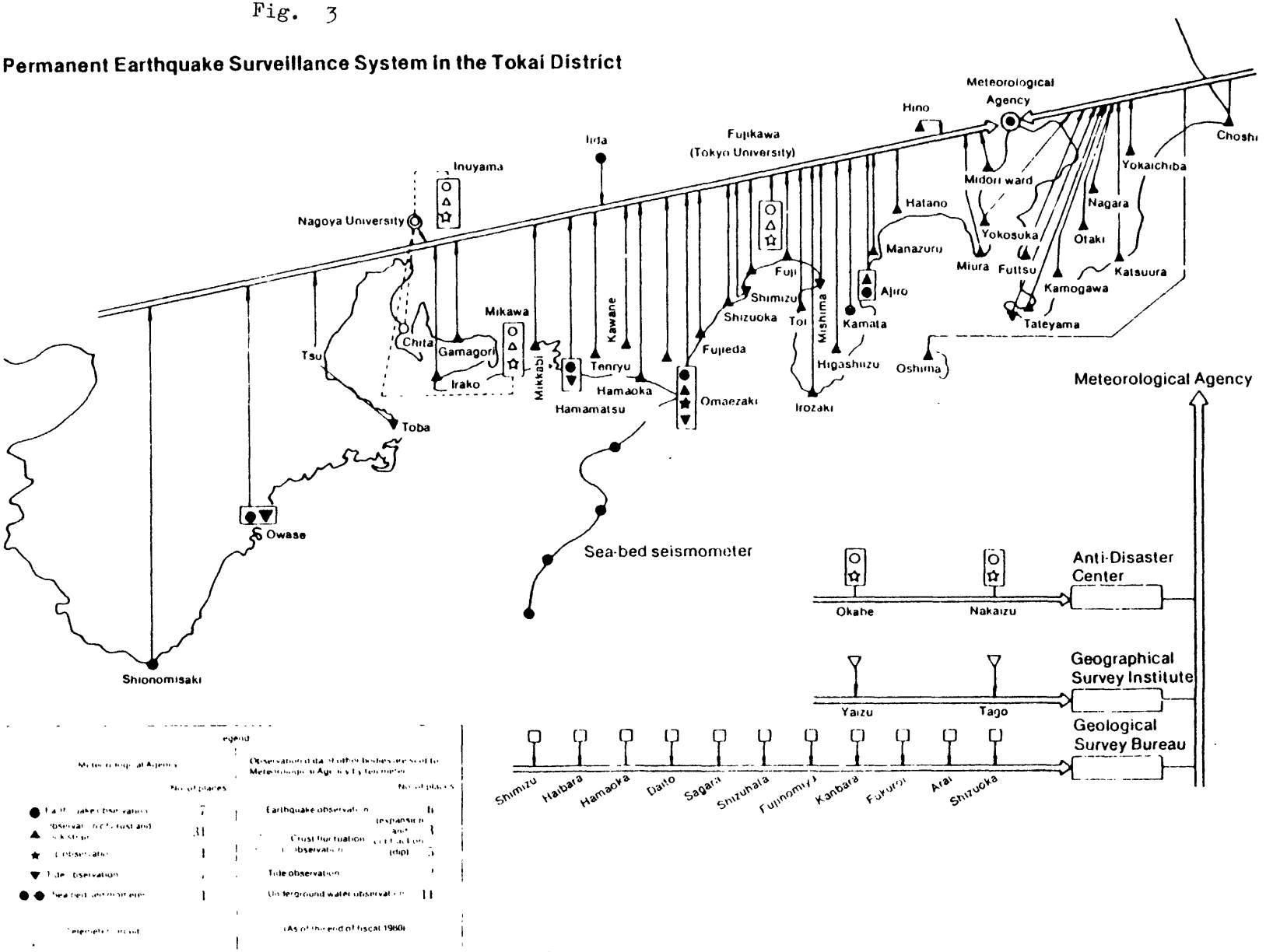

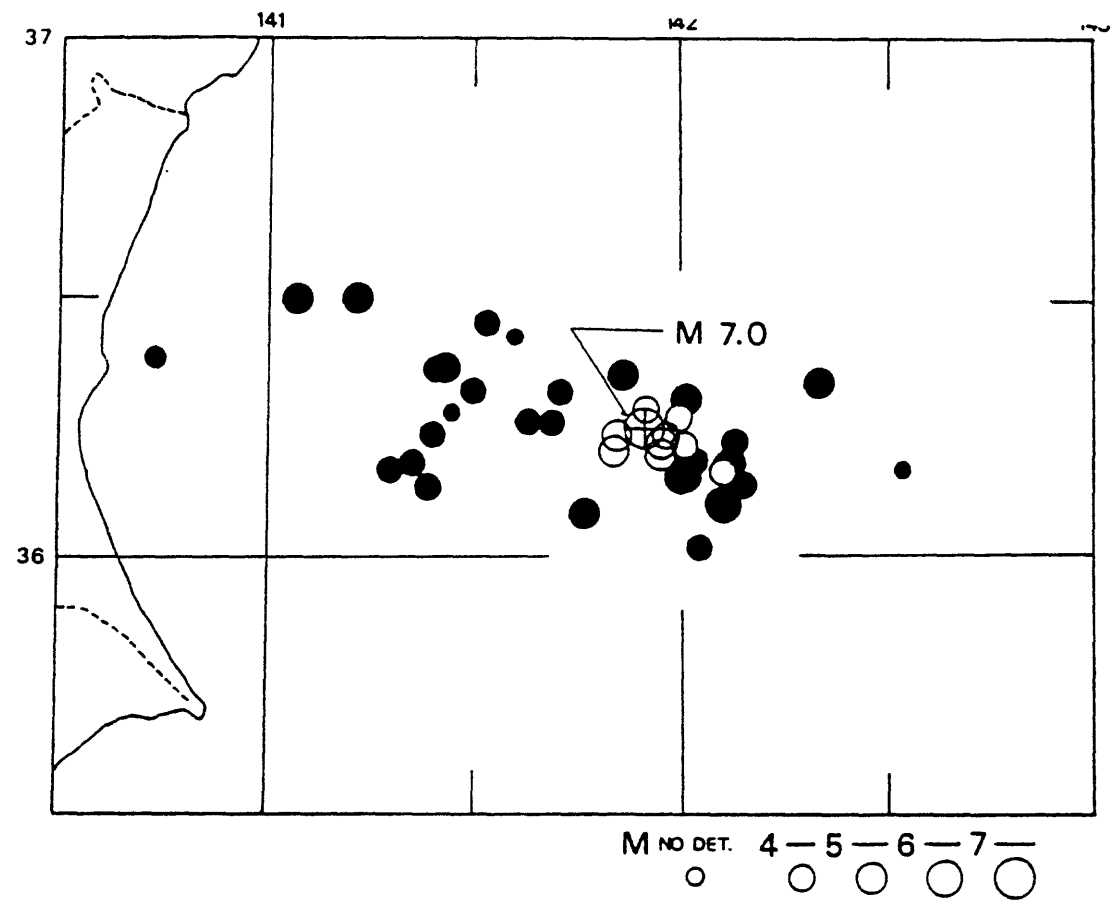

Fig. 4 Distribution of foreshock (open circle), main shock(cross) and aftershock (closed circle).

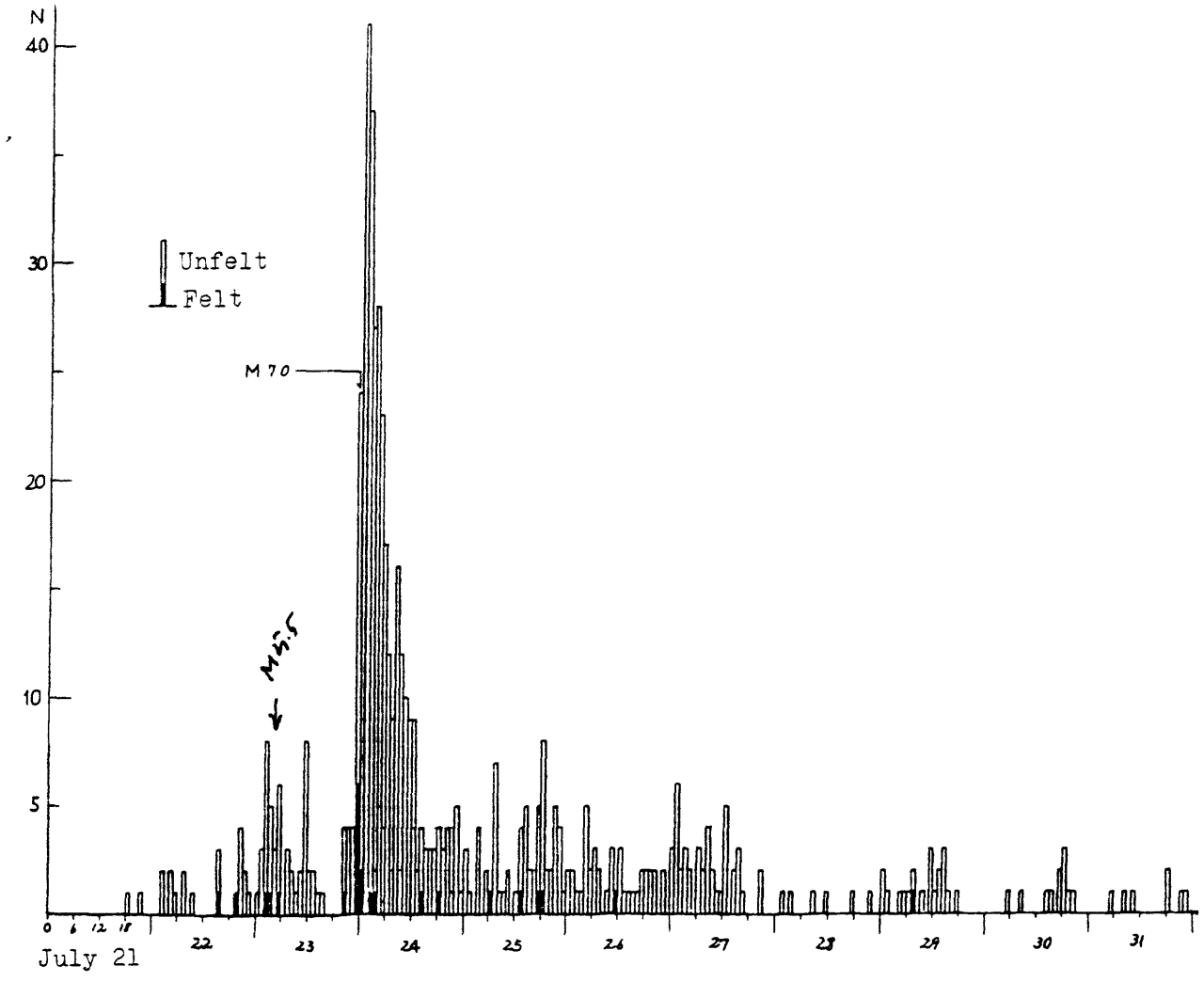

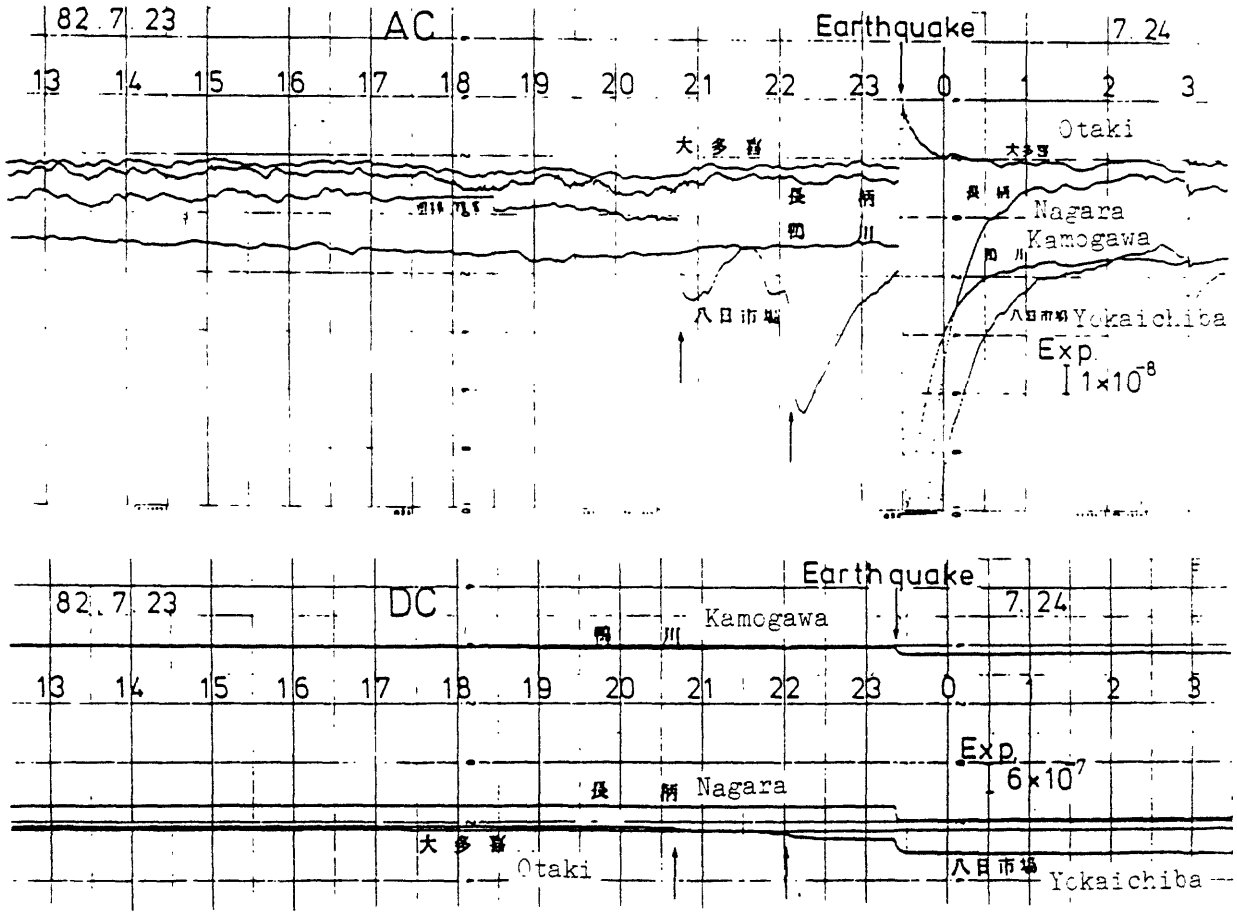

Fig. 6 Record of dilatational strainmeter

A Note on the Earthquake Off Urakawa of 1982

Takashi TADA and Naomi FUJITA

(Geographical Survey Institute)

1. General Description

A large earthquake(M:7.1) occurred off Urakawa town, Hidaka, Hokkaido (Lat:42° 04′, Long:142° 36′, H:40 km) at 11:32 on March 21, 1982(JST). It caused major damage in Hidaka district, such as 167 wounded persons, 9 total collapse houses and 16 half collapse houses. Fig.1 shows the hypocenter(open circle) and seismic intensity(JMA scale) distribution of the main shock. Maximum seismic intensity was VI in Urakawa town(after JMA, 1982).

This earthquake occurred at the north side of Hidaka trough that trends northwest from the junction between Kurile and Japan trenches as shown in Fig.1. Hidaka district is an active seismic region of shallow earthquakes in Japan and destructive earthquakes have occurred frequently as shown in Fig.2(Utsu, 1982), and the Earthquake Off Urakawa of 1982 was the largest destructive earthquake in this district.

The ocean side of the Earthquake Off Urakawa of 1982 is the seismic source regions of thrust type giant earthquakes associated with the subduction of the Pacific Plate(Fig.3).

2. Seismic Source Region and Focal Plane Solutions

Fig.4 shows the hypocenter distributions of main shock and after shocks (Hokkaido Univ., 1982). Some after shocks were located inland and the area of after shocks was about 30 km x 30 km and the focal depths distributed from 15 km to 55 km. Fig.5 shows the vertical focal distribution of back ground microearthquakes and after shock area of the Earthquake Off Urakawa of 1982. The after shock area, seismic source region, is above the deep seismic zone(Wadati-Benioff zone) associated with the subduction of the Pacific Plate, and then, it may be supposed that the Earthquake Off Urakawa of 1982 occurred in the leading edge of the Eurasian Plate.

Fig.6 shows the focal plane solutions of the main shock by manual fits to first P-motion data plotted on the lower focal hemisphere in an equal area projection. It is assumed that the nodal plane whose strike is N38W is the fault plane, based on the hypocenter distribution of after shocks, therefore

the fault of the Earthquake Off Urakawa of 1982 may be of high dip reverse type. The direction of P-axis is nearly northeast-southwest and this direction is parallel to the strike of Kurile trench and also is perpendicular to the direction of P-axis of giant thrust type earthquakes associated with the subduction of the Pacific Plate. And this focal plane solutions support the above mentioned consideration, that is, the Earthquake Off Urakawa of 1982 is an intra-plate earthquake occurred in the Eurasian Plate.

3. Crustal Movement and Fault Model

Fig.7 shows the vertical crustal movement on the leveling route which passes through the seismic source region of the Earthquake Off Urakawa of 1982(GSI, 1982a). The upper part of Fig.7 shows the result which obtained in the last summer, that is, half a year before the earthquake. The anomalous crustal uplift might have existed around the seismic source region (BM 7980-BM 7995). Even if it is anomalous crustal uplift, however, it may be difficult to judge from this data that this crustal uplift is a precursor of the earthquake. And also there is no anomalous sea level change during this 10 years at the Urakawa tidal station which located in the seismic source region.

The lower part of Fig.7 shows the crustal movement during the period from 1952 to 1970 including the after effect of the Earthquake Off Tokachi of 1952(M8.1, Fig.3) and the crustal movement associated with the Earthquake Off Tokachi of 1968(M7.9, Fig.3).

In order to study the crustal movement and the fault model of the Earthquake Off Urakawa of 1982, the leveling survey was carried out immediately after the earthquake by the Geographical Survey Institute. The result is shown in Fig.8(GSI, 1982b). A maximum crustal uplift of 17 cm was observed in the after shock area. A fault model of the Earthquake Off Urakawa of 1982 was determined by this crustal movement referring to the after shock distribution(Fig.4) and the focal plane solutions(Fig.6), as shown in Fig.9.

The fault is of high dip reverse type with lateral strike slip and dips the ocean side, as shown in inserted figure of Fig.9, and fault parameters are; fault length: 30 km, fault width: 40 km(15 km- 55 km), strike: N40°W, dip direction: N130°W, dip angle: 65°, dislocation: 60 cm(Ud:Us = 1:0.6), slip direction of hanging wall side: N20°E, and seismic moment: 2×10^{26} dyne·cm.

4. Conclusions

The Earthquake Off Urakawa of 1982 is an intra-plate earthquake occurred in the Eurasian Plate and whose fault is of high dip reverse type.

Although there are some reports concerning anomalous phenomena, such as the doughnut pattern of seismicity and the radio wave radiation, the clear precursors which are able to predict the occurrence of the earthquake were not observed.

References

GSI, 1982a, Vertical movement in the Hidaka area of Hokkaido district, Rep. Coord. Comm. Earthq. Pred., 27, 17-18.

GSI, 1982b, Vertical movement associated with 1982 Off Urakawa Earthquake in the southern part of Hokkaido, Rep. Coord. Comm, Earthq. Pred., 28, 21-23.

Hokkaido Univ., 1982, The Earthquake Off Urakawa(M7.1), March 21, 1982, presented at 59th meeting of the Coordinating Committee for Earthquake Prediction.

JMA, 1982, The Earthquake Off Urakawa of 1982, Rep. Coord. Comm. Earthq. Pred., 28, 14-18.

Utsu, T., 1982, Destructive earthquakes in and around Japan, presented at 60th meeting of the Coordinating Committee for Earthquake Prediction.

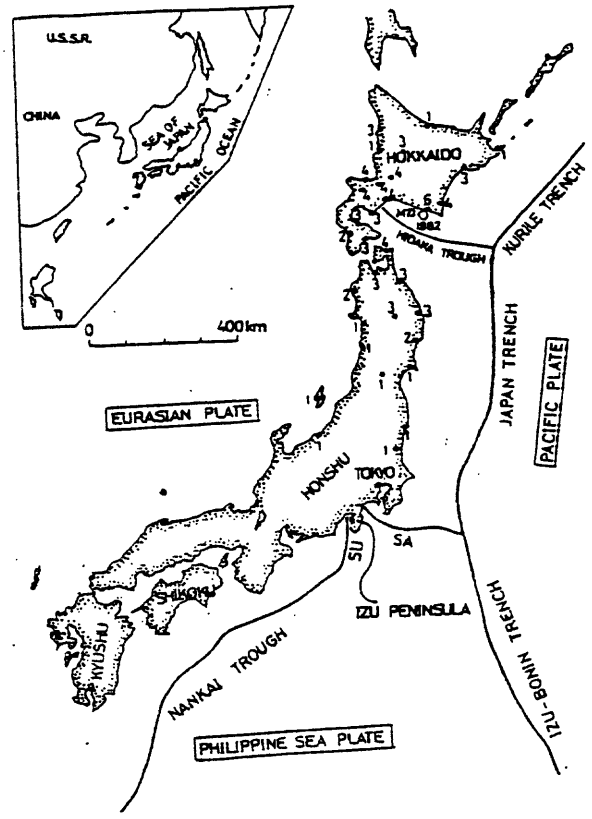

Fig.1 Location of main shock and distribution of seismic intensity (after JMA,1982).

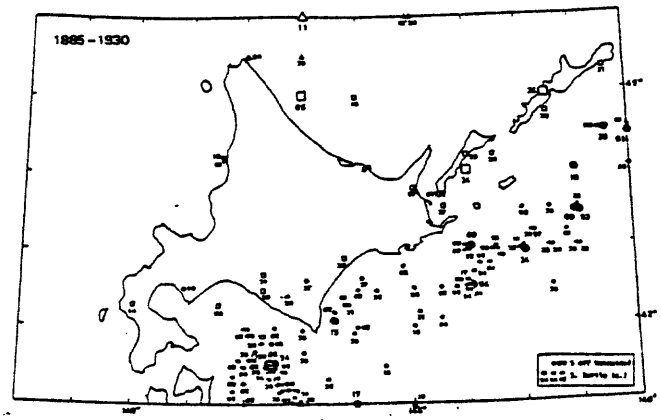

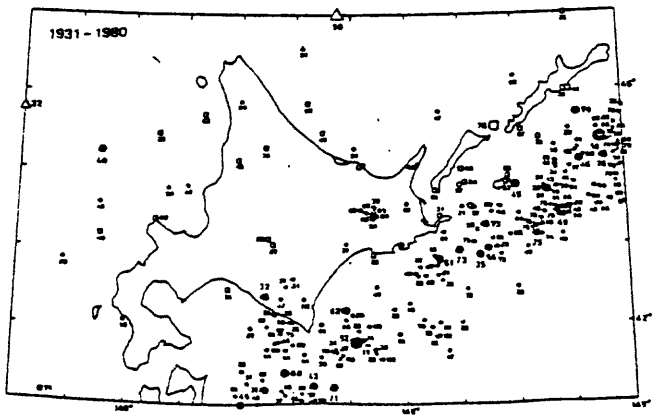

Fig.2 Distribution of destructive earthquakes in and around Hokkaido (after Utsu,1982).

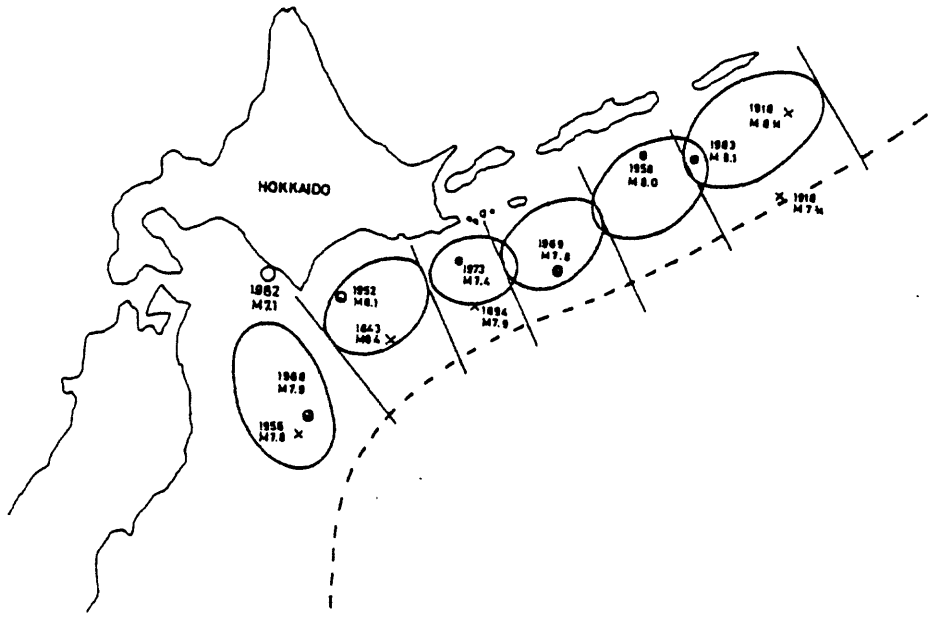

Fig.3 Seismic source regions of giant earthquakes associated with subduction of the Pacific Plate and hypocenter of the Earthquake Off Urakawa of 1982.

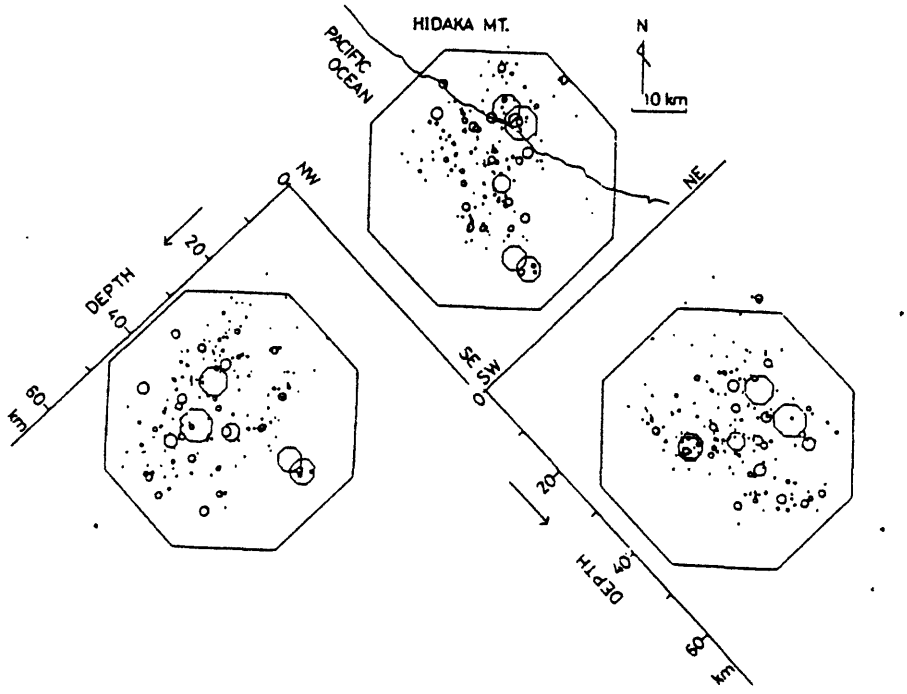

Fig.4 After shock distribution(upper) and focal depth distributions (lower). Scale of octagon is proportional to the magnitude of earthquakes(after Hokkaido Univ.,1982).

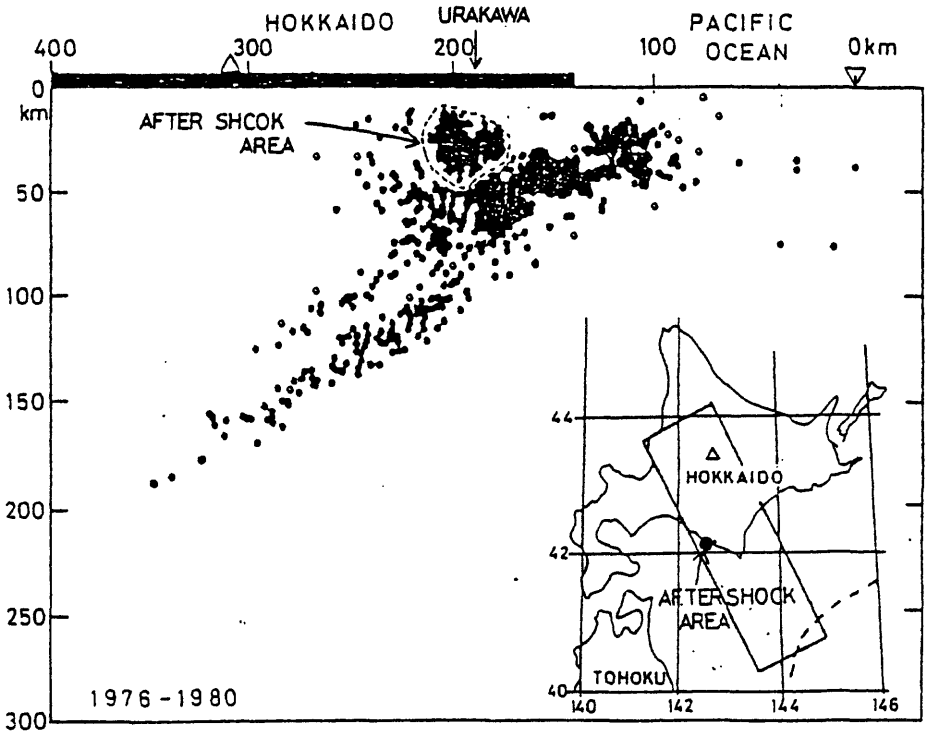

Fig.5 Focal depth distribution of back ground micro earthquakes and after shock area of the Earthquake Off Urakawa of 1982(after Hokkaido Univ.,1982).

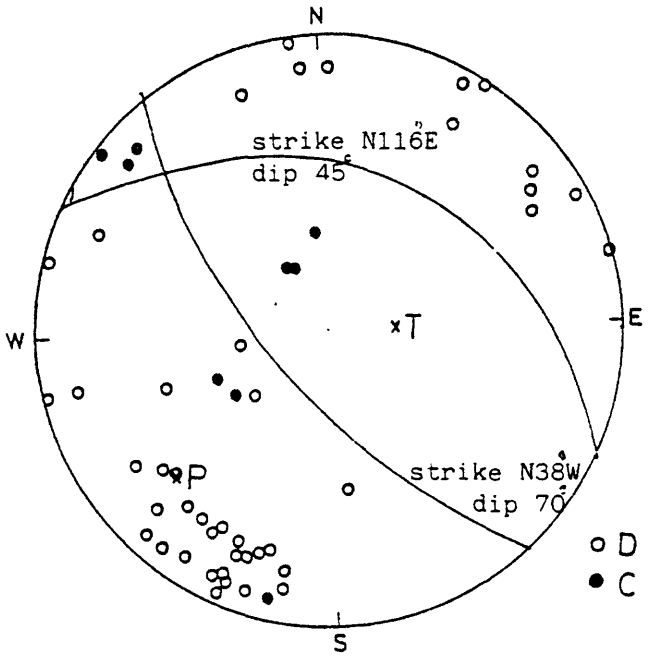

Fig.6 Focal plane solutions of main shock. Lower focal hemisphere in equal area projection.

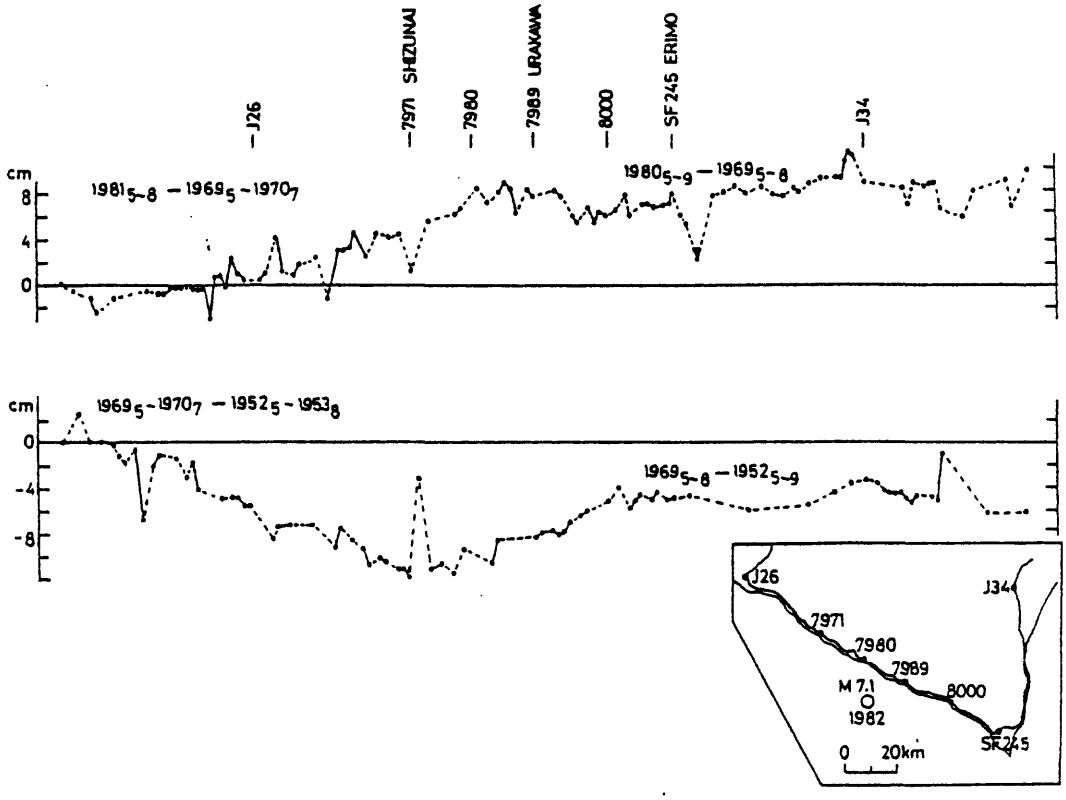

Fig.7 Vertical crustal movement before the Earthquake Off Urakawa of 1982(after GSI,1982a).

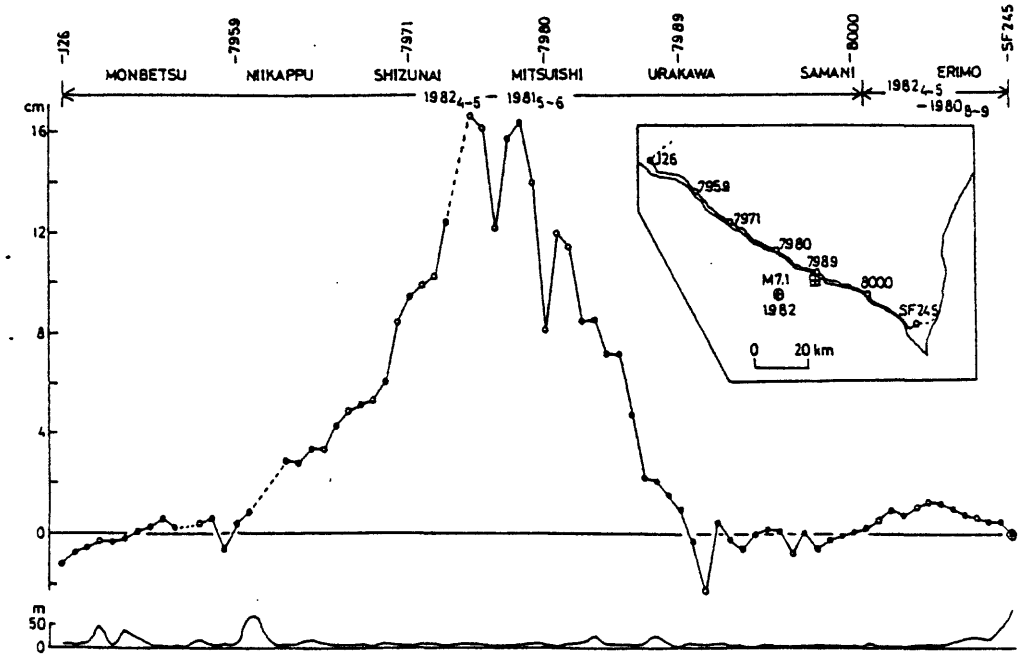

Fig.8 Vertical crustal movement associated with the Earthquake Off Urakawa of 1982(after GSI,1982b).

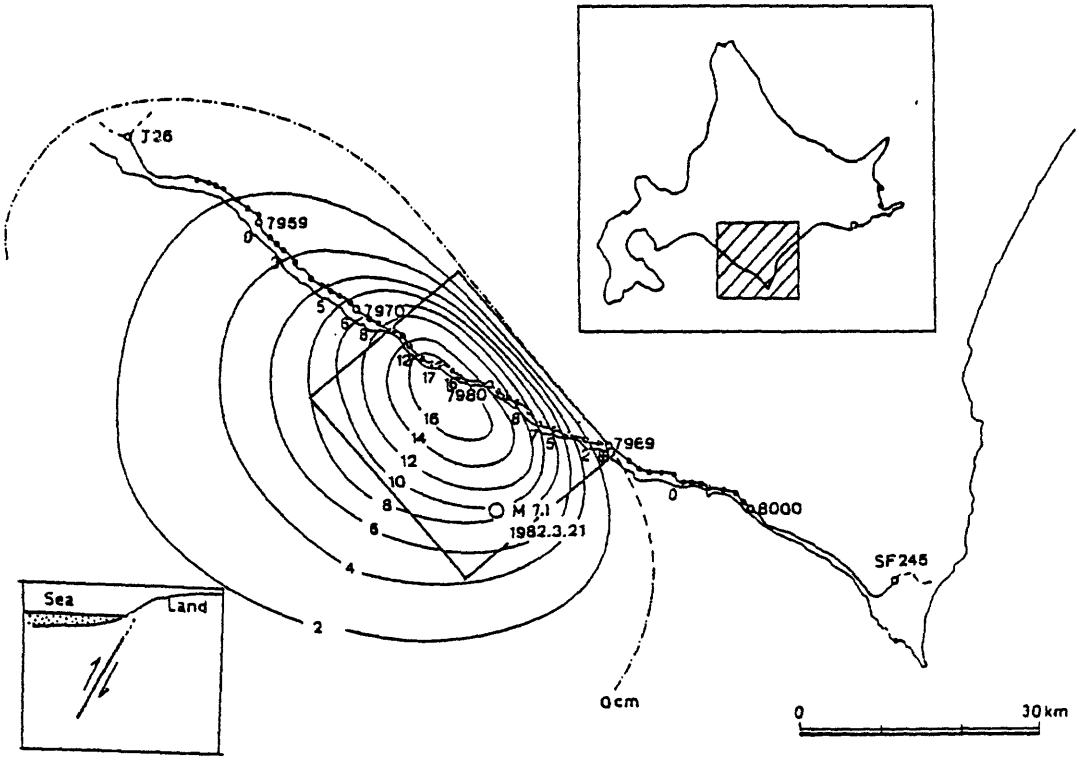

Fig.9 Fault model and calculated vertical crustal movement. Small numerals are observed data and contour lines show calculated crustal movement. Inserted figures show schematic fault motion(left) and location map(right).

THE MECHANISM AND PRECURSORS OF THE 1975 KALAPANA, HAWAII EARTHQUAKE

James H. Dieterich
U. S. Geological Survey
Menlo Park, California

The magnitude 7.2 1975 Kalapana, Hawaii earthquake resulted in up to 8 m of horizontal displacement and 3 m of subsidence along 50 km of the southern coast of the island of Hawaii. This region experienced an earthquake of comparable magnitude and apparently similar mechanism in 1868. The region affected by this earthquake has particularly good geodetic and seismic data prior to and following 1975. The data suggest a pattern of pre-seismic and post-seismic phenomena similar to some other earthquakes and analogous to processes observed in laboratory experiments and numerical simulations.

The Kalapana earthquake occurred on the south flank of Kilauea volcano and apparently owes its origin to processes related to the volcano. The driving force for the earthquake appears to have derived from semi-continuous injection of magma from the summit region of the volcano into the southwest and east rift zones of the volcano that resulted in rift zone spreading at an average rate of 5.5 cm/year for at least 79 years prior to the earthquake. Analysis of old triangulation data and recent trilateration surveys for the east rift zone for the period 1896-1970 by Swanson et al. (1979) show a continuous and consistent pattern of: a) horizontal extension across the rift zone and b) crustal shortening in a direction roughly perpendicular to the rift in the eventual source

region of the earthquake in the region south of the rift. The patterns of deformation are consistent with forceful expansion of the shallow rifts by continuous addition of magma into the rifts - an interpretation that is supported by several other lines of evidence. Aftershocks, first motion solutions, and dislocation models (Crosson and Endo, 1981; Ando, 1979) and finite element modeling conducted for this report indicate that the earthquake originated by slip along a shallow approximately horizontal fault. The fault plane apparently intersects the base of the rift zones and extends southward from the rift zones. The earthquake is interpreted to be the mechanism of accommodation to the strain induced by the shallow, forceful spreading of the rift zones. Finite element modeling of the coseismic horizontal and vertical displacements of the south flank of Kilauea indicate that passive extension of the rifts contributed significantly to the coseismic deformation.

Based upon evidence from a single geodimeter line that showed reversal from contraction to extension, Swanson et al. (1976) suggested that the south flank of Kilauea may have accumulated the maximum possible strain due to rift expansion and could experience a major earthquake in the near future (the paper was in press prior to the 1975 earthquake). Review of a more extensive data set by the present author indicates a clear pattern of strain reversal beginning from six months to five years before the earthquake depending on location. The region affected by the strain reversal is within the region of maximum coseismic strain change and is roughly 300

km^2 compared to the earthquake source area of 1000 km^2. Various explanations for the reversal of the pattern of strain accumulation have been considered including premonitory fault slip, contraction of the rifts due to removal of magma and local intrusion of magma. Only the fault slip explanation is supported by the data. The magnitude of the strain changes indicate that the premonitory fault displacements were up to 30 cm. The pattern of the strain reversals in space and time resembles in addition the pattern obtained in laboratory fault simulation experiments where large amounts of stable slip are sometimes observed prior to slip instability. In addition to the strain precursors other premonitory effects for the 1975 earthquake include P-wave velocity changes (Wyss, et al., 1981), and a short-lived foreshock sequence. The foreshocks and the velocity anomaly occurred within the region of the strain anomalies.

Following the earthquake, the south flank of Kilauea volcano experienced a prolonged period of afterslip. On the south flank the afterslip can be detected in the deformation data for an interval of six months while at the summit caldera the geodetic measurements indicate that afterslip continued for at least five years and may be continuing at present. The summit caldera was displaced southward 1.2 m by the earthquake and has been displaced at least 0.70 m subsequent to the 1975 earthquake apparently by afterslip.

References:

Ando, M., 1979, The Hawaii earthquake of November 29, 1975: Low dip angle faulting due to forceful injection of magma, J. Geophys. Res., 84, B13, 7616-7626.

Crosson, R. S., and E. T. Endo, 1981, Focal mechanisms of earthquakes related to the 29 November 1975 Kalapana, Hawaii, Earthquake: The effect of structure models, Bull. Seis. Soc. Am., 71, 3, 713-729.

Swanson, D. A., W. A. Duffield and R. S. Fiske, 1976, Displacement of the south flank of Kilauea volcano: The result of forceful intrusion of magma into the rift zones, Geol. Surv. Prof. Paper 963, 39p.

Wyss, M., F. W. Klein and A. C. Johnston, 1981, Precursors to the Kalapana M=7.2 earthquake, J. Geophys. Res., 86, B5, 3881-3900.

Temporal variation in the magnitude-frequency relation for the swarm activities off the east coast of the Izu Peninsula, Japan

by

Masajiro IMOTO

National Research Center for Disaster Prevention

Summary

Temporal variation in magnitude-frequency relation is studied for four swarm activities which recently occurred off the east coast of the Izu Peninsula, Japan. Characteristic patterns of the variation are found for all the swarms in common: (1) At the beginning of the swarm activity, b value is larger than the value before the swarm (normal value). (2) It decreases with time corresponding to activation of seismicity, attaining the smallest value at the time of the largest shock. (3) After this, b value increases to exceed the value at the beginning, and finally it resumes the normal value. By closely investigating magnitude-frequency relation, it is found that the number of shocks with magnitude larger than a certain threshold magnitude is so small that the exponential formula for magnitude-frequency relation is not satisfied at the beginning of the swarms. This threshold magnitude is in the range from 1.0 to 2.0. At the time of the highest activity, those shocks with magnitude larger than the threshold occur more frequently than would be expected from the

number of smaller shocks. This finding strongly suggests a difference in nature between the larger and smaller shocks belonging to the same seismic swarm. A physical process to acount for the temporal variation is proposed, and discussed with reference to the results of larboratory experiments of rock deformation.

1. Introduction

Seismicity in and near the Izu peninsula has been active for the last ten years (Yoshida, 1982). Prominent seismic events including the Izu-Oshima-Kinkai Earthquake of Jan. 14, 1978 (M=7.0), and several swarm activities off the east coast of the Izu Peninsula have been recorded by the microearthquake observation network of NRCDP since the first station was installed at JIZ in the middle part of the Izu Peninsula in April 1977 (Fig. 1). Monthly numbers of shocks detected at JIZ are shown in Fig. 2. The swarm activities indicated by S1, S2, ...,S6 in the figure occurred in the shaded area in Fig.1. In this report, magnitude-frequency characteristics of those swarm activities are investigated mainly by using the data at JIZ. Gross features of the six swarms are summarized in Table 1.

Temporal variation in b value or Ishimoto-Iida's coefficient m has already been reported for S1 (Imoto et al., 1979), S4 (Ohtake et al., 1980) and S5 (NRCDP, 1982). At first, we investigate in detail the magnitude-frequency relation for S2, for which the data set is the most complete. Next, the results for three other swarms, S1, S4 and S5 are reviewed. It is difficult to analyze S3 and S6, for lack

of data. Finally, we discuss the physical process of the change in b value during the swarm period, where focal mechanism solutions for S4 obtained by Imoto et al. (1981) are also taken into consideration.

2. Magnitude-frequency relation for the swarm of March 1979

The swarm activity of March 1979 (S2) is moderate in size among the six swarms (see Table 1). Figure 3 shows daily number of shocks at JIZ for the period from January to April 1979. This swarm activity began on the 13th March and lasted until the end of March. The largest shock, with magnitude 3.1, occurred on the 15th. Hourly numbers of shocks are shown in Fig. 4 for the most active period from the 13th to 20th. Several peaks of frequency can be seen. At each of them, a large number of shocks occurred within a few hours. The intervals of the peak activities were nearly constant, and the recurrence time was about one day. These features are common to all six swarms.

b values are estimated for the six periods by the maximum likelihood method, where shocks with magnitude greater than 1.0 are used for the computation. b value and its 95% confidence limits are indicated in Fig. 3 by solid line and shadow zone, respectively. Before the occurrence of the swarm, b value was about 1.0. At the beginning of the swarm, on 13th-14th, a large b value exceeding 1.5 appeared. For the most active period, on 15th-16th, it decreased to a value less than 0.9. After this, b value once increased to a larger

value of 1.8, and returned to the normal value of about 1.0 within a few days.

To assertain the change in b value, Fig. 5 shows the magnitude-frequency relation for each period, where the ordinate is the number of shocks in arbitrary log-scale. For the range of M=1.0-1.7, magnitude-frequency relations do not show large differences from one another. For the range of M1.7-2.4, however, the magnitude-frequency relation shows different features from period to period. For the period of 13th-14th, for example, the number of shocks with magnitude larger than 2.05 is remarkably smaller than the value which is extrapolated from the number of shocks of smaller magnitude. This contrast of magnitude-frequency distribution resulted in a larger b value.

Figures 6 and 7 make it clear that the temporal pattern of activity is different for different sizes of shocks. In the figure, the ordinate is the cumulative number of shocks which is normalized by the total number of shocks for each size range. The abscissa is the time axis, where a unit of time is proportional to the cumulative number of shocks for the 'standard' size range (M=1.0-1.7 for this case). At the active stage, however, the curve of certain size ranges shows a large deviation from the standard curve. Detailed features for this stage can be seen in Fig. 7. The pattern for both M1.7-2.4 and M2.05- greatly differs from the standard activity. M1.7-2.1 appears to give the boundary between non-standard and standard seismicity.

3. Other cases

Swarm of Nov-Dec. 1978 (S1)

This swarm began on Nov. 23, 1978, and became active with time. The largest shock (M=5.4) occurred on Dec. 3 (Fig. 8). Temporal variation in m value has already been reported by Imoto et al. (1979). The upper part of Fig. 8 shows the variations in b value calculated by the same method as mentioned above, where shocks with magnitude greater than 0.7 are used for the computation. At the beginning, b value was greater than 1.0, and decreased with time. After the occurrence of the largest shock, b value began to increase, attaining b=1.5 in later December. It decreased to about 1.2 in the next month. By examining time-number curves by the same method as used in the previous section, M1.4-2.1 is found to be the boundary which separates patterns of seismicity.

Swarm of June-July 1980 (S4)

This swarm has been investigated by many authors. Utsu (1981) classified this activity as 'Type 4', which is characterized by swarm-like activity with an exceedingly large main shock (M=6.7). Temporal variation in m value was investigated by Ohtake et al. (1980) on the basis of records at NSI (see Fig. 1). Figure 9 shows the result of reexamination by using the same data as Ohtake et al. (1980). b value is the lowest near the time of the largest shock. After this, it once increased up to 1.5, and gradually decreased to around 1.0.

Swarm of March 1982 (S5)

This swarm, beginning on March 10, was the most active during the period of 15th-16th, and ceased at the end of March. The source area of the swarm was no larger than 2x2 km^2 (NRCDP, 1982), which is consistent with S-P time distribution (Table 1). Figure 10 shows a magnitude-time plot of individual shocks. The two largest shocks are indicated by L1 and L2. The origin times of these two shocks and the 14th (quiescent time) divide the whole period into 4 stages (I-IV). b values for each stage are listed in Table 2. b value was comparatively small at the most active time, II-III, and increased after this. It is remarkable that in spite of the occurrence of larger shocks (M1.5-2.0), few smaller shocks (less than M1.5) were observed for the period from later on the 15th to early on the 16th. The absence of smaller shocks contributed to the apparent change in b value. The boundary of seismicity pattern is found at M1.0-1.5.

4. Discussion and conclusion

Characteristic patterns, which are commonly found for the magnitude-frequency relation of the four swarm activities are summarized as follows:

(1) At the beginning of the swarm activity, b value is larger than the value before the swarm (normal value).

(2) It decreases with time, attaining the smallest value at the time of the largest shock.

(3) After the occurrence of the largest shock, b value increases to exceed the value at the beginning, and finally it resumes the

normal value.

(4) The threshold magnitude which separates the patterns of seismicity is found in the range between 1.0 and 2.0.

With respect to S4, focal mechanism solutions of about 150 shocks with magnitude larger than 3.0 were determined by Imoto et al. (1981). According to the results, the fault strike of the shocks which occurred at the decreasing stage of b value (June 27-28, 1980) is scattered in a wide range, N0°-45°W. The mode of strike direction, however, is nearly N45°W, making a small angle with the direction of the regional principal stress. Taking these results into consideration, a process of temporal variations in magnitude-frequency relation is proposed as follows:

(1) At the beginning of the swarm, only smaller shocks with magnitude less than a threshold originate at weaker points in the swarm area.

(2) At the most active period, larger shocks occur so as to connect the weaker points. The focal mechanism of each shock may depend strongly on geometrical distribution of the weaker points and/or on the local stress field caused by smaller shocks. For this reason, fault strikes may be scattered over a wide range.

Hill (1977) proposed a model for earthquake swarms in volcanic regions. Ishida (1982) adapted his model to the 1980 swarm (S4). The core of his model is more or less similar to the second concept of our model. Shear failures of Hill's model correspond to larger shocks (larger than the threshold magnitude) mentioned above.

Our model is satisfactorily compared with results of laboratory experiments of rock deformation. Hypocenter distribution of AE events before and after a local fracture was investigated by Kusunose et al. (1982). They showed that a local fracture takes place in the gap between echelon type cracks connecting neighboring cracks. They determined the focal mechanism solutions of AE and concluded that the angle between the local fracture planes and compressional axis is about 20° in contrast with 40° for AE before the fracture. Based on a similar experiment, Nishizawa et al. (1982) suggested a small b value for occurrence of a local fracture. These results are consistent with our model in such points as change in b value and small angles between fault strikes and the direction of the principal stress.

In the above discussions, changes in b value were considered to be caused by changes in rock properties. It is also possible that temporal variations in b value appear to be associated with migration of seismic foci if rock properties are different from place to place. For the cases studied, however, the swarm activity was confined to a small area (see the case of S5), and evidence of systematic migration was not found. For this reason, we have not discussed change in b value from the viewpoint of seismicity migration.

Acknowledgments

I would like to express my sincere appreciation to Dr. M. Ohtake for much discussion and critical reading of the manuscript. I am also grateful to Dr. S.Matsumura for making the data available for this

study.

References

Hill,D.P.,A model for earthquake swarms, J.Geophy.Res., 82, 1347-1352, 1977

Imoto,M.,I.Karakama,R.S.Matsu'ura,F.Yamazaki,A.Yoshia and K.Ishibashi, Focal mechanisms of the 1980 earthquake swarm off the east coast of the Izu Peninsula, Japan, Zisin,2, 34, 481-493, 1981 (in Japanese).

Imoto,M.,M.Ohtake,S.Matsumura,K.Kasahara,F.Yamamizu,T.Ohkubo,M.Tatsukawa and K.Hamada, Earthquake swarm off Kawana-zaki, Izu Peninsula November 23 - December 31,1978, Research Note of the National Research Center for Disaster Prevention, 36, 1-14, 1979 (in Japanese).

Ishida,M.,Spatial-temporal variation of seismicity and spectrum of the 1978 and 1980 earthquake swarms off the east coast of the Izu peninsula, Japan, 1982 (in preparation).

Kusunose,K.,O.Nishizawa and K.Onai, AE gap in a rock under uniaxial compression, Zisin,2, 35, 91-102, 1982 (in Japanese).

National Research Center for Disaster Prevention, The March 1982 earthquake swarm near the east coast of the Izu Peninsula, Rep.Coord.Comm.Earthq.Predict., 28, 1982 (in Japanese, in Press).

Nishizawa,O.,K.Kusunose,T.Yanagitani,F.Oguchi and S.Ehara, Stochastic process of the occurrence of AE events and hypocenter distri-

butions during creep in Ohshima granite, Zisin,2, 35, 117-132, 1982 (in Japanese).

Ohtake,M.,M.Imoto,M.Ishida,T.Ohkubo,Y.Okada,K.Kasahara,M.Tatsukawa,S.Matsumura,F.Yamamizu and K.Hamada, The Izu, central Japan earthquake of June 29 of 1980 and related seismicity, Research Notes of the National Research Center for Disaster Prevention, 43,1-25, 1980 (in Japanese).

Yoshida,A., Recent seismic activity and its characteristics in the region in and around the Izu Peninsula, Zisin,2, 35, 142-144, 1982 (in Japanese).

Utsu,T., Seismicity of the Izu Peninsula and its vicinity from 1901 through 1980 with some remarks on the characteristics of foreshock activities, Bull.Earthq.Res.Inst., 56, 25-41, 1981.

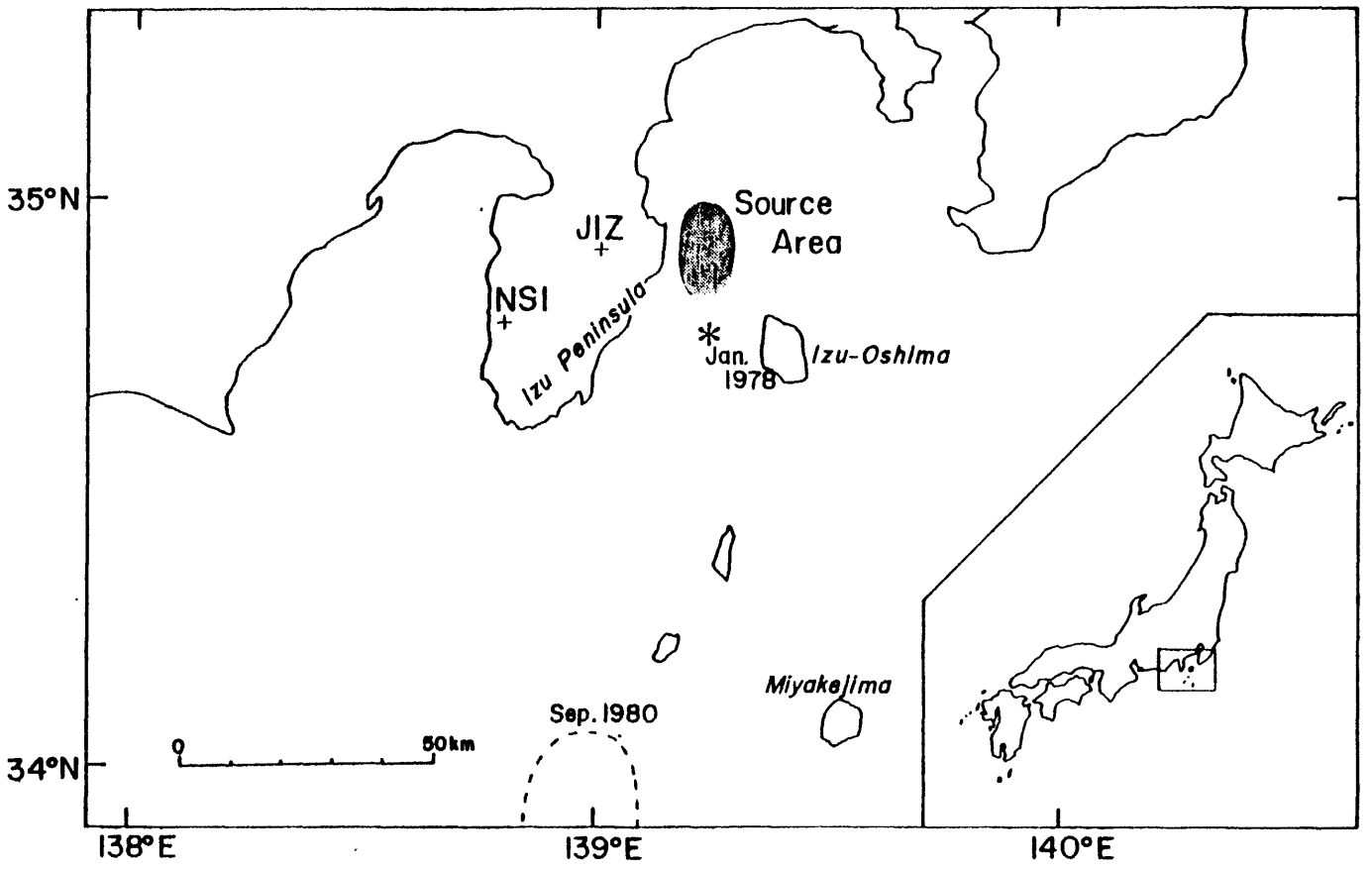

Fig.1 Index map indicating source area of the swarms and the epicenter of the 1978 Izu-Oshima Kinkai Earthquake. Observation stations JIZ and NSI are also shown.

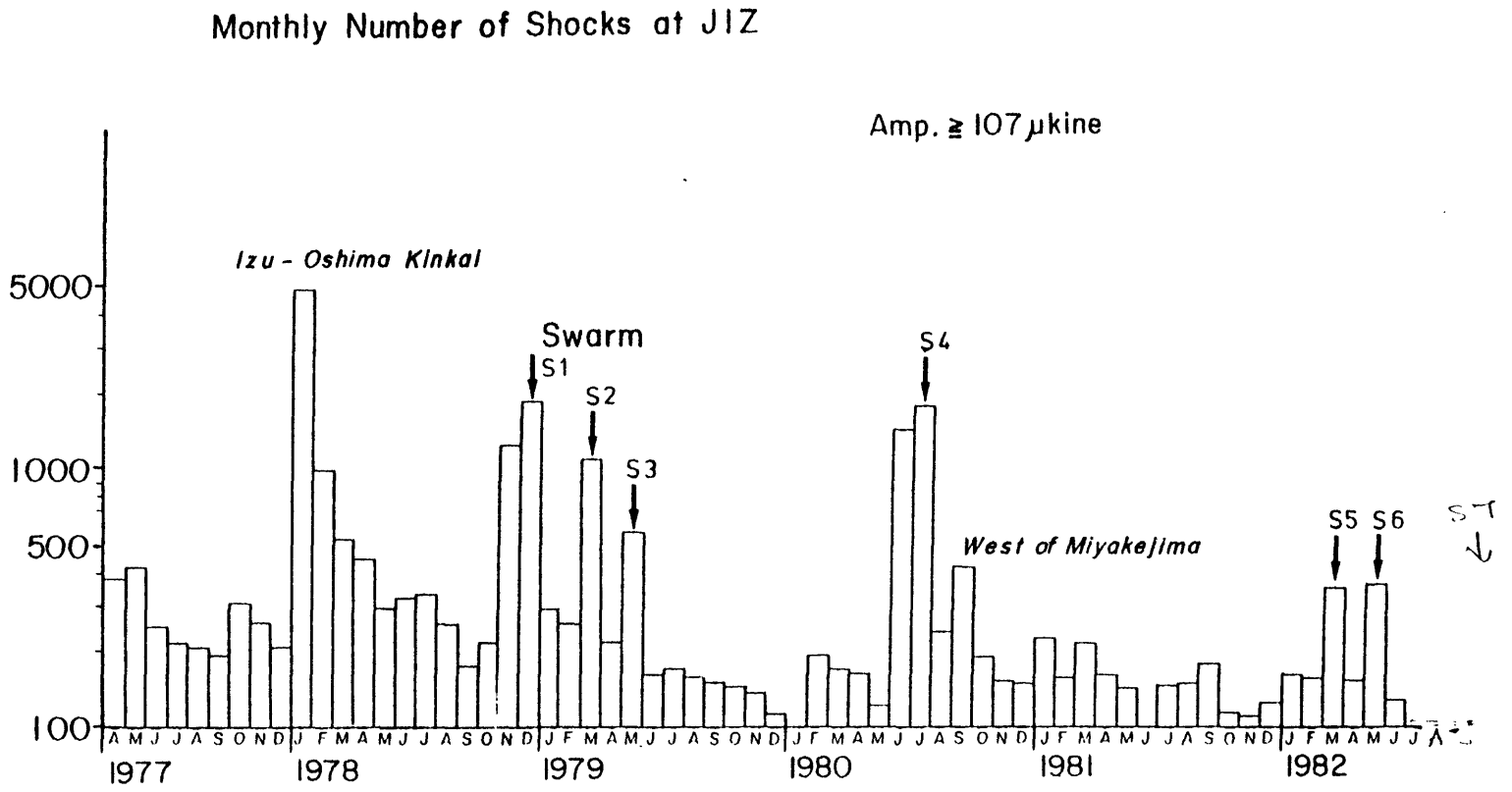

Fig.2 Monthly number of shocks at JIZ for Apr.1977-June 1982. Swarm activities are indicated by arrows.

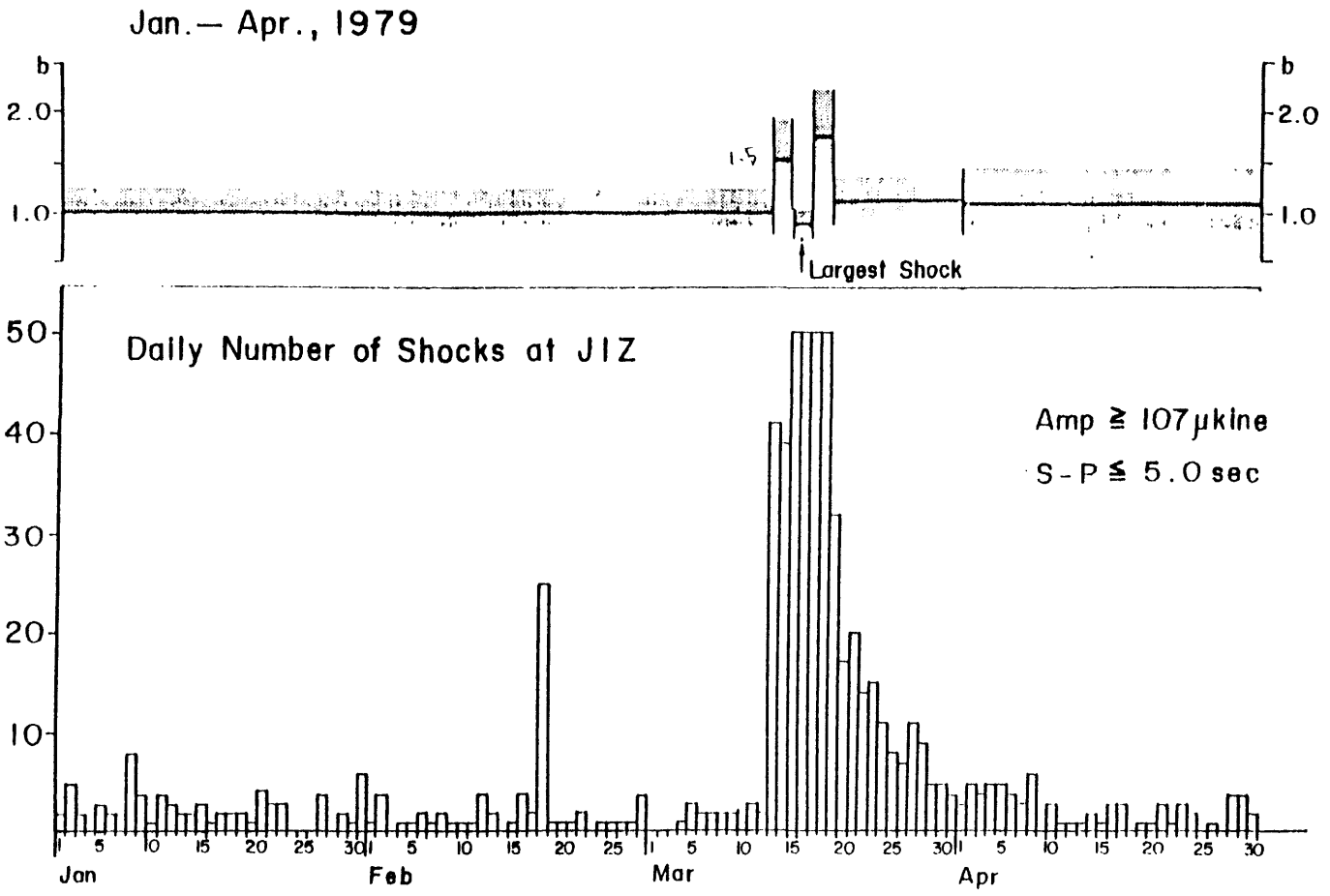

Fig.3 Daily number of shocks at JIZ and temporal variation in b value for Jan.-Apr., 1979. 95% confidence limit of b value is shown by shadow zones.

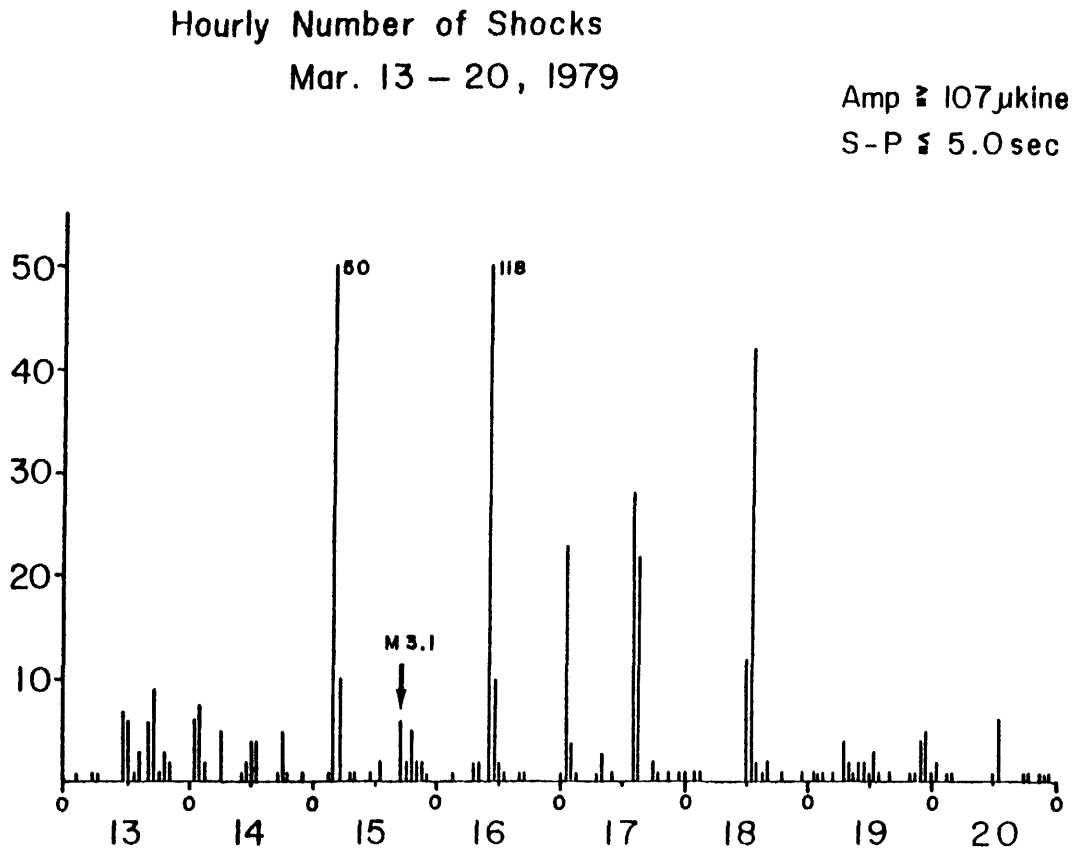

Fig.4 Hourly number of shocks at JIZ for Mar.13-20, 1979.

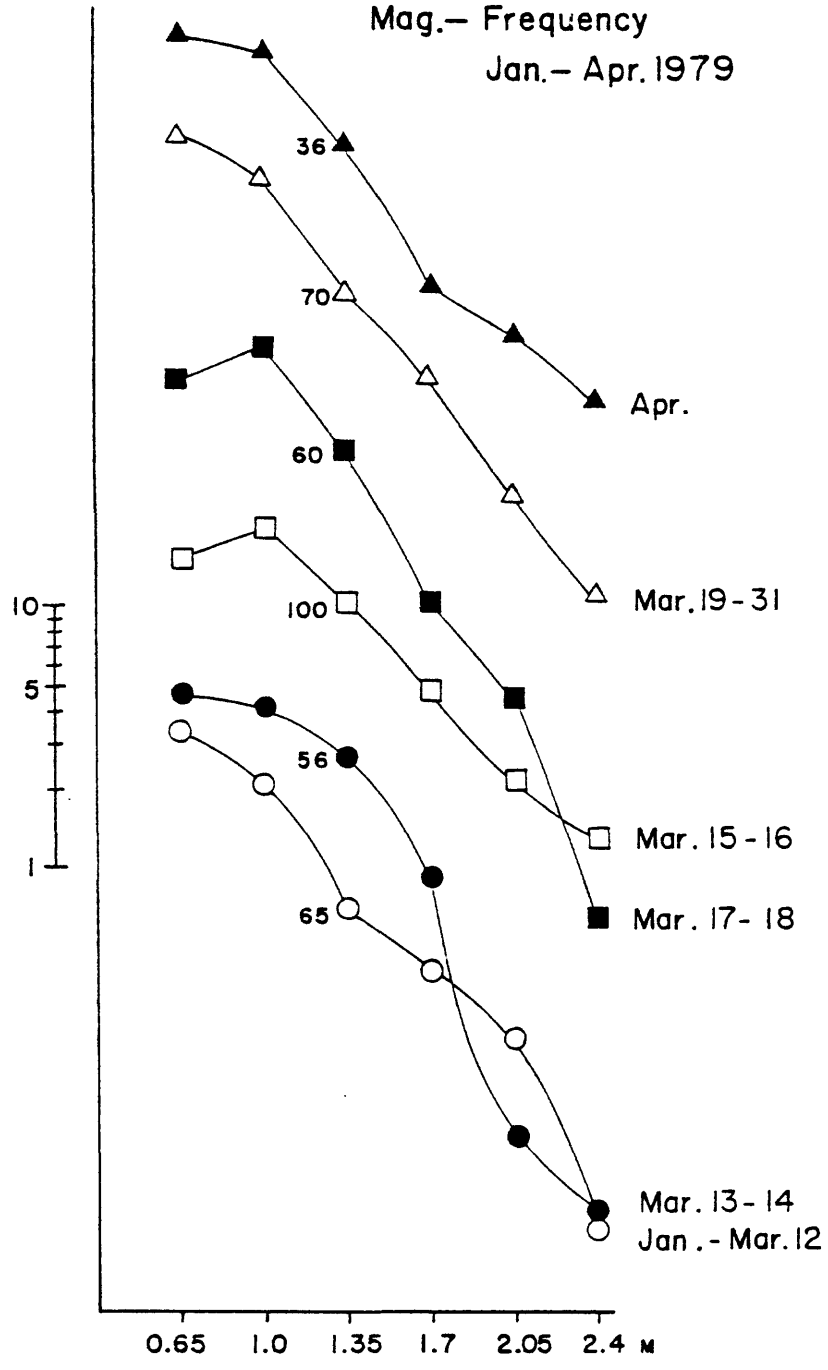

Fig.5 Magnitude-frequency relation for each period of S2 activity. Ordinates indicate numbers of shocks in log scale.

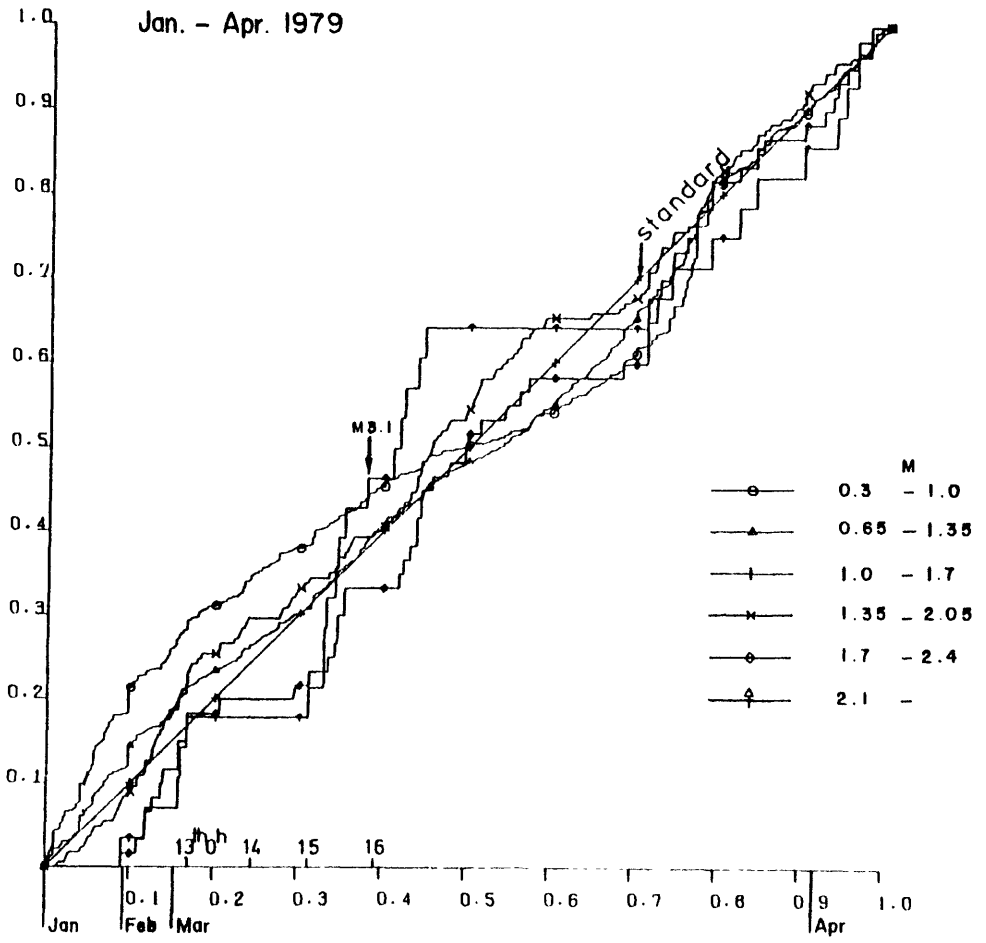

Fig.6 Cumulative numbers of shocks for each magnitude range for the period Jan.-Apr., 1979. Ordinate is the ratio of the cumulative number to the total number. Abscissa is the time axis, where unit is proportional to the cumulative number of shocks for the 'standard' size range, M1.0-1.7.

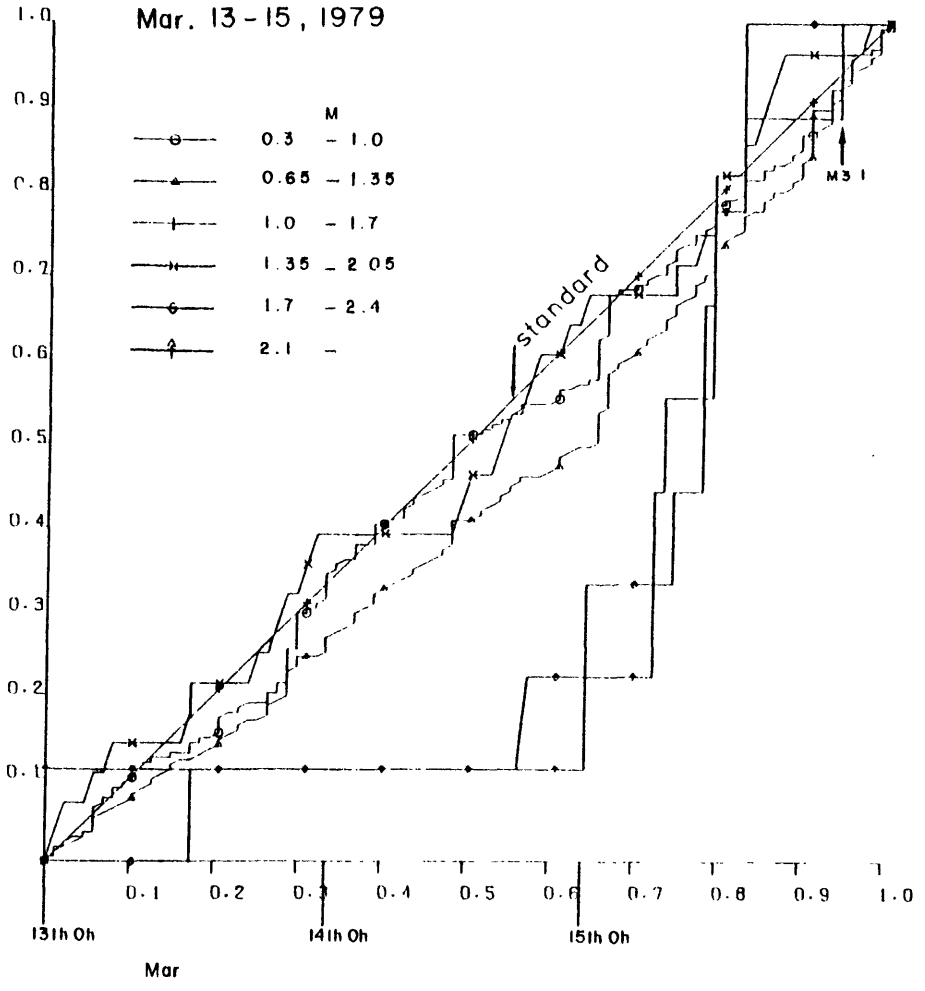

Fig.7 Same as Fig.6 but for the period, Mar.13-15.

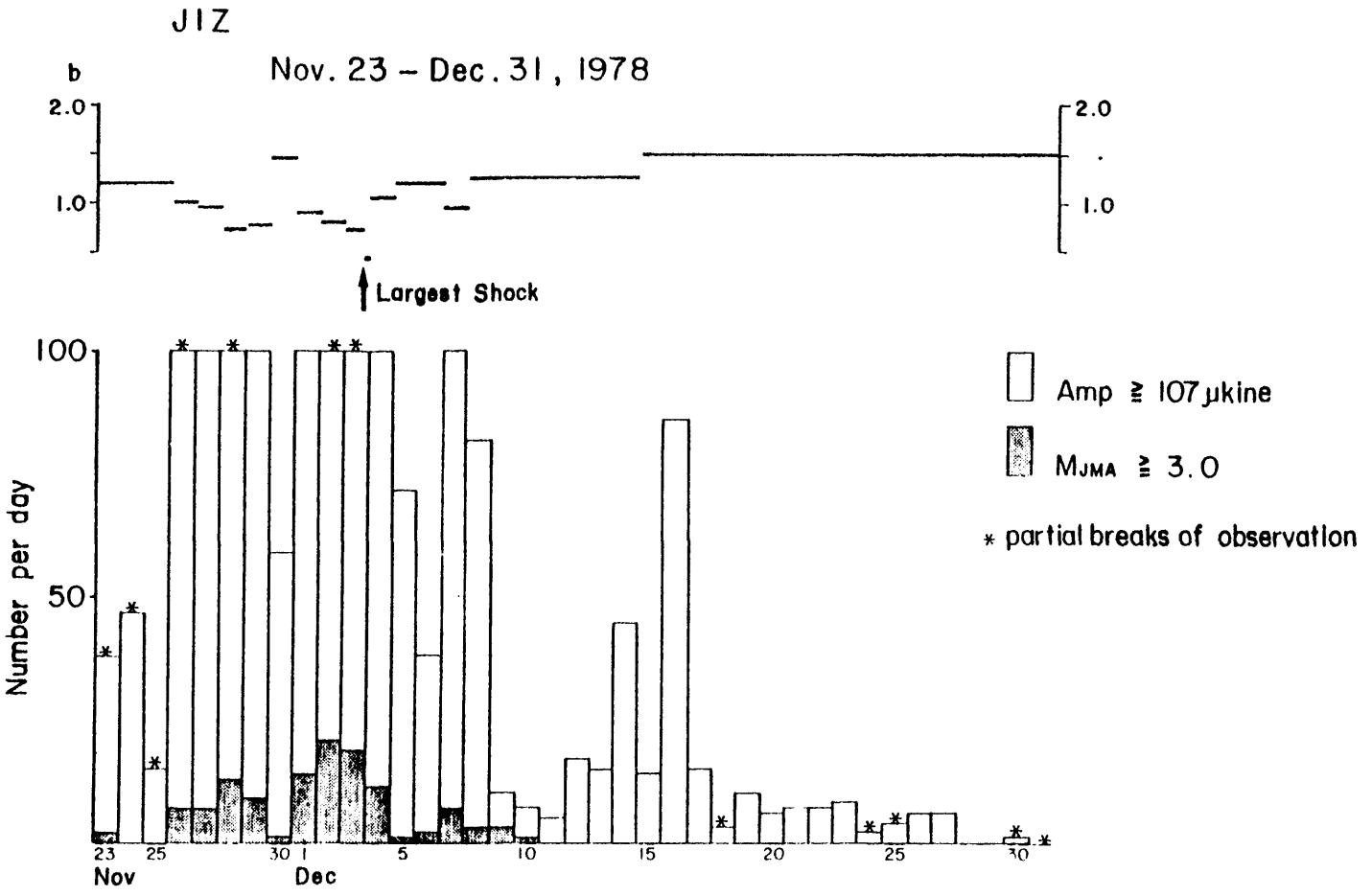

Fig.8 Daily number of shocks at JIZ and temporal variation in b value for S1.

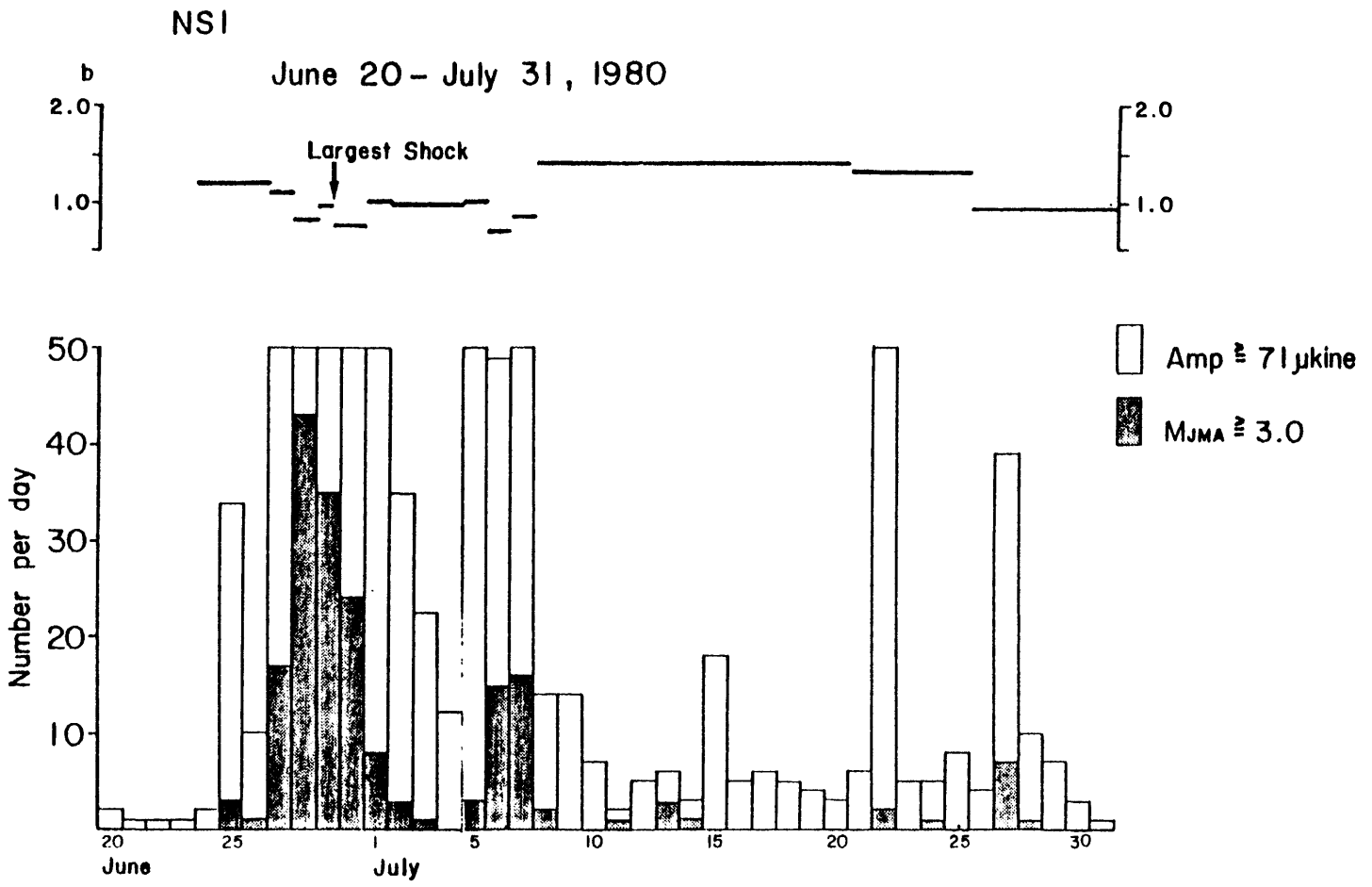

Fig.9 Daily number of shocks at NSI and temporal variation in b value for S4.

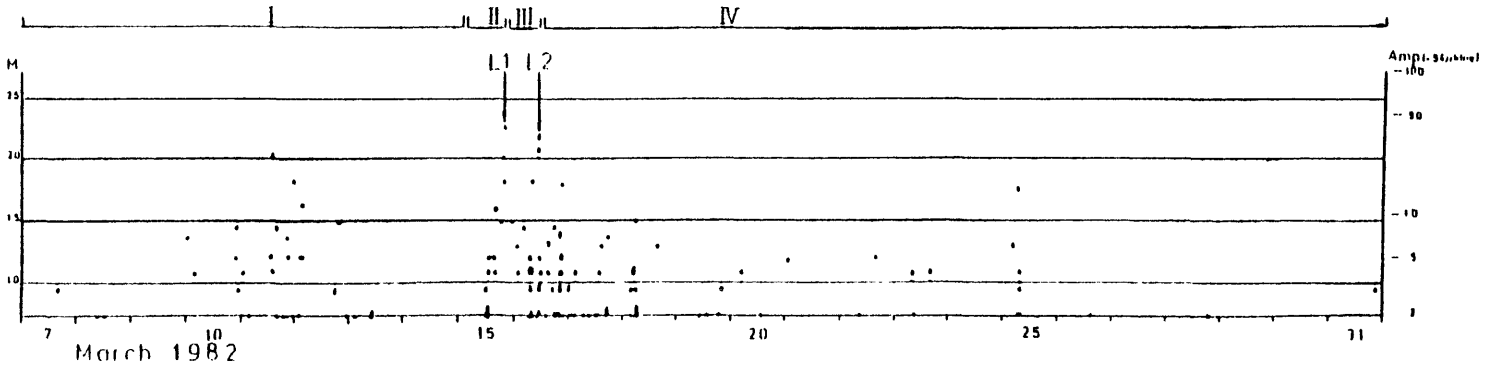

Fig.10 Time-magnitude plot for S5. L1 and L2 indicate the two largest shocks.

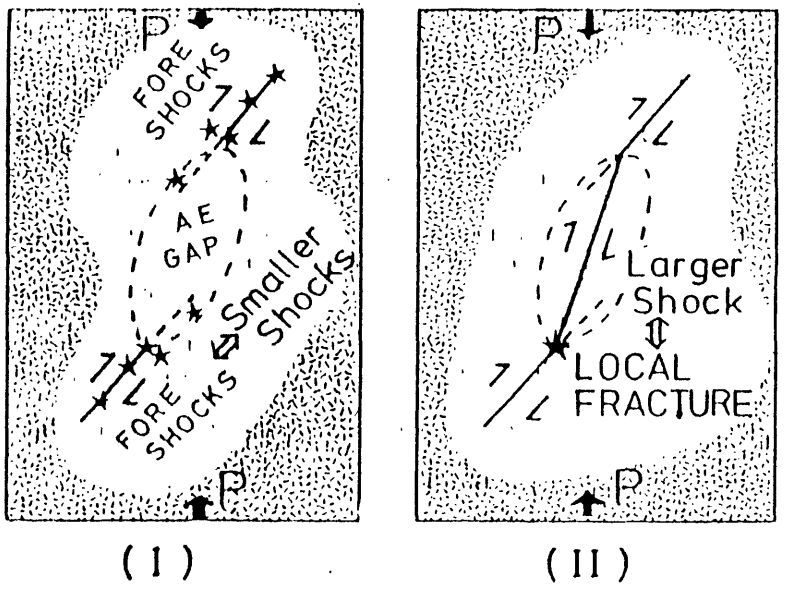

Fig.11 Schematic representation of smaller and larger shocks. (I) and (II) correspond to the first and second concept of our model, respectively. (Taken after Kusunose et al.,1982 and modified)

Swarm No.	S-1	S-2	S-3	S-4	S-5	S-6
Largest Shock						
Date	Dec.3,1978	Mar.15, 1979	May.20, 1979	Jun.29, 1980	Mar.15, 1982	May.10, 1982
M	*5.4	*3.1	*3.8	*6.7	2.2	2.0
**Number of shock$	3153	611	456	3000	144	160
(Period)	(Nov-Dec)	(Mar.13-31)	(May.18-26)	(June-July)	(Mar.7-31)	(May.8-12)
**S-P time(sec)	2.6-2.8	2.4-2.8	2.7-2.9	2.8-3.2	2.3	2.5-2.7

Table 1 List of the earthquake swarms off the east coast of the Izu Peninsula.

* after Japan Meteorological Agency.

** JIZ. Those shocks with a maximum amplitude of 107μkine or larger are counted.

Table

M_l	I	II	III	IV
0.3	1.08±0.26 (68)	0.94±0.38 (24)	0.70±0.26 (29)	
0.7	1.19±0.43 (30)	1.05±0.34 (37)		1.81±0.40 (77)

Table 2 b value and its 95% confidence limit for stages I-IV of SS. Upper and lower values correspond to the cases where the lower limit of magnitude for the estimation, M_l, is 0.3 and 0.7, respectively.

Precise determination of the focal depth of offshore earthquakes in the northern Honshu arc and its implications

Tetsuzo Seno and Makoto Watabe

International Institute of Seismology and Earthquake Engineering, Building Research Institute, Ministry of Construction, Ohho-machi, Tsukuba-gun, Ibaraki Pref., Japan 305

Abstract

We study earthquakes along the northern Honshu arc, Japan, which were previously thought to have occurred within the downgoing slab, landward of the trench axis and seaward of the double seismic zone. We use P wave synthetic seismograms to determine precise focal depth and mechanism.

We examine six earthquakes in the zone from 50 km to 150 km landward of the trench axis whose published focal mechanisms showed T axes subparallel to the dip of the slab; these events have been considered as being within the slab due to their focal mechanisms. When we computed body wave synthetics, however, five of these six events were showen to be of thrust type and located at the plate interface. Our synthetics confirm that the sixth event, which is located about 100 km landward of the trench axis, definitely occurred within slab 15 km below the plate interface. We obtain a focal mechanism with T axis dipping at an angle of 60°.

The bending-unbending theory of an elastic-plastic plate cannot explain the stress axis of this event; however, the gravitational pull or sagging of the plate is consistent with this stress orien-

tation.

Introduction

Sismicity in subduction zones can be separated into three groupes: activity whithin the continental plate, activity at the plate interface, and activity within the oceanic plate. The activity within the oceanic plate is well known in the Wadati-Benioff zone and also in the region seaward of the trench axis. However, the activity within the slab between these two regions is less known or have not been studied well. We concentrate our efforts on this activity in this study. The northern Honshu arc is the best place to study this activity because the double seismic zone is well defined there and precise focal depth determination is possible based on the known crustal structure along the arc in the offshore region (Asano et al., 1981). We determine precise focal mechanism and depth for the events which have occurred in this area using body wave synthetics.

Events

We searched events which possibly have occurred within the slab during the period 1964-1978 June from file MEl of Yoshii (1979b) and Seno and Pongsawat (1980). We listed events which have non-thrust type mechanisms and T axes subparallel to the dip of the slab and whose body-wave magnitudes are greater than 5.4. There are six events which satisfy these conditions; they are listed in table 1 and their epicentral locations are shown in Fig. 1. We selected events with T axes subparallel to the dip of the slab because there are

previous studies which suggested that normal fault type earthquakes dominantly occur in the region between the trench axis and the double seismic zone (Sasatani, 1971; Yoshii, 1979a). We also selected events larger enough of which long period seismograms allow the body wave synthetics.

Method

The method of computation of P wave synthetics is described by Kroeger and Geller (1982). The method is essentially based on the first motion apporximation of generalized rays (Langston and Helmberger, 1975). However, it was improved to include all reflections from the structure near the source. The crustal structure revealed by seismic refraction studies (Asano et al., 1981) is used to compute the synthetics.

Results

Out of six earthquakes in Table 1, five events were found to be of thrust type. The sixth event (1969 03 16, mb=5.5), which is located 100 km landward from the trench axis, definitely has a mechanism different from the thrust type mechanisms which are usually seen in this region. It has one nodal plane dipping shallow to the south and the other dipping steeply to the northeast; thus this event cannot be interpreted as indicating the differential motion between the Pacific and Eurasian plates. The depths determined for these earthquakes are also listed in Table 1. The accuracy of determination is about +-3km if the given crustal structure is correct. The sixth events has the deepest focal depth of 33 km. The foci of other

five events lineup in the cross-section normal to the trench axis (Fig.2); because the shallower fault planes dip along this lineup (fig.2), we interprete this as a plate interface.

Discussions and conclusions

Out of the five events, two events were previously determined as normal fault type by Ichikawa (1971) based on the short period data reported in the ISC Bulletins; P-wave first motions of the long period data clearly show that they are not of normal fault type but of thrust type. The first motion data for the other events are not enough to determine the focal mechanism type. Body-wave synthetics was used effectively to determine the mechanism type in such case. Comparison of waveforms can determine the dip angle of the fault plane if the strike is fixed. Strikes of the fault plane were constrained well by the first motions of P wave and S wave polarization angles. The uncertainty of the slip angle does not effect the waveform much.

Faulting within the slab between the trench axis and the double seismic zone is not significant on the contrary to the previous works (Sasatani, 1971; Yoshii, 1979a). However, the sixth event definitely occurred within the slab 15 km below the interface. The stress orientation of this event (Fig. 2) shows that bending or unbending (Engdahl and Sholz, 1977; Isacks and Barazangi, 1977) cannot explain this stress orientation. Thus this gives an piece of evidence that the force other than expected by unbending-bending is acting within the slab in this reigon. Gravitational pull or sagging of the downgoing plate (Sleep, 1979) is a possible mechanim for this stress orientation.

We selected events from file MEl which does not necessarily include all the larger events. There are still events which are large enough and whose mechanism solutions have not been analysed. Moreover, the time period treated is only about 15 years. Thus we have to await future studies to conclude that the faulting within the slab between the trench axis and the double seismic zone is not significant.

Acknowledgements

This work was done with Glenn Kroeger while one of the authors stayed at Stanford University under the support of NSF grant EAR80-19463. We express our thanks to Bob Geller for his encouragement.

Asano, S., T. Yamada, K. Suyehiro, T. Yoshii, Y. Misawa, and S. Iizuka, Crustal structure in a profile off the Pacific coast of northeastern Japan by refraction method by ocean bottom seismometers, J. Phys. Earth, 29, 267-282, 1981.

Engdahl, E. R. and C. H. Sholz, A double Benioff zone beneath the central Aleutians and unbending of the lithosphere, Geophy. Res. Lett., 4, 473-476, 1977.

Ichikawa, M., Reanalysis of mechanism of earthquakes which occurred in and near Japan, and statistical studies on the nodal plane solutions obtained, 1926-1968, Geophys. Mag., 35, 207-273, 1971.

Isacks, B. L., and M. Baraazangi, Geometry of Benioff zones Lateral segmentation and downward bending of the subducted lithosphere, in Island Arcs Deep Sea Trenches and Bac Arc Basins, Maurice Ewing Series, 1, edited by M. Talwani and W.C. Pitman III, AGU, Washington, D.C., pp. 99-114, 1977.

Kroeger, G. C. and R. J. Geller, An efficient method for synthesizing teleseismic body waves for sources in a vertiacaly layered crust, J. Geophys. Res., Submitted, 1982.

Langston, C. A. and D. V. Helmberger, A procedure for modelling shallow dislocation sources, Geophys. J. R. Astron. Soc., 42, 117-130, 1975.

Sasatani, T., distribution of the P-wave initial motions by earthquakes occurred on the Pacific side in the northeast of Japan, Geophys. Bull. Hokkaido University, 25, 243-258, 1971 (in Japanese).

Seno, T. and B. Pongsawat, A triple-planed structure of seismicity and earthquake mechanisms off Miyagi prefeclture, northern Japan,

Honshu, Japan, Earth. Planet. Sci. Lett. 55, 25-36, 1981.

Sleep, N. H., The double seismic zone in downgoing slabs and the viscosity of the mesosphere, J. Geophys. Res., 84, 4565-4571, 1979.

Stauder, W., and L. Mualchin, Fault motion of the larger earthquakes of the Kurile-Kamchatka arc and of the Kurile-Hokkaido corner, J. Geophys. Res., 81, 297-308, 1976.

Yoshii, T., A detailed cross-section of the deep seismic zone beneath Japan, Tectonophysics, 55, 349-360, 1979a.

Yoshii, T., Compilation of geophysical data around the Japanese islands, Bull. Earthq. Res. Inst., Univ. of Tokyo, 54, 75-117, 1979b (in Japanese).

Figure Captions

Fig. 1 Epicentral location of the events analysed in this study. Focal mechanism solutions from previous studies are also shown; I1 and I2 are from Ichikawa; Y, from Yoshii (1979a); SM, from Stauder and Maulchin (1976); SP1 and SP1 from Seno and Pongsawat (1980).

Fig. 2 Cross-section of the foci determined by body-wave synthetics. Shallower fault planes for thrust type events and T axis for the non-thrust type event are also shown in this cross-section.

Table 1. Earthquakes analysed

Event	Date	Location (°N)	(°E)	m_b	*Depth – ISC** (km)	*Depth*** (km)	Reference
I1	1965 03 16	40.75	142.96	5.8	29	26	Ichikawa (1971)
I2	1968 05 24	40.91	143.11	5.7	23	23	Ichikawa (1971)
Y	1968 06 22	40.31	143.68	5.8	19	16	Yoshii (1979a)
SM	1971 09 15	39.17	143.39	5.8	20	16	Stauder&Mualchin (1976)
SP1	1968 04 21	38.68	142.99	5.4	41	18	Seno&Pongsawat (1981)
SP2	1969 03 16	38.57	142.83	5.5	37	33	Seno&Pongsawat (1981)

* pP-P depths corrected for the water layer (Yoshii, 1979a)
** Depths determined by the body wave synthetics in this study

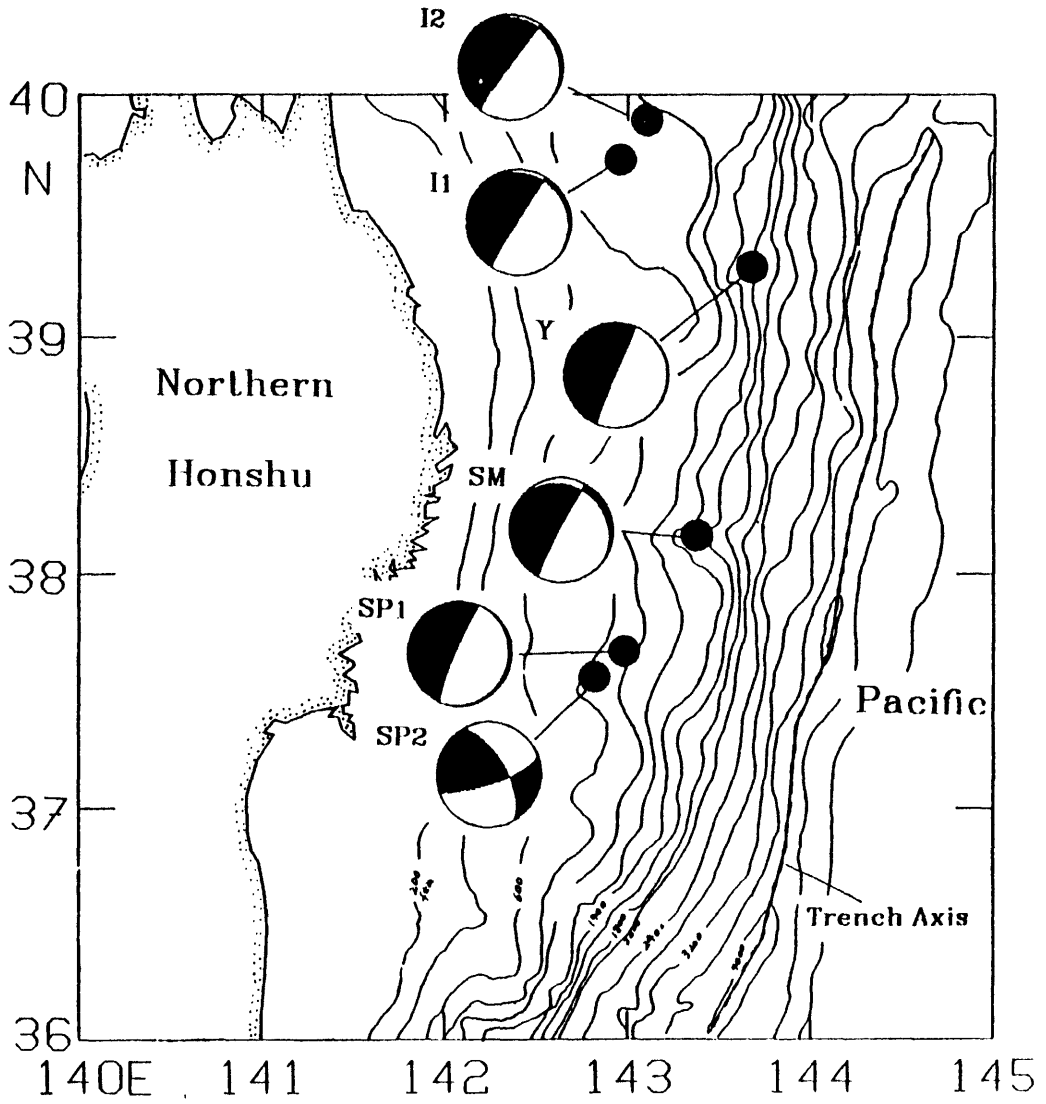
I2
I1
Y
SM
SP1
SP2
Northern
Honshu
Pacific
Trench Axis
40
N
39
38
37
36
140E
141
142
143
144
145

Fig. 1

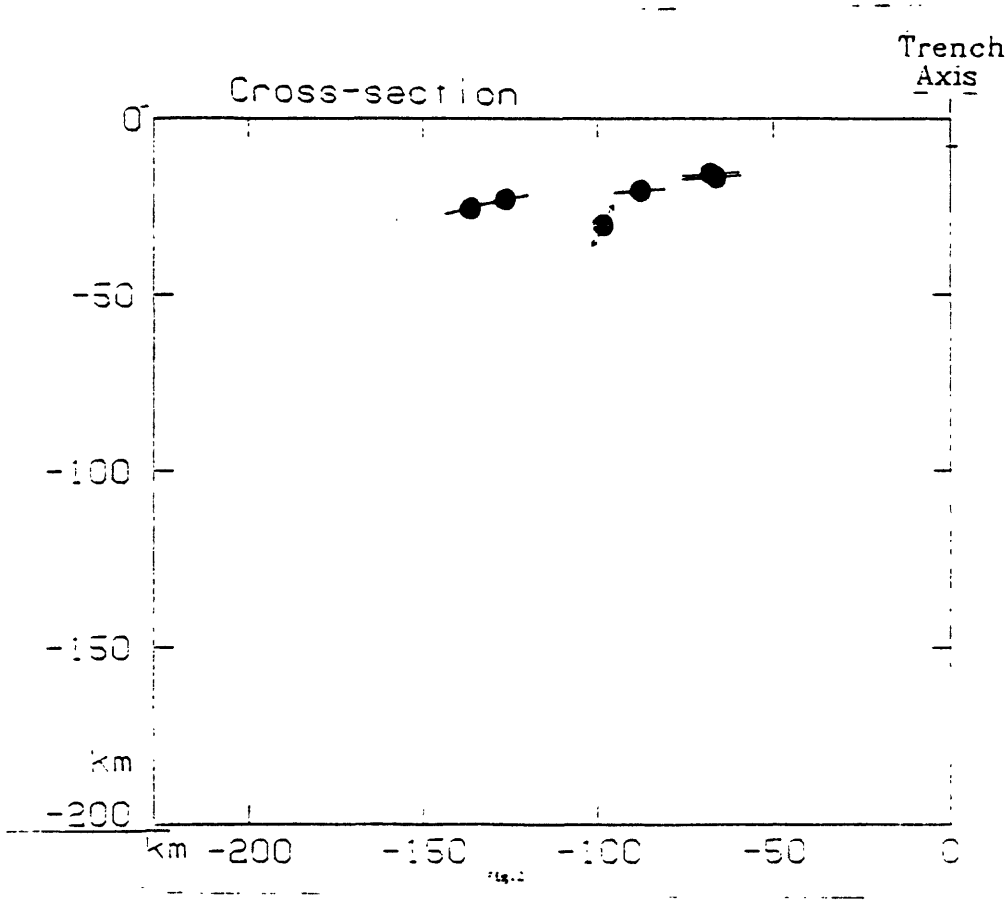
Cross-section
Trench Axis
0
-50
-100
-150
km
-200
km -200
-150
-100
-50
0

Seimicity along the Pacific-North American Plate Boundary in California and Western Nevada: 1980

by

David P. Hill, Jerry P. Eaton, Robert S. Cockerham,
William L. Ellsworth, and Carl E. Johnson

INTRODUCTION

Beginning in 1980, the number and distribution of telemetered, high-gain seismic stations operated in California and western Nevada provided the capability for locating earthquakes of magnitude 1.5 and greater occurring throughout the broadly-deforming Pacific-North American plate boundary from the Salton Trough to the Mendocino triple junction and as far inland as the eastern Sierra Nevada escarpment and the western Great Basin. The objectives of this paper are to 1) present the pattern of earthquake occurrence that emerged during 1980 from standard processing of the data recorded by the three networks which, taken together, form a 550-station array spanning the transform boundary between the Pacific and North American plates, and 2) highlight a few aspects of this pattern in relation to recognized active faults, regional tectonic processes associated with deformation of the plate boundary, and the recurrence of major earthquakes.

THE SEISMIC NETWORKS

Locations of the 550 stations forming the three telemetered networks of short-period, high-gain seismograph stations in California and western Nevada are plotted in Figure 1. Data from the stations within a given network are telemetered to a central site where they are recorded and processed on a routine basis for origin time, hypocentral locations, and

magnitudes. Thus, data from the Central California Network are processed by the U.S. Geological Survey (USGS) in Menlo Park, California; data from the southern California network are processed in a cooperative Caltech-USGS effort at the California Institute of Technology (Caltech) Seismological Laboratory in Pasadena, California; and data from the western Nevada network are processed by the Seismological Laboratory at the University of Nevada in Reno, Nevada.

Each of the stations plotted in Figure 1 involves a moving-coil, vertical-component seismometer with a 1 Hz natural frequency and a low-power amplifier-VCO (Voltage-Controlled Oscillator) unit that prepares the signal for FM-multiplexed transmission (with up to eight signals on a single telemetry channel). At the present time, most of the signals are transmitted over available telephone lines, although a concerted effort is underway to convert as much telemetry as possible to more economical FM-radio or microwave links. Representative system-response curves for the telemetered stations are plotted in Figure 2. Note that a typical station operates with a magnification of about 1×10^6 at a frequency of 10Hz. The attenuated response of southern California stations at frequencies above 3 Hz reflects a dealiasing filter introduced to accommodate the 50 sample/second digital recording rate for data in this network.

The digitally-recorded data from the southern California network have been processed using the interactive computer system CEDAR since 1976 (Johnson, 1979). An enhanced version of this system based on 100 samples/second digital recording rate is currently being implemented for all three networks. Earthquakes recorded on the Central California and

western Nevada networks for the period covered in this paper (1980), however, were largely processed by hand timing from film (Develecorder) records and paper playbacks of FM signals recorded on magnetic tapes.

Routine hypocenter locations for earthquakes occurring within each network are determined by least-squares inversion of measured P-wave arrival times using a horizontally-layered P-wave velocity model (Lee and Lahr, 1975) appropriate for the region. Magnitudes are calculated principally from the duration of the earthquake coda waves measured on the network-stations (Lee et al., 1972). For earthquakes larger than M 3.5 magnitudes are obtained from acmplitude measurements on Wood-Anderson seismograms reported by either Caltech or U.C. Berkeley.

The accuracies of hypocenter locations vary within the networks depending primarily on local station-density and knowledge of the local crustal structure. As a rule, calculated epicenter- and focal-depth errors for well-recorded earthquakes in the most densely instrumented sections of the central California network are less than 1 and 2 km, respectively. The corresponding errors in areas with average station spacing are generally less than 2.5 and 5 km, respectively, but for earthquakes occurring near the network margins or beyond, these errors may increase to 5 and 10 km or more.

The system of telemetered, high-gain stations pictured in Figures 1 and 2 began in late 1966 with the installation of a small cluster of eight stations along the San Andreas Fault near the south end of San Francisco Bay (Eaton and others 1970). This cluster was gradually extended to form the 175-station Central California Network by 1977. With the increase in funding for earthquake research accompanying passage

of the National Earthquake Hazards Reduction Act in 1977, the number of stations was expanded to the current system of over 500 stations distributed between three major networks pictured in Figure 1. Although the majority of the stations in these networks are supported by funds administered by the USGS under the Earthquake Hazards Reduction Program, a significant fraction have been supported by other sources, including the U.S. Geological Survey and Department of Energy Geothermal Programs, the U.S. Bureau of Reclamation, and U.S Army Corps of Engineers, and the Reactor Hazards Program under the Nuclear Regulatory Commission.

This dense array of high-gain, telemetered stations complements the regional networks in northern and southern California that have been operated by the University of California, Berkeley and the California Institute of Technology, respectively, beginning as early as 1910 (Bolt and Miller, 1975; Heilman et al, 1975). In addition to sparse arrays of telemetered stations these networks contain a number of broad-band and special-purpose low-gain stations. They provide long-term continuity for the locations and magnitudes of earthquakes with local magnitudes M_L greater than about 3 as well as on-scale data for special studies of the larger earthquakes occurring in California.

1980 SEISMICITY

Epicenters for earthquakes of magnitude 1.5 and greater recorded during 1980 by the three seismic networks illustrated in Figure 1 are plotted in Figure 3 together with the surface traces of major Quaternary faults. The resulting seismicity pattern can be described in terms of a quasi-stationary pattern that seemingly shows only modest fluctuations in form over the past ten years or more (at least for the parts of central

and southern California where data of uniform quality are available), and a more transient pattern dominated by the aftershock sequences of larger earthquakes ($M \gtrsim 5$) and occassional earthquake swarms.

Stationary pattern. The stationary seismicity pattern along the San Andreas fault for at least the past ten years and very likely for the last 50 or 60 years (Ellsworth and others, 1981), has been characterized by the remarkable absence of even the smallest earthquakes along the sections of the fault that broke with the great historical earthquakes ($M \simeq 8$) of 1857 in southern California and 1906 in northern California. These two quiet segments are separated by the equally remarkable creeping segment of the fault in central California characterized by the persistant activity of small-to-moderate earthquakes ($M < 6$), which are tightly confined to the actively slipping planes of the San Andreas and Hayward-Calaveras faults (Wesson and others 1977). South of the now quiet 1857 break, the San Jacinto, Brawley, and Imperial branches of the San Andreas fault system have also been persistantly active with small to moderate earthquakes during the past ten years (see Allen, 1981).

The two parallel strings of epicenters extending northwestward from San Francisco Bay toward the Mendocino triple junction also appear to be part of the stationary seismicity pattern, although a few more years of monitoring with the newly established stations in northern California will be required to establish the stability of this pattern.

Several rather diffuse seismicity patterns also show a tendency to maintain relatively stable levels of activity over the last decade or so. The most noteworthy examples are 1) an irregular cluster elongated in an east-west direction that generally includes the southern section of

the Transverse Ranges plus the Los Angeles Basin and the southwestern part of the Mojave Desert, 2) a cluster elongated in a northeasterly direction that runs parallel to but north of the Garlock fault (the Tehachapi-Walker Pass-Coso trend), 3) an elongated, rectangular-shaped cluster in the Coast Ranges immediately east of the long, straight stretch of the San Andreas fault central California, 4) a persistant cloud of activity covering the Cape Mendocino area (the particular triangular-shaped pattern in Figure 3, however, represents the aftershock sequence of the November 11 magnitude 7 event to be mentioned below. The diffuse pattern of epicenters that crosses the north end of the Great Valley and the northern Sierra Nevada mountains also appears to be stable, as least over the couple of years for which adequate data are available.

In contrast, three large areas are noteworthy for their persistently low levels of seismicity. Few earthquakes are reliably located in the Mojave Desert either east of a line extending between Death Valley and the east margin of the Salton Trough or in the western wedge that forms the "prow" between the Garlock and San Andreas faults. (Note, however, that these two quiet areas are seperated by a band of seismicity and mapped Quaternary faults in the central Mojave Desert).

Similarly, few earthquakes are located within the large oval-shaped area that includes the central sections of the Great Valley and the Sierra Nevada Range. (The absence of epicenters plotted in Figure 3 for northern-most California reflects the lack of network coverage during most of 1980. Data from newly installed stations in the Mount Shasta-Mount Lassen region show a moderate level of earthquake activity).

Transient pattern. The more transient part of the seismicity pattern for 1980 is dominated by the occurrence of six earthquakes of magnitude 6 or greater. Excluding the aftershocks of major earthquakes, this is the largest number of magnitude 6 or greater earthquakes to occur in California and western Nevada during any single year back at least as far as the turn of the century (Bufe and Toppozoda, 1981). Interestingly, the two largest events were located at the extreme northern and southern ends of the San Andreas fault system: a M 6.1 earthquake on the Cerro Prieto fault (Mexico) in the Salton Trough on June 9 and a M 7.0 earthquake just off Cape Mendocino on November 8. (The Cerro Prieto fault is one of a series of right-stepping, en-echelon faults forming the transition from the San Andreas transform fault system to the east PAcific Rise in the Gulf of California). The remaining for M=6 events occurred in the remarkable Mammoth Lake sequence just south of Long Valley along the eastern escarpment of the Sierra Nevada range on May 25, 26, and 27.

Also contributing to the transient pattern were several earthquake sequences in which the largest events were in the range $5 \leq M < 6$. On January 24, and M 5.8 mainshock initiated an intense aftershock sequence on the previously quiet Greenville fault just north of Livermore and east of the persistantly active Calaveras fault. The clusters of epicenters extending to the northeast into Nevada from Mammoth Lakes developed as a series of swarm-like sequences each with one or more M 5 events during June, September, and December. A tight cluster of epicenters just northwest of Lake Tahoe represents the aftershock sequence of a M 5.2 earthquake on November 28 (see Smith and Ryall, 1982).

Depth Distribution. As has been recognized for some time, most earthquakes in California and Nevada are confined to the upper 15 km of the crust (Allen, 1981, Wesson and others, 1977, Hill, 1978). With the improved areal coverage and resolution afforded by the array of stations shown in Figure 1, however, some interesting variations in the pattern of focal depths have begun to emerge.

The series of cross-sections plotted in Figure 4 illustrate a few of the more notable variations. In particular:

1) Maximum focal depths systematically increase from 20 to 60 km along profile AA' extending to the southwest from Cape Mendocino. This pattern of deep earthquakes very likely reflects the southern edge of the Juan de Fuca plate as it is being subducted beneath the North American plate (Cockerham, in press).

2) The distribution of focal depths along the San Andreas fault system in northern California (Profile D-D') emphasizes the abrupt transition from the deep seismicity ($h \lesssim 40$km) beneath the Mendocino triple junction to the shallower seismicity ($h \lesssim 15$km) typical of the San Andreas system. This step probably represents the southern edge of the Juan de Fuca plate.

3) The tendency for earthquakes to occur on the vertical planes of the major branches of the San Andreas system in central California is emphasized in profile B-B'.

4) Maximum focal depths increase to about 20 km beneath the Transverse Ranges in southern California (Profile C-C'). (Because focal depths are generally the least reliably determined parameter in a routine hypocenter location, some

caution must be exercised in interpreting detailed patterns in cross-sections of the sort presented in Figure 4).

DISCUSSION

The spatial pattern of earthquake occurrence emphasized here represents only a small part of the information that can be extracted from these networks on seismotectonic processes operating along the San Andreas transform fault system and the western margin of the North American plate.

For example, we have made only passing reference to temporal variations of seismicity in terms of stationary and transient patterns with respect to a one-year time frame, although the data affords the possibility of a wide range of space-time studies. Such studies are critical as we attempt to access the validity of the "seismic cycle" concept as it applies to the recurrence of major earthquakes on transform plate boundaries (Ellsworth and others, 1981). In particular, we should expect to see a change in the "stable" seismicity pattern as we move in time from the relatively quiet period (stage I) in the "Seismic gaps" along the sections of the fault that broke with major events in 1857 and 1906 to a period of increased activity (stage II) leading to the next major, gap-filling earthquake (stage III). Clearly, however, our ability to resolve such changes will depend on our ability to maintain a uniform capacity to collect and process the data from a stable array of stations over the coming years.

Information on earthquake source parameters (Fault plane solutions, seismic moment, stress drops) that can be extracted from the network data provide fundamental clues on the kinematics of the deformation process

and the nature of the associated stress field. Although solutions for source parameters are not yet produced by routine processing of network-data, a number of special studies based on subsets of the network data have been completed. The results show that, in general, 1) earthquakes on the San Andreas fault and its many sub-parallel branches have right-lateral, strike-slip focal mechanisms with slip on planes more or less parallel with the surface trace of the associated fault, 2) earthquakes in the Transverse Ranges have focal mechanisms showing both reverse slip (thrust) on east-striking planes and strike-slip on either northeast of northwest striking planes, and 3) earthquakes in the Basin and Range province (north of the Garlock fault) and east of the Sierra Nevada) have normal slip on north-striking planes and strike slip on either northeast of northwest striking planes. All of these focal mechanisms are consistant with a stress field dominated by the interaction of the Pacific and North American plates in which the greatest compressive horizontal stress has a north-south orientation and the least compressive horizontal stress has an east-west orientation (Hill, 1982, Zoback and Zoback, 1980). Local deviations of focal mechanisms from this regional pattern, however, are not unusual. A notable example is provided by the Mammoth Lake sequence and earthquakes to the northwest along the boundary zone between the Sierra Nevada and Great Basin in which the extention directions (T-axes) of the focal mechanisms are systematically rotated by nearly 45^0 in a counterclockwise direction with respect to the regional trend (see VanWormer and Ryall, 1980).

CONCLUSIONS

The pattern of earthquake occurrence in California and Nevada illustrated in Figures 3 and 4 is symptomatic of the wide-spread deformation of the western margin of the United States as the Pacific and North American plates grind past on another along the San Andreas transform fault system. The data recorded from these earthquakes on the array of seismic stations illustrated in Figure 1, clearly contain a wealth of information on the nature of the processes driving this wide-spread deformation and the properties of the lithosphere undergoing deformation.

REFERENCES

Allen, C.R., (1981), The modern San Andreas fault, in The Geotectonic Development of California, Ruby Volume 1, W.G. Ernst, eds., Prentice-Hall, New Jersey, pp. 511-534.

Bolt, B., and R. D. Miller, (1975), Catalog of Earthquakes in Northern California and Adjoining Areas, 1 January 1910 - 31 December 1972: University of California, Berkeley. 567 p.

Bufe, C. G., and T. R. Toppozada (1981), End to seismic quiescence, California Geology, v. 34, pp. 111-114.

Cockerham, R. S., (198), Evidence for a 180 km-long subducted slab beneath northern California, to be submitted to the Bulletin of the Seismological Society of America (BSSA).

Eaton, J. P., W. H. K. Lee, and L. C. Pakiser (1969), Use of microearthquakes in the study of the mechanics of earthquake generation along the San Andreas fault in central California, Tectonophysics, v. 9, pp. 259-282.

Ellsworth, W. L., A. G. Lindh, W. H. Prescott, and D. G. Herd, (1981), The 1906 San Francisco earthquake and the seismic cycle, in Earthquake Prediction - An International Review, Maurice Ewing Series 4, American Geophysical Union, Washington D.C., pp. 126-140.

Hileman, J. A., C. R. Allen, J. M. Nordquist (1975), Seismicity of the Southern California Region, 1 January 1932 to 31 December 1972; California Inst. of Technology, Pasadena, 497 p.

Hill, D. P. (1978), Seismic evidence for the structure and Cenozoic tectonics of the Pacific coast states in Cenozoic Tectonics and Regional Geophysics of the western Cordillera, eds. R. B. Smith and G. P. Eaton, Mem. Geol. Soc. Am. 152, pp. 145-174.

Hill, D. P. (1982), Contemporary block tectonics: California and Nevada Jour. of Geophys. Res., v. 87, pp. 5433-5450.

Johnson, C. R., (1979), I. CEDAR - An Approach to the computer Automation of Short-Period Local Seismic Networks, PhD Thesis, California Inst. of Tech., Pasadena 332p.

Lee, W.H.K., and J. Lahr, (1975). HYPO71 (revised): A computer program for determining hypocenter, magnitude, and first motion pattern of local earthquakes. Open-File Report 76-169, U.S. Geological Survey, Menlo Park.

Lee, W.H.K., R. E. Bennett, and K.L. Meagher, (1972), A method of estimating magnitude of local earthquakes from signal duration, U.S.G.S. Open File Report, 28p.

Smith, G. M., and F. D. Ryall, (1982), Bulletin of the Seismological Laboratory for the Period January 1 to December 31, 1980. Mackay School of Mines, University of Nevada, Reno.

Vanwormer, J. D., and A. S. Ryall, (1980) Sierra Nevada-Great Basin boundary zone: Earthquake hazard related to structure, active tectonic processes and anomalous patterns of earthquake occurence, Bull. Seis. Soc. Am. 70, 1557-1572.

Wesson, R. L., R. Robinson, C. G. Bufe, W. L. Ellsworth, J. H. Pfluke, J. A. Steppe, and L. C. Seekins, (1977), Seach for seismic forerunners to earthquakes in central California, Tectonophysics v. 42, pp. 111-126.

Zoback, M. L. and M. D. Zoback, (1980) Interpretative stress map of the counterminous United States, Jour. of Geophys. Res., v. 85, pp. 6113-6154.

FIGURE CAPTIONS

Figure 1 Locations of short-period, telemetered seismic stations forming the Central California Network (C), the Southern California Network (S), and the Western Nevada Network (N) in 1980.

Figure 2 Typical system response for telemetered stations in Figure 1. Dashed curve shows effect of dealiasing filter used in Southern California Network.

Figure 3 Earthquakes located in California and western Nevada during 1980. Symbol size is proportional to magnitude. Profiles are keyed to cross-sections in Figure 4.

Figure 3a Map showing major Quaternary faults mapped in California and Nevada together with geographic features mentioned in the text. Striped area indicates Sierra Nevada mountains and cross-ruled area indicates the Transverse Ranges. Faults and other features are: B = Brawley seismic zone, BP = Big Pine f., C = Calaveras f., CM = Cedar Mt. f., DV = Death Valley f., E = Elsinor f., G = Garlock f., GV = Green Valley f., H = Hayward f., I = Imperial f., M = Maacama f., NI = Newport-Inglewood f., PM = Pinto Mt. f., PV = Pleasant Valley f., SA = San Andreas f., SJ = San Jacinto f., SY = Santa Ynez f., WL = Walker Lake, LV = Long Valley Caldera, LT = Lake Tahoe, MTJ = Mendocino triple junction.

Figure 4 Cross-sections showing depth distribution of earthquakes along profiles in Figure 3. Earthquakes occurring within 20 km on each side of a profile have been projected onto the corresponding cross-sections.

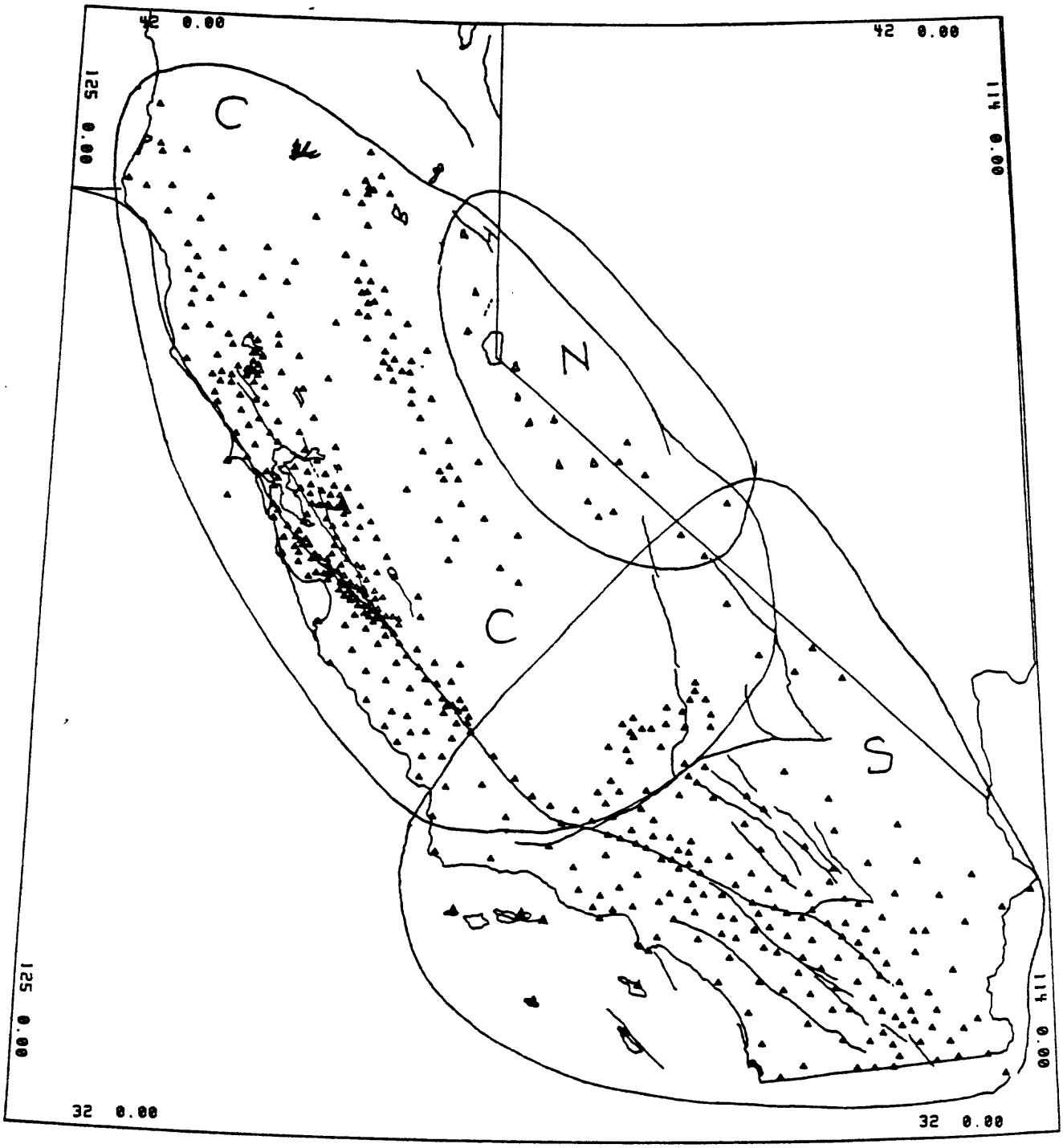

FIGURE 1

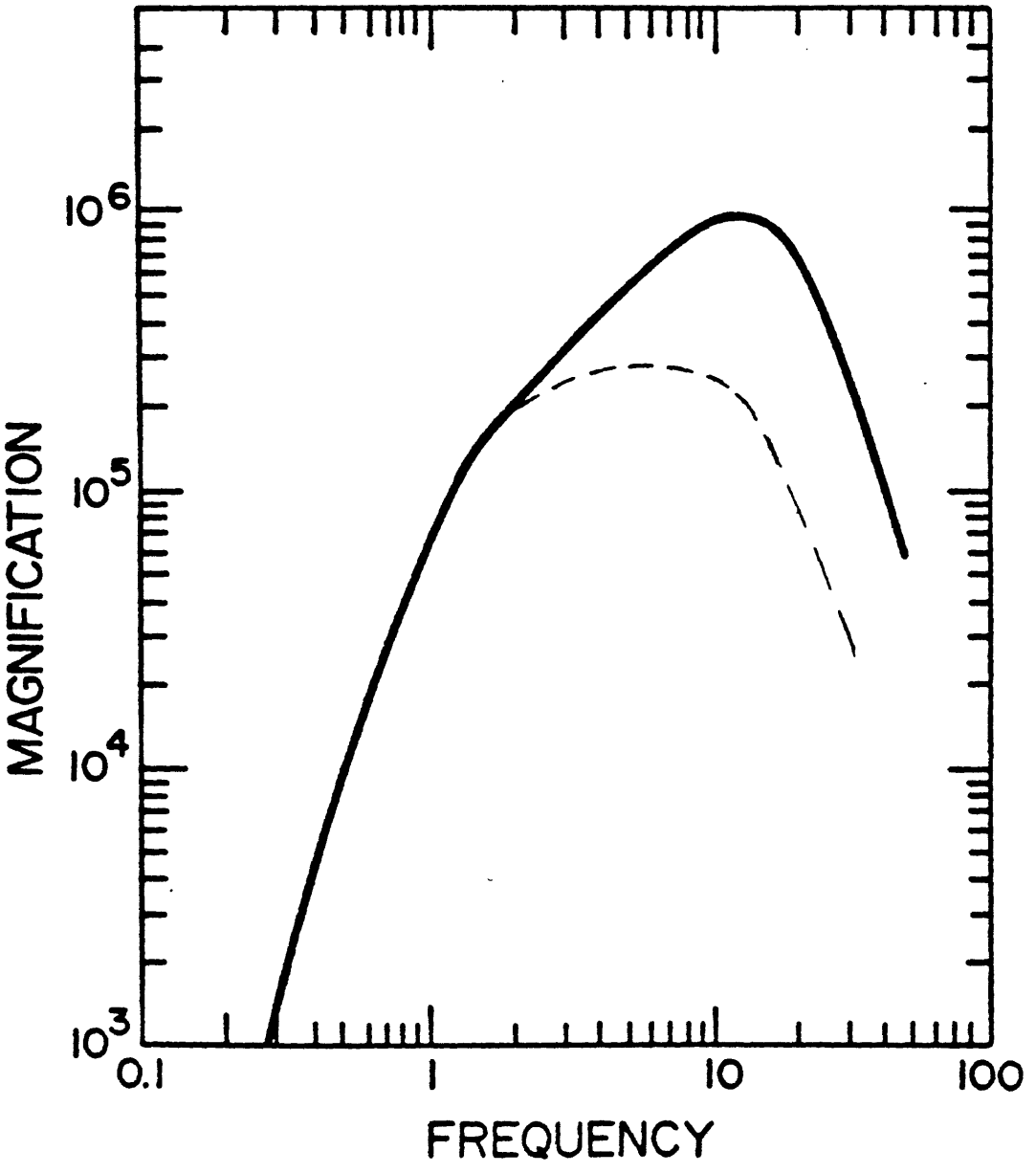

FIGURE 2

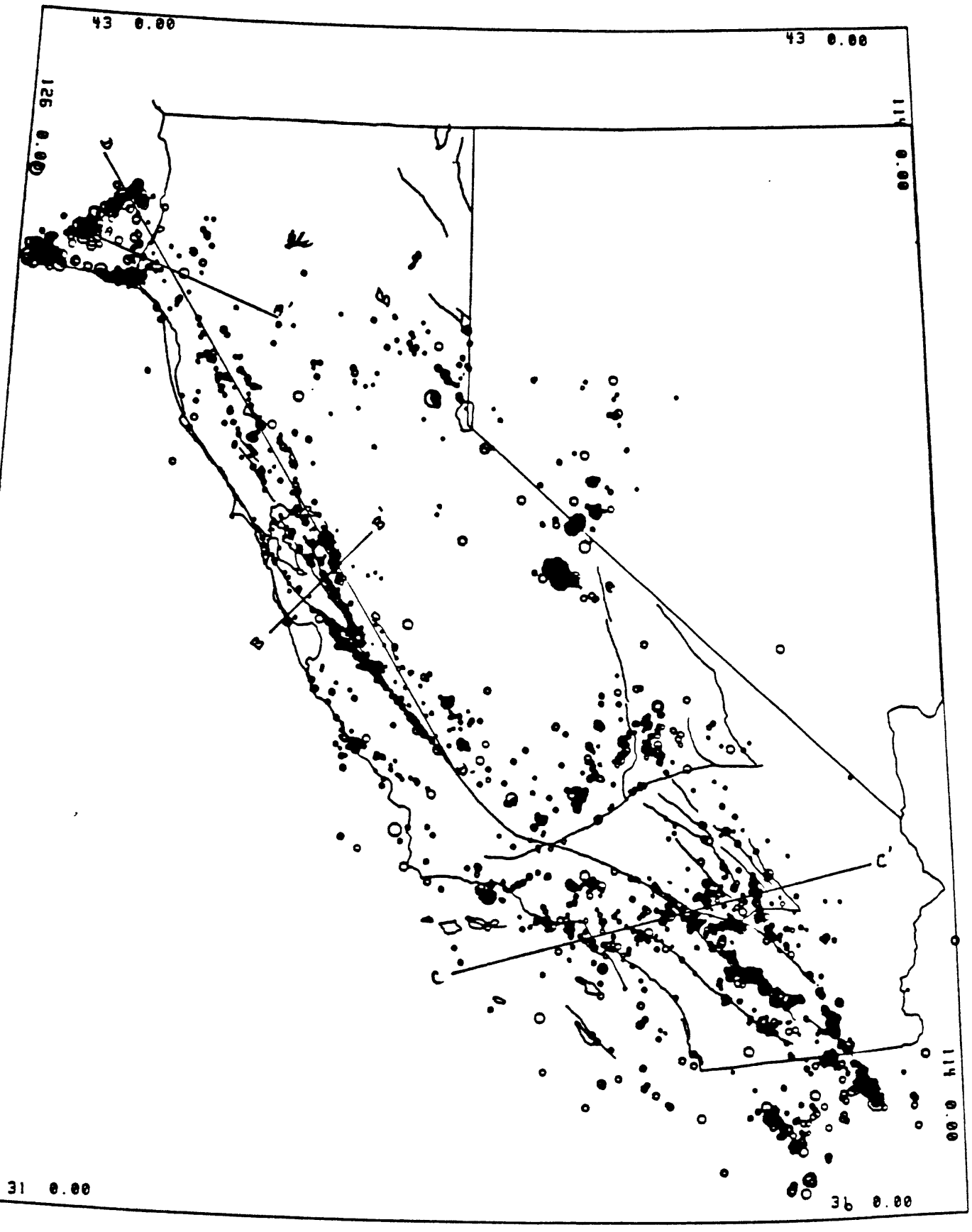

Figure 3

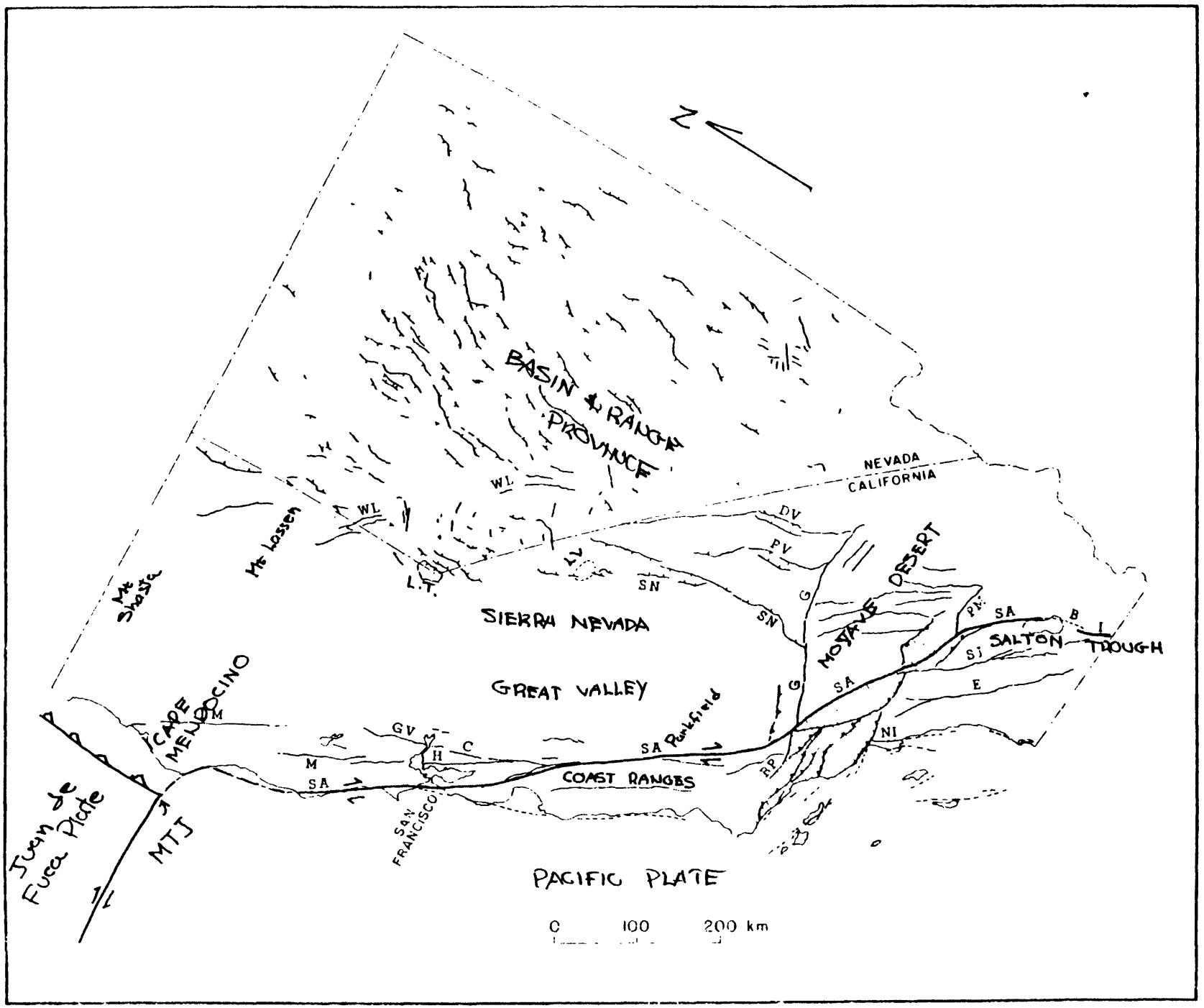
N
BASIN & RANGE PROVINCE
NEVADA
CALIFORNIA
WL
Mt Shasta
Mt Lassen
DV
PV
LV
SN
SIERRA NEVADA
GREAT VALLEY
MOJAVE DESERT
PN
SA
B
I
SJ
SALTON TROUGH
E
G
CAPE MENDOCINO
M
GV
H
C
SA Parkfield
NI
RP
COAST RANGES
SAN FRANCISCO
Juan de Fuca Plate
MTJ
PACIFIC PLATE
0 100 200 km

FIGURE 3C:

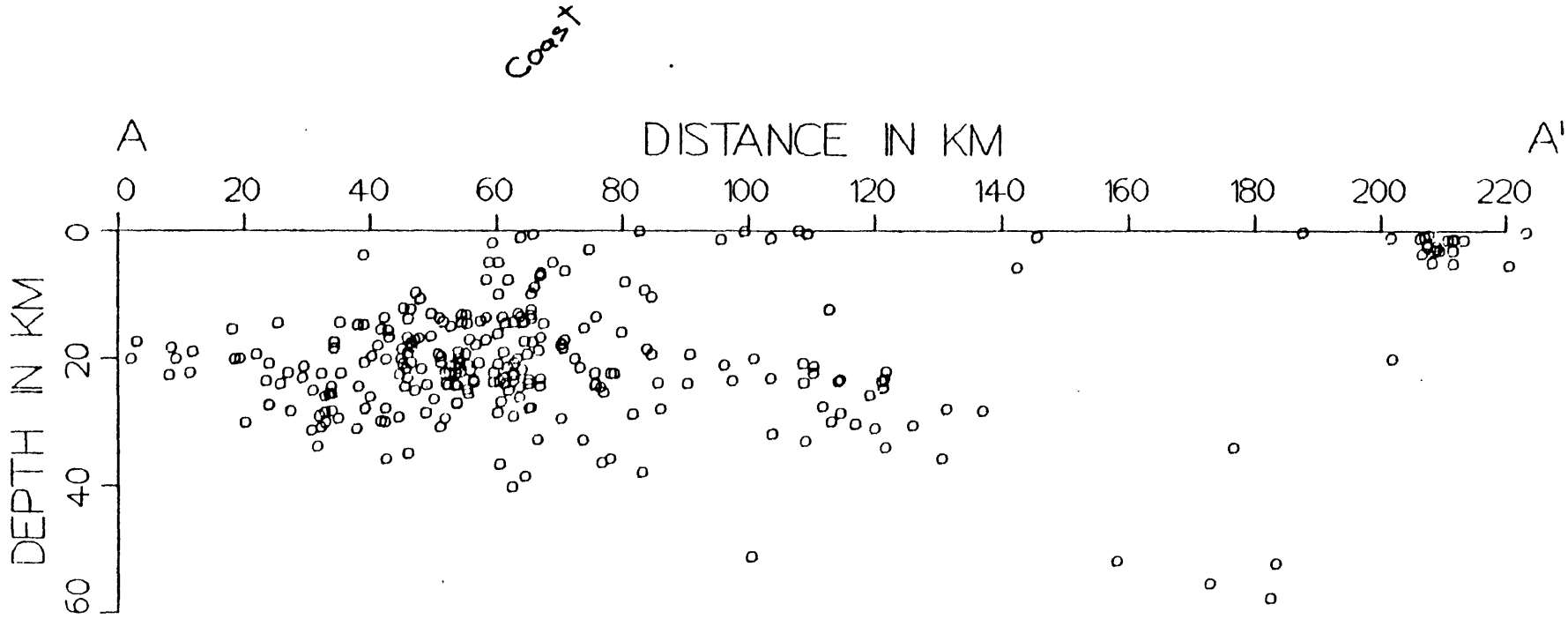
Coast
A
DISTANCE IN KM
A'
0
20
40
60
80
100
120
140
160
180
200
220
DEPTH IN KM
0
20
40
60

Figure 4a

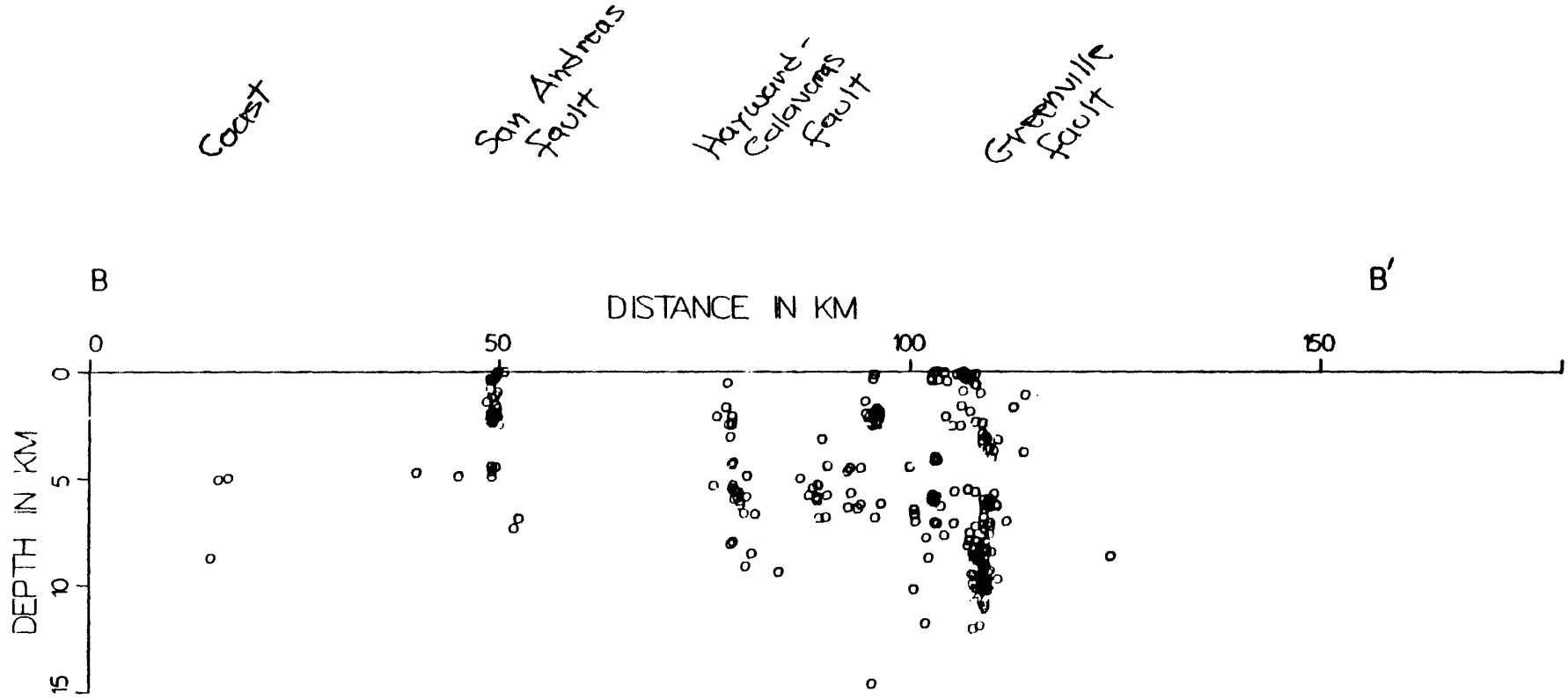
Coast
San Andreas fault
Hayward-Calaveras fault
Greenville fault
B
B'
DISTANCE IN KM
0
50
100
150
DEPTH IN KM
0
5
10
15

FIGURE 4b

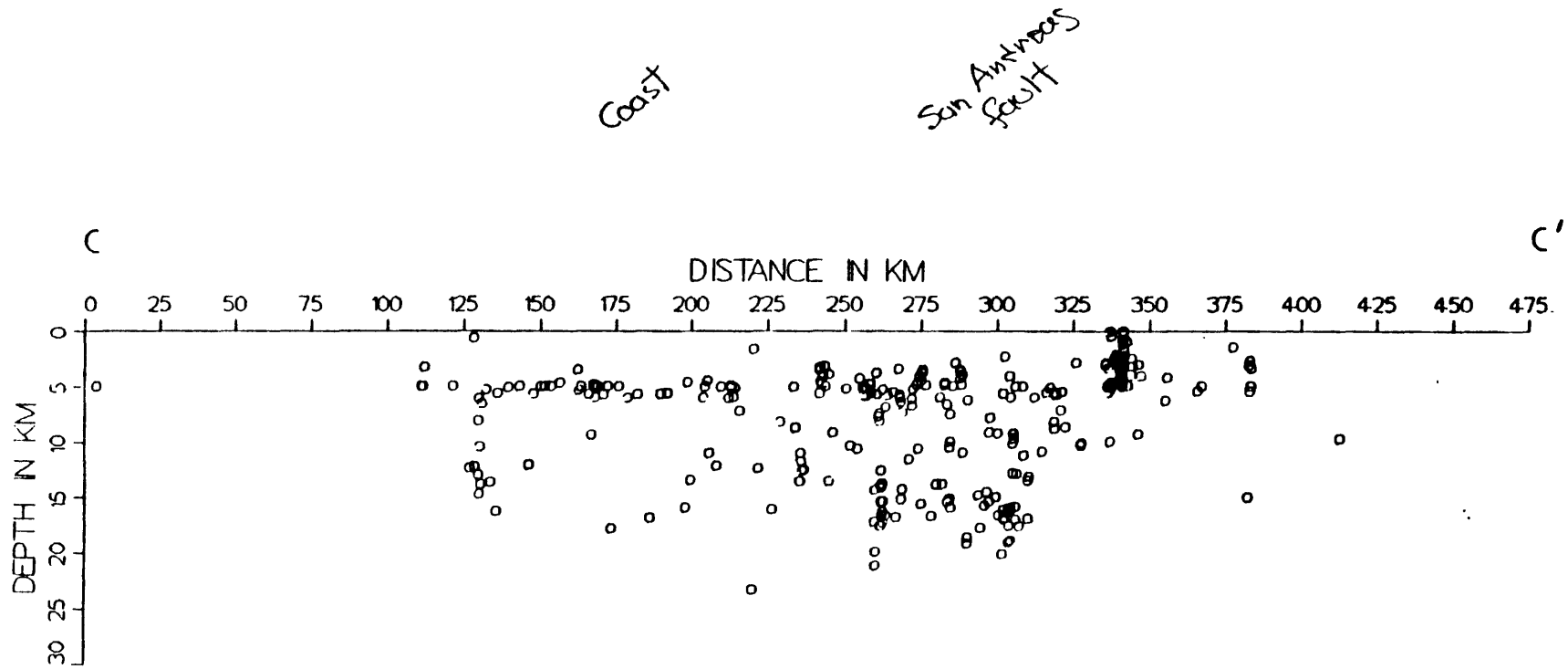
Coast
San Andreas Fault
C
C'
DISTANCE IN KM
0 25 50 75 100 125 150 175 200 225 250 275 300 325 350 375 400 425 450 475
DEPTH IN KM
0 5 10 15 20 25 30

Figure 4c

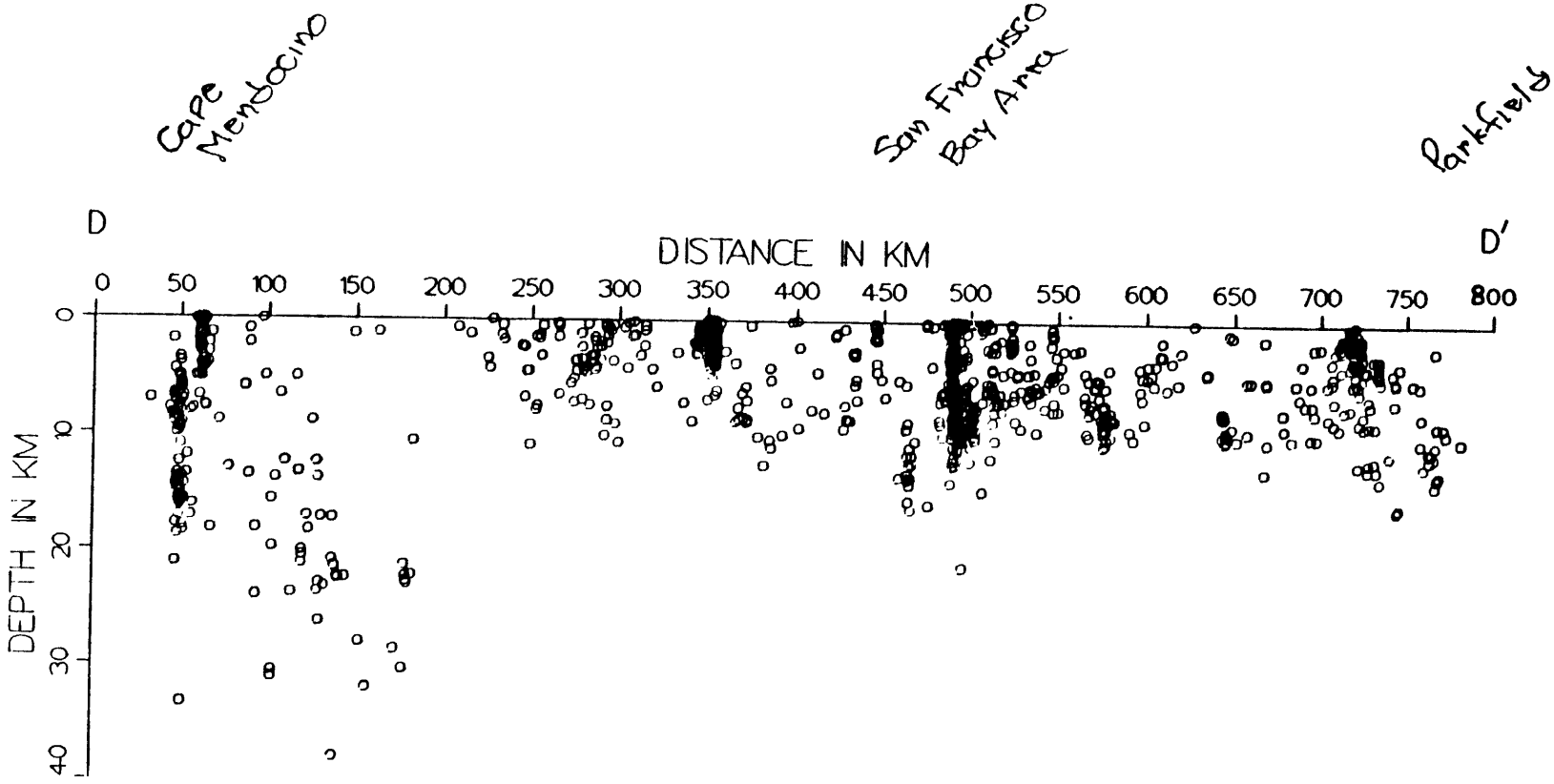
Cape Mendocino
San Francisco Bay Area
Parkfield
D
D'
DISTANCE IN KM
0
50
100
150
200
250
300
350
400
450
500
550
600
650
700
750
800
DEPTH IN KM
0
10
20
30
40

Figure 4d

The interpretation of changes in groundwater level caused by earthquakes

Tagutschi,Y., Takahashi,M., Nagai,S., and Tono,N.
Geological Survey of Japan
Tsukuba, Ibaraki 305, Japan

Abstract

The swarm earthquake occurred off the east coast of the Izu Peninsula for about three months from June 25, 1980. Among them, the earthquake of magnitude 6.7, which occurred at 16:20 hours on June 29, 1980 was the main shock.

Pre- or coseismic changes in groundwater level caused by the main shock were examined at the two observation wells at Atami and Haibara, Shizuoka Prefecture, Japan.

Based on groundwater level fluctuation caused by earthquakes, one model called a sponge model is proposed. According to the model, the mechanism of fluctuation in groundwater level by earthquake can be reasonably interpreted.

1. Introduction

The swarm earthquake occurred off the east coast of the Izu Peninsula for about three months from June 25, 1980. Among them, the earthquake of magnitude 6.7(by the Japan Meteorological Agency) which occurred at 16:20 hours on June 29, 1980 was the main shock.

The authors examined the fluctuations of groundwater levels at two observation wells at Atami and Haibara(Fig. 1) from a hydrological point of view.

A groundwater level decrease of about 80 cm was observed for 40 minutes after the occurrence of the main shock at the Atami observation well. The groundwater level was stabilized at the decreased level after the main shock.

For 16 hours before the main shock, the groundwater level at the Haibara observation well could not be correlated to barometric pressure change.

The purpose of this paper is to interpret the fluctuation of the groundwater level caused by earthquakes using a model based on their examinations.

2. Coseismic changes in groundwater level at the Haibara observation well

1) Description of the well

The Atami observation well(80 m in depth) is situated on the active Baien fault at 96 m above sea level(Fig. 2). Strainers are installed from 15 to 30 m and from 60 to 70 m in depth based on temperature logging and other data, but the well below 60.73 m is buried with debris.

This well had been a source of water supply to Atami City only

in summer, but the pumping was stopped after 1974. GSJ installed an automatic water gauge in October, 1979.

2) Fluctuation of groundwater level

Figure 3 shows the groundwater level at 30 minute intervals at the observation well, hourly precipitation, and barometric pressures at 6 hour intervals observed at the Ajiro Weather Station from 21:00 hours on June 25 to 24:00 hours on June 30, 1980. During this period, earthquakes in magnitude over 4.0 occurred nine times as shown in Table 1. Earthquakes A, B, C, and D were relatively large, among which C was the main shock. It took 14 months for the groundwater level to return to the former level after the main shock. The decrease in groundwater level by earthquake C occurred exponentially during a time span of 40 minutes.

3) Relationship between the net difference of groundwater level and energy of earthquake

The net difference of groundwater level(ΔH in mm) before and after each earthquake is related with its energy(E in joule) as shown in Fig. 4. The equation between two is as follows;

$$\Delta H = 5.75 \times 10^{-9} E^{0.75} \qquad (1)$$

4) Hydrological aspects of groundwater level fluctuation

Groundwater level is greatly affected by the amount of the precipitation. But barometric pressure does not affect it in signifi-

cant way(Fig. 5). The groundwater at this well is unconfined both hydrologically and hydrochemically. The relationship between precipitation and net increase of groundwater level by precipitation is not identical, but it is nearly linear on a log-log scale when the total precipitation exceeds 10 mm(Fig. 6). This relationship holds regardless of earthquake occurrence. A scattering of circles in Fig. 6 such as A7, A8, A10, B3, and B7 mainly depends on each antecedent condition.

The recession segment of groundwater hydrograph after the peak can be expressed by the following equation(2).

$$H = H_o e^{-\alpha(t-t_o)} + b \qquad (2)$$

Replacing $e^{-\alpha}$ with K, equation(2) can be rewritten by equation(3).

$$H = H_o K^{(t-t_o)} + b \qquad (3)$$

where H:groundwater level at the time t on a recession segment of hydrograph, H_o:that at the peak($t=t_o$), K:recession constant, $t-t_o$: passed time after the peak, b:constant.

Table 2 shows recession constant calculated from equation(3), after the peak of hydrograph before and after earthquake C. The mean value before and after earthquake C is 0.97. Significant difference cannot be observed between them. On the other hand, the decrease of groundwater level after earthquake C is 0.81 for the first five minutes and 0.88 after that. They are small enough compared to those under normal conditions. It is clear that earthquake C did not affect the hydraulic properties of aquifers significantly.

3. Preseismic changes in groundwater level at the Haibara observation well

1) Description of the well

The observation well at 58 m above sea level is 170 m in depth and its strainer is installed from 71 to 154 m in depth. This well was drilled in December, 1978 for the purpose of earthquake prediction research.

Geological formations of the well are loam(0 - 3 m), sandstone (3 - 51 m), clay(51 - 52 m), sandstone(52 - 110 m), sand and gravel(110 - 115 m), sandstone(115 - 130 m), and mudstone(130 - 170 m) from the surface downward.

2) Relationship between the groundwater level and the barometric pressure

As the occurrence of groundwater at this well is confined, the groundwater level is directly related to barometric pressure. The ratio of groundwater level change to the barometric pressure change, in equivalent units, is termed the barometric efficiency. The effect is inverse, that is, as the barometric pressure rises the groundwater level declines(Fig. 7).

Table 3 shows changes of barometric efficiency during a period of one month from June 15 to July 15, 1980. The mean values of barometric efficiency for both increasing and decreasing segments of barometric pressure are about 10.

Figure 8 shows changes of barometric efficiency from June 25 to July 4, when swarm earthquake occurred. The barometric efficiency before earthquake A was 8.6 to 9.5, but that after earthquake A decreased to 3.7. After earthquake A, the barometric efficiencies were unstable.

Since 0:00 hours on June 29, the groundwater level was independent of barometric pressure and the main shock occurred. It was about 16 hours after observing the anomalous barometric efficiency.

The barometric efficiency increased to 15.8 by the effect of the main shock, but it returned to the normal value of 9.4 from July 1.

4. Interpretation by a sponge model

Considering phenomena mentioned above, one model called a sponge model is proposed for the mechanism of fluctuation in groundwater level as follows.

A sponge is filled with water from the bottom to D(Fig. 9-B). As this model is hypothesized to be a closed system, water does not change in quantity.

If compressive stress increases, water level in a sponge will gradually rise. In this process, a correlation between the groundwater level and the barometric pressure will be changed. The anomalous values of the barometric efficiency observed for 16 hours

EXPLANATIONS OF FIGURES AND TABLES

Fig. 1 Location map of the two observation wells and epicenter of the main shock.

Fig. 2 Location of the Atami observation well, and distributions of epicenters and active faults

Solid lines in lower left figure are nodal lines derived from the focal mechanism of the earthquake. Slip vector is shown by a pair of arrows. Area circled by broken line indicates that of epicenters of swarm earthquake.

Fig. 3 Changes in the groundwater level at the Atami observation well, the barometric pressure and hourly precipitation at the Ajiro Weather Station

Fig. 4 Relationship between energy of earthquake and decrease of groundwater level caused by the earthquake

Fig. 5 Seasonal changes in the groundwater level at the Atami observation well, the barometric pressure and precipitation at the Ajiro Weather Station

Fig. 6 Relationship between total precipitation and increased groundwater level by it at the Atami observation well

Numbers in this figure correspond to those in Table 2.

Fig. 7 Fluctuations of the groundwater level and the barometric pressure at the Haibara observation well

Fig. 8 Changes of barometric efficiencies before and after the main shock at the Haibara observation well

Fig. 9 Schematic interpretation of decrease of the groundwater level caused by the earthquake after a sponge model

(B):before, and (A):after earthquake

Table 1 List of earthquakes of magnitude over 4.0 from 21:00 on Jun. 25 to 24:00 on Jun.30, 1980

Table 2 Comparison of recession constants before and after earthquake C at the Atami observation well

Table 3 Barometric efficiencies at the Haibara observation well

Table 4 Comparison of increase of storage coefficient with a thickness of an aquifer in case of the Atami observation well

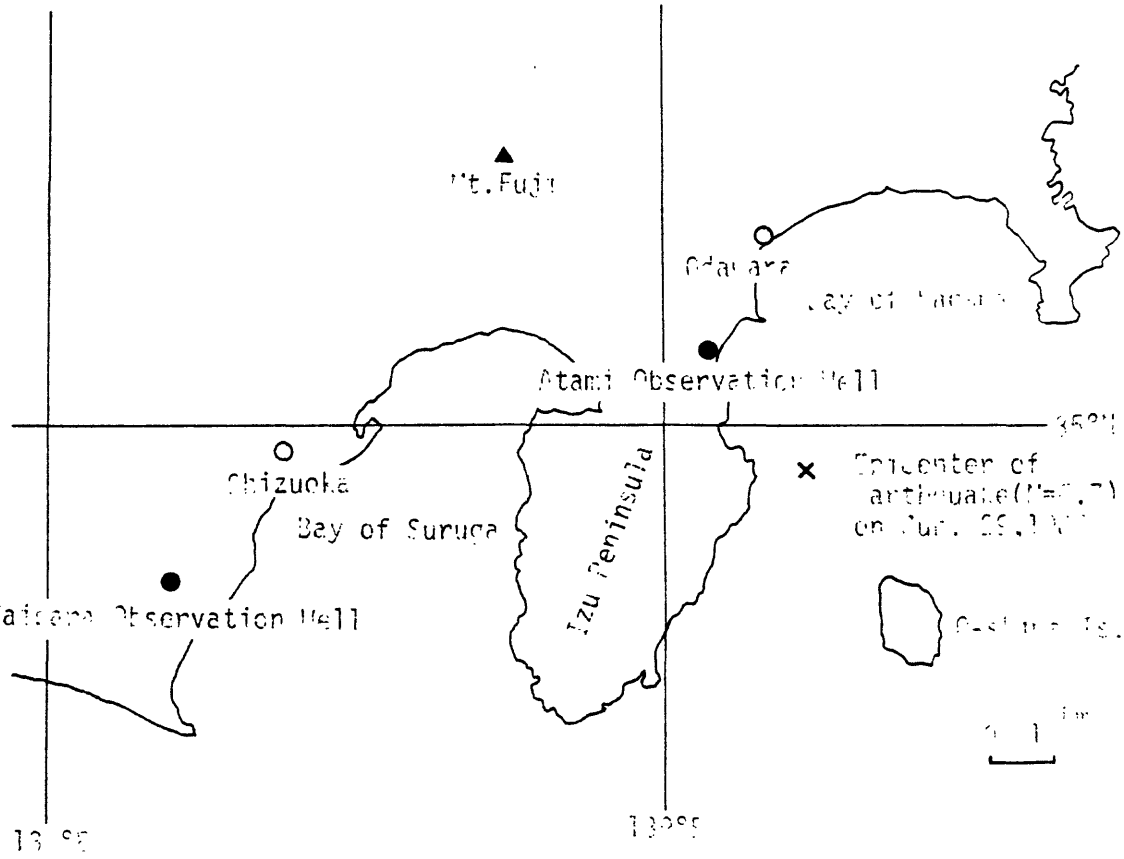
Mt.Fuji
Odawara
Atami Observation Well
Shizuoka
Bay of Suruga
Izu Peninsula
Hamaoka Observation Well

before the main shock at the Haibara observation well were due to this stress change. In case of an unconfined aquifer as the Atami observation well, these phenomena will not be found significantly.

When this sponge is stretched toward both sides(the occurrence of an earthquake), the water level will go down. Water-bearing conditions(hydraulic constants) in a sponge(an aquifer) may slightly be changed by tension. At last, water level becomes stable at somewhat lower than the former level(before the earthquake). In case of the Atami observation well, coseismic decrease of groundwater level was observed in about 80 cm.

Putting water volume into Q and storage coefficient into S in (B) stage(Fig. 9-B),

$$Q = SD$$

On the other hand, putting storage coefficient into S' in (A) stage (Fig. 9-A),

$$Q = S'(D - d)$$

where d is the net difference of groundwater level before and after the earthquake.

Therefore,

$$S' = \frac{D}{D - d} S$$

When D is sufficiently large in comparison with d, $D/(D-d)$ is nearly equal to 1. The net difference of groundwater level(d) before and after the main shock at the Atami observation well was about 0.8 m. Table 4 shows the calculated result of the comparison of increase of

storage coefficient with the thickness of an aquifer at this well. Then,

$$S' \simeq S$$

If a thickness of an aquifer is deep enough, storage coefficient after the earthquake will increase slightly, but the change of it will not give the remarkable difference of groundwater occurrence both before and after the earthquake. The groundwater occurrence after the main shock at the Atami observation well did not change significantly as shown in Table 2 and Fig. 6.

5. Conclusion

Groundwaters on an active fault such as the Atami observation well or in a confined aquifer without artificial disturbances such as the Haibara observation well have important informations as a parameter showing the movement of earth's crust. A practical application of the model proposed by the authors and further detailed observations should be expected to obtain the useful data for earthquake prediction.

Reference

Tagutschi,Y. and Nagai,S.(1982): Anomalous changes in groundwater level at the Atami observation well, Shizuoka Prefecture, caused by the swarm earthquake off the east coast of the Izu Peninsula, Japan, 1980. *Geogr. Rev. Jpn.*, 55(4), 239-257(in Japanese with English summary).

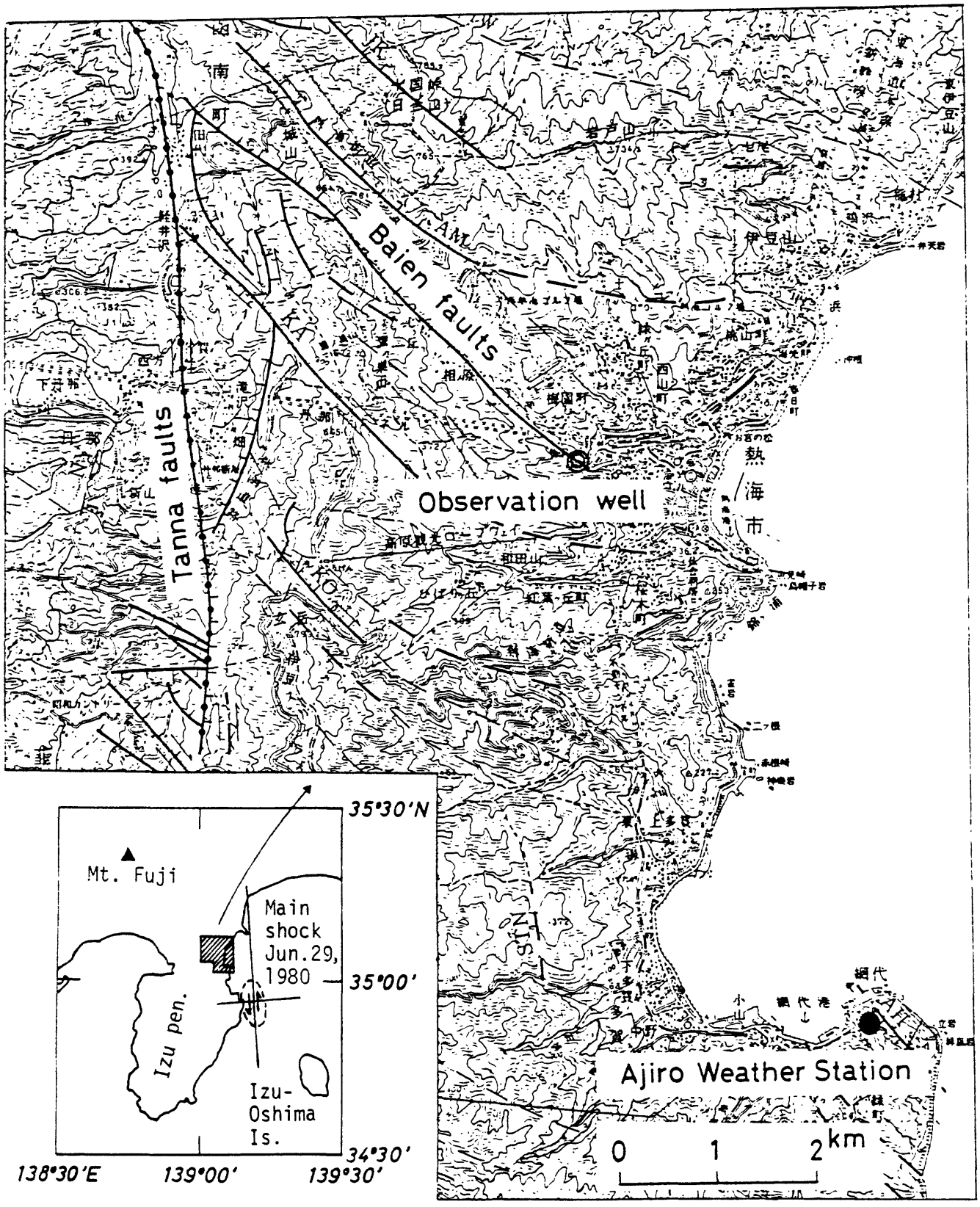
Tanna faults
Baien faults
Observation well
熱海市
Ajiro Weather Station
0 1 2 km
Mt. Fuji
Main shock Jun.29, 1980
Izu pen.
Izu-Oshima Is.
35°30'N
35°00'
34°30'
138°30'E
139°00'
139°30'

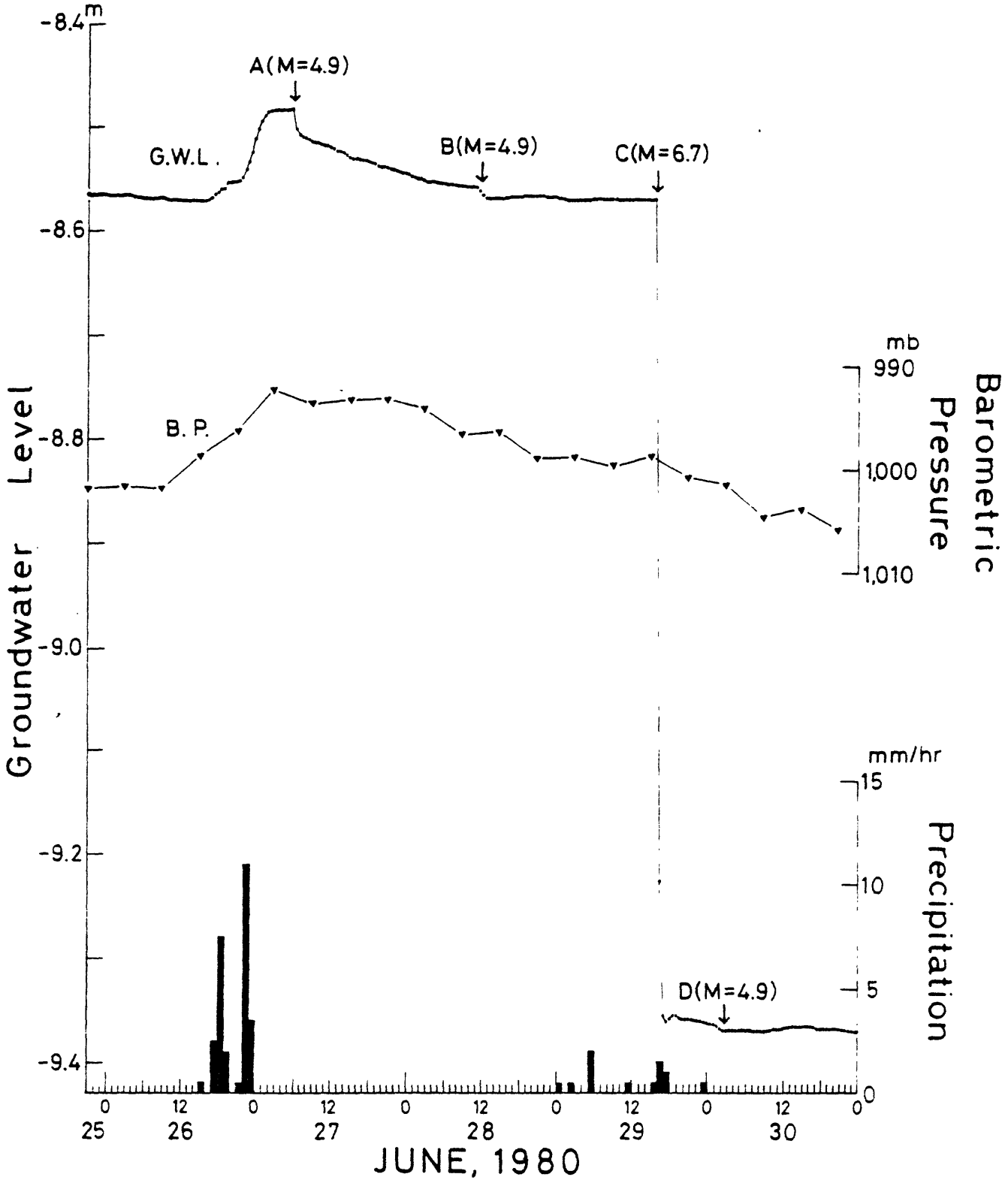
-8.4 m
A(M=4.9)
G.W.L.
B(M=4.9)
C(M=6.7)
-8.6
-8.8
B. P.
-9.0
-9.2
-9.4
Groundwater Level
mb
990
1,000
1,010
Barometric Pressure
mm/hr
15
10
5
0
Precipitation
D(M=4.9)
0 12 0 12 0 12 0 12 0 12 0
25 26 27 28 29 30
JUNE, 1980

Net Difference of Groundwater Level
between before and after Earthquake
mm
10^3
10^2
10
1
10^{11}
10^{12}
10^{13}
10^{14}
10^{15}
Energy of Earthquake in Joule
M = 4.1
M = 4.4
M = 4.9
M = 6.7
Eq.A
Eq.B
Eq.C
Eq.D

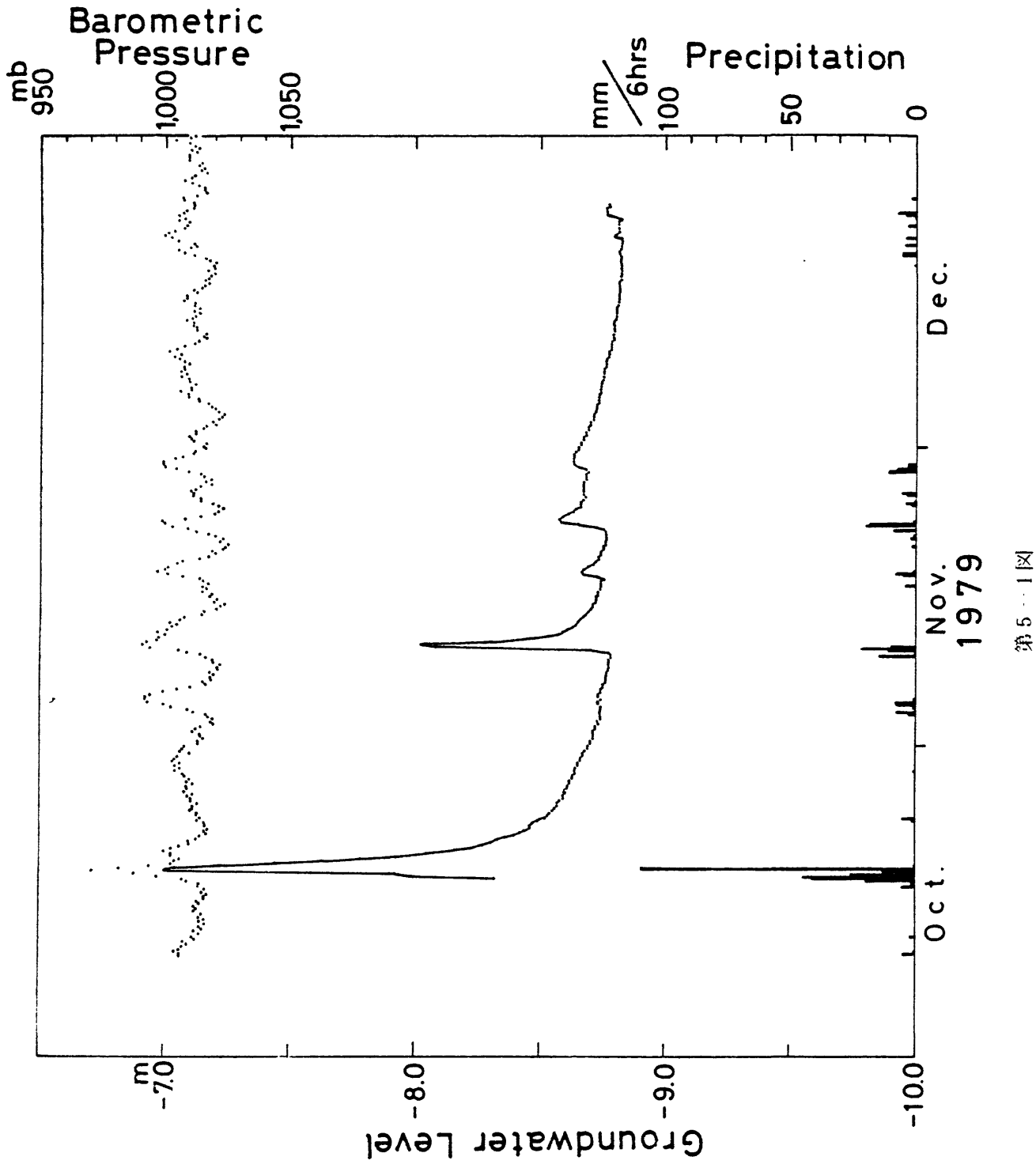
Barometric Pressure
mb
950
1,000
1,050
Precipitation
mm / 6hrs
100
50
0
Groundwater Level
m
-7.0
-8.0
-9.0
-10.0
Oct.
Nov.
1979
Dec.

第5-1図

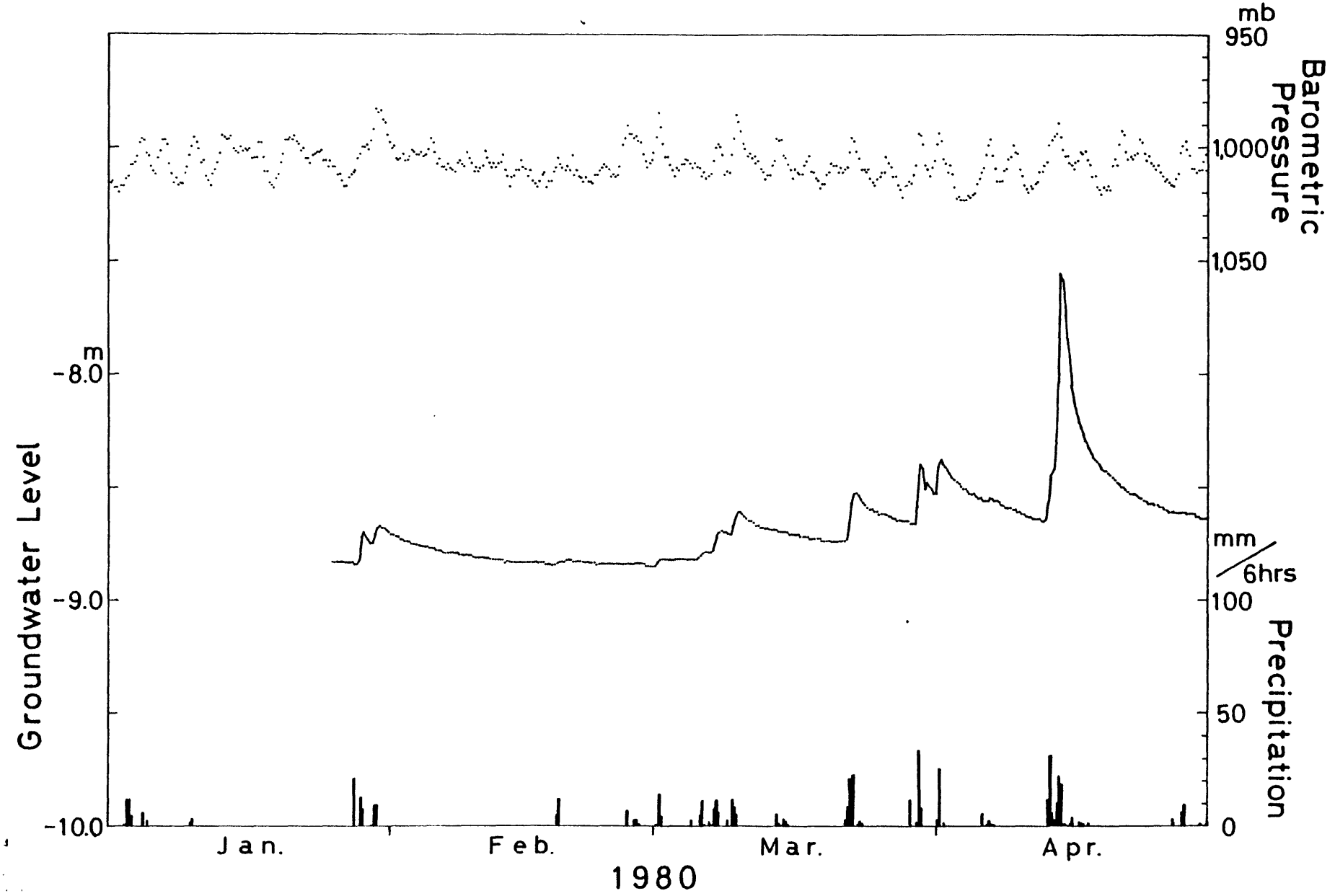
mb
950
1,000
1,050
Barometric Pressure
m
-8.0
-9.0
-10.0
Groundwater Level
mm
6hrs
100
50
0
Precipitation
Jan.
Feb.
Mar.
Apr.
1980

第5-2図

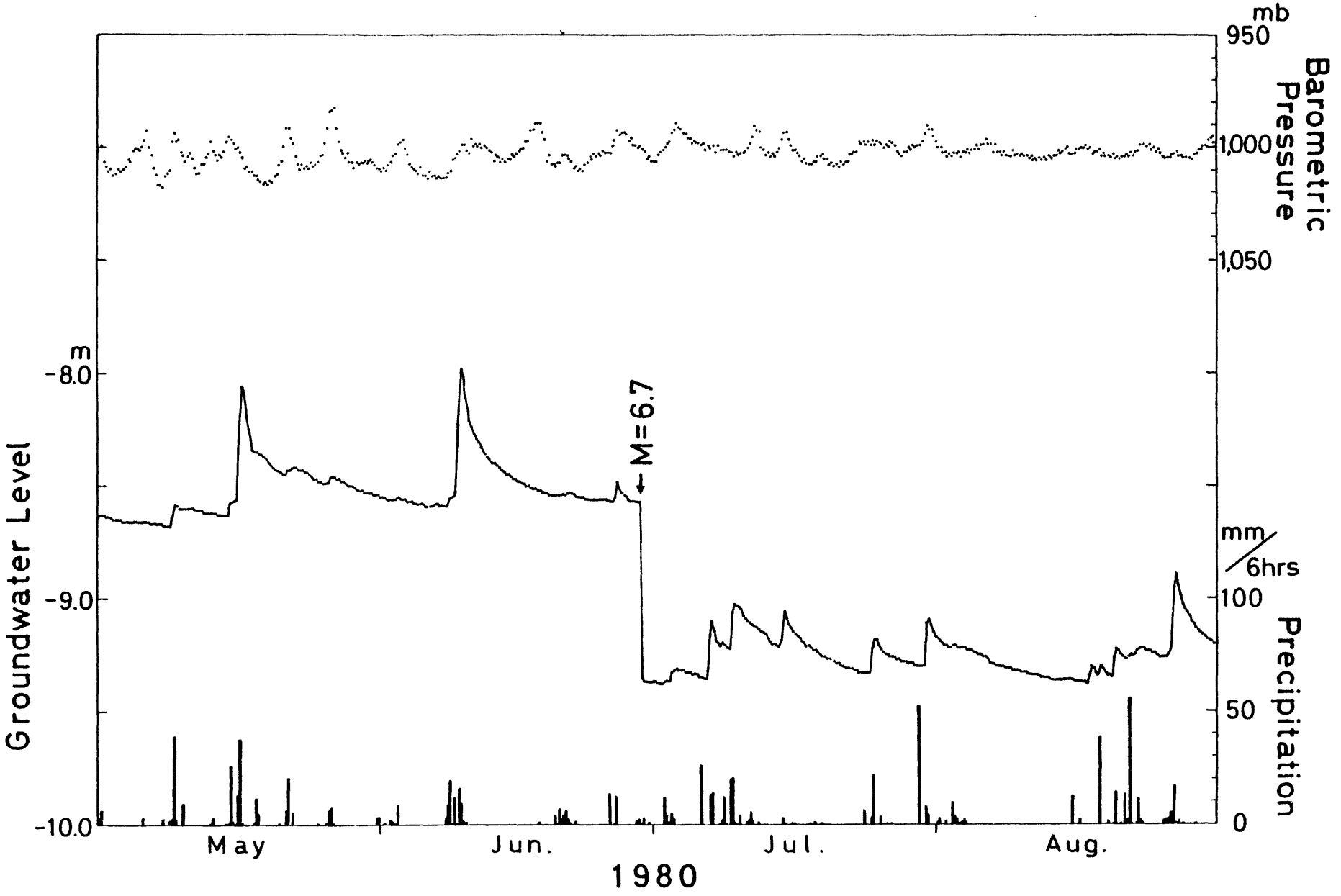
mb
950
1,000
1,050
Barometric Pressure
m
-8.0
-9.0
-10.0
Groundwater Level
M=6.7
mm/6hrs
100
50
0
Precipitation
May
Jun.
Jul.
Aug.
1980

第5　3図

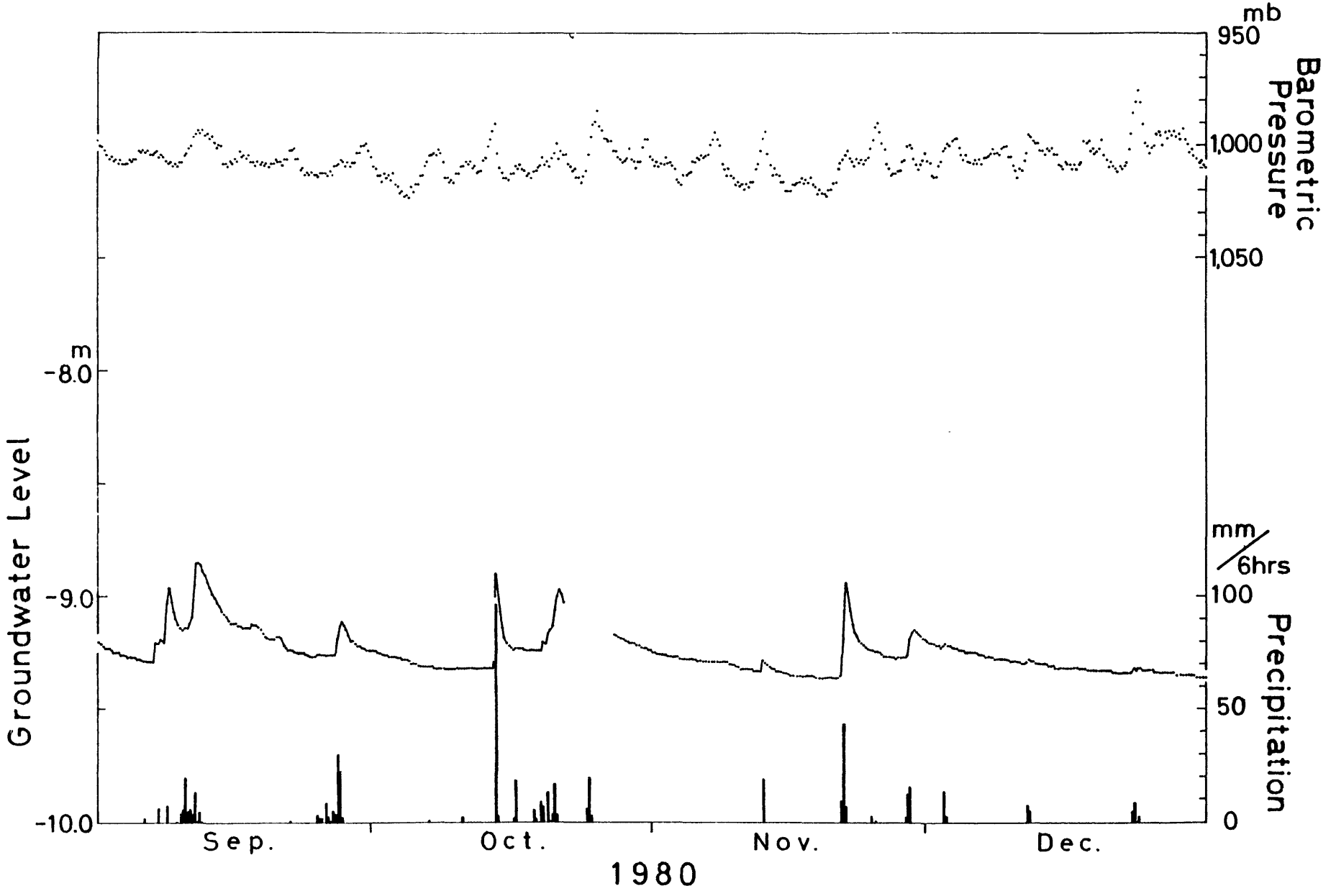
mb
950
1,000
1,050
Barometric Pressure
m
-8.0
-9.0
-10.0
Groundwater Level
mm/6hrs
100
50
0
Precipitation
Sep.
Oct.
Nov.
Dec.
1980

第5　4図

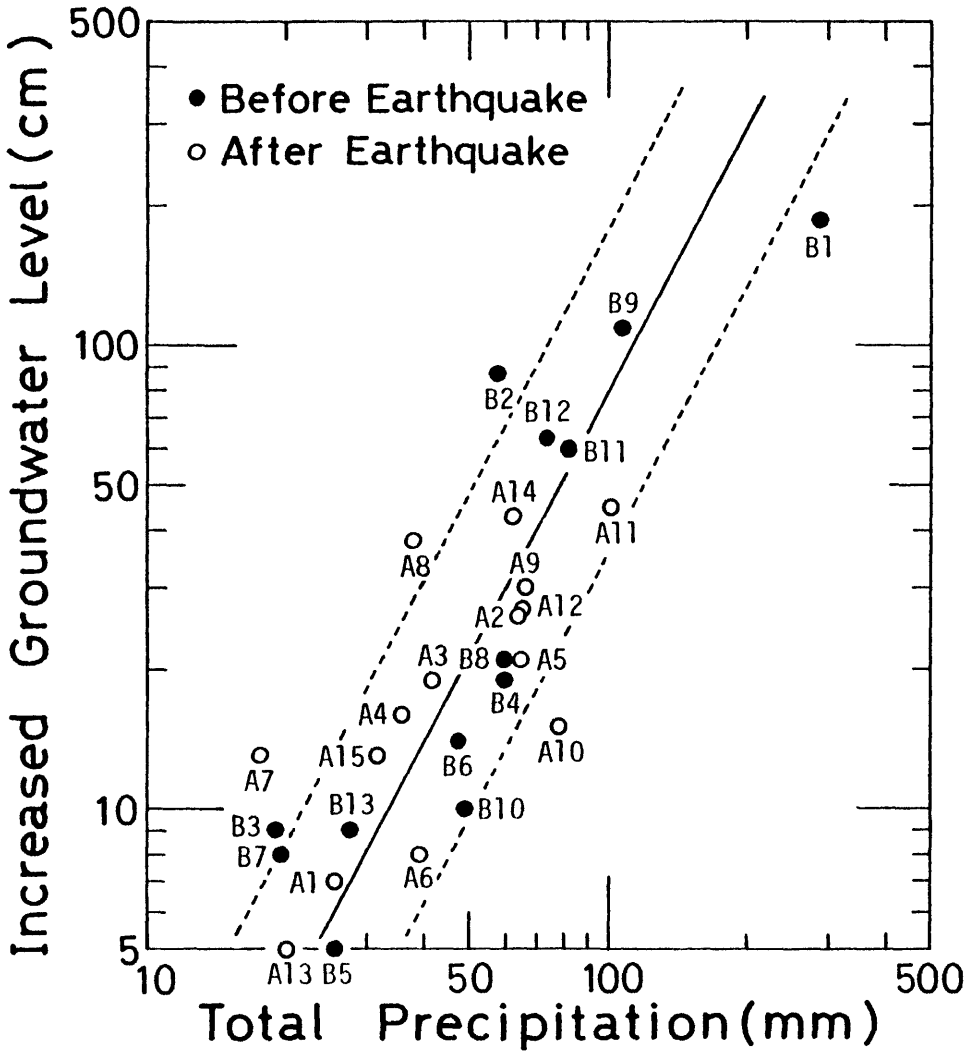
500
100
50
10
5
10
50
100
500
Increased Groundwater Level (cm)
Total Precipitation (mm)
● Before Earthquake
○ After Earthquake
B1
B9
B2
B12
B11
A14
A11
A8
A9
A2
A12
A3
B8
A5
B4
A4
A10
A15
B6
A7
B13
B10
B3
B7
A1
A6
A13
B5

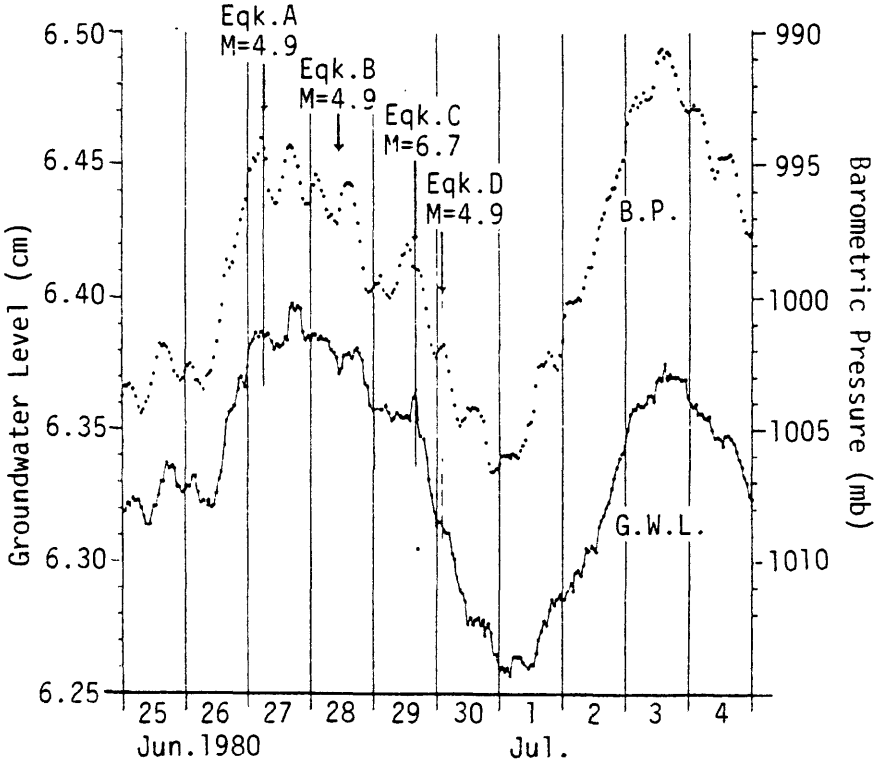
Eqk.A
M=4.9
Eqk.B
M=4.9
Eqk.C
M=6.7
Eqk.D
M=4.9
B.P.
G.W.L.
Groundwater Level (cm)
Barometric Pressure (mb)
6.50
6.45
6.40
6.35
6.30
6.25
990
995
1000
1005
1010
25
26
27
28
29
30
1
2
3
4
Jun.1980
Jul.

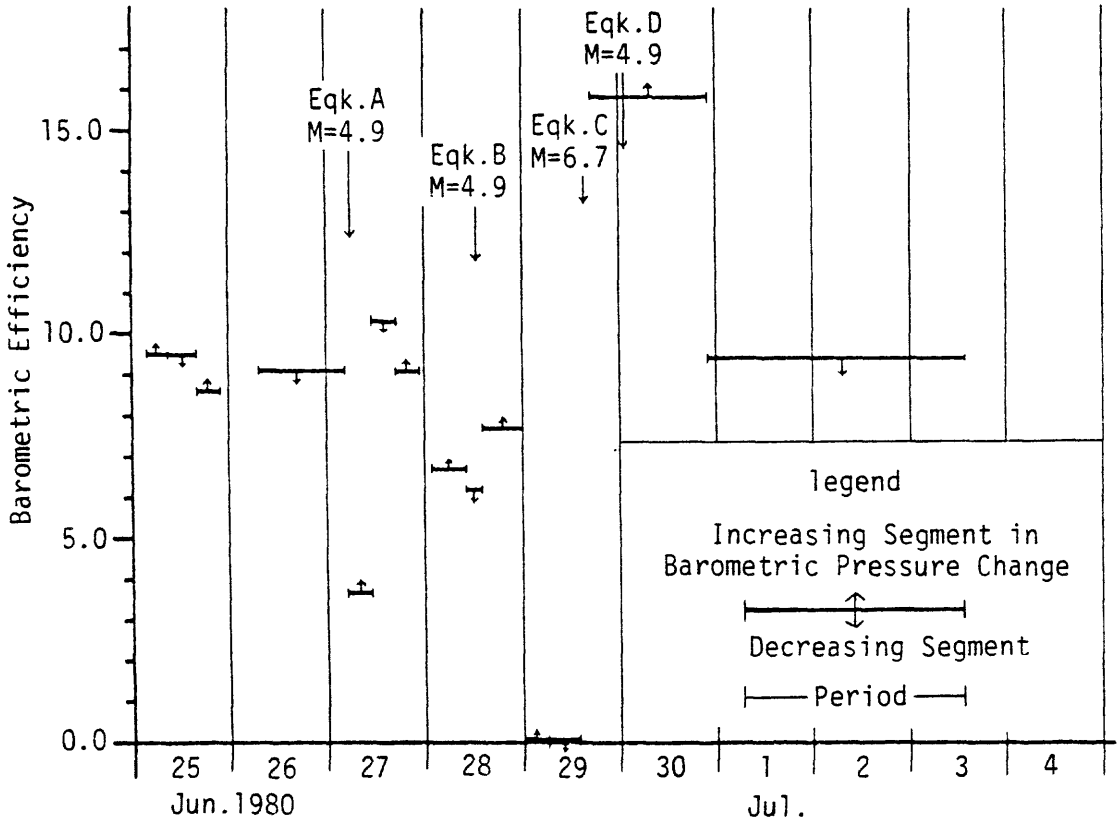
Eqk.D
M=4.9
Eqk.A
M=4.9
Eqk.B
M=4.9
Eqk.C
M=6.7
15.0
10.0
5.0
0.0
Barometric Efficiency
legend
Increasing Segment in
Barometric Pressure Change
Decreasing Segment
Period
25
26
27
28
29
30
1
2
3
4
Jun.1980
Jul.

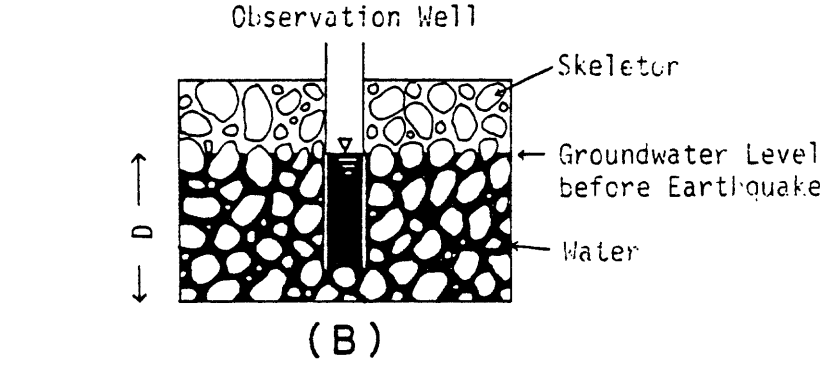
Observation Well
Skeleton
Groundwater Level
before Earthquake
Water
D
(B)

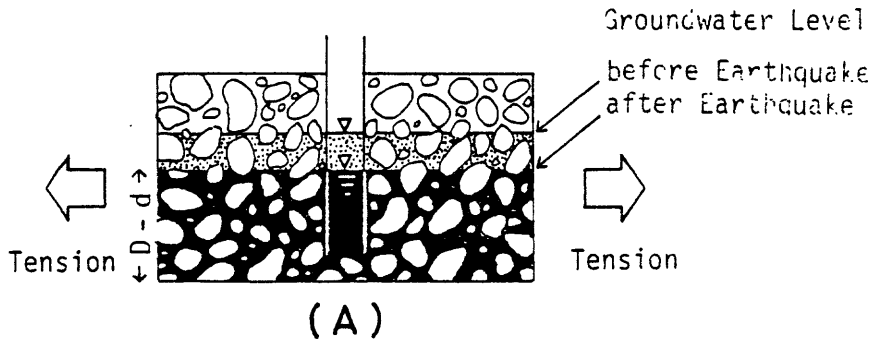
Groundwater Level
before Earthquake
after Earthquake
Tension
D - d
Tension
(A)

Date	Time	Longitude	Latitude	Depth of focus	M	Note
27	0555	139°13'E	34°56'N	0 km	4.6	
27	0606	139°13'E	34°56'N	0	4.9	Earthquake A
28	1150	139°12'E	34°57'N	0	4.4	
28	1205	139°12'E	34°56'N	0	4.9	Earthquake B
29	0147	139°12'E	34°55'N	0	4.1	
29	1620	139°14'E	34°55'N	10	6.7	Earthquake C
29	1636	139°11'E	34°56'N	0	4.1	
30	0223	139°14'E	34°51'N	10	4.9	Earthquake D
30	0243	139°17'E	34°53'N	10	4.6	

Data source: Japan Meteorological Agency

No.	Date	Increased Groundwater Level(cm)	Period of Precipitation	Total Precipitation (mm)	Recession Constant
B 1	Oct.19-26,'79	178	Oct.17-19,'79	290.5	0.98
B 2	Nov.11-17	87	Nov.10-11	57.5	0.94
B 3	Nov.18-20	9	Nov.17-18	19.0	0.96
B 4	Nov.23-25	19	Nov.21-23	59.5	0.98
B 5	Nov.29-30	5	Nov.28-29	25.5	0.98
B 6	Jan.29-30,'80	14	Jan.28-29,'80	47.5	0.98
B 7	Jan.31-Feb.2	8	Jan.30	19.5	0.98
B 8	Mar.23-25	21	Mar.22-23	59.5	0.99
B 9	Apr.14-18	109	Apr.13-15	107.0	0.98
B10	May 9-11	10	May 8- 9	49.0	0.98
B11	May 16-20	60	May 15-16	81.5	0.97
B12	Jun. 9-13	63	Jun. 8-10	73.0	0.98
B13	Jun.27-28	9	Jun.26	27.5	0.94
Mean Value of Recession Constant before Earthquake C					0.97
A 1	Jul. 3- 6	7	Jul. 2- 3	25.5	0.98
A 2	Jul. 7- 8	26	Jul. 6- 7	63.5	0.98
A 3	Jul.10-13	19	Jul. 9	41.5	0.98
A 4	Jul.25-26	16	Jul.24-25	35.5	0.98
A 5	Jul.31-Aug.1	21	Jul.30-31	64.5	0.98
A 6	Aug.19-20	8	Aug.19	39.0	0.97
A 7	Aug.21-22	13	Aug.20-21	17.5	0.98
A 8	Aug.27-28	38	Aug.26-27	37.5	0.98
A 9	Sep.12-14	30	Sep.10-12	66.0	0.99
A10	Sep.27-29	15	Sep.25-27	78.5	0.96
A11	Oct.14-16	45	Oct.14-15	101.0	0.94
A12	Oct.21-22	27	Oct.19-21	65.0	0.98
A13	Nov.13-14	5	Nov.13	20.0	0.91
A14	Nov.22-23	43	Nov.21-22	62.0	0.97
A15	Nov.29-30	13	Nov.28-29	31.5	0.98
Mean Value of Recession Constant after Earthquake C					0.97

In case of the barometric pressure decrease

Observation period	Net difference of groundwater level (mm)	Net difference of barometric pressure (mmHg)	Barometric efficiency
00:00 on Jun.15 - 00:00 on Jun.18	70	7.5	9.3
10:00 on Jun.20 - 05:00 on Jun.21	35	3.5	10.0
07:00 on Jun.26 - 00:00 on Jun.27	54	5.6	9.6
11:00 on Jul. 1 - 14:00 on Jul. 3	110	10.6	10.4
12:00 on Jul.10 - 05:00 on Jul.12	87	8.6	10.1
12:00 on Jul.14 - 17:00 on Jul.15	71	6.7	10.6
		Average	10.0

In case of the barometric pressure increase

16:00 on Jun.18 - 17:00 on Jun.19	94	10.7	8.8
15:00 on Jun.21 - 08:00 on Jun.23	70	6.6	10.6
18:00 on Jul. 3 - 00:00 on Jul. 8	96	9.1	10.5
15:00 on Jul.12 - 07:00 on Jul.14	90	9.3	9.7
		Average	9.9

In case of the barometric pressure increase after the main shock

17:00 on Jun.29 - 22:00 on Jun.30	95	5.7	16.7

D (m)	$\frac{D}{D-0.8}$
10	1.09
20	1.04
30	1.03
40	1.02
50	1.02
60	1.01
70	1.01
80	1.01

AE under Cyclic Loading

Kinichiro Kusunose, Osamu Nishizawa and Koji Ono

Geological Survey of Japan

Abstract

For application of the Kaiser effect to the tectonic stress measurement, the stress memorial mechanism of rocks must be clarified. We have attempted the cyclic loading tests and located hypocenters of AE emitted during the test. Though the AE activity changes remarkably, no difference can be found at the distribution of hypocenters and the crack type of AE between the first loading cycle and the following cycles.

Introduction

Tectonic stress measurement is an effective technique for the estimation of the risk of the earthquake. The hydrofracturing method and the overcoring method have already been established and seem to be useful for this purpose. However, only limited numbers of measurements have been performed by use of these methods, partly due to their high costs. Thus less expensive method such as the Kaiser effect method is favorable. Kaiser effect is a stress memorial effect usually observed during cyclic loading tests of rock specimens. In a rock specimen under loading process, the AE activity increases drastically beyond the maximum stress of

previous cycle (virgin load). The Kaiser effect is considered to be applicable to tectonic stress measurement whenever a core sample can be collected.

Kanagawa et al. (1976) showed that stress values at the Seikan tunnel, Japan, obtained from the Kaiser effect method agree with those from the overcoring method. The preliminary study for the stability of the Kaiser effect against temperature and water contents was performed by Yoshikawa and Mogi (1980). Despite recent advance in this field, the stress memorial mechanism has not been well understood. We are studying the mechanism of the Kaiser effect from the AE source process during cyclic loading tests of rock specimens. Some of our preliminary results agree with those reported by Sondergeld and Estey (1981).

Results

Fig.1 shows the relation of AE activity to the axial stress during a cyclic loading test. AE activity increases drastically beyond the maximum loading of the previous cycle, namely, the virgin load. The Kaiser effect is remarkable when the virgin load is low, but it becomes obscure as the virgin load increases. These difference may be caused by the difference of the AE source process.

Variation in the distribution of AE hypocenters from incipient loading to just before the final fracturing is shown schematically in Fig.2 (Nishizawa et al. 1981). At low stress, the AE occur randomly in the specimen. As the axial stress increases, their

hypocenters gradually cluster and migrate around an eventual fracture plane. Kusunose et al. (1982) reported that AE tends to occur in succession, such as the main shock-after shock sequence, under the high axial stress due to the local stress concentration. As the stress becomes higher, local fractures corresponding to the clusters of AE hypocenters develop and the distribution of the local stress responsible for these fracture changes within the rock specimen. The local stress concentration remains when the sample is unloaded. This may be the main mechanism of the Kaiser effect being inconspicuous in the progressive loading cycle (Kusunose et al. 1980). We investigate the focal mechanism of the AE for more than 1000 AE from the distribution of the first motion direction (Fig.3). The shear type cracking is the dominant mechanism of the AE throughout the low stress region and the high stress region (Kusunose et al. 1981a, 1982) It is also observed during the creep experiment (Nishizawa et al. 1982b, Yanagidani et al. 1982).

When the virgin load is low, any difference can not be found between the AE under the first loading cycle and those under the progressive cycles from the statistical investigation of the AE hypocenter distributions and their focal mechanism (Kusunose et al. 1981). Though the AE activity decreases remarkably under the progressive cycle, the unelastic volumetric strain is almost the same as compared to that under the first cycle. This means that the tensile cracks open without sliding of the shear cracks or with smooth sliding of them in the progressive loading.

Kusunose et al. (1980) showed that the stress drop of the AE increases exponentially with waveform gradually dominated by high frequency component as the axial stress increases in the higher stress region (Fig.4). On the other hand, from the investigation of the distribution of the first motion directions, the change in the stress drop dose not result from the change in the crack type; in both stages, the source of the AE is the shear type cracking irrespective of the axial stress. The high stress drop may be caused by the local stress concentration around the eventual fracture plane produced by the trapping of the micro-cracks by some asperities.

Reference

Kanagawa,C.,M.Hayashi and H.Nakasa, Estimation of Spatial Geo-Stress Components in Rock Samples Using the Kaiser Effect of Acoustic Emission, 3rd AE Symp. Tokyo, 229-248, 1976.

Kusunose,K., K.Yamamoto and T.Hirasawa, Source Process of Microfracture in Granite with Reference to Earthquake Prediction, Sci.Rep. Tohoku Univ., Ser. 5, 26, 111-121, 1980.

Kusunose,K., O.Nishizawa, H.Ito, T.Ishido and I.Hasegawa, Source Mechanism of Acoustic Emission in Rocks under Uniaxial Compression, Zishin Ser. 2, 34, 241-250, 1981a. (in Japanese).

Kusunose,K., O.Nishizawa and T.Miyajima, AE Hypocenter Distribution of Granite during the Cyclic Loading Test, Abstracts of the Seism. Soc. Japan. 1981, 2, 152, 1981b. (in Japanese).

Kusunose,K., O.Nishizawa and K.Onai, AE Gap in a Rock under Uniaxial Compression, Zishin Ser. 2, 35, 91-102, 1982. (in Japanese).

Nishizawa,O., K.Kusunose and K.Onai, A Study of Space-Time Distribution of AE Hypocenters in a Rock Sample under Uniaxial Compression, Bull.Geol.Surv.Japan, 32, 473-486, 1981. (in Japanese).

Nishizawa,O., K.Kusunose, T.Yanagidani, F.Oguchi and S.Ehara, Stochastic Process of the Occurrence of AE Events and Hypocenter Distributions during Creep in Ohshima Granite, Zishin Ser.2, 35, 117-132, 1982a. (in Japanese).

Nishizawa,O., K.Kusunose and K.Onai, Hypocenter Distribution and Focal Mechanism of AE Events during Creep in Yugawara Andesite, 1982b, (in preparation).

Sondergeld,C.H., and L.H.Estey, Acoustic Emission Study of Microfracturing during the Cyclic Loading of Westerly Granite, J.Geophys.

Res., 86, 2915-2924, 1981.

Yoshikawa,S. and K.Mogi, A New Method for Estimation of the Crustal Stress from Cored Rock Samples:Laboratory Study in the Case of Uniaxial Compression, Tectonophysics, 74, 323-339, 1981.

Fig.1 AE activity during the cyclic loading test. The AE rate is constant in the first loading cycle and it decreses remarkably in following loading cycle (the Kaiser effect).

Fig.2 Schematic view of spatial distribution of AE hypocenters during the first loading cycle. As the axial stress increases, AE events occur randomly in the specimen under low axial stress and concentrate around an eventual fracture plane as stress increses.

Fig.3 An example of a focal mechanism solution of AE. Open circles indicate dilatation of P-wave initial motion direction of AE and closed ones indicate compression. The solution is projected on a equal area net of upper hemisphere.

Fig.4 Variations of stress drop T and m-values in amplitude-frequency relation with respect to axial stress σ_z.
T_1; stress drop for the lowest axial stress in the figure.
σ_f; fracture strength.
The dash-dot line shows the case in which the stress drop increases in proportion to the axial stress.

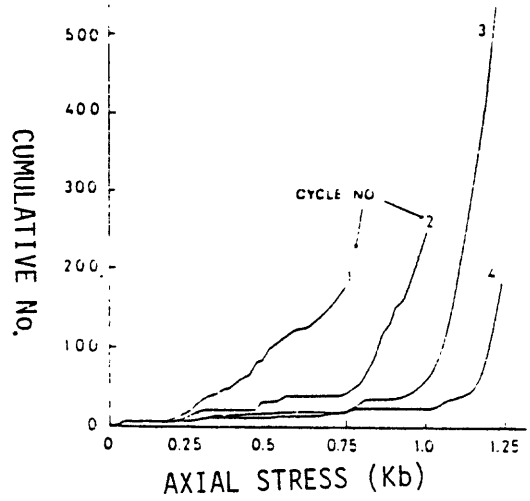
CUMULATIVE No.
500
400
300
200
100
0
0
0.25
0.5
0.75
1.0
1.25
AXIAL STRESS (Kb)
CYCLE NO
1
2
3
4

Fig. 1

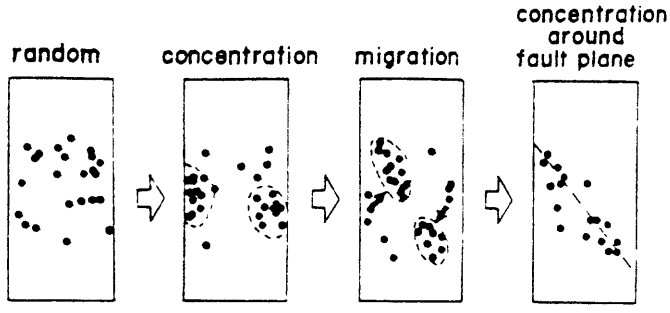
random
concentration
migration
concentration around fault plane

Fig 2

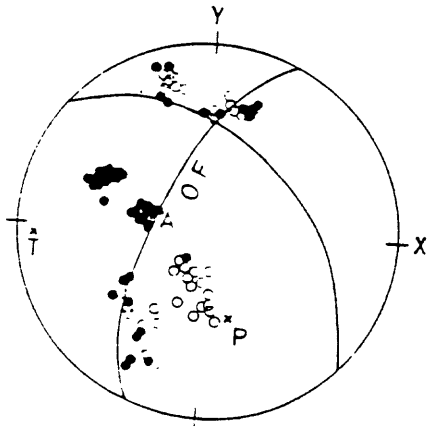

Fig. 3

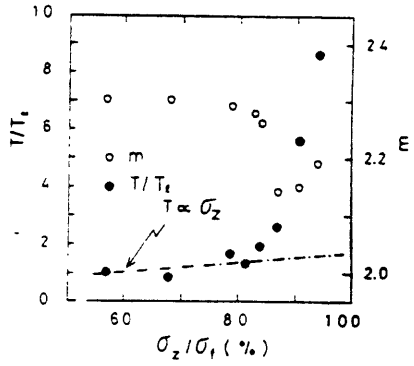

Fig. 4

Excavation Survey of Active Faults

Haruo Yamazaki, Eikichi Tsukuda and Yoshihiro Kinugasa

Geological Survey of Japan

Summary

The outline and brief history of trench excavation survey for active faults in Japan are described. Since the late 1970's, the study of active faults in Japan has progressed to a stage where it is possible to reveal the detailed movement history of each fault. Trench survey plays an important role in the study of the Holocene fault movement. Although the physical conditions in Japan provide large advantage for the excavation, the social conditions make it difficult to find suitable sites for the survey.

Owing to the excellent results of the trench survey carried out in the late 1970's, the excavation survey has been adopted as an item of the 4th Program of Japanese Earthquake Prediction Project in 1979. Since then, Geological Survey of Japan, Earthquake Research Institute and Kyoto University have been carring out the trench survey every year. In this project, Geological Survey of Japan has excavated the Tanna fault system in 1980 and the Atera fault in 1981. Both excavations revealed the recurrence interval of a few thousand years. Particularly, in the Atera fault it is inferred that the fault movements have occurred every 2000-3000 years accompanied with great earthquakes during the last 12000 years.

1. Recent trends of the study of active faults in Japan

The study of active faults in Japan has made remarkable progress in the 1970's and the results of the studies in this decade were summarized and published in 1980 as "Active Faults in Japan -- Sheet Maps and Inventories" by the Research Group for Active Faults of Japan (RGAFJ), more than 40 geologists and geomorphologists took part in the group. Although of preliminary nature, general features of the active faults in Japan have been clarified by this compilation.

Since then, the following two types of the study have become major trends in Japan. One is the continuous observation on and around the active faults by geophysical and geochemical methods such as gravity measurement, precise geodetic survey, groundwater level monitoring, monitoring of chemical composition of groundwater and radon gas emanation. The main purpose of these observations is to obtain the distribution of these quantities in time and space. The other type of study is to clarify the history of the fault movement in the recent geologic period by geological and geomorphological methods. The aims of this study are to obtain data on the recurrence interval of each fault and the time of the last earthquake. Various investigations such as field survey, boring and trench excavation are carried out in this type of study. Among these

investigations, trench excavation survey has attracted much attention of many researchers.

In general, we may only accidentally meet the chance to observe the details of active faults at some natural outcrops and outcrops cut for other purpose than geological survey. In such case, researchers described and discussed the history of the fault movement (Okada and Matsuda; 1976, Hirano and Nakata; 1981). The trench survey intends to reveal the history of the fault movement through the detailed observation of faulted strata at man-made outcrops.

2. Some problems of the trench excavation survey in Japan

Because of thick vegitation, high rate of erosional and depositional process due to the climatic condition in Japan, tectonic features accompanied with faults of low activity are easily worn away in the regions where erosional processes prevail. On the other hand, when the fault movement occur in the depositional region, the deformed strata and tectonic landforms are rapidly covered by the overlying deposits and are preserved. As these deposits contain peat, wood remains and other carbonaceous material, we can obtain the radiocarbon dating data. Also several wide spreading air fall ash layers and the archaeological remains burried in these deposits help the chronological study for the fault movement. As mentioned above, the natural conditions in Japan are advantageous for the studies of the fault movement from the deformed strata compared with arid regions where it is difficult to find a radiocarbon dating sample.

So it can be said from the physical view point that Japan is one of the most suitable regions in the world to conduct the excavation survey of active faults. The following is a list of conditions favourable for excavating sites.

(1). Alluvium with accumulation of peat and wood remains.

(2). Detailed knowledge of the fault trace. It is difficult to know the precise fault trace in regions of thick alluvial deposits where the faults appear as monoclinal flexure of surficial strata or as a group of scattered minor faults.

(3). Sufficient open space to conduct the trench opening work.

In Japan, it is not very easy to find places which satisfy the above three conditions, because such places are usually already developed for other purposes.

Another problem is artificial modification of the land for various purposes. These modifications disturb the valuable data of recent history of faulting. For example, at the trench site of the Atera fault where the Geological Survey of Japan (GSJ) excavated in 1981, we could not appraise the time of the last event due to the artificial modification of the shallow part of the strata.

In short, although the physical condition in Japan is very advantageous for the trench excavation, it is not so easy to find the suitable site for the survey by social limitations.

3. A brief history of excavation survey in Japan.

The excavation survey of active faults in Japan began in the

late 1970's stimulated by the several excellent results in the United States such as the works of Clark et al. (1972) and Sieh (1978).

The first trench excavation survey in Japan was done at the Tachikawa fault by Geographical Survey Institute (GSI) in 1977. The Tachikawa fault has dislocated the Musashino upland in the western suburbs of Tokyo with 20 km in length and 0.3 m/1000 y. vertical slip rate (Yamazaki, 1978). Although the slip rate of this fault is small, we have been concerned with it from the view point of disaster prevention, because the fault is located in the metropolitan area of Japan. However, the history of fault movement was not obtained from the trench as the site did not satisfy the above conditions.

In 1978, Okada of Aichi Prefectural University, Ando and Tsukuda of Kyoto University excavated the Shikano fault in Tottori Prefecture which is associated with the Tottori earthquake (M. 7.4) in 1943 (Okada et al., 1981). Three trenches were excavated at two places along the Shikano fault. The precise trace of the fault was confirmed by the displaced paths and stone walls. The faulted strata were clearly recognized on the side walls of the trench. As a result of this survey, it was ascertained that the last fault movement before the 1943 event had occurred in the period between 1940 y.B.P. and 2580 y.B.P.

After that, they excavated the Yamasaki fault in Hyogo Prefecture which has no historical record of great earthquake (Okada et al., 1980). The Yamasaki fault with 80 km in length shows many evident tectonic landforms such as left lateral offset of streams and ridges,

wind gaps and fault scarps. Since the late 1960's this fault has been a center of attention as a conspicuous active fault in Southwest Japan. In this survey, long trench of 25m in length was excavated because of the uncertainty of the fault trace. On the trench walls, it was recognized that the faulted strata with many peat layers and overlying unfaulted strata. It was inferred from the radiocarbon dating and archaeological remains that the event occurred in the period between the 8th and 12th century. As it is known from the historical data that a great earthquake occurred at 868 in this region, above findings indicate that the Yamasaki fault caused the earthquake in 868.

The data obtained from the trench excavation survey conducted in the late 1970's were appraised to be useful for earthquake prediction. Excavation survey of active faults was included in the 4th Program of Japanese Earthquake Prediction Project which started in 1979. Based on this project, GSJ initiated a comprehensive survey of active faults in which the excavation survey occupied the main part of the study. GSJ excavated two trenches along the major active faults in 1980 and 1981, and is now arranging for another trench which will be conducted in this winter. The results of the two trenches carried out will be described later in detail.

On the other hand, Ando and Tsukuda of Kyoto University and some member of RGAFJ have started the excavation survey project in 1980. This study is going on under the leadership of the Earthquake Research Institute (ERI) and Kyoto University, and they have excavated several active faults in 1980 and 1981. Figure 1 shows the location

of trenches in Japan made by various institutes.

4. Excavation survey by GSJ

4-1. Excavation survey of the Tanna fault system in 1980

GSJ has excavated the Ukihashi central fault in 1980 (Yamazaki et al., 1981). This fault is one of the southern portion of the Tanna fault system which caused the Kita-Izu earthquake of 1930 (M. 7.0). This fault system traverses the northern half of the Izu Peninsula in N-S direction and shows left lateral movement with high long-term slip rate of 2m/1000y. The purpose of this excavation is to disclose the movement history of that system.

The excavation site is located at the western margin of a small basin called Ukihashi. This basin is a large scale fault depression dammed up by the upheaval of western side of the fault. Figure 2 shows the locality of the site and the outline of the Tanna fault system.

The trench was excavated in 'T' shape to observe the three dimensional pattern of the fault trace. Length and depth of the trench are 20m and 3m respectively. String was used to set a one meter grid on the trench wall. Stratigraphic details were observed grid by grid. Figure 3 shows a summarized sketch of the wall.

As shown in Figure 3, the sheared zone of 20cm in width and overlying faulted gravel and sand layers with charcoal-rich zone were observed on the trench wall. The west dipping main break in the lower part of the trench splits into two minor faults in the upper

part. Though the western minor break offsets the fine sand, charcoal-rich zone which is dated as 4670 y.B.P. and pebble layer, the displacement of this fault does not continue to the overlying layers in which a layer of air fall pumice is contained. This pumice is correlated to Kawagodaira pumice (KgP) erupted from the Amagi volcano in 2900 y.B.P. From this fact, it is estimated that the west minor break has moved in the period between 4670 y.B.P. and 2900 y.B.P.

On the other hand, the eastern minor surface break displaced the KgP with west side drop. It is known that the eastern break indicates the movement of the earthquake of 1930. From these data, the recurrence interval of the Ukihashi central fault is inferred to be 3000-4000 years.

Another trench data in Tanna basin by ERI shows the 1000 years recurrence interval of the Tanna main fault since 7000 y.B.P.(Matsuda et al., 1982). The difference of the recurrence intervals obtained at two trench sites can be explained by the different nature of the faults, that is, one is the main trace and another is one of the branching fault. An additional trench will be opened in 1982-1983 by GSJ.

4-2. Excavation of the Atera fault in 1981

The Atera fault, which dissects central Japan with NW-SE strike and 80km length, is one of the most active faults in Japan. The fault shows left lateral slip with northeastern upheaval component (Sugimura and Matsuda, 1965). The long-term slip rate is estimated

to be 3-5m/1000y. by Okada (1975). In spite of this extraordinary high slip rate, there are no records of historical great earthquakes from this fault.

As the Atera fault passes through mountainous region, large efforts were expended for finding a favourable site for trenching. At Tsukechi Machi, Gifu Prefecture, we found a small but suitable flat place, where a fault scarplet is covered by talus deposits derived from a small valley overlying the river terrace deposits. At this place, GSJ excavated the trench in the fall of 1981 (Tsukuda and Yamazaki, 1982).

The trench was 8m at the deepest and over 25m long. The strata and faulted zone which were exposed on the trench wall were sketched in detail using one meter string grids. Detailed sketches of the trench walls are shown in Figure 4. The principal fault with fault gouge 10cm wide is exposed at the northeast end of the trench. As shown in Figure 4, completely different geologic units are exposed on both sides of the fault. Sediments on the northeast side of the fault consist of boulder layer of river terrace overlying the basement rhyolite. On the other hand, layered coarse sand and sandy humic soil are exposed on the southwest side of the fault. In spite of clearly identifiable fault trace and well bedded strata on one side of the fault, the lack of corresponding sediments on the other side makes it difficult to estimate the age of fault movement. We estimated the age in following way. Assuming that the minor faults are formed near the ground surface associated with the movement of

the main fault and these minor faults never repeat the fault slip, the age of the main fault movement can be estimated from the age of talus layers which directly cover each minor fault.

Figure 5 shows the radiocarbon dating of the layered talus deposits and the age of the slip of each minor fault with solid circles. The obvious concentration of the solid circles to several ages suggests that the movement of the main fault occurred at those ages. From Figure 5, we can distinguish at least 4 events of fault movement, ages of these events can be estimated to be about 12000 y.B.P., 10000 y.B.P., 6500 y.B.P. and younger than 5500 y.B.P. Because of the artificial modification of the ground surface, it was impossible to reveal the ages of the events younger than 5500 y.B.P. at this site.

From the data mentioned above, it is inferred that the Atera fault have repeated the movements with 2000-3000 years recurrence interval since 12000 y.B.P. This long recurrence interval and high long-term slip rate of the Atera fault suggest that this fault has a high potential of causing great earthquake with displacement of 6-15m.

References

Clark,M.M., Grantz,A. and Rubin,M. (1972) Holocene activity of the Coyote Creek fault as recorded in sediments of lake Cahuilla. The Borrego Mountain Earthquake of April 9, 1968, U.S.Geological Survey Prof. Paper, 787, p.112-130.

Hirano,S. and Nakata,T. (1981) Prehistoric large earthquakes deduced from fault activities along the Atera fault, central Japan. Geogr. Rev. of Japan, vol.54, p.231-246. (in Japanese)

Matsuda,T. and the Group for the Excavation Survey of the Tanna Fault, (1982) Trench survey to the active faults : a case of the Tanna fault. Program and abstracts, Geol. Soc. of Japan, 1982, p.550. (in Japanese)

Okada,A. (1975) Geomorphic development and fault topography in the Butai-pass area along the Atera fault zone, central Japan. Geogr. Rev. of Japan, vol.48, p.72-78. (in Japanese)

Okada,A. and Matsuda,T. (1976) A fault outcrop at the Onosawa pass and recent displacements along the Atera fault,central Japan. Geogr. Rev. of Japan, vol.49, p.632-639. (in Japanese)

Okada,A., Ando,M. and Tsukuda,T. (1980) Trenches across the Yamasaki fault in Hyogo Prefecture. Rep. Coordinating Committee for Earthquake Prediction, vol.24, p.190-194. (in Japanese)

Okada,A., Ando,M. and Tsukuda,T. (1981) Trenches, late Holocene displacement and seismicity of the Shikano fault associated with the 1943 Tottori earthquake. Disaster Prevention Res. Inst. Annuals, no.24B-1, p.105-126. (in Japanese)

Sieh,K. (1978) Prehistoric large earthquakes produced by slip on the San Andreas fault at Pallet creek. California, Jour. Geophys. Res, vol.83, p.3907-3939.

Sugimura,A. and Matsuda,T. (1965) Atera fault and its displacement vectors. Geol. Soc. Am. Bull., vol.81, p.2875-2890.

The Research Group for Active Faults of Japan (1980) Active faults in Japan -- sheet maps and inventories. University of Tokyo Press, Tokyo, 363p. (in Japanese)

Tsukuda,E. and Yamazaki,H. (1982) Holocene fault movement of the Atera fault revealed by the trench excavation survey. Program and abstructs, Seism. Soc. of Japan, 1982, no.1, p.175. (in Japanese)

Yamazaki,H. (1978) Tachikawa fault on the Musashino upland, central Japan and its late Quaternary movement. The Quat. Res., vol.16, p.231-246. (in Japanese)

Yamazaki,H., Kakimi,T., Tsukuda,E. and Awata,Y. (1981) Trench survey of the Ukihashi-chuo fault, Tanna Fault System. Program and abstracts, Seism. Soc. of Japan, 1981, no.1, p.118. (in Japanese)

Caption of the Figures

Figure 1. Location map showing the excavated active faults and the trench sites (open circles) in Japan.
1: Tachikawa fault
2: Shikano fault
3: Yamasaki fault
4: Tanna fault system (Tanna fault, Ukihashi central fault)
5: Nobi fault system (Umehara fault)
6: Atera fault
7: Atotsugawa fault
8: Senya fault
9; MTL (Hatano fault)

Figure 2. Trace of the Tanna fault system and location of the trench site. Heavy lines represent the earthquake faults of 1930. Contour interval is 100 m.
TN: Tanna basin
UK: Ukihashi basin

Figure 3. Summarized sketch of the trench wall across the Tanna fault.

Figure 4. Logs of the trench across the Atera fault. Solid circles show the point where the samples for radiocarbon dating were obtained.

Figure 5. Radiocarbon datings of the layered talus deposits observed on the trench wall and age of the slip of each minor fault. Solid circle indicates the horizon of the base of unfaulted layer. Layer's number corresponds to that in Figure 4.

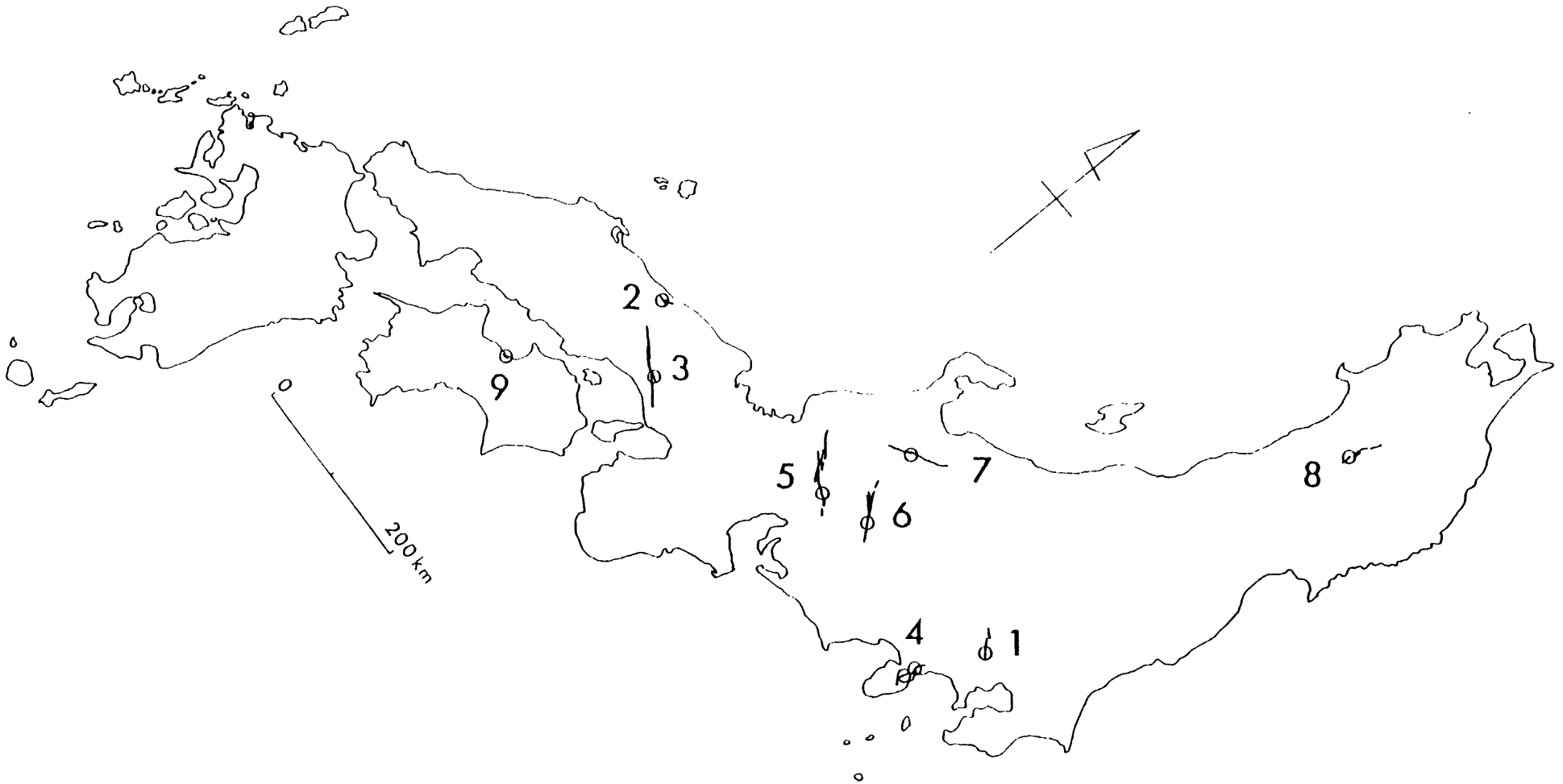
2
3
9
5
7
8
6
4
1
200 km

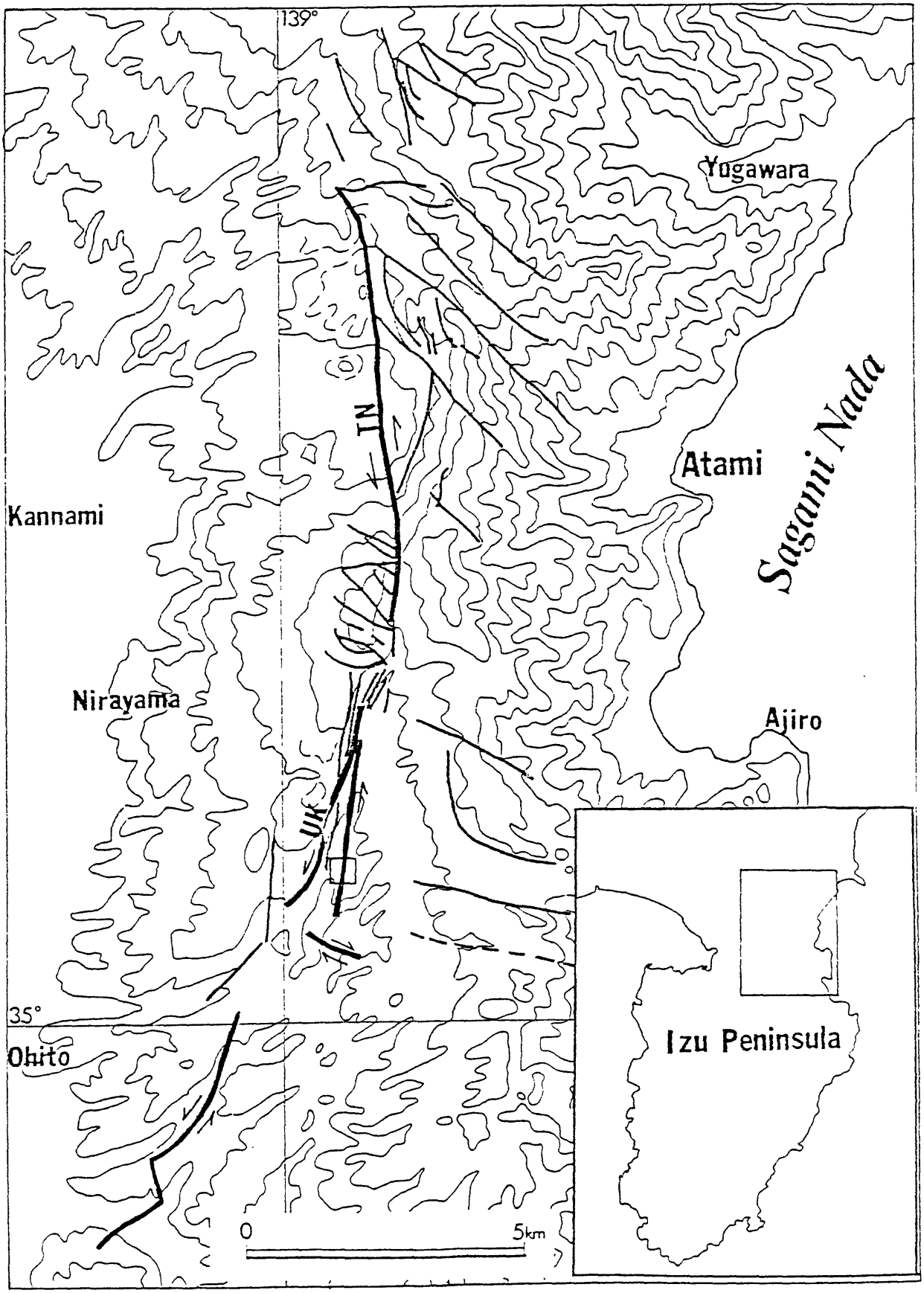
139°
Yugawara
Sagami Nada
Atami
IN
Kannami
Nirayama
Ajiro
UK
35°
Ohito
Izu Peninsula
0
5km

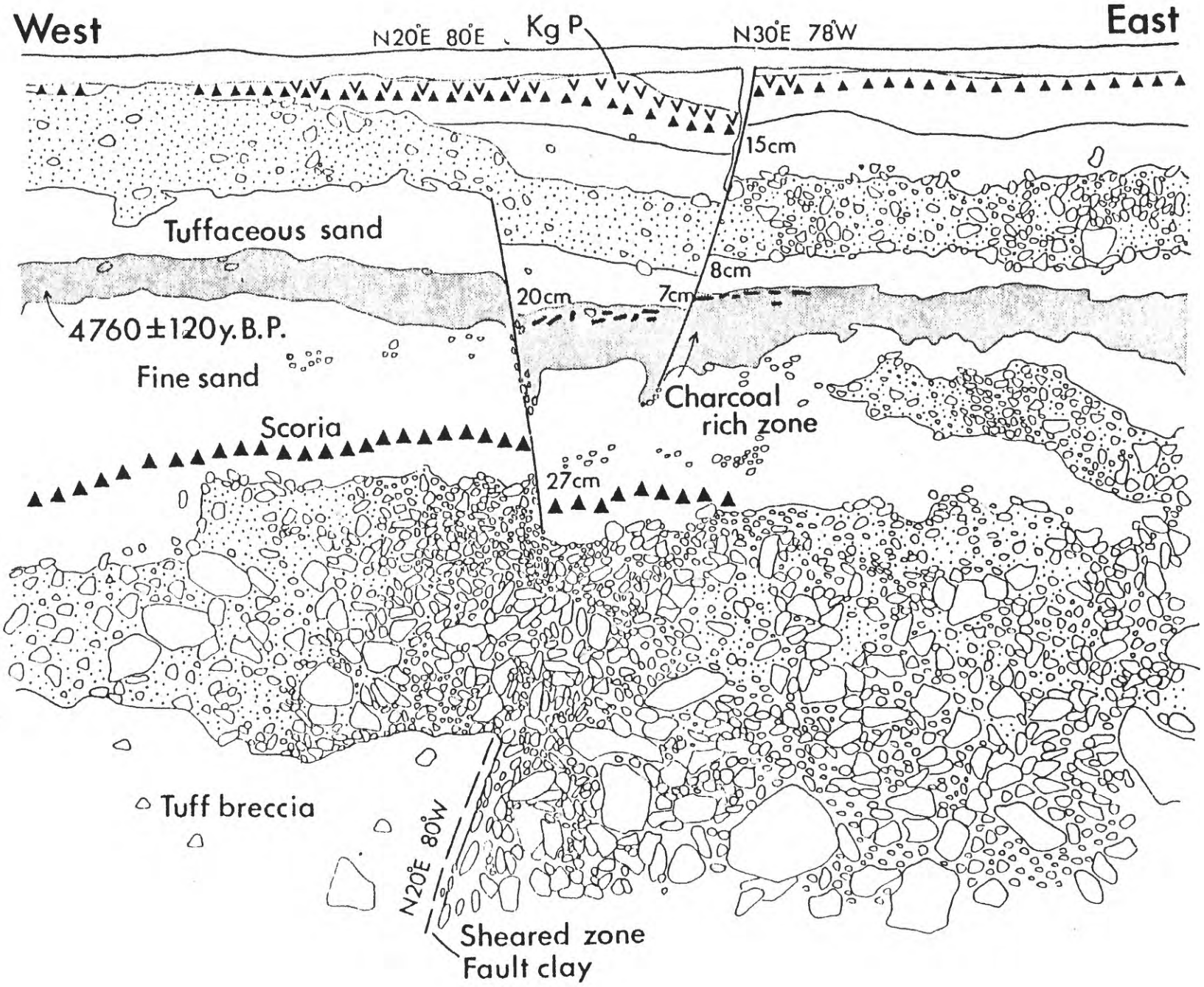
West
N20°E 80°E
Kg P
N30°E 78°W
East
15cm
Tuffaceous sand
8cm
20cm
7cm
4760±120y.B.P.
Fine sand
Charcoal
rich zone
Scoria
27cm
Tuff breccia
N20°E 80°W
Sheared zone
Fault clay

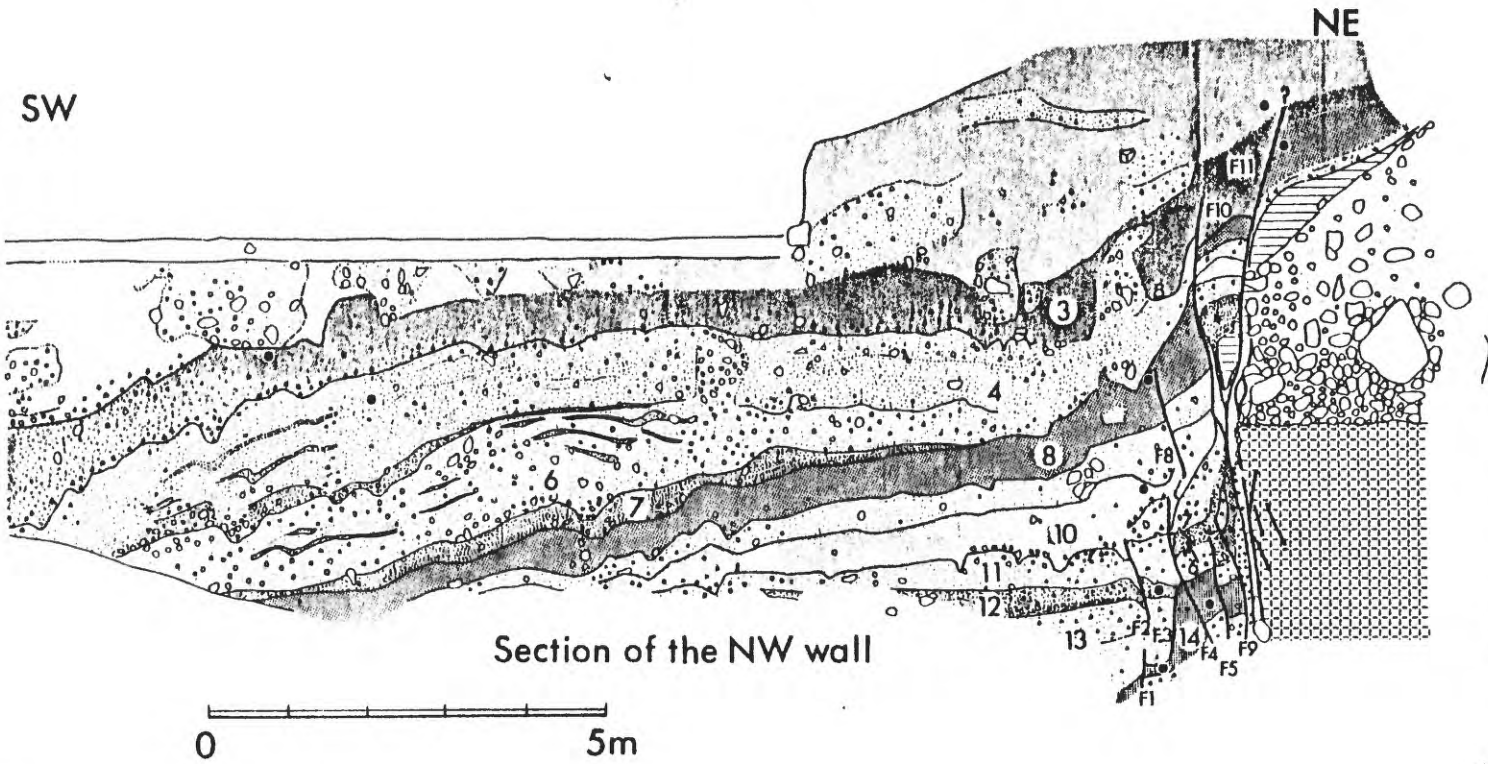

Section of the NW wall

0 5m

Section of the SE wall

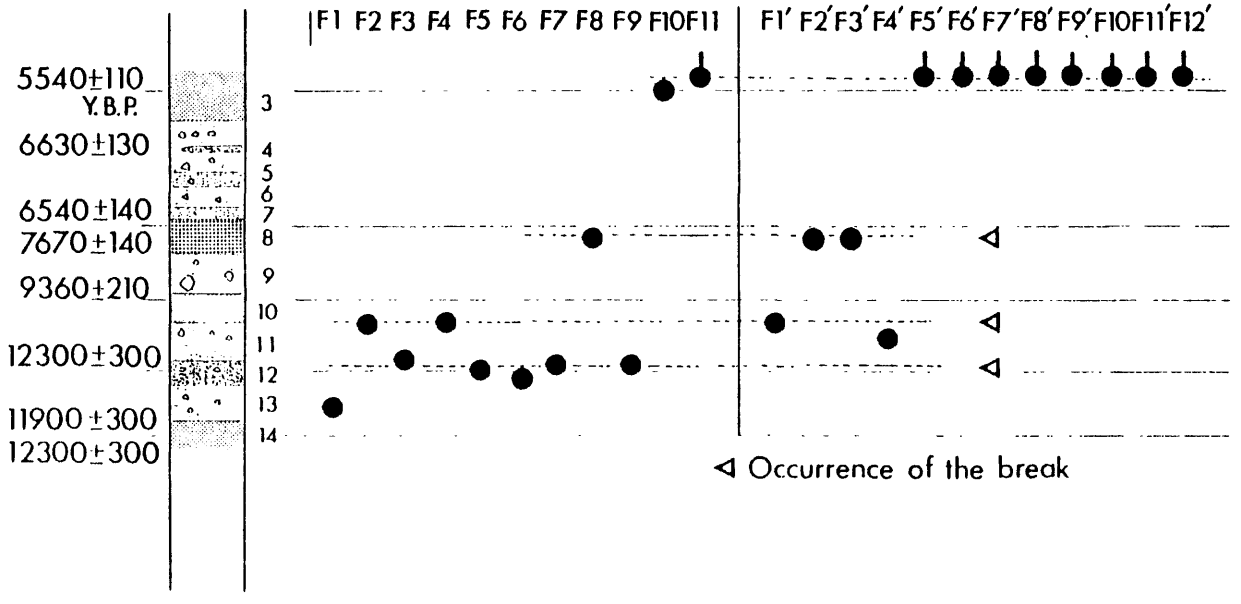
F1 F2 F3 F4 F5 F6 F7 F8 F9 F10F11
F1' F2' F3' F4' F5' F6' F7' F8' F9' F10F11' F12'
5540±110 Y.B.P.
6630±130
6540±140
7670±140
9360±210
12300±300
11900±300
12300±300
3
4
5
6
7
8
9
10
11
12
13
14
◁ Occurrence of the break

Hydraulic Fracturing Stress Measurements in the Kanto-Tokai Area, Japan

Hiroaki TSUKAHARA, Ryuji IKEDA and Hiroshi TAKAHASHI

National Research Center

for Disaster Prevention

SUMMARY

Over 60 sets of in-situ stresses were obtained by using hydraulic fracturing technique in eight wells of 450 m depth and in two wells of 100 m depth. The maximum and minimum horizontal compressive stresses increase linearly with depth; their gradients with depth are different for each measurement site. The maximum differential stresses also increase with depth. This can be understood by considering large stress relaxation in shallow regions in the measurement wells where low confining pressure and many pre-existing microcracks are dominant. The ratios of shear stress/normal sress decrease with depth, and in some measurement wells the ratios are almost constant below certain depths. This suggests that the stress relaxation takes place in a steady state by frictional sliding. As isotropic stress relaxation does not cause stress direction change, the direction measured in a well is applicable to estimation of the stress direction at depths. The measured stresses are consistent with stress conditions estimated from the focal mechanism of shallow earthquakes and active faults.

High in-situ stress areas are not always active in seismicity. A map of horizontal stress orientations is compiled from in-situ stress, seismic and geologic data. The stress orientations are understood in terms of interaction of the three plates, the Pacific, Philippine Sea, and Eurasian plates. Seismic activity is low in the area where the in-situ stress direction does not agree well with the accumulated strain direction observed by geodetic survey. The present strain accumulation does not work efficiently to increase the in-situ differential stress. This might be a reason for low seismicity there.

1. Stress measurement

All holes were drilled into sedimentary rocks: sandstone, mudstone and tuff of Late Miocene to Late Cretaceous age (see Fig. 1). Fracturing was carried out by pumping water into a straddled interval 2.2 m in length between two inflated packers at constant rates which varied between 5 and 100 l/min (see Fig. 2). After fracturing, operations (pumping water, halting and venting water) were repeated several times to obtain the reopening pressures of the fracture and the instantaneous shut-in pressures (see Fig. 3). The in-situ stresses were calculated from the reopening pressure and the instantaneous shut-in pressure.

The following relationships were used in calculating the maximum and minimum horizontal compressive stresses: S_{Hmax} and S_{Hmin} (Bredehoeft et al., 1976, Zoback et al., 1977, and Haimson, 1978).

$$S_{Hmim} = P_s \qquad (1)$$

$$S_{Hmax} = 3P_s - P_b^r - P_p \qquad (2)$$

where P_b^r, P_s and P_p are the reopening pressure of the hydraulic fracture, the instantaneous shut-in pressure (the pressure necessary merely to keep the fracture open), and the normally existing pore pressure in the rock, respectively. We take the value of P_p as hydrostatic pressure because the well water level was near the surface at all the sites.

The fracture azimuth of each experiment which indicates the azimuth of the maximum horizontal compressive stress was observed by an ultrasonic borehole televiewer (see Fig. 4) and/or an impression packer (see Fig. 5).

2. Results and discussion

(1) Stress magnitude

The data are plotted against the depth in Fig. 6. Dot-dash-lines are vertical stresses calculated from density. Solid straight lines are best fits obtained by a least squares method. The scattering of S_{Hmax} is larger than that of S_{Hmin}. As is to be expected from Eqs. (1) and (2), the values of S_{Hmin} are more reliable than those of S_{Hmax} generally.

Since the site M is apart from OK and K by only 4 km, the stresses are in good agreement with the best fit straight line obtained from the data from OK and K.

The following characteristics are seen in Fig. 6:

(i) Both stresses S_{Hmax} and S_{Hmin} increase linearly with depth. The straight lines along S_{Hmin} data are a fairly good approximation of the data.

(ii) At the measurement sites in the Izu Peninsula, Nishiizu(N), Shuzenji(SZ) and Shimoda(SM), S_{Hmin} is estimated to be smaller than S_v below about 600 m. In the case of Nishiizu(N), S_v will exceed S_{Hmax} at depths. The results in the central and east Izu Peninsula (SZ and SM) are consistent with the stress condition estimated from the focal mechanisms of shallow earthquakes and active faults which are of strike-slip type: $S_{Hmax} > S_v > S_{Hmin}$. In the case of the west Izu Peninsula, the focal mechanisms are of strike-slip type but there are two types of active faults: normal and strike-slip types. The data from the west Izu Peninsula (Nishiizu: N) indicate normal fault stress condition at depths.

(iii) It is well known in the Izu Peninsula that crustal movement and shallow earthquakes have been very active in recent decades. However, the measured differential stresses, $S_{max} - S_{min}$, at SZ and SM are rather small. Further, though the region near Nakaminato(NA) is inactive in crustal movement and seismicity of shallow earthquakes, large differential stresses are obtained. This suggests that the differental stress level does not simply correspond to current crustal activity.

(2) Stress variation with depth

As shown in Fig. 6, the differential stresses increase with depth except for Yokosuka. This is generally observed (e.g., Zoback et al., 1980). We must discuss the reason why differential stresses increase with depth in our measurement wells.

The increase in differential stress with depth will not be due to the topographic effects, because it is observed in most measurements although the topography around each measurement site is different. Local upheaval or subsidence has not been observed in most measurement sites. Rocks are assumed to be strained almost uniformly from the surface to 500 m.

If elastic constant increase with depth under conditions of uniform strain, the differential stress increases with depth, but the rates of increase of most measurements are too large to be explained in terms of the elastic constant increase. Therefore, it is reasonable to believe that the differential stress has been reduced due to the anelastic relaxation of rocks in shallow parts. The relaxation of stress differences in shallower parts is greater than that in deeper parts due to the mechanical properties of rocks and low confining pressure in shallower parts.

If the relaxation obeys known physical mechanisms, we can extrapolate the stress data to the depth. The dominant mechanism for the relaxation is not the steady state plastic deformation of rocks because of low temperature (e.g., Tsukahara, 1976). The relaxation should be caused by frictional sliding in many pre-existing micro-cracks. There are many pre-existing cracks in rocks and the cracks

which have proper direction for sliding are used for stress relaxation by frictional sliding. It is known that the coefficient of friction, μ = shear stress/normal stress, is almost constant for the same kind of rocks regardless of stress level, and most of the values are less than 0.85 (e.g., Byerlee, 1978).

In Fig.7 the ratio m = shear stress/normal stress is shown against depth. The ratio m is a parameter indicating stsress condition and μ is a physical constant: $\mu \geq m$. It is noteworthy that the values of m are almost constant below some depths for more than 200 m in some measurement wells, which are shown by solid straight lines in Fig. 7; F: 0.37, OK: 0.43, NA: 0.44, and SM: 0.27. This phenomenon is similar to that from rock friction experiments in the laboratory. This suggest that we can estimate the stresses at depths using the m values if there is no marked change of rock property with depth. Further, isotropic stress relaxation does not cause stress direction change. Therefore, the directions measured in the well indicate the stress direction at depths.

In the stress-depth plot for Shimoda(SM) in Fig. 7 a set of stresses measured by the overcoring method (O.C.; Koide et al., 1981) is plotted together with our data. The value of S_{Hmax} obtained from the overcoring method is rather large. As the rocks where the stress measurements were conducted were hard, and thick dike, the large S_{Hmax} will be due to the small stress relaxation.

(3) Stress orientation.

In Fig. 8 the directions of S_{Hmax} measured by and estimated from various methods are shown: focal mechanism solutions of shallow (depth < 20 km) and more than moderate sized ($M > 6.5$) earthquakes (Abe, 1974 and 77, Maki, 1974, Ishibashi, 1976b, Japan Meteol. Agen., 1978 and Imoto et al., 1980), Quaternary dike trends (Nakano et al., 1980 and Shirao, 1981), Quaternary cinder cone alignments (Nakamura, 1977), active faults of class A (average slip rate more than 1/1000 m/year) and certainty ranking I and II defined by the Research Group for Active Faults (1980a and b), in-situ stress measurements by the hydraulic fracturing method (present data) and by the overcoring method (Koide, 1980 and Koide et al., 1981). Dashed lines show active major tectonic lines.

The distribution of S_{Hmax} is complex. However, it is understandable when the relative motion of the Pacific, Philippine Sea, and Eurasian plates is taken into account. The Philippine Sea plate is consiered to be moving northward and subducting at the Suruga and Sagami troughs under the Eurasian plate, and the Pacific plate is moving westward and subducting at the Japan trench (e.g., Ishibashi, 1976a and 81, Seno, 1977, and Minster and Jordan, 1979). We interprete the S_{Hmax} direction distribution in terms of the interaction among the plates in the following discussion.

We can divide the area into some provinces where the stress directions appear almost uniform. Fig. 9 is a stress province (Zoback and Zoback, 1980 and Kobayashi, 1980) map, and lines indicate the average direction of S_{Hmax} in the province. The classification

is made on the basis of the S_{Hmax} direction considering the plate interaction. The area is divided into two large zones by line F-G, the southern part (P, Q_1, Q_2, QR, R, and S) ruled by the northwestward movement of the Philippine Sea plate, and the northern part (T_1 and T_2) ruled by the westward movement of the Pacific plate against the Eurasian plate. Further, the southern part consists of two subzones: the region ruled directly by the northwestward movement of the Philippine Sea plate (P, R, and S), and that ruled by the downward bending of the Philippine Sea plate at the Suruga trough (Q_1, Q_2, and QR). The stress state of each stress province is explained as follows.

(i) The stress direction in area R is simply ruled by the NW movement of the Philippine Sea plate against the Eurasian plate. The stress state of $S_v > S_{Hmin}$ in this area is caused by the downward bending of the Philippine Sea plate (Nakamura, 1979 and 80).

(ii) The stress state of $S_v > S_{Hmin}$ in area Q_1 is also caused by the same (Nakamura, 1979 and 80). This is illustrated in Fig. 10a.

(iii) QR is transition area. It is remarkable that changing from R to Q is not gradual and that area QR is very narrow.

(iv) The stress state in area Q_2 is ruled by the downward bendings at both east and west sides and also ruled by compressional stresses produced by the NW movement of the Philippine Sea plate. As the space between the two troughs Suruga and Sagami becomes narrow with the movement of the Philippine Sea plate, S_{Hmin} will increase gradually with movement northward, and it will exceed S_v: $S_{Hmin} > S_v$.

In this area, reverse faults are observed. The focal mechanisms of earthquakes in the lower crust (depth $\gtrsim$ 20 km; the earthquake swarm in east Yamanashi Prefecture) give the direction of S_{Hmax} as about N45°W (e.g., Ishibashi, 1976b). This is resonable from the above mentioned bending model as shown in Fig.10c.

(v) The upper crust of area P has enough distance not to be disturbed by the downward bending, and the stress direction is dominated by the NW compression by the Philippine Sea plate as shown in Fig. 10a.

(vi) Area S is dominated by almost the same stress conditions as area P, as shown in Fig. 10b.

(vii) The stress state in areas T_1 and T_2 is basically controlled by the westward motion of the Pacific plate. The direction will change gradually from T_1 to T_2.

Geodetic survey data in the Kanto-Tokai area have been reported (Nakane and Fujii, 1979, Dambara, 1980 and Geograph. Surv. Inst., 1979 and 80). Comparing the map of the stress direction with that of accumulated strain direction, we can see that both the directions do not always agree; there is close agreement in stress provinces P and R, and disagreement in Q_2 and S. Activity of shallow earthquakes is low in areas Q_2 and S. Current strain accumulation does not work efficiently to increase the in-situ differential stresses. It might be a reason for low seismicity there.

Acknowledgement Dr. K. Hamada (National Research Center for Disaster Prevention) kindly read and criticized the manuscript.

REFERENCES

Abe,K., 1974. Seismic displacement and ground motion near fault: The Saitama earthquake of September 21, 1931. J. Geophys. Res., 79: 4393-4399.

Abe.K., 1977. Focal mechanisms of earthquakes occurred in the Izu Peninsula. Abstracts, Seismol. Soc. Japan, No. 1: 82. (in Japanese)

Bredehoeft.J.D., R.G.Wolff, W.S.Keys and E.Shuter, 1976. Hydraulic fracturing to determine the regional in situ stress field, Piceance Basin, Colorado. Geol. Soc. Amer. Bull., 87: 250-258.

Byerlee,J., 1978. Friction of rocks. Pure Appl. Geophys., 116: 615-626.

Dambara,T., 1980. Some Problems on prediction of the Tokai earthquake in future. Proc. Earthq. Predic. Res. Symp. 1980: 85-95. (in Japanese with English abstract)

Geograph. Surv. Inst., 1979. Horizontal earth's strain in the northern part of the Boso Peninsula. Rep. Coordinating Committee Earthq. Predic., 21: 60-61. (in Japanese)

Geograph. Surv. Inst., 1980. Horizontal strain in the Kanto district. Rep. Coordinating Committee Earthq. Predic., 24: 73-81. (in Japanese)

Geol. Surv. Japan, 1978a. 1:1,000,000 Geological Map of Japan, Second Edition.

Geol. Surv. Japan, 1978b. 1:2,000,000 Map Series 18, Active Fault in Japan (Main Lands).

Haimson,B.C., 1978. Near-surface and deep hydrofracturing sterss measurements in the Waterloo quartzite. Proc. 19th U. S. Symp. Rock

Mech.:345-361.

Ikeda,R. and H. Takahashi, 1981. Stress measurement by hydrofracturing at Futtsu City, Chiba Prefecture. Zisin, 34: 565-576. (in Japanese with English abstract)

Imoto,M. I.Karakama, R.S.Matsu'ura, F.Yamazaki, A.Yoshida and K.Ishibashi, 1981. Focal mechanisms of the 1980 earthquake swarm off the east coast of the Izu Peninsula, Japan. Zisin, 34: 481-493. (in Japanese with English abstract)

Ishibashi,K., 1976a. Re-examination of a great earthquake expected in the Tokai district: Possibility of the Suruga Bay earthquake Abstracts, Seismol. Soc. Japan, 1976, No. 2: 30-34. (in Japanese)

Ishibashi,K., 1976b. Re-evaluation of the 1923 Kanto earthquake (1) Abstracts, Seismol. Soc. Japan, 1976, No. 1: 55. (in Japanese)

Ishibashi,K., 1981. Specification of soon-to-occur seismic faulting in the Tokai district, central Japan, based upon seismotectonics Earthquake Prediction - An International Review, Maurie Ewing Series 4, Amer. Geophys. Union, U. S. A.: 297-332.

Japan Meteol. Agency, 1978. Report on the earthquake of January 14 1978, near Izu-Oshima. Quaterly J. Seismol., 43: 21-57. (in Japanese)

Kobayashi,Y., 1980. On "Tectonic stress province". The Earth Monthly Kaiyo Shuppan, Tokyo, 2: 569-572. (in Japanese)

Koide,H., 1980. Problems on in situ stress measurements for earthquake prediction. The Earth Monthly, Kaiyo Shuppan, Tokyo, 2: 578-585. (in Japanese)

Koide,H., K.Hoshino, K.Kusunose, K.Inami, Y.Nishimatsu, S.Koizumi and

M.Akiyama, 1981. Stress measurements by a stress relief method at Izu Shimoda. Abstracts, Seismol. Soc. Japan, 1981, No. 2: 20. (in Japanese)

Maki,T., 1974. On the earthquake mechanism of the Izu-Hanto-oki earthquake of 1974. Spec. Bull. Earthq. Res. Inst., Univ. Tokyo, 14: 23-36.

Minster,J.B. and T.B.Jordan, 1979. Rotation vectors for the Philippine and Rivera plates. EOS, 60: 958.

Nakamura,K. 1977. Volcanoes as possible indicators of tectonic stress orientation - principle and proposal. J. Volcanol. Geotherm. Res., 2: 1-16.

Nakamura,K. 1979. $\mathcal{T}_{Hmax}$ trajectories east of Suruga trough, Japan - an effect of flexure of lithospheric plate. Zisin, 32: 370-372. (in Japanese)

Nakamura,K. 1980. Tectonics of Izu and flexure of lithospheric plate. The Earth Monthly, Kaiyo Shuppan, Tokyo, 2: 94-102. (in Japanese)

Nakane,K. and Y.Fujii, 1979. On accumulation and release of the earth's strain in the south Kanto district. J. Geodetic Soc. Japan, 25: 26-37. (in Japanese with English abstract)

Nakano,Y., O.Sugita, H.Inokuchi and Y.Kobayashi, 1980. Tectonism at the Izu Peninsula from the viewpoint of dike trends. The Earth Monthly, Kaiyo Shuppan, Tokyo, 2: 103-109. (in Jaspanese)

The Research Group for Active Faults, 1980a. Active Faults in Japan - Sheet Maps and Inventories. Univ. Tokyo Press, Tokyo, pp 363. (in Japanese)

The Research Group for Active Faults, 1980b. Active faults in and

around Japan: The distribution and the degree of activity. J. Natural Disaster Sci., 2: 61-99.

Seno,T., 1977. The instantaneous rotation vector of the Philippine Sea plate rlative to the Eurasian plate. Tectonophys., 42: 209-226.

Shirao,M., 1981. Geology of Daruma volcano and adjacent areas, Izu Peninsula, Japan. J. Geol. Soc. Japan, 87: 641-655.

Tsukahara,H., 1976. Diffusion and diffusion creep in olivine and ultrabasic rocks. J. Phys. Earth, 24: 89-103.

Tsukahara,H., R.Ikeda, H.Satake, M.Ohtake and H.Takahashi, 1978. Hydrofracturing stress measurements at Okabe Town, Shizuoka Prefecture. Zisin, 31: 415-433. (in Japanese with English abstract)

Tsukahara,H., R.Ikeda, H.Satake and H.Takahashi, 1980. Stress measurements by hydrofracturing at Nishiizu Town, Shizuoka Prefecture. Zisin, 33: 317-327. (in Japanese with English abstract)

Tsukahara,H., R.Ikeda, H.Satake, and Takahashi, 1981. Stress measurements by hydrofracturing at Choshi City, Chiba Prefecture. Zisin, 34: 13-20. (in Japanese with English abstract)

Zoback,M.D., J.D.Healy and J.C.Roller, 1977. Preliminary stress measurements in central California using the hydraulic fracturing technique. Pure Appl. Geophys., 115: 135-152.

Zoback,M.L. and M.D.Zoback, 1980. State of stress in the conterminous United States. J. Geophys. Res., 85: 6113-6156.

Zoback,M.D., H.Tsukahara and S.Hickman, 1980. Stress measurements at depth in the vicinity of the San Andreas Fault: Implications for the magnitude of shear stress at depth. J. Geophys. Res. 85: 6157-6173.

Figure Captions

Fig. 1 Measurement sites (black circles) and their geological and tectonic settings. Simplified from Geological Map of Japan, and Active Fault in Japan (Geol. Surv. Japan, 1978a,b). 1: The post-Miocene, 2: The Miocene, 3: The pre-Miocene, 4: Quaternary extrusives, 5: Tertiary extrusives, 6: Intrusives, 7: Active faults, 8: Major tectonic lines (MT: the Median tectonic Line, IS: the Itoigawa-Shizuoka Tectonic Line, SU: the Suruga trough, and SA: Sagami trough), 9: Depth in m, 10: Measurement sites (M, K and OK: Okabe; K and OK are located within 10 m of each other, SZ: Shuzenji, SM: Shimoda, N: Nishiizu, Y: Yokosuka, F: Futtsu, C: Choshi, and NA: Nakaminato), 11: Sedimentary rocks, 12: Igneous rocks. In the inserted figure, EU: the Eurasian plate, PH: the Philippine Sea plate, NAN: the Nankai trough, and JA: the Japan trench.

Fig.2 Equipment for the hydraulic fracturing stress measurement. 1: Clock, 2: Magnetic tape recorder, 3: Multipen chart recorder, 4: Water tank, 5: Flow rate meter, 6: Water Pump, 7: Pressure transducer, 8: Casing pipe (16 cm, 50 m), 9: Inflatable packers, 10: Fluid outlet, and 11: Downhole pressure transducer with a hydrophone.

Fig. 3 Typical records of water pressure and flow rate vs. time plot (at 248 m in the Nakaminato well). Pumping was maintained in each injection cycle between points A and B, and water pressure is

vented at point C. P_b^o: Breakdown pressure, P_b^r: Reopening pressure, and P_s: Instantaneous shut-in pressure.

Fig. 4 Comparison of an ultrasonic borehole televiewer log taken after the hydraulic fracturing (right-hand picture), which shows new vertical cracks created by the hydraulic fracturing with that taken before the hydraulic fracturing (left-hand). Nishiizu, 263 m depth.

Fig. 5 Newly created cracks printed on the impression packer for the 225 m deep experiment at the Okabe site.

Fig. 6 Stress variations with depth. Solid lines are best fits obtained by a least squares method. The linear variation of the lithostatic pressure which is calculated from density log data and/or core density are also shown for reference by dash-dot-lines. M, K and OK: Okabe (Tsukahara et al., 1978), N: Nishiizu (Tsukahara et al., 1980), Y: Yokosuka, F: Futtsu (Ikeda and Takahashi, 1981), C: Choshi (Tsukahara et al., 1981), NA: Nakaminato, SZ: Shuzenji, and SM: Shimoda. O.C.: Data measured by the overcoring method (Koide et al., 1981). SM and O.C. are located about 4 km of each other.

Fig.7 Variation of maximum shear stress/normal stress with depth; maximum shear stress = $(S_{Hmax} - S_{Hmin})/2$, and normal stress = $(S_{Hmax} + S_{Hmin})/2$ - pore pressure. Solid lines indicate the average value over the interval of depths extending over 200 m where the data do not change monotonically. Dashed lines are freehand curves along the data.

Fig. 8 The maximum compressive stress directions measured by the hydraulic fracturing method and by the overcoring method, and those estimated from seismic and geologic evidence. 1 and 2: Hydraulic fracturing method (present study; 1, one point datum, and 2, average of two and more data at one measurement site), 3: Focal mechanism solutions of shallow (depth < 20 km) and more than moderate sized (magnitude > 6.5) earthquakes (Maki, 1974, Abe, 1974, Ishibashi, 1976 and 77, Japan Meteol. Agen., 1978, and Imoto et al., 1980), 4: Cinder cone alignments around Quaternary volcanoes (Nakamura, 1977), 5: Active faults analyses (data from Res. Group Active Faults, 1980a), 6: Overcoring method (Koide, 1980, and Koide et al., 1981), 7 and 8: Quaternary dike trends (Nakano et al., 1980, and Shirao, 1981; 7, average of four dike trends, and 8, average of five and more dike trends), and 9: Major tectonic lines.

Fig. 9 The maximum compressive stress directions in the upper crust. Short segments are the same data as shown in Fig. 8. Straight lines indicate the average directions of the data in the stress provinces; P, Q_1,Q_2, QR, R, S, T_1, and T_2. F-G line indicates the limit of the influence of the Philippine Sea plate on the stress conditions in the upper crust of the Eurasian plate estimated from the stress direction.

Fig. 10 Simplified current stress directions in the upper crust (top), and illustrations of a model (bottom). Dotted lines indicate diretions of the maximum horizontal compressive stresses. Large arrows show the relative movement of the Philippine Sea plate (PH)

and the Pacific plate (PA) with respect to the Eurasian plate (EU). Small arrows show directions and relative magnitude of stresses in the cross sections schematically. P, Q_1, Q_2, QR, S, and T_1 are the stress provinces as shown in Fig. 9. H (bottom right): East Yamanashi Prefecture earthquake swarm.

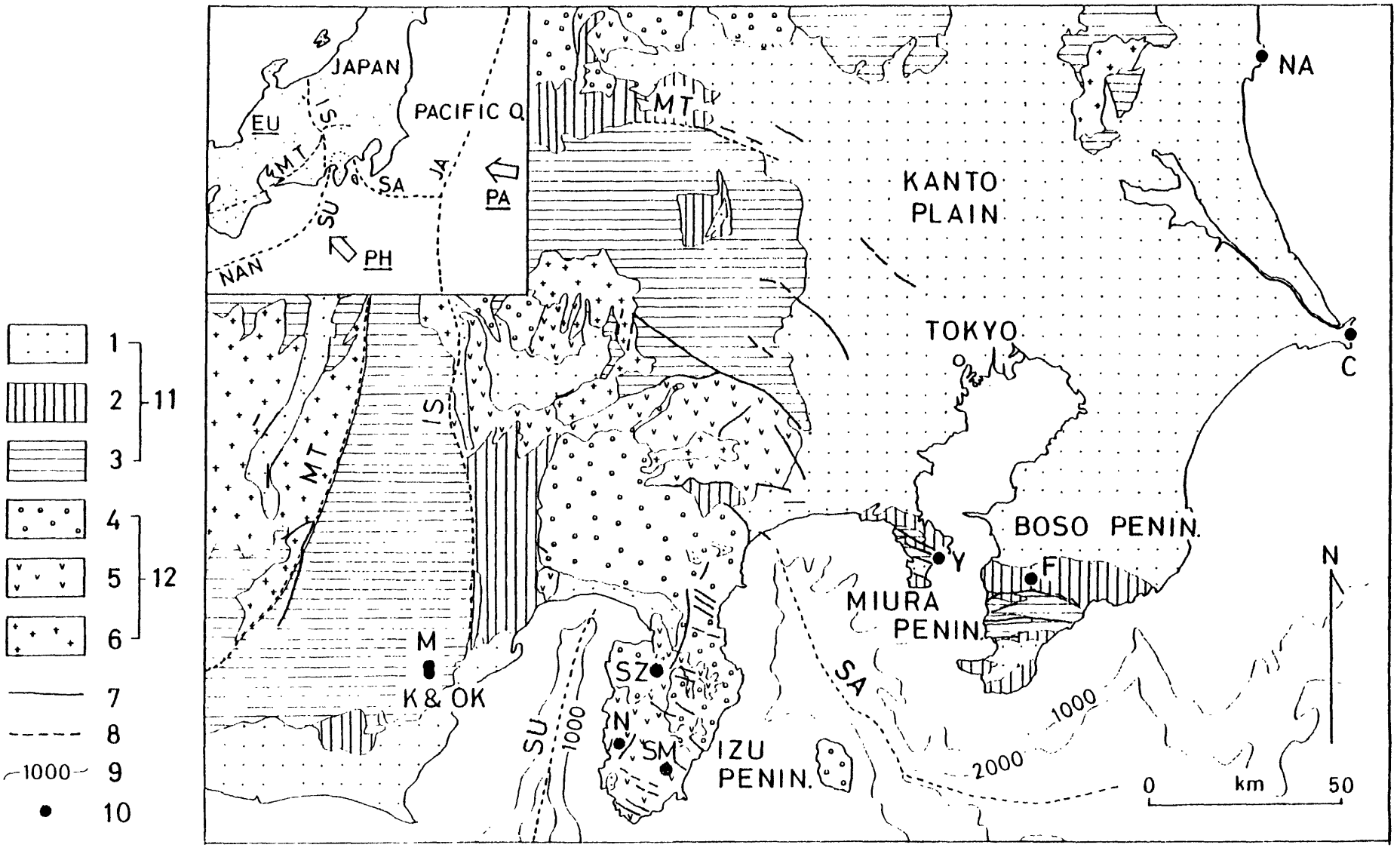
JAPAN
EU
IS
PACIFIC O.
MT
SA
JA
PA
SU
PH
NAN
NA
KANTO
PLAIN
TOKYO
C
BOSO PENIN.
Y
F
MIURA
PENIN.
N
M
K&OK
SZ
N
SM
IZU
PENIN.
SA
1000
2000
0
km
50
1
2
3
11
4
5
6
12
7
8
9
10

Fig. 1

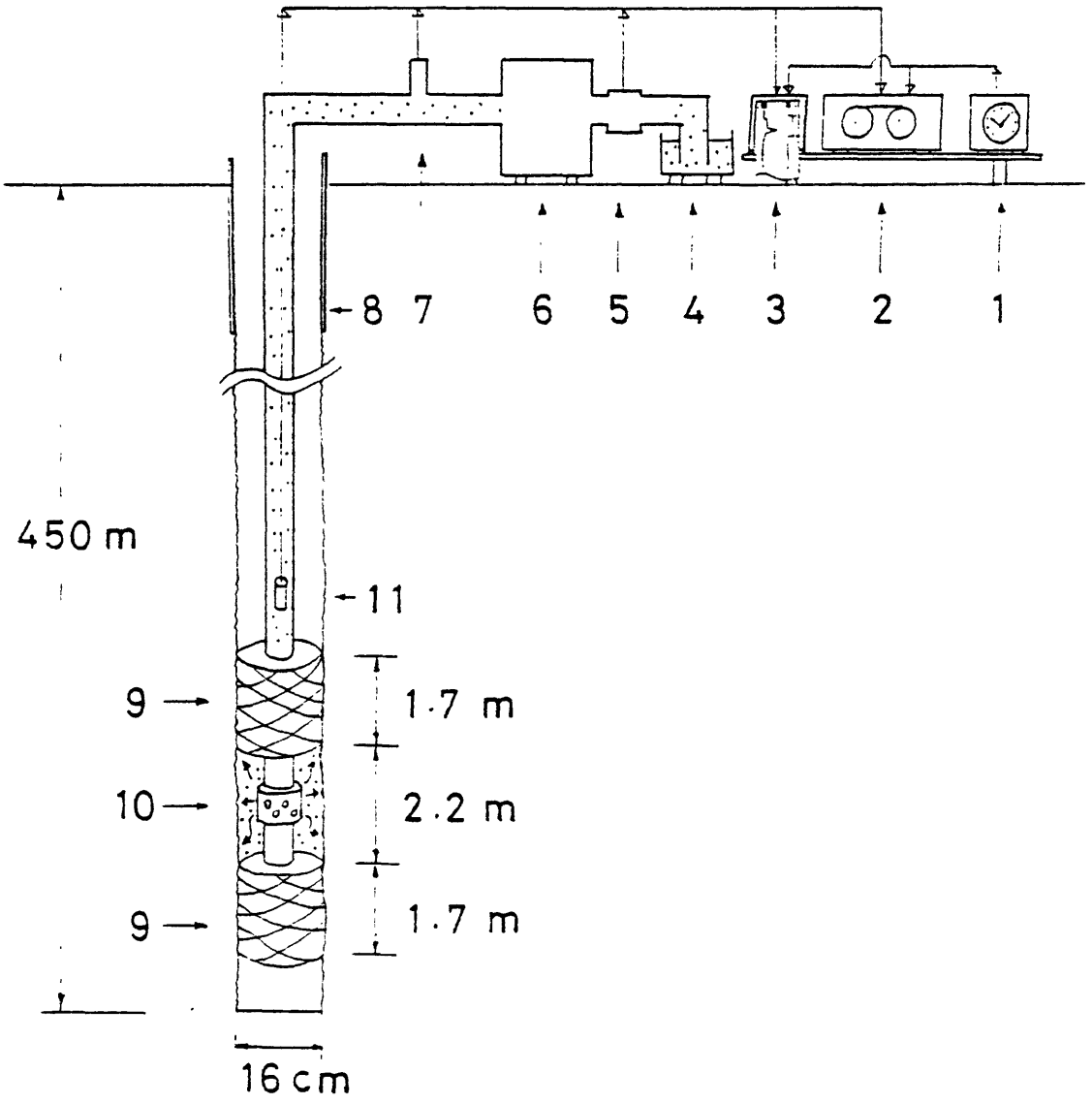

Fig. 2

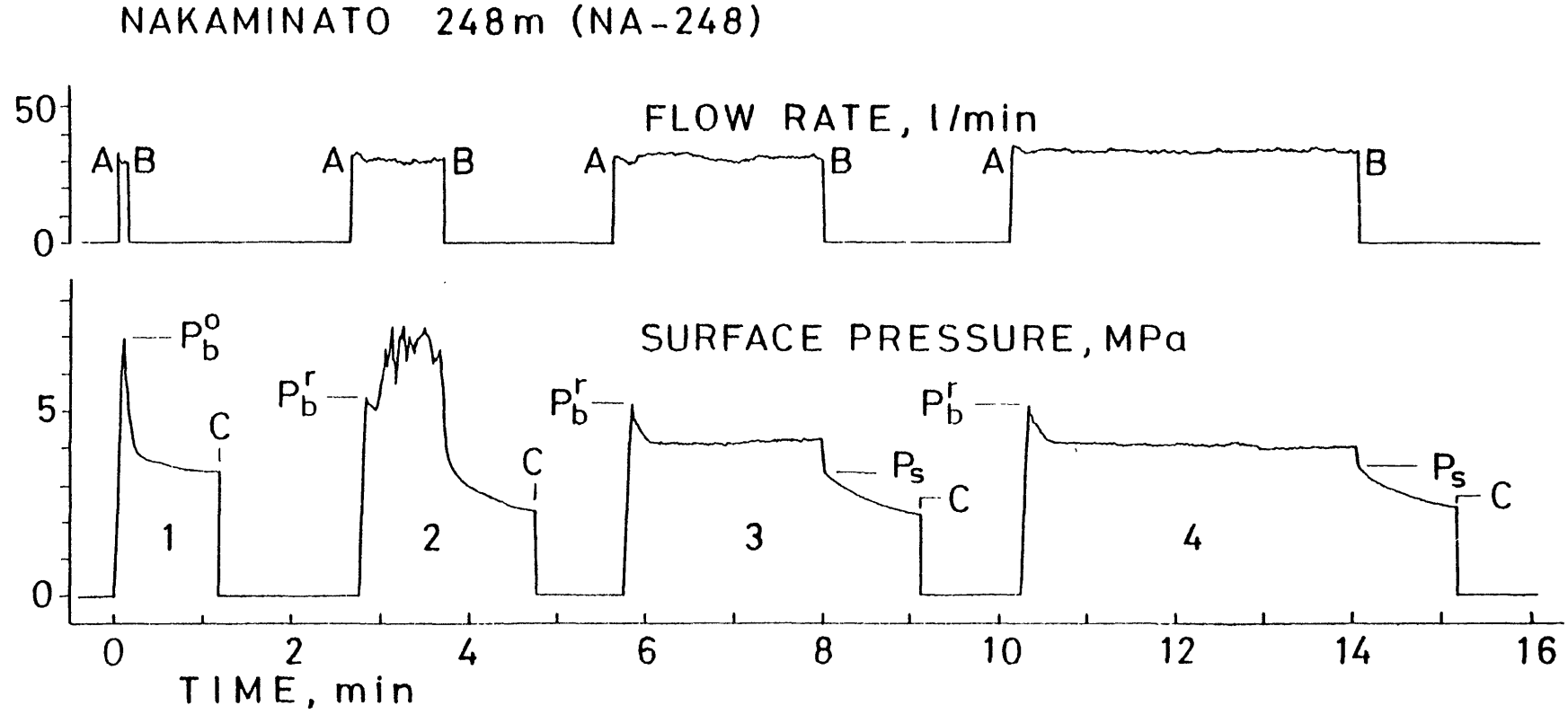
NAKAMINATO 248m (NA-248)
FLOW RATE, l/min
50
0
A
B
SURFACE PRESSURE, MPa
5
0
P_b^o
P_b^r
C
P_s
1
2
3
4
0
2
4
6
8
10
12
14
16
TIME, min

Fig. 3

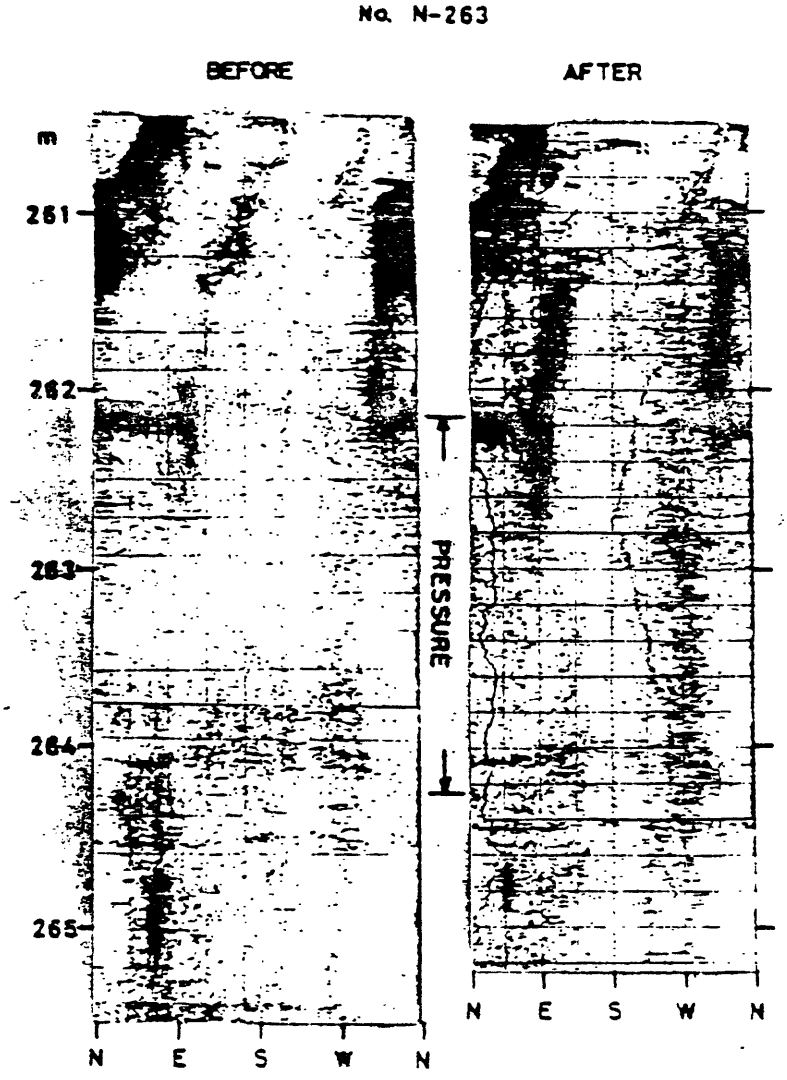
No. N-263
BEFORE
AFTER
m
261
262
263
264
265
PRESSURE
N E S W N
N E S W N

Fig. 4

OK 225

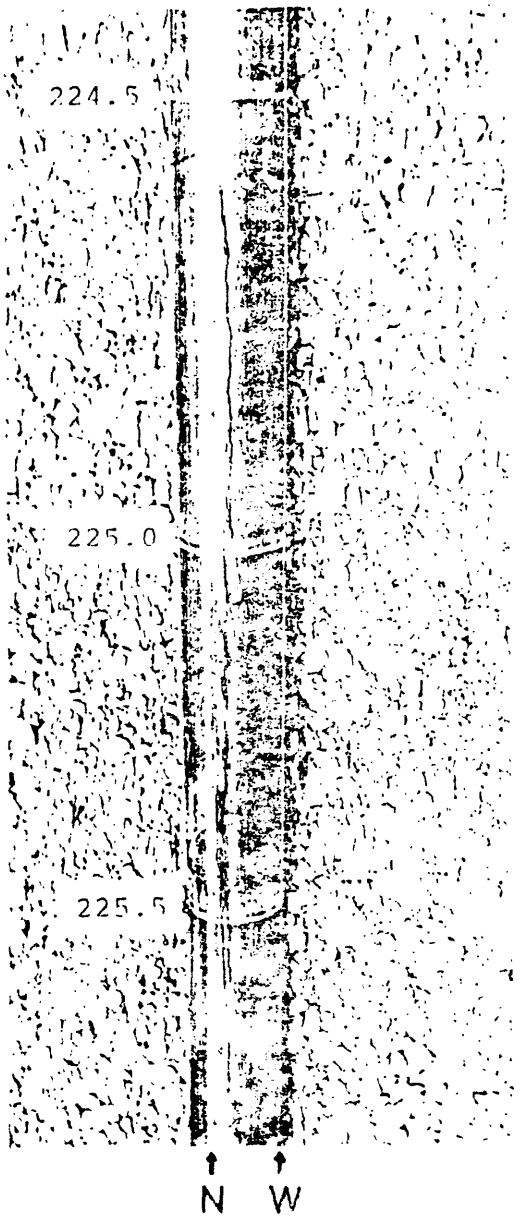

Fig. 5

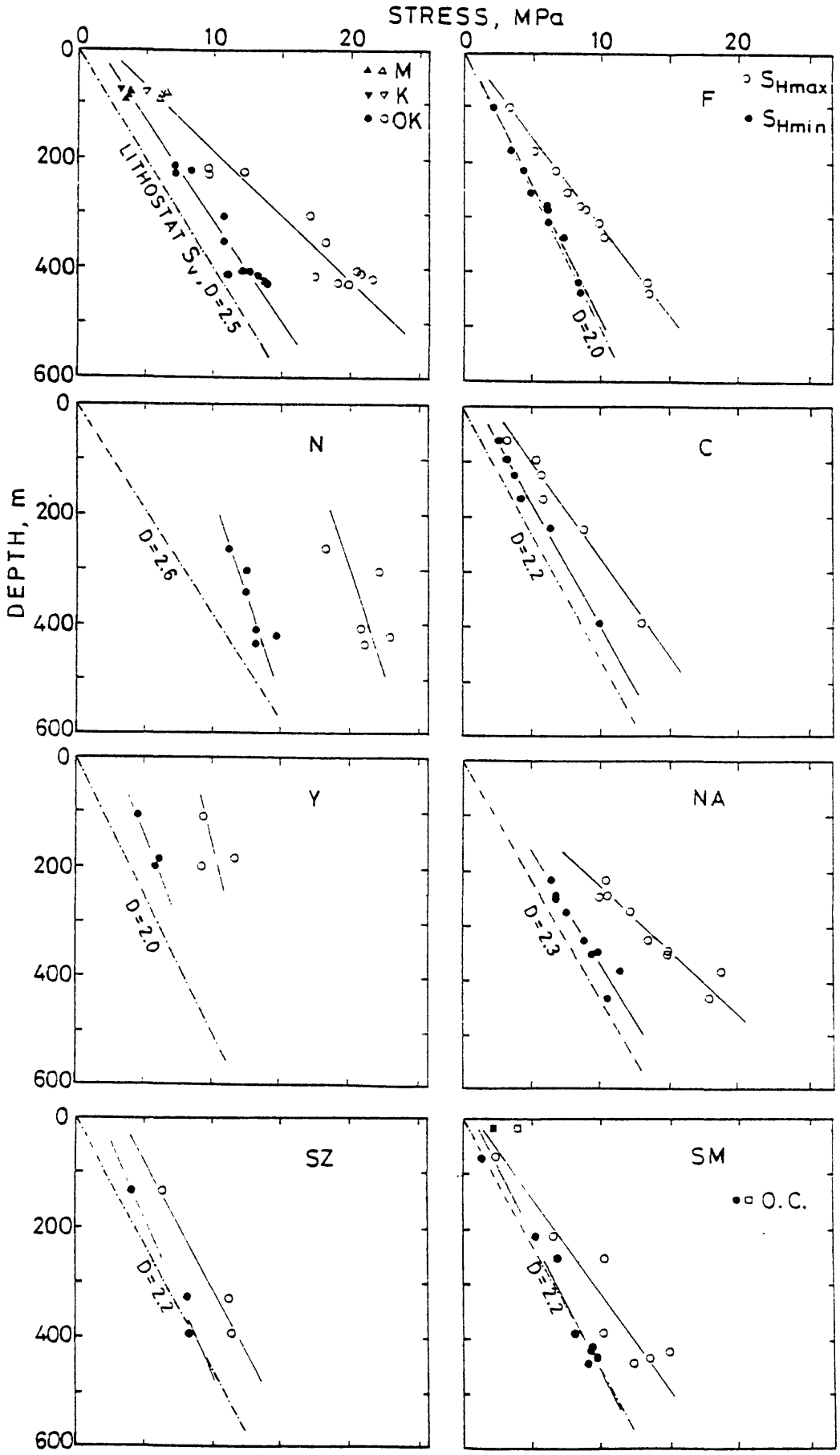
STRESS, MPa
0
10
20
DEPTH, m
0
200
400
600
M
K
OK
LITHOSTAT Sv, D=2.5
F
SHmax
SHmin
D=2.0
N
D=2.6
C
D=2.2
Y
D=2.0
NA
D=2.3
SZ
D=2.2
SM
O.C.
D=2.1

Fig. 6

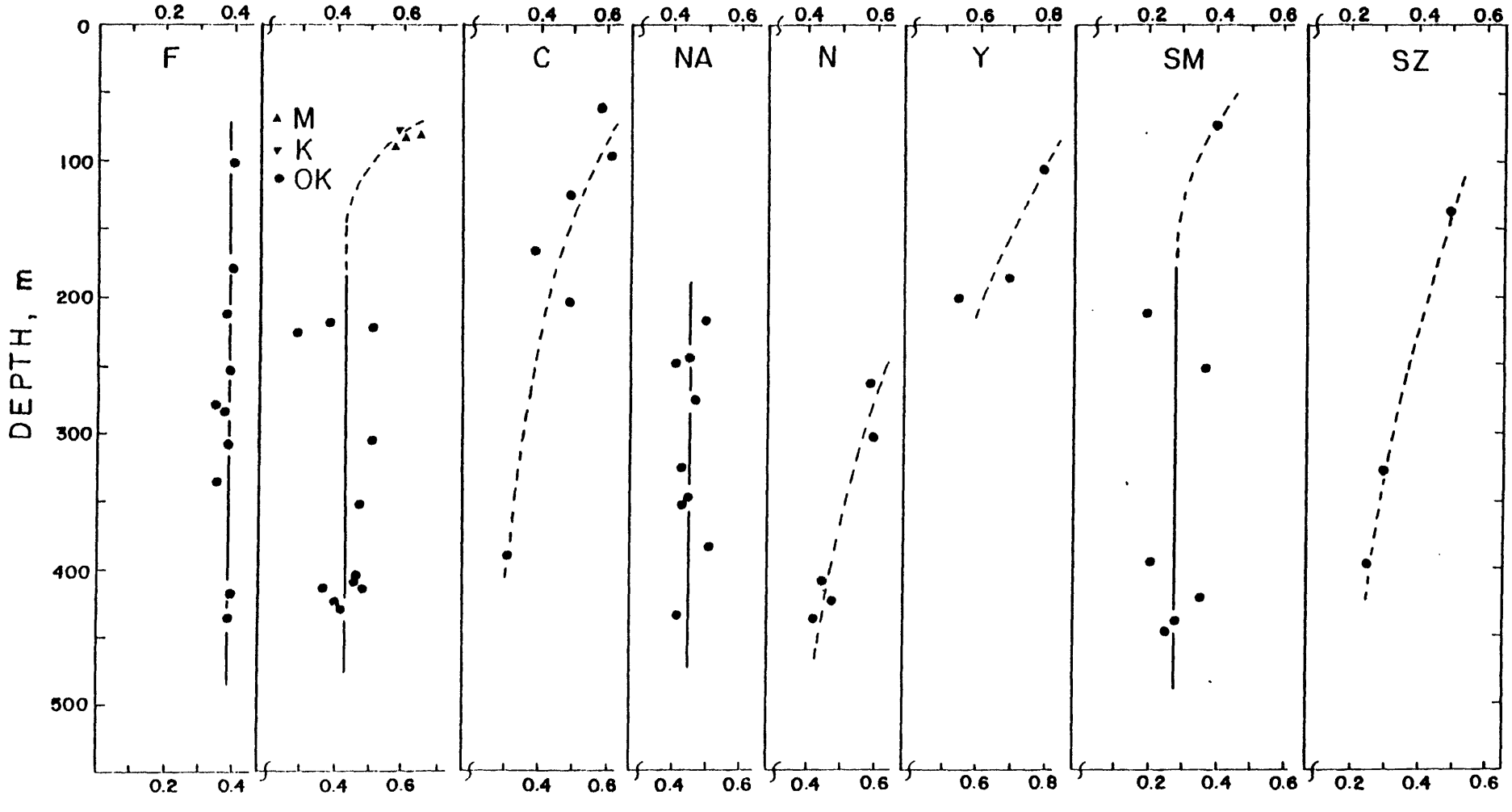
MAXIMUM SHEAR STRESS / NORMAL STRESS
DEPTH, m
0
100
200
300
400
500
F
C
NA
N
Y
SM
SZ
M
K
OK
0.2
0.4
0.6
0.8

Fig. 7

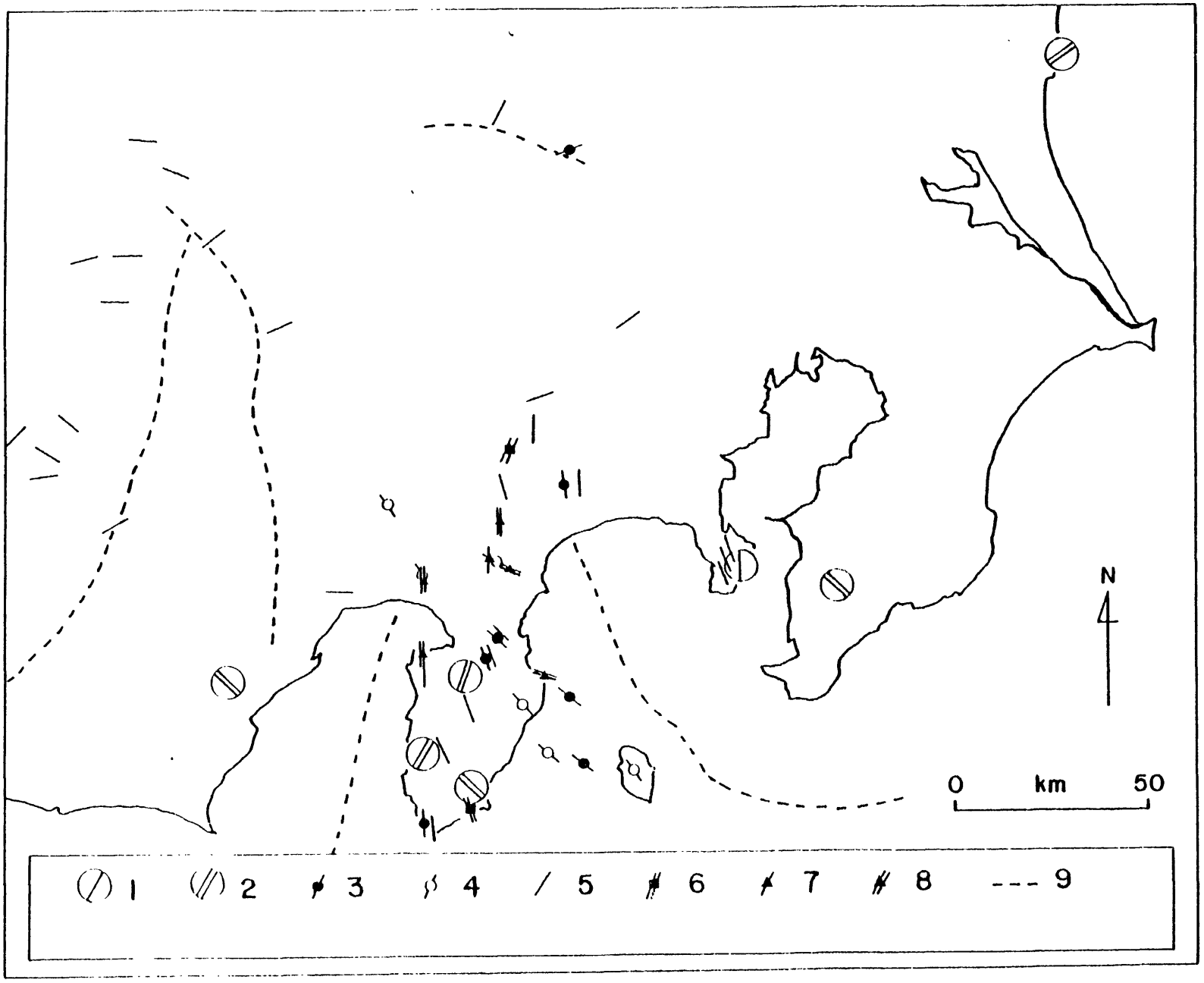

Fig. 8

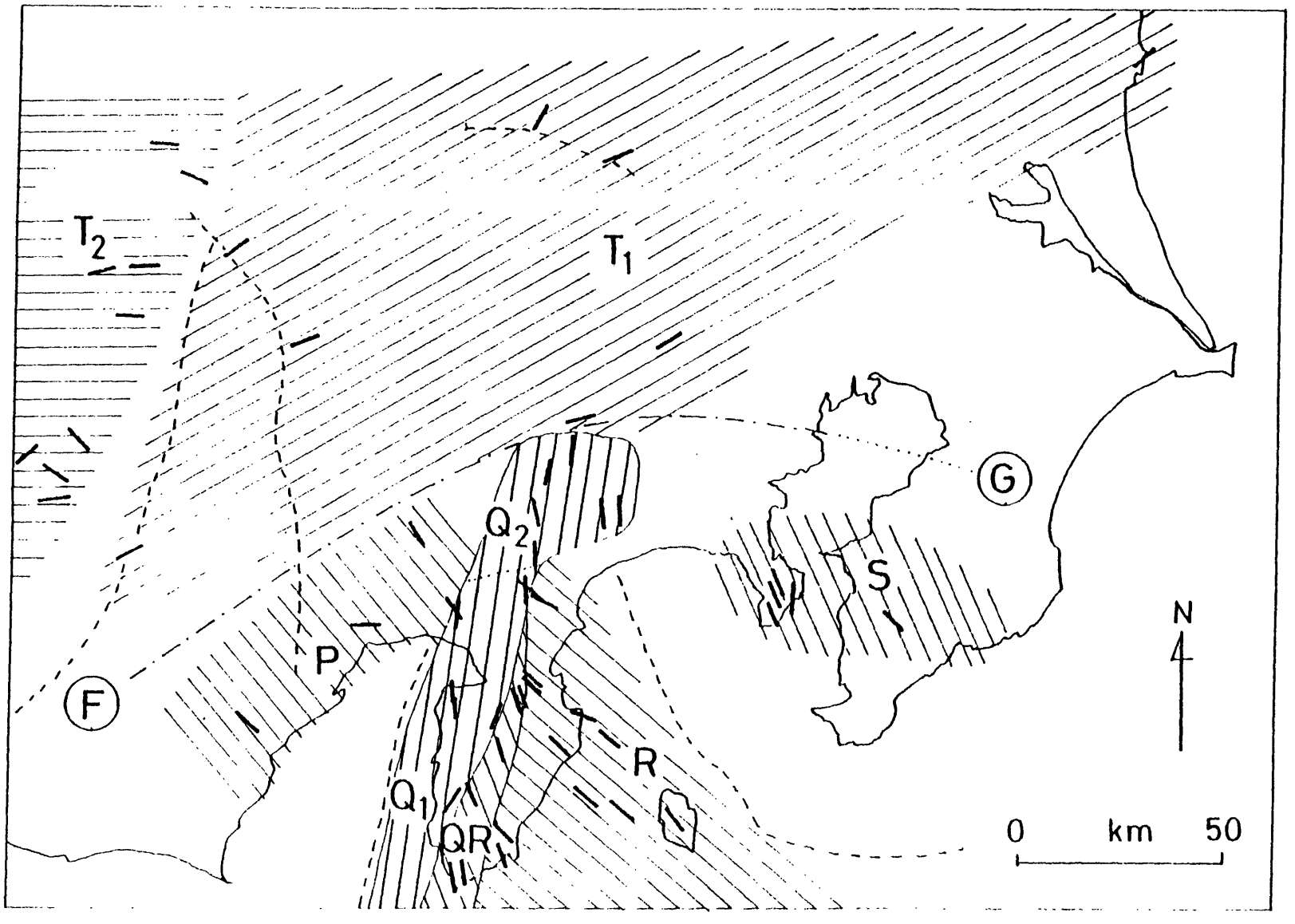

Fig. 9

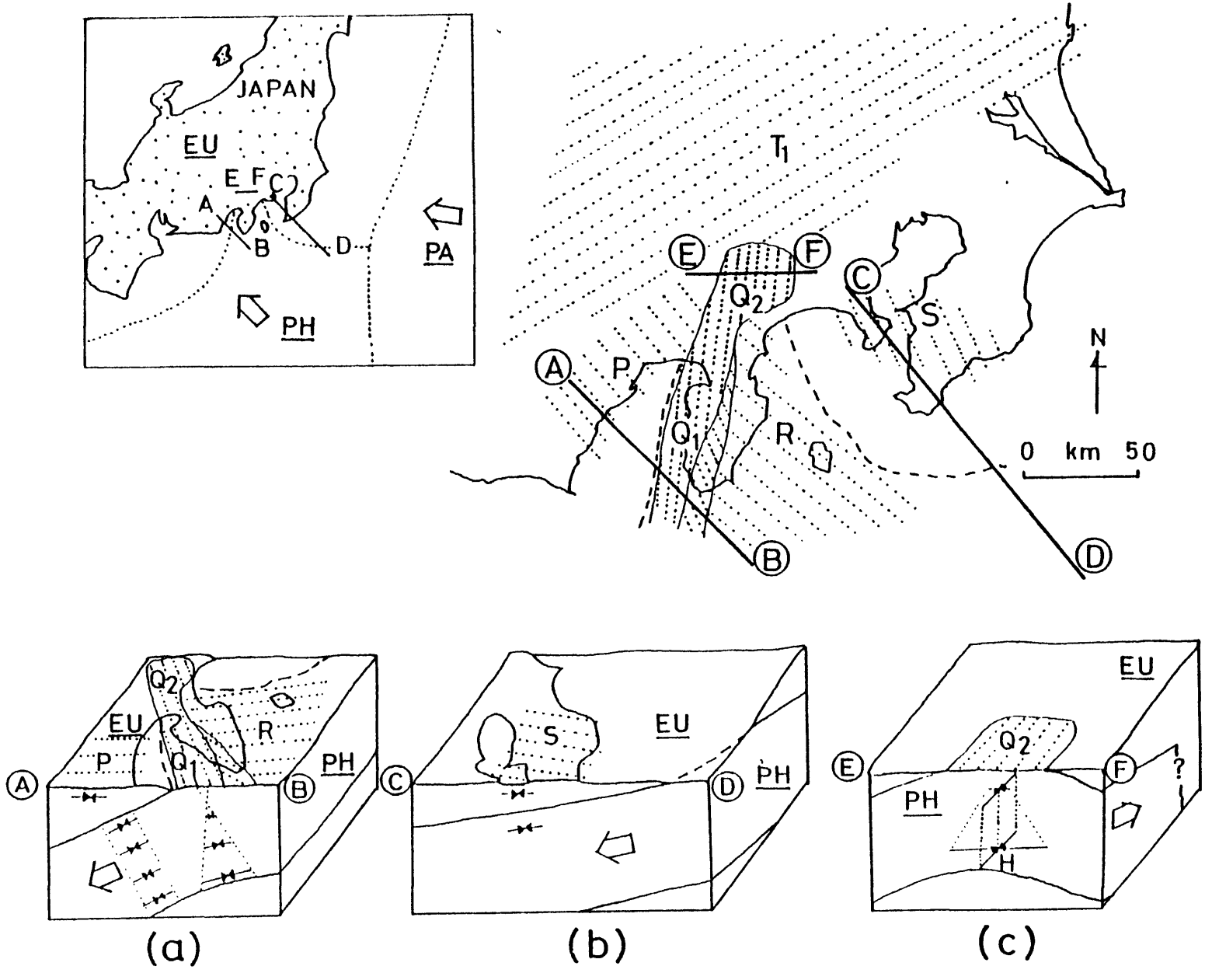
JAPAN
EU
E F
C
A
B
D
PA
PH
T1
E
F
Q2
C
S
N
A
P
Q1
R
0 km 50
B
D
Q2
EU
R
P
Q1
PH
A
B
(a)
S
EU
C
D
PH
(b)
EU
Q2
E
F
?
PH
H
(c)

Fig.10

Multi-channel seismic reflection survey in the Nankai, Suruga and Sagami Troughs

by: Takahiro SATO
Shigeru KATO
Misao SAKURAI

Surveying Division,
Hydrographic Department,
Maritime Safety Agency

Abstract

In 1980 and 1981, nine lines of multi-channel seismic reflection survey were carried out by the Hydrographic Department of Japan, in the Nankai, Suruga and Sagami Troughs bordering the northern subducting margin of the Philippine Sea Plate. Data were obtained by R/V Kaiyo-Maru of the Japan Petroleum Exploration Co., and processed for following methods; deconvolution, velocity analysis, 24-fold stacking, time migration, and depth conversion. Subduction of oceanic crust of the Philippine Sea Plate beneath the Japanese Islands is clearly recognized on migrated depth sections. Subducting oceanic crust is pursued for at least 30 km landward from the axis of the Nankai Trough with the inclination of 3°-5°. On the landward slope of the Nankai Trough, distinctly imbricated sediment bodies with many thrust faults were found. In the Suruga Trough, basement forming Izu Peninsula is traced beneath the Trough and western slope of it for about 8 km with the inclination of 7°-23°. In the Sagami Trough the basement forming Izu Peninsula is recognized beneath the Trough to the Misaki Knoll located eastern slope of the trough, with inclination

of about 10°.

Purpose of investigation

The project aims to clarify the deep crustal structure in the subducting plate boundary between the Philippine Sea and Eurasia Plates, by multi-channel reflection records along the Nankai, Suruga and Sagami Troughs.

Methods and operations

The investigation includes data acquisition on board as well as preparation of 24-fold stack sections along A-C lines in 1980, and preparation of migrated time sections and depth sections along A-C lines, and 24-fold stack sections and migrated time and depth sections along D-I lines in 1981. All operation of data acquisition and data processing were carried out by the Japan Petroleum Exploration Co. under the supervision of the Hydrographic Department of Japan.

(1) Track lines

Positions of track lines A to I summed up to 675 km are listed below and shown in Fig. 1.

Line A 34°54.3'N, 139°12.4'E and 35° 4.6'N, 139°35.0'E

Line B 34°27.4'N, 137°43.0'E and 34°26.9'N, 139° 4.4'E

Line C 34°13.7'N, 137°30.3'E and 34° 9.1'N, 138°35.4'E

Line D 34° 8.2'N, 138°17.7'E and 34° 0.2'N, 138°38.3'E

Line E 34° 6.7'N, 138° 2.3'E and 33°35.6'N, 138°33.6'E

Line F 33°56.2'N, 137°47.4'E and 33°25.3'N, 138°18.8'E

below sea level, depth of receiving 15 m below sea level, interval of emission and receiving points 50 m respectively, interval of sampling 4 miliseconds, recording time range to 11 seconds and methods of recording by MT of 1600 BPI.

(3) Data processing

Obtained data were processed by computer system of IBM 370 utilizing soft-ware packages for analysis of integrated position fixing data, and for multi-channel reflection records. The flow of data process was shown in Fig. 2. For each track line, 24-fold stack section, migrated time section and migrated depth section were prepared. The interval of common reflection points was 25 m in distance. Velocity analysis was done according to CVSTACK method which determines velocities by 5 fold stacking for each 2.5 or 3 km.

Results

Migrated depth sections of surveyed nine lines are shown Figs 3 to 11.

(1) Line A (Fig. 3)

Basement reflector of the Izu Peninsula is pursued from west to east with inclination of about 10° to beneath the Misaki Knoll. Trough sediments thickens towards east up to 4000 m beneath the west slope of the Misaki Knoll. The sediments are divisible into two parts; the upper part is thick at the center of trough and the lower part thickens towards the Misaki Knoll. The declining of sediment layers towards northeast in the small basin northeast of the Misaki Knoll suggests the uplift of the Knoll and tilting of

Line G 33°24.8'N, 137° 3.2'E and 32°54.0'N, 137°34.6'E

Line H 33°14.1'N, 136°38.5'E and 32°35.4'N, 136°53.1'E

Line I 33° 7.8'N, 136° 0.1'E and 32°29.2'N, 136°15.1'E

Line A is about 40 km long traversing northern part of the Sagami Trough from eastern continental slope of the Izu Peninsula to the southern continental shelf of the Miura Peninsula. It traverses Misaki Knoll.

Line B and C are about 125 km and 100 km long respectively traversing southern part of the Suruga Trough and the northern part of the Nankai Trough along E-W direction. The former traverse includes the Izu Spur and Omaezaki Spur, and the latter includes southern part of the Kanasu-no-Se and Tenryu Canyon.

Line D, E and F are about 35 km, 75 km and 75 km long respectively, traversing northern part of the Nankai Trough. Latter two lines are across the Zenisu Ridge in their southeastern part.

Line G, H and I are about 75 km long and across the Sikoku Basin, Nankai Trough and continental slope off the Kumano Trough.

(2) Details of data acquisition on board

On board operations were carried out in September, 1980 for A-C lines and January to February, 1981 for D-I lines. Details of operation are as follows;

Vessel: R/V Kaiyo-Maru of Japex, 991 tons.

Positioning system: Magnavox navigation/positioning system utilizing integrated satellite, Loran C and doppler sonar.

Equipment of reflection exploration: Air-gun array of explosion power up to 140 kg/cm^2, 48-channel SEC streamer of 2400 m long and DFS V recording system of Texas Instruments Co.

Parameters of reflection exploration: Depth of emission 8-10 m

the basin.

(2) Line B (Fig. 4)

General structure in the Suruga Trough is similar to that of the Sagami Trough but in reverse order; the basement of the Izu Spur declines toward west with inclination about 23° and is pursued to the foot of continental slope of the Omaezaki Spur. Distinct foldings and thrust faults beneath the foot of the continental slope of Omaezaki Spur suggest the subduction of the basement of the Izu Spur belonged to the Philippine Sea Plate under the Omaezaki Spur belonged to the Eurasia Plate, and the accretion of trough sediments to overriding plate margin.

Thick sediments more than 2000 m are found in the west of the Omaezaki Spur. This is the sedimentary basin formed behind the outer ridge on the landward slope. Although Ishibashi(1976) postulated so-called East-off-Izu Tectonic Line which was supposed plate boundary between the Philippine Sea and Eurasia Plates, such tectonic zone was not recognized on the eastern part of this section.

(3) Lines C and D (Figs 5 and 6)

The basement of the Zenisu Ridge declines towards W to WNW with inclination of 7° along both sections. The lower continental slopes of the Kanesu-no-Se shows stepped slope and thrust faults dipping to west. The trough sediments layered horizontally or slightly inclined towards west have thickened from east to west and formed wedge-like shape which suggests the turbidite origin like other trenches.

There is a thick sediments dipped to west at the western slope

of the Kanesu-no-Se, which suggest relative uplift of the Kanesu-no-Se. This fact is similar to the uplift of the Misaki Knoll recognized along line A despite the direction of subduction is reverse. Another basin including thick sediments of 1000 to 1500 m gently folded is found in the environs of the Tenryu Canyon, beneath of which acoustic basement is observed. These sediments are pursued from the west of the Kanesu-no-Se so that line C traverses the peripheral part of the sedimentary basin backward of the outer ridge.

There are two remarkable reflectors at about 300 m deep beneath sea bottom 12 to 23 km and 48 to 60 km from the west end of the both records. These reflectors are considered as the lower plane of the gas-hydrate layer which contains ice dissolving much gas of methane.

(4) Lines E and F (Figs 7 and 8)

On the records of lines E and F, there are two reflectors inclined to landward. The upper one is the basement of the Zenisu Ridge, and the lower one is the surface of oceanic crust of the Sikoku Basin which becomes distinct in lines G to H.

Wedge sediments of 2500 m thick in line E and 3000 m thick in line F, are deformed and displaced by horizontal compression, which resulted in foldings and thrust faults. Although steps on continental slope are supposed to be effected by the compressional force, the inside structure are too obscure to discriminate foldings or faults.

The distinct reflector at the northwestern end of the line F is also gas-hydrate layer.

(5) Lines G, H and I (Figs 9, 10 and 11)

On the records of line G to I, remarkable reflector which is considered as the surface of oceanic crust, is continuously pursued from the Sikoku Basin to the landward slope. The average inclination of these basement reflectors ranges 3-5° and it is traced to about 30 km in line G, about 35 km in line H and about 20 km in line I beyond the foot of the continental slope.

In the Sikoku Basin sedimentary layer of 1000-1500 m thick deposited in parallel to the basement is recognized, above which wedge sediments in the bottom of the Nankai Trough is formed. The wedge sediments are nearly horizontal along lines H and I, but is gently undulated along line G.

Landward slope which was called 'ridge and trough zone' by Iwabuchi (1970), is composed of alternating small highs and lows parallel to the direction of the Nankai Trough. At the foots of landward slope in lines G and I, wedge sediments of trough bottom intrude beneath the slope or landward slope overrides above wedge sediments with thrust fault. The landward slope in line I is structured by thrust faults and compressional folds, which result in the topographical highs in the 'ridge and trough zone'. These features suggest compressional stress of the subduction of the Philippine Sea Plate. The landward slope are underlain by a series of accreted sediments that overlie the trough bottom and the Sikoku Basin.

Another distinct feature observed in lines G and H is big fault on the seaward swell of the Nankai Trough, of which downthrow to SE is about 3000 m in line G and about 600 m in line H. Although the distance between two lines is 70 km,

these faults are supposed to be continuous because they are located at the outer part of the seaward swell and both faults have same direction of down throw.

Discussions

(1) Subduction of the Philippine Sea Plate along the Nankai and Suruga Troughs

All records of line B to I show the basement continued from trough bottom to the foot of landward slope. Some records in the western region show further continuation of the basement beneath the landward slope. This clearly proves the subduction of the Philippine Sea Plate beneath the Eurasia Plate along the southern part of the Suruga Trough and the eastern part of the Nankai Trough. Fig. 12 shows the subbottom topography of the surface of the basement; oceanic crust of line G to I dips 3-5° towards NNW and has some complicated relieves, it dips 5-10° toward NW in lines E and F, and 7-23° toward WNW in lines B to D. The reflector shown in line B to D is the surface of the basement of the Izu Spur and Zenisu Ridge, which is pursued to line E and F where is observed another reflector recognized at lower horizon than it. It is correlated to the surface of oceanic crust in lines G to I, so that the contour lines in Fig. 13 are shown in dashed line for the upper one and solid line for the lower one.

(2) The structure of landward slope

All records beneath landward slope are very complicated by intense deformation and displacement and become obscure to

analyse. However, there are many compressional thrust faults and foldings. As seen in lines G and I, folded sediments overlie the wedge sediments in trough bottom and the boundary of them is thrust fault. The anticlinal high at the northwestern margin of the Nankai Trough in line E is considered as the embryonic folding of wedge sediments which will convert to compressionaI folding of landward slope. These features are well explained by the concept of imbrication structure of the accretionary prism at trench slope. The ridge and trough relieves at intervals of 20-30 km on the landward slope of the Nankai Trough in lines E to I and the stepped slope of the Suruga and Nankai Troughs in lines B to D are surface expression accreted sedimentary bodies. This difference of the bottom topography is considered as the result of the difference of subducting inclination of the underlain plate and the original landform of landward slope.

(3) P-wave velocities

During the data processing, velocity analysis by CVSTACK method were carried out before stacking and migration. The results are summarized below.

(a) Wedge sediments of trough bottom

The P-wave velocity of the wedge sediments ranges 1.8 to 3.0 km/sec which increase from surface to lower horizon. The velocity more than 3.0 km/sec was measured at the lowest part of the Sagami Trough in line A.

(b) Ocenic sediments in the Sikoku Basin

It ranges 1.6 to 2.9 km/sec similar to that of the wedge

sediments. However, it becomes 2.2 to 3.2 km/sec in trough where wedge sediments overlie.

(c) Deformed sediments beneath landward slope

Although detailed velocity is not obtained as there is scarece of remarkable reflector, it is supposed to range about 2 km/sec at surface and up to about 4 km/sec near to acoustic basement.

(d) Oceanic crust in the Sikoku Basin

As there is no reflector other than the surface of the basement, velocity is not obtained except one place about 15 km from the southeastern end of the line H'(Fig.13), where deep reflector was recognized and velocity of 4-6 km/sec was obtained.

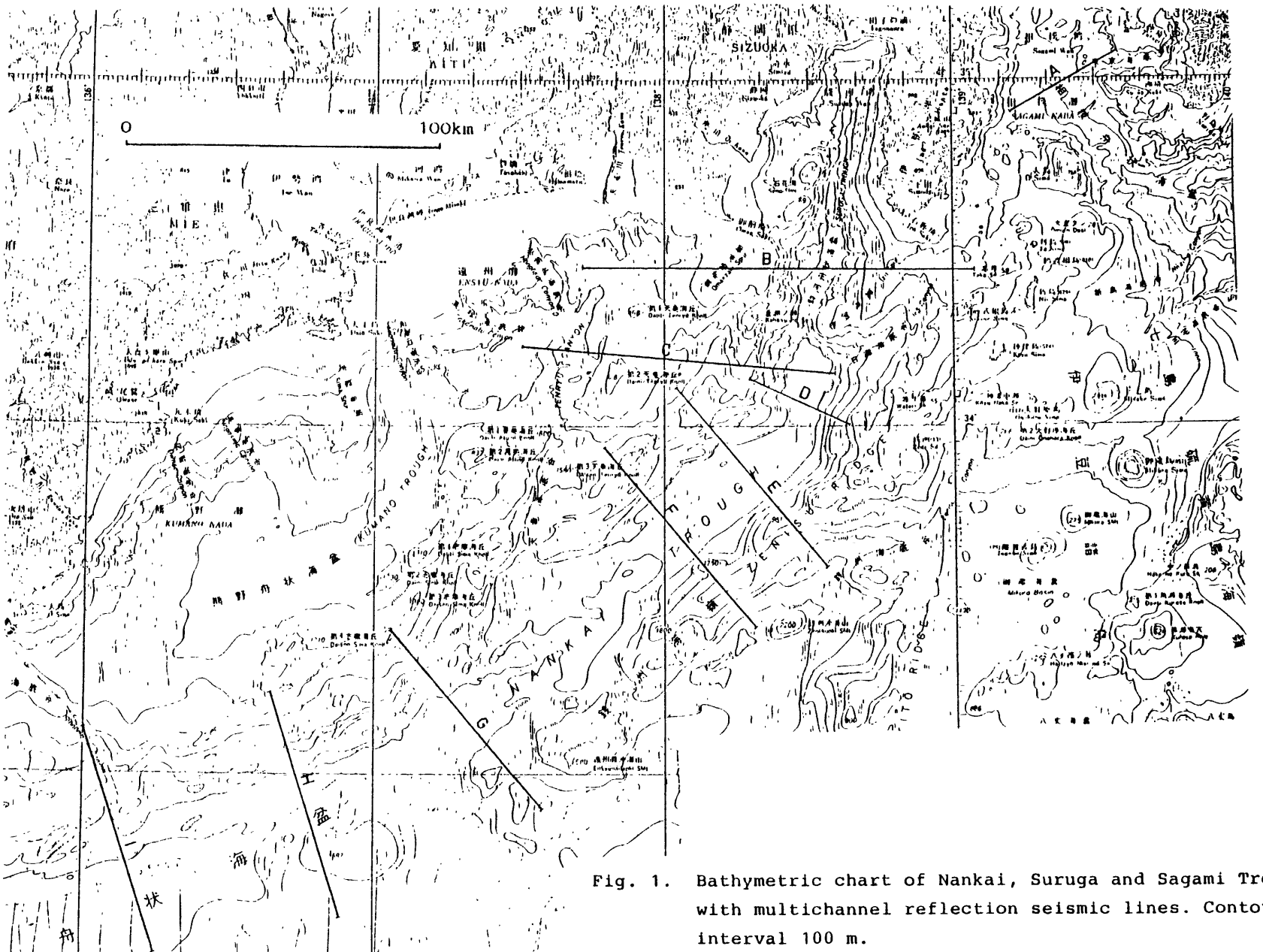

Fig. 1. Bathymetric chart of Nankai, Suruga and Sagami Trough with multichannel reflection seismic lines. Contour interval 100 m.

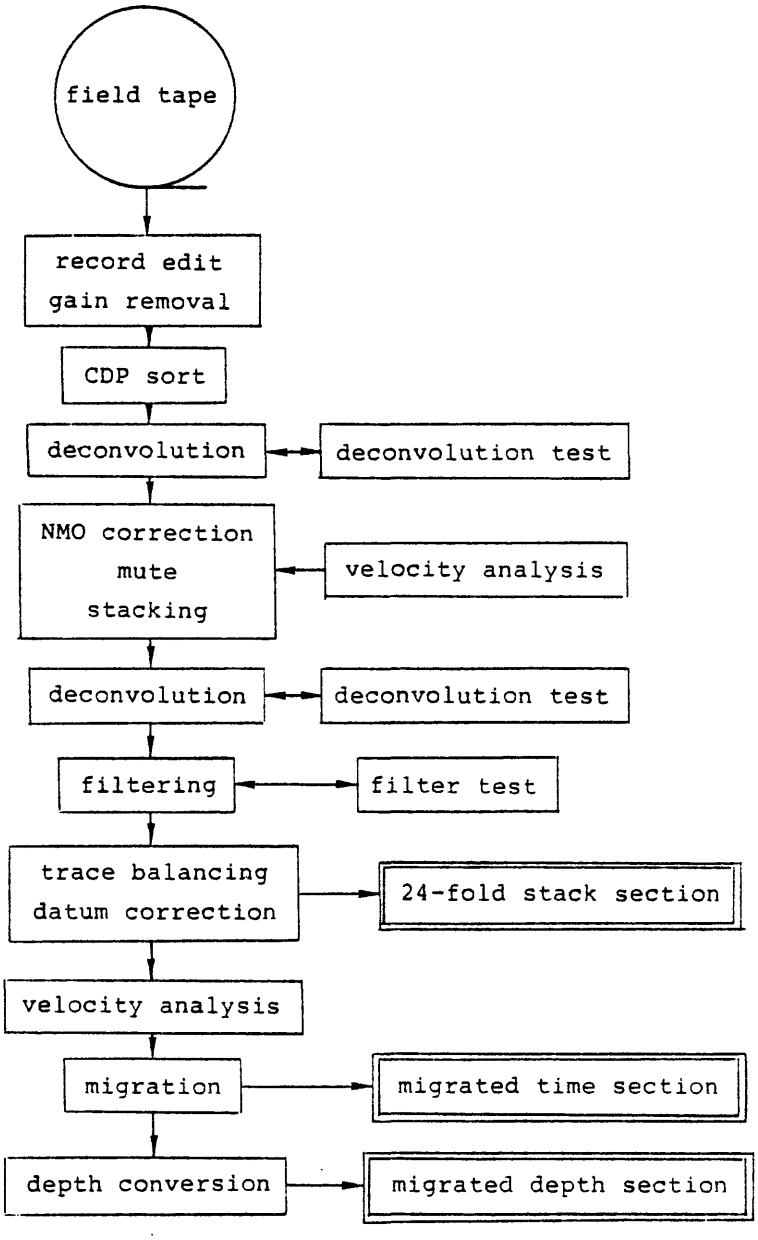

Fig. 2. Flow chart of seismic data processing.

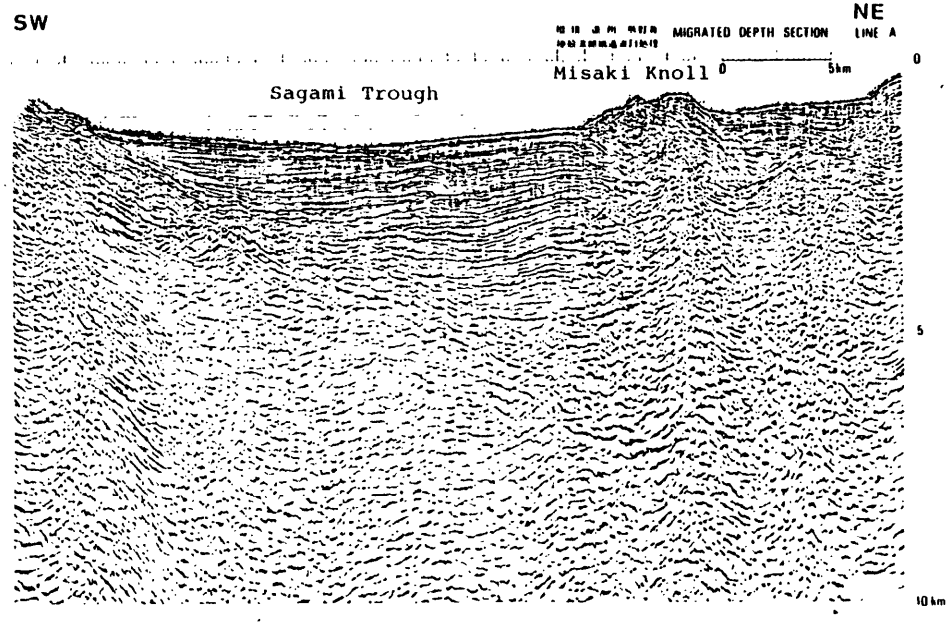

Fig. 3. Migrated depth section of line A. Figure location is indicated in Fig.1. Vertical exggeration 2.5x.

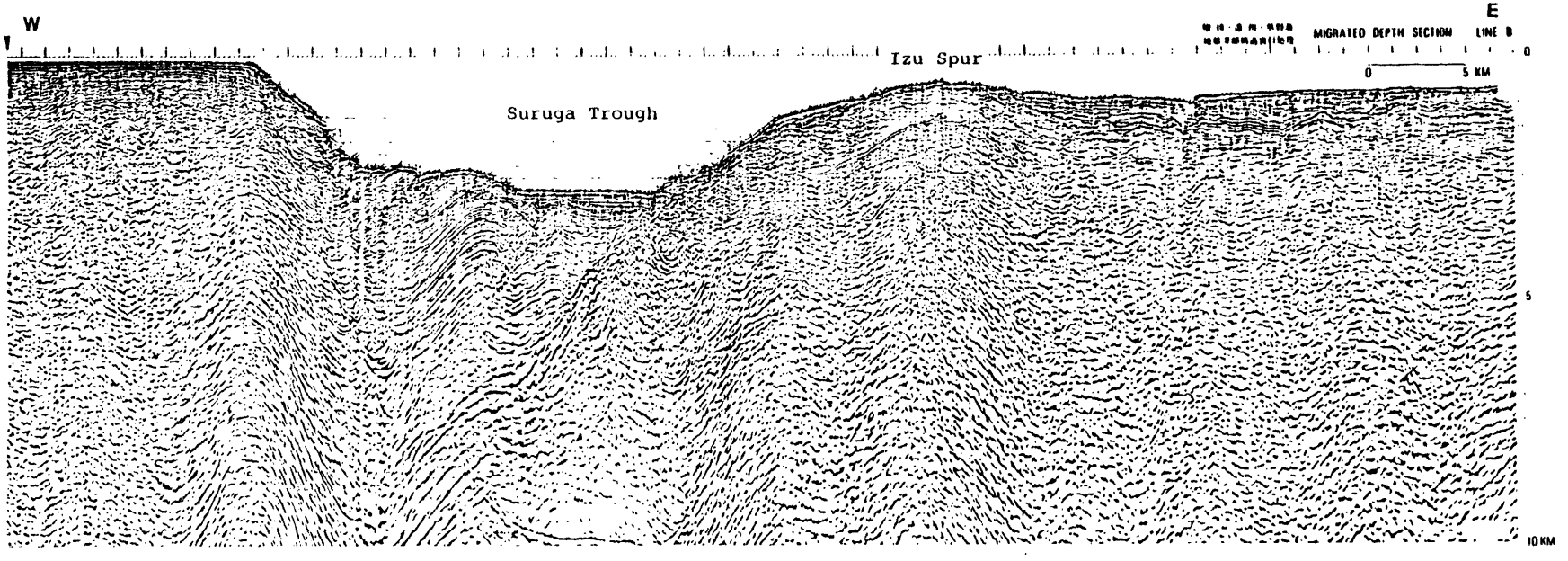
W
E
MIGRATED DEPTH SECTION
LINE B
Izu Spur
Suruga Trough
0
5 KM
5
10KM

Fig. 4 Line B

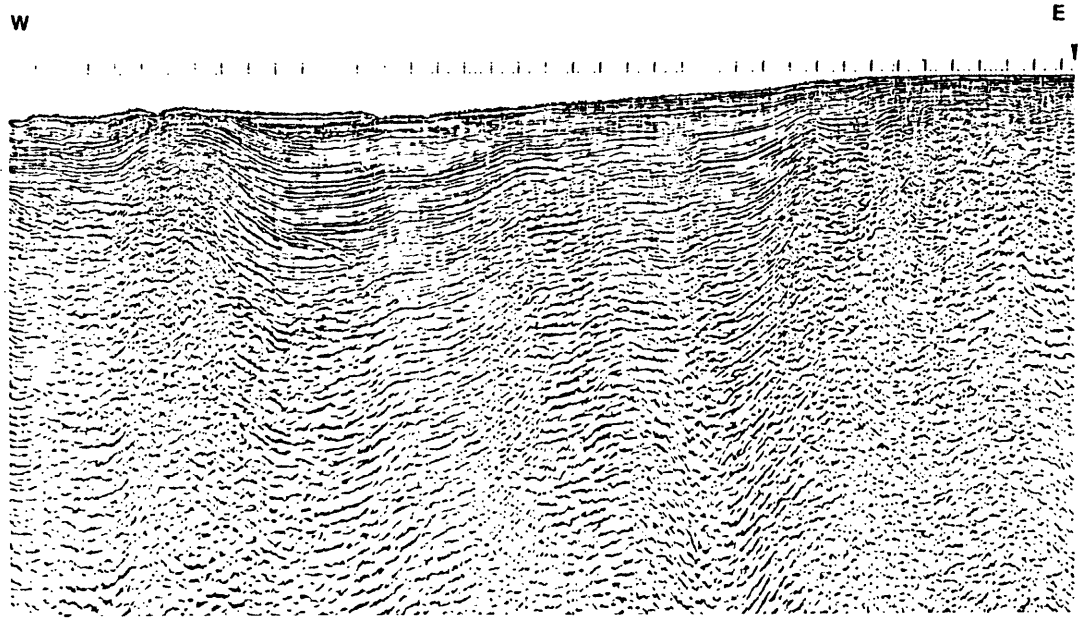

Fig 4' Line B

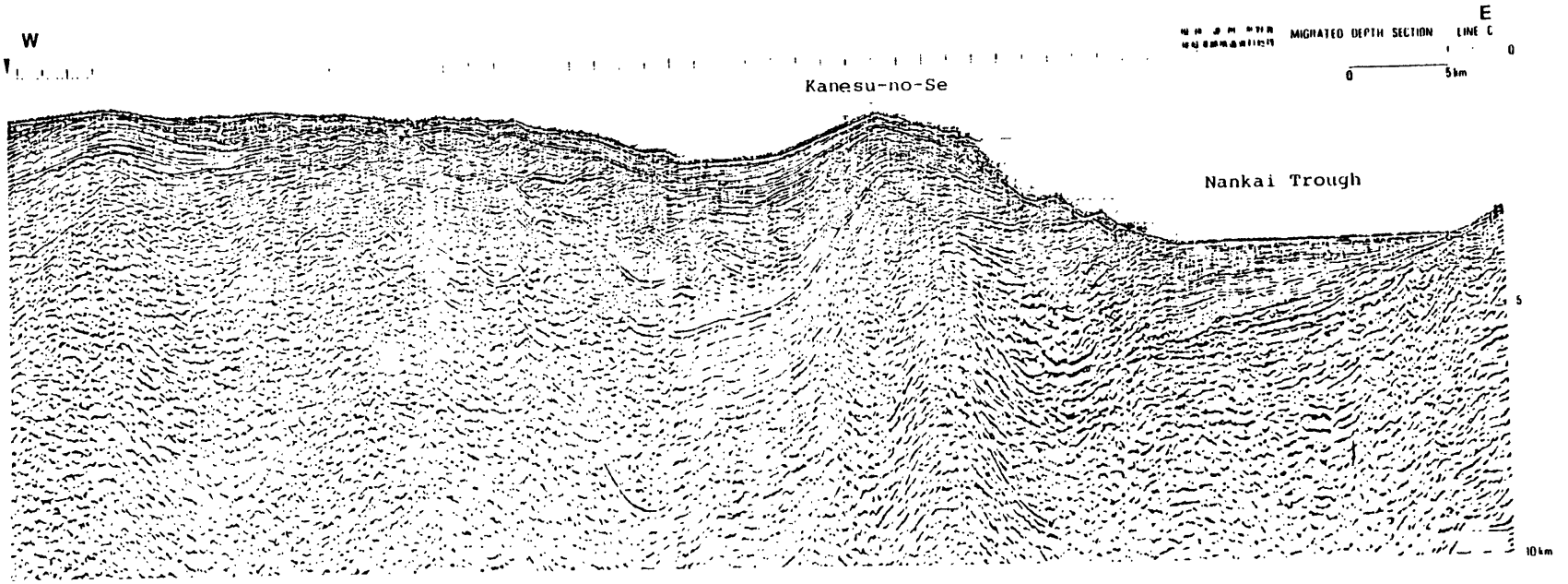
W
E
MIGRATED DEPTH SECTION LINE C
0
0 5km
Kanesu-no-Se
Nankai Trough
5
10km

Fig. 5 Line C

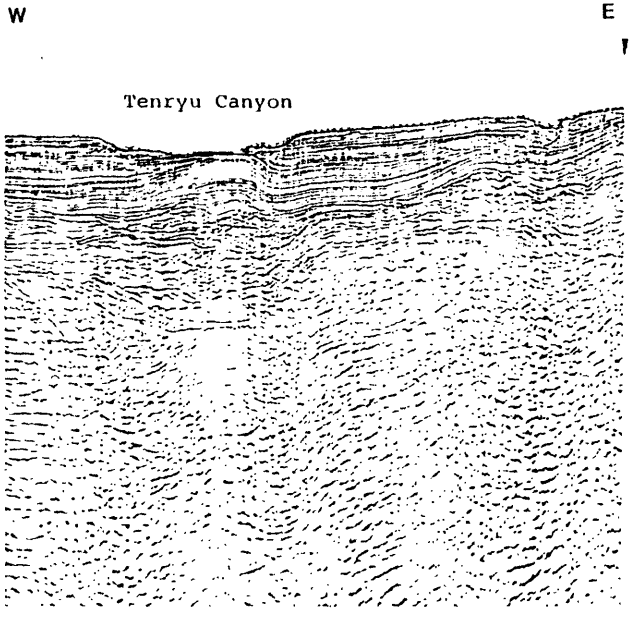

Fig. 5' Line C

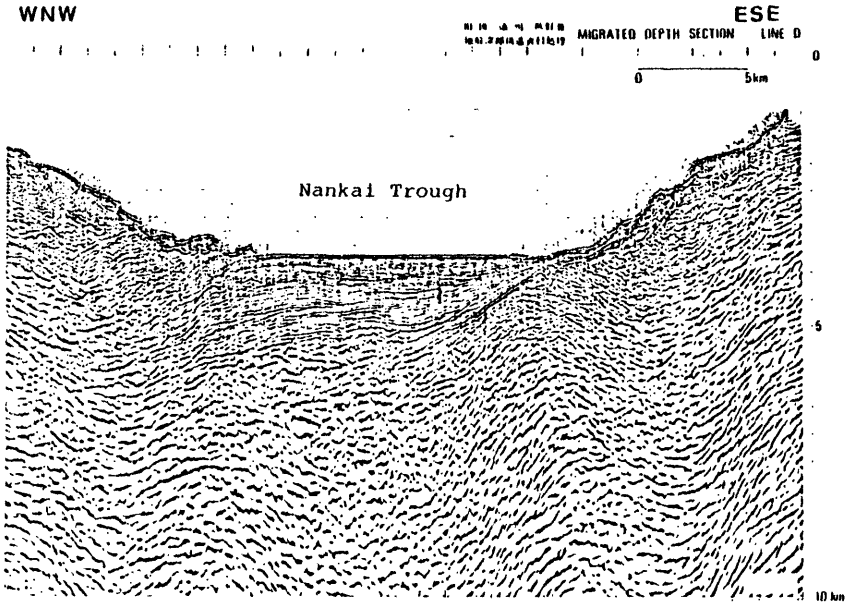
WNW
ESE
MIGRATED DEPTH SECTION LINE D
0
0
5km
Nankai Trough
5
10 km

Fig. 6 Line D

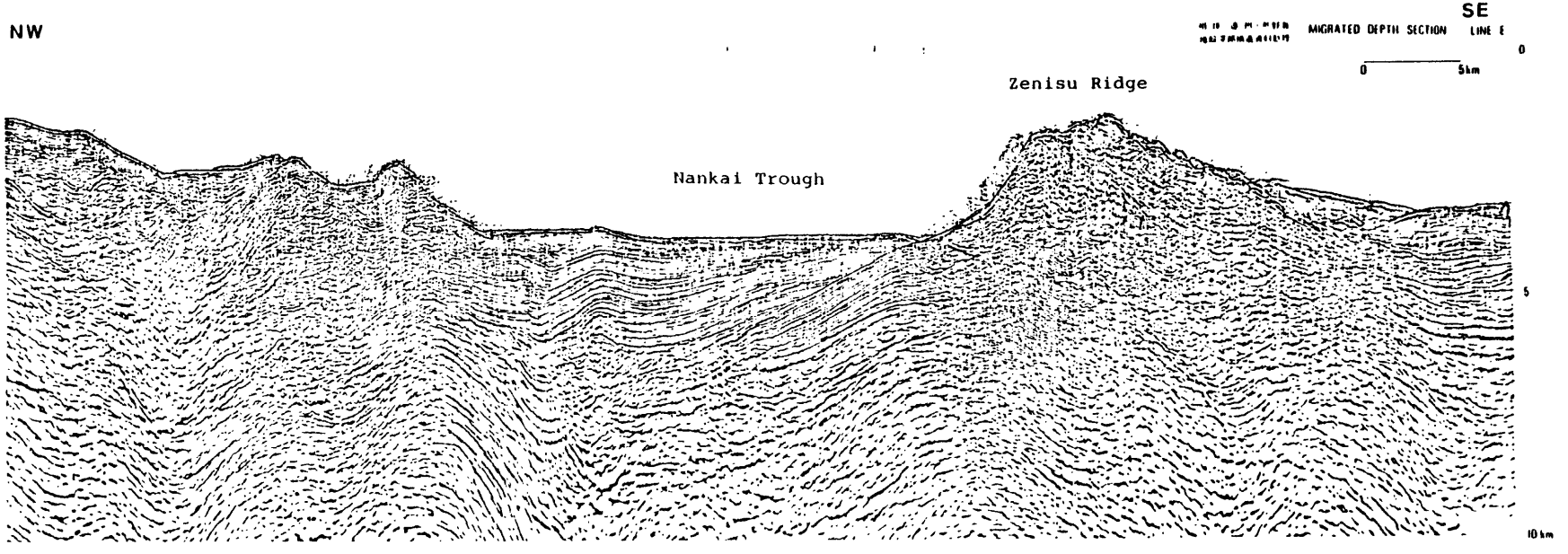
NW
SE
MIGRATED DEPTH SECTION LINE E
0
0
5km
Zenisu Ridge
Nankai Trough
5
10km

Fig. 7 Line E

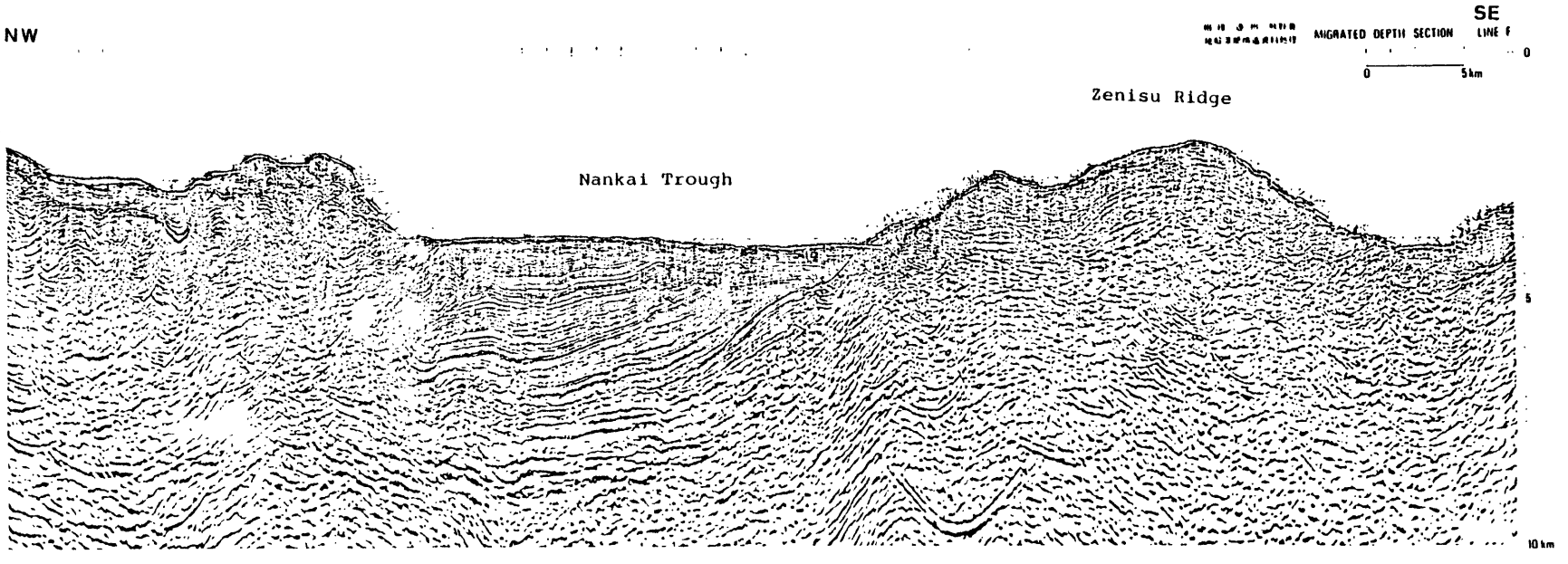
NW
SE
MIGRATED DEPTH SECTION
LINE F
0
0
5km
Zenisu Ridge
Nankai Trough
5
10km

Fig. 8 Line F

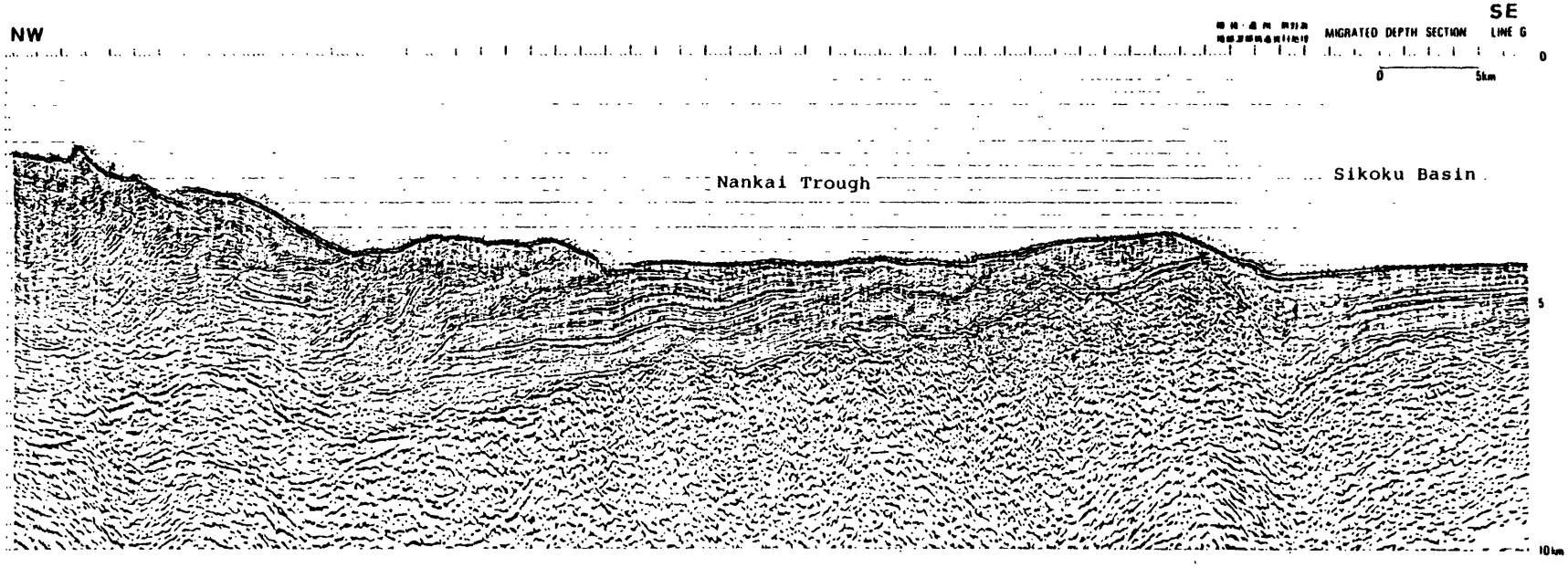
NW
SE
MIGRATED DEPTH SECTION
LINE G
0
0
5km
Nankai Trough
Sikoku Basin
5
10km

Fig. 9 Line G

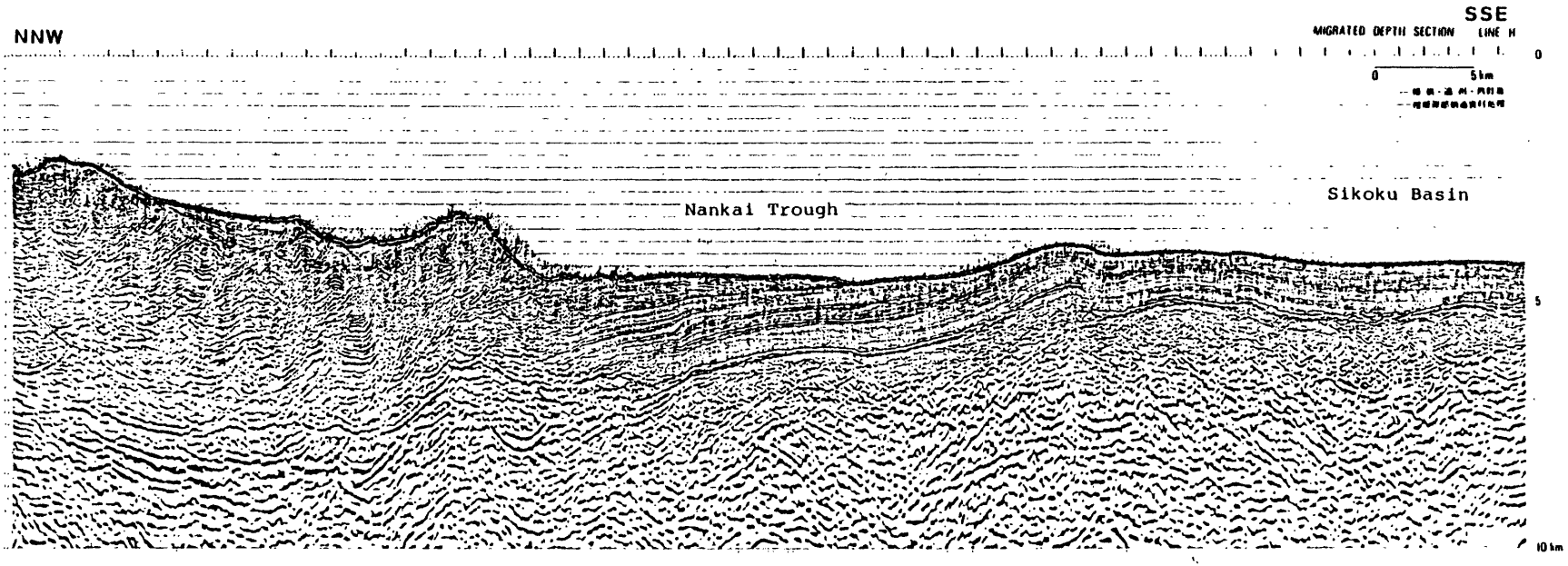
NNW
SSE
MIGRATED DEPTH SECTION LINE H
0
0 5km
Nankai Trough
Sikoku Basin
5
10 km

Fig. 10 Line H

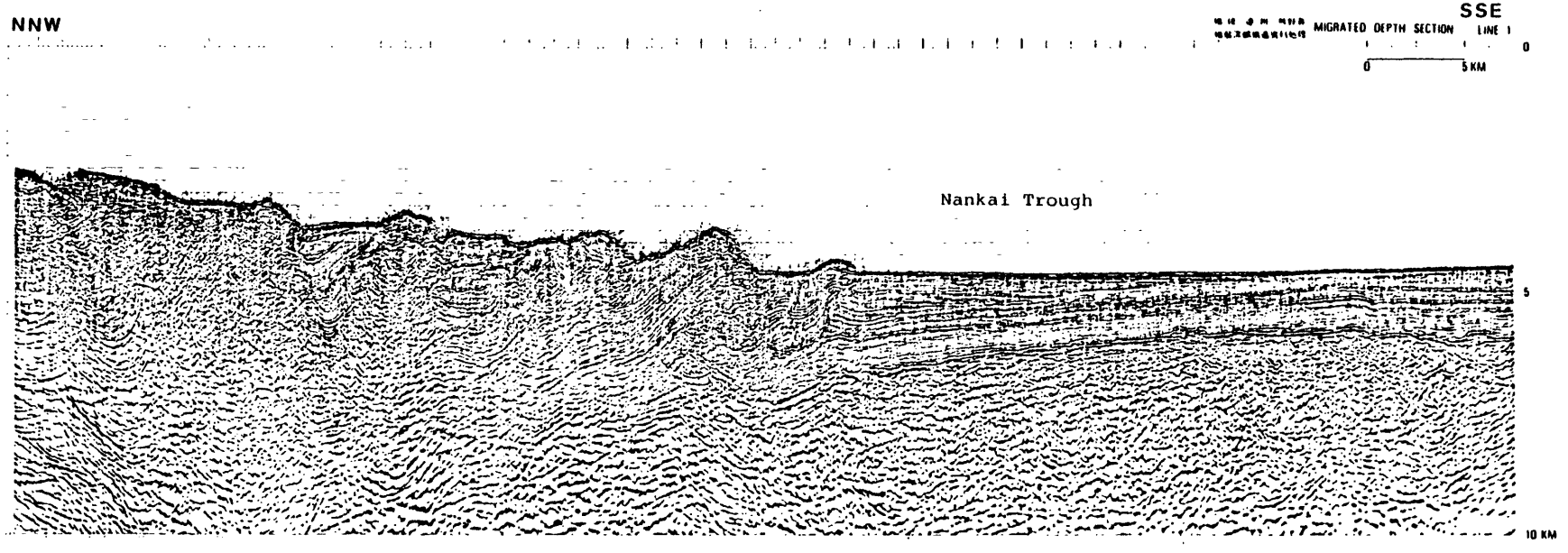
NNW
SSE
MIGRATED DEPTH SECTION LINE I
0
0 5 KM
Nankai Trough
5
10 KM

Fig. 11 Line I

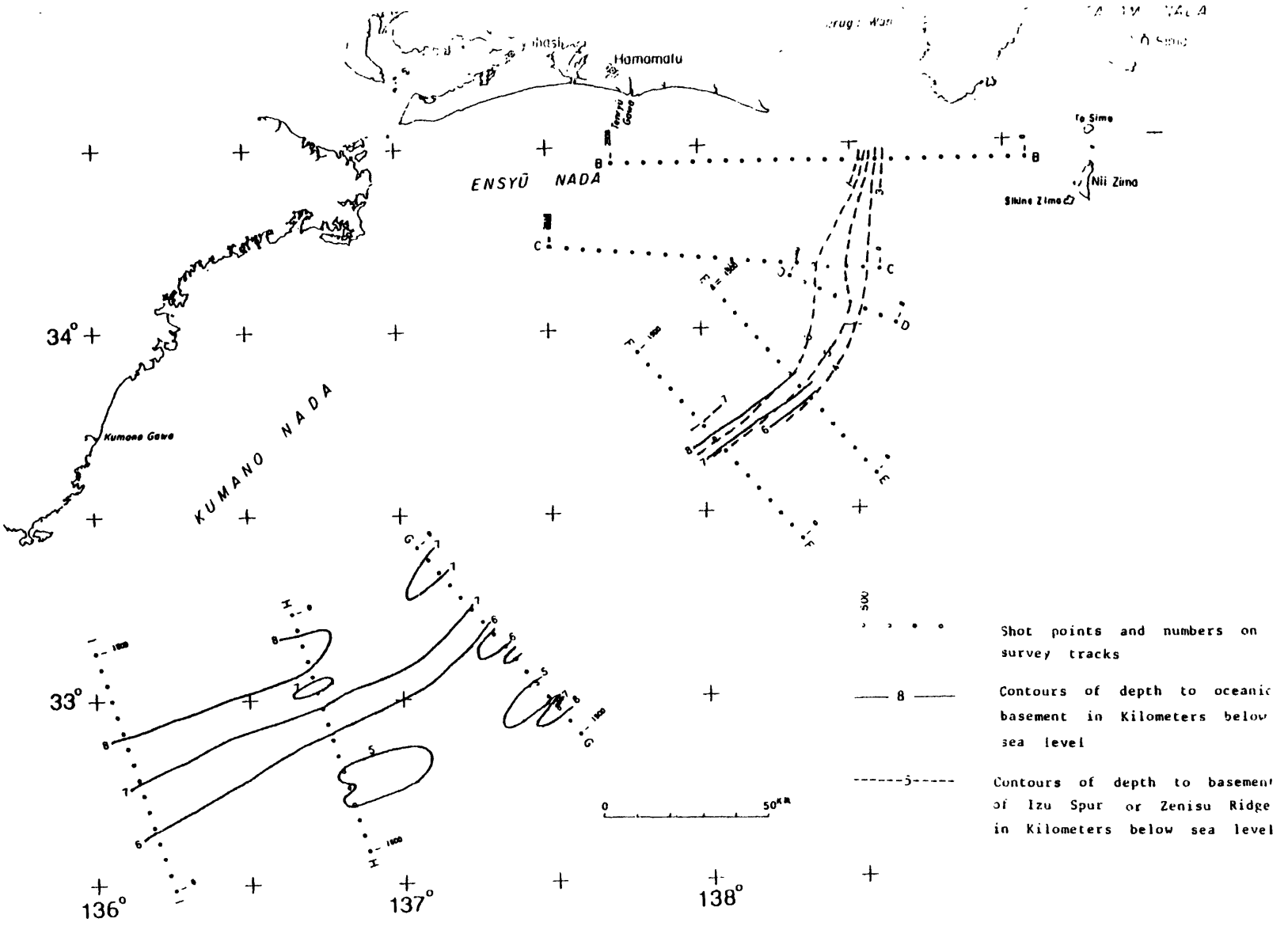

Fig. 12 Contours map of oceanic basement subducted in Nankai Trough.

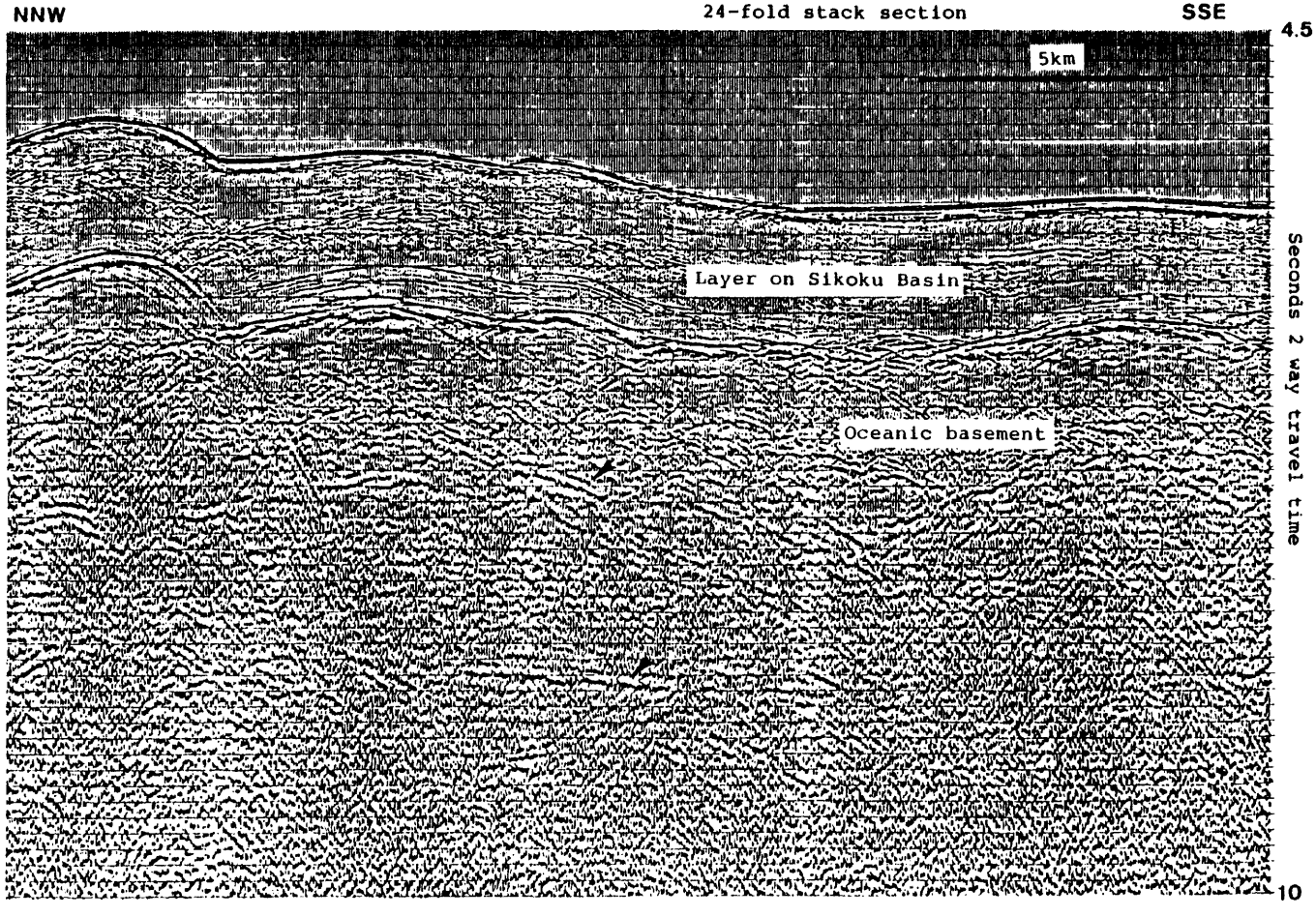

Fig. 13. Southeastern portion of the 24-fold stack section of line H. Notes to reflectors (➘) below the oceanic basement.

OVERVIEW OF NSF SUPPORTED FUNDAMENTAL EARTHQUAKE RESEARCH

Leonard E. Johnson

Seismology and Deep Earth Structure Program

National Science Foundation

Abstract

A brief overview is given of fundamental earthquake research supported by the Earth Sciences Division of the National Science Foundation. Some major accomplishments in several areas are outlined and some possible future directions for research are identified.

1. Introduction

In NSF, the Fundamental Earthquake Studies Element is supported primarily through the Seismology and Deep Earth Structure Program of the Division of Earth Sciences. Seismology is perhaps the most important area of geophysics in that it is the primary method of studying the structure and physical properties of the earth's interior and is a primary method of outlining the plates making up the earth's lithosphere. As such, seismology and other earthquake related areas have been of long term interest to the Earth Sciences Division and have in fact constituted an important part of the Division's program for some 20 years. The NSF program on fundamental earthquake studies consists of detailed studies and measurements directed at understanding the natural phenomena involved in an earthquake. The major goal is to establish a fundamental base of knowledge necessary for the potential prediction of earthquakes and destructive ground motion. An independent program of fundamental studies will provide the basic scientific framework on which more empirical programs of earthquake prediction can be based. Such a framework will help assure that an empirical program is scientifically sound and flexible, will provide direction for the optimal use of resources and, of course, will provide a reservoir of imaginative ideas, new experiments and basic theory if a particular empirical approach proves inadequate.

The program of fundamental earthquake studies at NSF can be defined in terms of two broad categories: plate tectonics and the earthquake process. The concept of plate tectonics states that a small number of rigid plates form the earth's outer surface and that the movement of these plates relative to one another is responsible for earthquakes and mountain building. The deposition of ores, burial of plant and animal life to form fossil fuels, volcanic eruptions, and many other phenomena are the consequences of plate tectonic processes. There is still much that we do not know about this revolutionary concept, including the answer to the underlying question of what causes the plates to move in the first place. When we know much more about why and how the plates move, we will have the basis of a much better understanding of many processes in the earth, including the prediction of earthquakes.

Our present concepts of the nature of the details of the earthquake process are derived mainly from seismic signals measured at large distances from the source. Consequently, the models used by seismologists today are generally not able to describe the variety of observed near-source features completely.

However, the prediction of earthquakes and destructive ground motion hinges on the thorough understanding of the mechanical processes leading to and constituting an earthquake. Both pre-earthquake phenomena and the ground motion caused by the

earthquake are tightly linked with the faulting process itself. Detailed measurements of geophysical fields associated with near-source pre-earthquake deformation must be made, therefore, in the neighborhood of the seismic fault.

We do not yet know what physical parameters are the most critical or the details of rock properties that cause an earthquake. The failure criteria of crustal rocks and the role of pre-earthquake deformations must be understood in order to calculate the re-initiation of motion on the fault and to determine the total seismic energy that is released. In addition, the material properties and the nature of the geology affect the amount of energy released and the characteristics of the generated motion.

Theoretical work is leading to a model of the initiation and propagation of catastrophic failure in rock, and this work must continue if we are to understand earthquakes. Experimental rock mechanics has been important in developing our concepts of the physics of the earthquake source, but extrapolation from the laboratory to nature has been only qualitative because of the difficulty of scaling both in size and in time. The range of temperatures and pressures in laboratory experiments should be representative of conditions in the earth's crust and upper mantle.

In short, to solve the problem of earthquake prediction, a blend of theoretical, laboratory and field studies is essential.

2. Major Accomplishments

Substantial advances have been made in recent years in each of the areas mentioned above. Some of them are outlined below. Taken together, the list comprises a partial statement of the current status (where we now stand) in each of the two broad categories of fundamental earthquake studies at NSF:

Plate Tectonics

Delineation of "Seismic gaps" and a map of seismic potential for the simple major plate boundaries of the world.

Increased knowledge of the nature of subduction zone earthquakes and the physical processes by which they are generated.

Better knowledge and understanding of the state and magnitude of stress in the Earth's lithosphere.

Evidence that most large plate boundary earthquakes are complex multiple shocks that consist of a number of smaller events.

The association of the location of particular intraplate earthquakes with faults and other tectonic features.

The improved delineation and understanding of lateral heterogeneity in the Earth.

The Earthquake Process

A better understanding of the processes that go on in rocks prior to an earthquake and of the details of the final rupture and energy release.

The introduction of a new, more quantitative measure of the "size" of an earthquake, the moment.

The inversion of seismic data to determine the moment tensor as a function of time - a measure of the temporal pattern of stress release.

The improvement of discrimination between earthquakes and nuclear explosions.

Improved procedures to compute synthetic seismograms.

A better understanding of the dynamic processes of faulting -- how a fault rupture nucleates, spreads, and finally stops, and the effects seen in seismograms from each of these three stages in the faulting process.

An increased knowledge of the phenomena that occur on a fault within the zone of crushed material referred to as "gouge."

The discovery that a number of major earthquakes have been preceded by a premonitory clustering of small earthquake events in their epicentral regions.

Research on tilt, magnetic field, resistivity and gas emanation has furnished some suggestive but not universally accepted precursory data.

3. Additional Activities of Special Note

Detailed Study of Continental Structure

The Consortium for Continental Reflection Profiling (COCORP) project is using deep seismic profiling to provide several types of information of importance to the understanding of earthquakes and to the reduction of earthquake hazard.

Ultra Long Period Seismology

A new network of very long period seismographic stations is being established around the world; the International Deployment

of Accelerometers (IDA) network. Data from this network is providing a unique set of high-quality, very long period digital seismic data for a number of new and important studies of the earth. Such data, previously not available, can be used to study the mechanism of earthquakes.

Instrumentation

The needs of geodesists for better benchmarks and for better methods to measure regional deformation, strain and tilt have led to the development of new "state-of-the-art" instruments. Notable among these are: 1) the cryogenic, superconducting gravimeter; 2) the long baseline (about 1 km) laser strain meter; 3) the long baseline (500m) tiltmeter; 4) the two and three color laser geodimeters; and 5) the stable laser interferometric benchmark.

Ocean Bottom Seismology

Recent developments in ocean bottom seismographs (OBS) have greatly improved both the quality and quantity of data from offshore events.

4. Future Directions

Results from past work have indicated a number of important directions in which research should currently be directed. It is not possible to predict what a fundamental studies program will be

in future years. We can only plan to continue and complete the most interesting and promising work currently in progress, realizing that the actual work over the next few years will be guided by major discoveries that emerge, often unpredictably.

We, can, however, list some important areas that must be continued or initiated:

Initiation of new studies and expansion of current effort is needed to investigate the deep continental lithosphere.

The development of reliable ocean-bottom seismometers (OBS) for long term ocean floor recording of seismicty, particularly along ridge crests, fracture zones, and near subduction zones.

There is a need for an increased understanding of the relationship of earthquakes to tectonics and geology. A better understanding of the distribution of stress in the earth, obtained from surface geodetic and stress measurements and from earthquake studies, may answer some of these questions.

In the past, seismologists were limited to studies of abrupt seismic sources because the existing technology was not sufficiently advanced for study of long term

dynamical effects. New instrumentation now allows us to open up the whole important area of dynamical source mechanics, i.e., seismic source phenomena with very long-term characteristics. At low frequencies, we can study the longer time history of earthquake sources and particularly the hypothesized "slow earthquakes" that may precede the more usual ones with which we are familiar. Continued augmentation of global broadband digital networks is desirable.

Lack of knowledge about the inelastic properties of the earth represents a major gap and is one of the most pressing problems in seismology. In order to determine the structure of the earth from broadband seismic data, it is necessary to incorporate the effects of seismic-wave attenuation. The use of synthetic seismograms in the quantitative study of amplitudes of seismic waves is a recent advance in this area, but further observational, theoretical, and laboratory investigations are needed.

We need to know the properties of the large-scale rock mass, i.e. the rock as it occurs in nature, with its ensemble of joints, fractures and inhomogeneities.

Laboratory studies are needed on the time-dependent mechanical properties of rock since these are poorly

understood and may dominate processes at geological strain-rates.

International cooperation in research will be especially important in the near future as seismologists seek ways to predict earthquakes. Opportunities to acquire data and experience related to the prediction of major earthquakes, which are rare events at any one location, are essential to progress. By preparing cooperatively to make observations related to occurrences of strong earthquakes in many parts of the world, the international seeismological community can optimize its chances of being in the right place, with the right instrumentation, at the right time, for the benefit of all nations afflicted by earthquake disasters.

The following table gives the funding history of fundamental earthquake studies in NSF from the inception of the National Earthquake Hazards Reduction Program. Fiscal years (FY) run from October 1 to September 30. The numbers are millions of dollars.

FY 78	FY 79	FY 80	FY 81	FY 82
5.3	6.0	6.6	7.0	7.1

It is not realistic to attempt to predict the outcome of a fundamental research program in terms of "technical milestones." Nevertheless, we can reasonably predict that a basic research effort, focused on projects with a strong potential for application to earthquake prediction and hazard reduction, will result in a more comprehensive understanding of the earthquake process. Progress in such basic understanding can be expected to increase the efficiency as well as the reliability of earthquake prediction. Some present approaches to the problem, although promising, may conceivably fail. This is good reason to have a reservoir of imaginative ideas, new experiments, and basic theory that fundamental studies can generate.

A LASER EARTH STRAINMETER WITHOUT VACUUM-PIPE

Shoichi Seino and Tadanao Ohishi

National Research Laboratory of Metrology

Abstract

A vacuum-pipeless laser strainmeter has been designed, tested, and is described. The strainmeter has a compensator for the change of the refractive index of air which is determined by Edlén's formula using measured values of atmospheric pressure and temperature. The effect of air-condition change was compensated by the compensator, and residual of the effect was less than 5×10^{-9} for 75 h. The strainmeter has successfully recorded solid tidal strains.

INTRODUCTION

A simple and portable earth strainmeter enables active measurements at many places. Untill now the most widely used are Benioff type strainmeters using quartz or invar rods. This type of strainmeter is not mobil because these instruments require large amounts of labour and time for construction and installation.

Long path laser interferometers are beginning to be used to measure strains in the earth's crust.[1-7] Some of them are easier to move than the Benioff-type, but all require vacuum pipes to avoid being affected by the change of the refractive index of air. The vacuum pipe is too long to move; it must be divided into several units, and those units must be reassembled every time the strainmeter is moved. Moreover, the vacuum pipe requires rotary pumps, which radiate heat and generate vibration; these undesirable effects on the measurement.

Searching for a portable unit we considered the possibility of a vacuum pipeless laser strainmeter. When length or displacement measurement is made in air with an interferometer, the measured value is affected by the variation of the refractive index of air. In spite of the disadvantages, measurements of end standards or line standards have been made in air; in this case the refractive index of air is measured by other means, and its effect is corrected. When this method is introduced into the earth strain measurement, the most important problem is how accurately the variation of the refractive index is measured. In the measurement of line standards, for an optical path shorter than 1 m, the refractive index of air determined with an accuracy of better than 1×10^{-7} by measuring the air conditions: atmospheric temperature, atmospheric pressure, and water vapor pressure. It is, however, expected that the longer the optical path, the lower

the accuracy of the determined refractive index of air. Therefor, the accuracy in the refractive-index measurement was investigated for a 25-m long optical path in a tunnel. Unexpectedly, the accuracy in the refractive index measurement was about $\pm 5\times10^{-9}$. Moreover, using this type of strainmeter, tidal strains of 1×10^{-8} in amplitude have been recorded.

DESCRIPTION OF APPARATUS

The vacuum-pipeless strainmeter consists of a frequency stabilized laser, a Michelson-type interferometer with corner cubes, an interference fringe readout, and a compensator for the refractive index of air. The laser should have good frequency stabilty; we used a HP 5500C laser. The frequency stability of the laser was measured by Iwasaki and Sakurai[8]; using an iodine stabilized He-Ne laser as the reference. The stability was found to be 1×10^{-9}. The interferometer, as shown in Fig. 1, and most of the elements are mounted on a steel bench, and one of the reflectors is on another bench. These benches are installed on concrete bases which are fixed to rock in the earth's crust. The separation between them was 25 m. The interferometer has an optical path length modulator and a phase shifter. The optical path length modulator is a glass plate which makes rotational vibration around the vertical axis and generates vibration in interference fringes. The phase shifter consists of two glass plates: one is supported rigidly, and the other has a mechanism to tilt with a screw. The optical beam is divided into two halves; one of the beams tranmits through the fixed glass plate, and the other transmits through the tiltable glass plate. The phase difference between the two beams can be continuously varied by the screw.

To make the analog readout for fringe movement more convenient,

a rapid vibration is superimposed on the measuring fringes by the optical path length modulator. Then the fringes obtained will be vibrating, and the center will be slowly shifting. Two photodiodes are placed to receiv each half of the fringe pattern, and phase separation between them is adjusted to 90 using the phase shifter. The signals from the detectors are applied to an interference order to voltage converter. The converter consist of a bidirectional fringe counter, a digital-to-analog converter, and a low-pass filter: the bidirectional counter counts four for one fringe shift; the DAC generates an electric voltage corresponding to the count totalized by the counter: the low-pass filter eliminates the components of fringe vibration and the components of distortion in digital measurement. Then an output voltage from the converter is proportional to the movement of the interference fringes.[9,10]

As the output from the fringe readout contains a component caused by the change of the air conditions, this component should be eliminated. The elimination was performed by a compenstor which has three potentiometers and an operational amplifier. In measuring atmospheric pressure and temperature, the same is the case of the interference fringe readout, outputs from each measuring instrument are electric signals. As the outputs from the atmospheric pressure gauge and the thermistor are too small to be fed to the compensator, the signals are preliminarily amplified. The compensation is carried out with the operational amplifier by adding or subtracting the signals. The elimination of the components caused by the change of air conditions is carried out automatically by the compensator, and earth strains are recorded in real time.

MEASUREMENT OF THE CHANGE OF THE REFRACTIVE INDEX OF AIR

The refractive index of air depends on its content, such as water vapor or carbon dioxide. It also depends on the condition of the air: atmospheric pressure and temperature. Formulas to determine the refractive index of air as a function of atmospheric pressure, atmospheric temperature, and its contents were introduced by Edlén[11] and Masui.[12] According to Edlén, the refractive index of air containing 0.03% of CO_2 and in atmospheric pressure p mm Hg (133 × p Pa), atmospheric temperature t°C is given by

$$(n-1)_{t,p} = (n-1)_s \frac{0.0013823p}{1+0.003671t}, \qquad (1)$$

where $(n-1)_s = \{8342.13 + 2406030(130-\sigma^2)^{-1} + 15997(38.9-\sigma^2)^{-1}\} \times 10^{-8}$, and σ is the wave number in vacuum in micrometers. Using this formula, the change of the refractive index of air in a tunnel was measured. The tunnel, in Matsushiro in Nagano city, 200-km northwest of Tokyo, is in a hill surrounded by mountains. A part of the tunnel was enclosed by doors and used for the measuring place; the space was 30 m in length, 2.5 m in width, and 2 m in height. Next to this space was a small room for the measuring instruments. Dewdrops were always on the walls of the space, and the air in the space was very calm. In such conditions the air is almost saturated with water vapor. Therefore, it is considered that the variation in humidity is small. For this reason, factors affecting the refractive index, barometric pressure, and atmospheric temperature were adopted. By substituting the measured values of the above two factors into the formula, the refractive index of air was calculated.

To measure atmospheric pressure, a Texas Instruments precision pressure gauge model 145 was used with a type 2 fused quartz Bourdon

capsule. Its resolution is 0.00033% of the full scale (32.5 In. HgA; 1.1 x 10^5 Pa), namely, 0.37 Pa. The value corresponds to 1 × 10^{-9} of the refractive index of air. A change in pressure is converted into a rotational angle by the Bourdon capsule. This deflection of the capsule is optically converted into an electric signal. When the 150-Ω resistor is connected across the output terminals of the gauge, a voltage across the resistor is linearly proportional to the change in the atmospheric pressure. But the linear region of the output characteristics is limited.

To measure atmospheric temperature, a thermometer manufactured by Sibaura Electronics was used. The thermometer employs thermistors as sensors. Its range is from 13.7 to 14.7°C, and its relative accuracy is 1 mK. The output impedance is 3 kΩ. The thermistor is coated with glass and protected with a metal tube. Its heat releasing constant is 0.6-1.2 mW/K, and the risetime constant is 30-50 sec (both measured in air).

With these instruments, variations in atmospheric temperature Δt(K) and atmospheric pressure Δp(Pa) are obtained. Using these values, a variation in the refractive index of air Δn is calculated from Eq. (1):

$$\Delta n = (n-1)_s \left[\frac{ac}{1+bt} \Delta p - \frac{abcp}{(1+bt)^2} \Delta t \right], \qquad (2)$$

where a = 0.00138823, b = 0.003671, and c = 0.00750.

In the tunnel, the average values of the atmospheric pressure and temperature are 96 kPa (720 mm Hg) and 14°C, respectively. For the He-Ne laser of 633-nm wavelength, σ is 1.580. Substituting these values into Eq. (2), we obtain

$$\Delta n = (0.2738\Delta p - 91.78\Delta t) \times 10^{-8} \qquad (3)$$

A change in the refractive index of air is obtained by substituting the measured values Δp and Δt into Eq. (3). This caluculation, described in detail later, was made with an analog computer in real time.

COMPENSATION OF THE REFRACTIVE INDEX OF AIR

As before, measurements of the refractive index of air using the measured values of atmospheric pressure and temperature have been made; but most of them are for lengths < 1 m, and the accuracy is $\sim 10^{-7}$. The possibility of more accurate measurement of the refractive index of air for a longer path, such as 25 m, is not clear. Before measuring earth strain, a study of the accuracy of the refractive index of air calculated with Edlén's formula was made. For this purpose an interferometer having equal arm lengths of 25 m, as shown in Fig. 2, was used. As both reflectors of the interferometer are mounted on the same steel bench, earth strains do not cause any movement in the interference fringes. Fluctuations of wavelength of the laser, also, do not influence the fringes. The reason is that the interferometer has zero optical path difference. Only the difference of the refractive index of air in both arms makes movement of the interference fringes.

One arm was laid along a 25-m long steel pipe in which a quantity of air was sealed. Therefore, in this arm, the refractive index of air is constant. The other arm was covered with a plastic pipe which has several small holes every 3 m and a glass window at each end. The holes are for equilibration of inner and outer pressures of the pipe. The plastic pipe, 25 m in length and 80-mm i.d. inhibits air currents. Without the plastic pipe, stable measurement of the refractive index of air is not possible. In the plastic pipe the atmospheric temperature and pressure varied, namely, the refractive index of air varied. Atmospheric pressure was measured outside but near the pipe, and

atmospheric temperature was measured in the middle of the pipe. The output from the interferometer represents the whole sum of the refactive-index variation of each part in the optical path. On the other hand, the refractive index calculated by Edlén's formula using atmospheric pressure and temperature represents that of a point. By recording the difference between these refractive indices, the accuracy of this correction method was revealed.

As mentioned above, the atmospheric temperature and pressure and a shift of interference fringes are represented by electric voltages. To obtain the difference of these refractive indices by operating these voltages, an operational amplifier was used. As shown in Fig.3, each electric voltage has an operational coefficient by each potentiometer and is operated by the operational amplifier. Output voltage from the interferometer was 2.44 mV per one count(four counts correspond to one fringe shift). As one fringe shift is 1.27×10^{-8} of 25 m, th output was 7.71 mV/1×10^{-8}. External output voltage from the pressure gauge was 73.3 μV/Pa when a type 2 Bourdon capsule and a 150-Ω resister were used. On the other hand, from Edlén's formula, 3.65 Pa corresponds to a change of the refractive index of air of 1×10^{-8}(at 14 C, λ = 633 nm). Therefore, the output was 0.267 mV/1×10^{-8}. The output voltage from the thermometer was 10.7 mV/K; the output was o.117 mV/1×10^{-8}.

The output voltages from the pressure gauge and the thermometer were so small, compared with that of the interferometer, that they were preliminarily amplified. The amplification degree of the pressure signal was 18.3 and that of the temperature signal was 100. Weighting resistors for the interference fringe shift, for atmospheric pressure and temperature were chosen to be 7.67, 4.87, and 11.7 kΩ, respectively. The feedback resistor of the operational amplifier

was 49.8kΩ. The output from the operational amplifier V_c is described by

$$V_c = 5.00(\Delta F - \Delta p + \Delta t) \qquad (mV), \qquad (4)$$

where ΔF, Δp, and Δt are the fringe shift, pressure change, and temperature change in 1×10^{-8} of the refractive index, respectively.

An example of the refractive-index difference between that measured with the interferometer and that calculated is shown in Fig. 4. The variation of the difference was less than $\pm5\times10^{-9}$.

MEASUREMENT OF EARTH STRAINS

For the measurement of each strains, the configuration shown in Fig. 1 was used. The movement of fringes was mainly caused by atmospheric pressure variation, amounting to 3 ppm(see Fig. 5). By precise compensation for air factors, tidal strains of 1×10^{-8} in amplitude were clearly recorded. The record of strains (S) is compared with the record of a quartz strainmeter (Q) installed about 150 m apart. As shown in Fig. 5, both of them agreed with each other within experimental error. In other words, although the fringe movement caused by the variation of atmospheric pressure 300 times larger than that due to earth strains, the earth strains were recorded with relatively high accuracy. By this experiment, the possibility of a portable starainmeter is demonstrated.

EXTENSION OF WORKING RANGE

Linear region of the output characteristics of the atmospheric pressure gauge is limited and it does not cover ordinary barometric pressure change. The output characteristics of the gauge is shown in

Fig. 6: horizontal axis is atmospheric pressure change in counter reading(1 count reading corresponds to 375 Pa), and vertical axis is output voltage in mV. The output characteristics has nonlinear components. The nonlinear components are shown in Fig.7. From Fig. 7 it is found that: (1) to obtain an accuracy of 2×10^{-9} with linear compensator, working region of the compensator is limited within 2.5×10^{-6} (948 Pa), on the other hand, (2) the working region of a nonlinear compensator (digital compensator) is extended to twice of the linear one. A digital compensator, shown in Fig. 8, was adoped to next experiments. To check the performance of the digital compensator the configuration shown in Fig. 2 was used. The results of the experiment are shown in Fig.9 and Fig. 10. It become clear that the accuracy of the digital compensator is about $\pm1\times10^{-8}$. Then using the digital compensator and the interferometer configuration shown in Fig. 1, earth strains was recorded. The result is shown in Fig. 11. Earth tides of 2×10^{-8} in amplitude was observed.

The authors are grateful to the members of the Matsushiro Seismological Observatory for their permission to use the tunnel, for their data recorded with a quartz strainmeter, and for their good wishes.

REFERENCES

1. V. Vali, R. S. Krogstad, and R. W. Moss, Rev. Sci. Instrum.36, 1352 (1965).
2. V. Vali and R. C. Bostrom, Rev. Sci. Instrum. 39, 1304 (1968).
3. J. Berger and R. H. Lovberg, Rev. Sci. Instrum. 40, 1569 (1969).
4. J. Levine and J. L. Hall, J. Geophys. Rev. Res. 79, 2595 (1972).
5. N. R. Gaulty, G. C. P. King and A. J. Wallard, Geophys J. R. Astron. Soc. 39, 269 (1974).
6. S. Seino, T. Ohishi, and Y. Sakurai, Trains. Soc. Instrum. Control Engrs. 13, 174 (1977), in Japanese.
7. Y. Sakurai, S. Seino, and T. Ohishi, Jpn. J. Appl. Phys, 15, 1859, (1976).
8. S. Iwasaki and T. Sakurai, Oyo Burtsuri 49, 870 (1980), in Japanese.
9. T. Ohishi, Y. Sakurai, and S. Seino, Trans. Soc. Instrum. Control Engrs. 10, 114 (1974), in Japanese.
10. T. Ohishi, Rev. Sci. Instrum. 49, 629 (1978).
11. B. Edlén, Metrologia 2, 71 (1966).
12. T. Masui, Rev. Opt. 36,281 (1957).
13. T. Ohishi, Y. Sakurai, and S. Seino, Kogaku 5, 176 (1976), in Japanese.

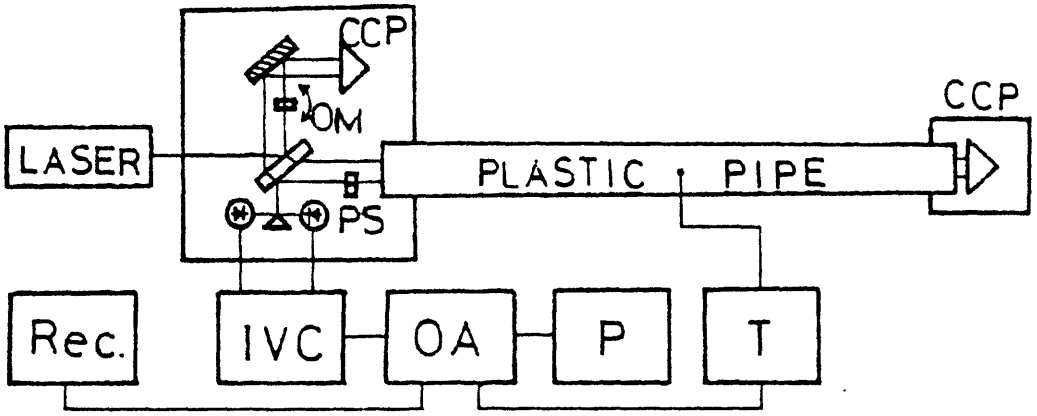

Fig.1 Block diagram of vacuum-pipeless laser strainmeter: CCP is corner-cube prism; OM is optical path length modulator; PS is phase shifter; Rec. is chart recorder; IVC is interference order to voltage converter; OA is operational amplifier; P is atmospheric pressure gauge; and T is thermometer.

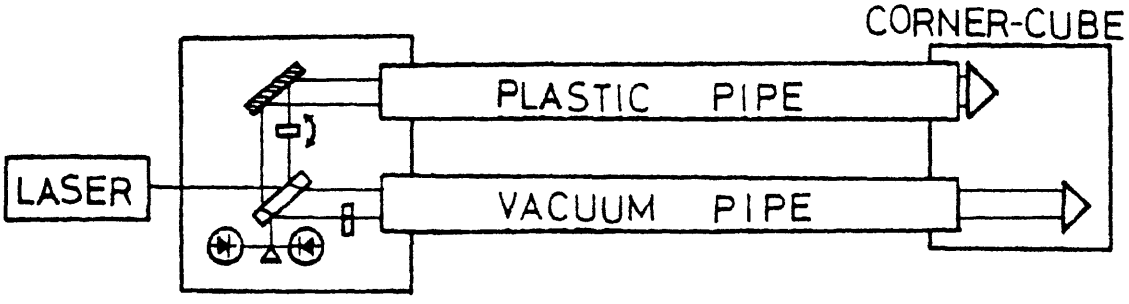

Fig.2 Configuration of interferometer to check the perfromance of compensating the effect of refractive index change.

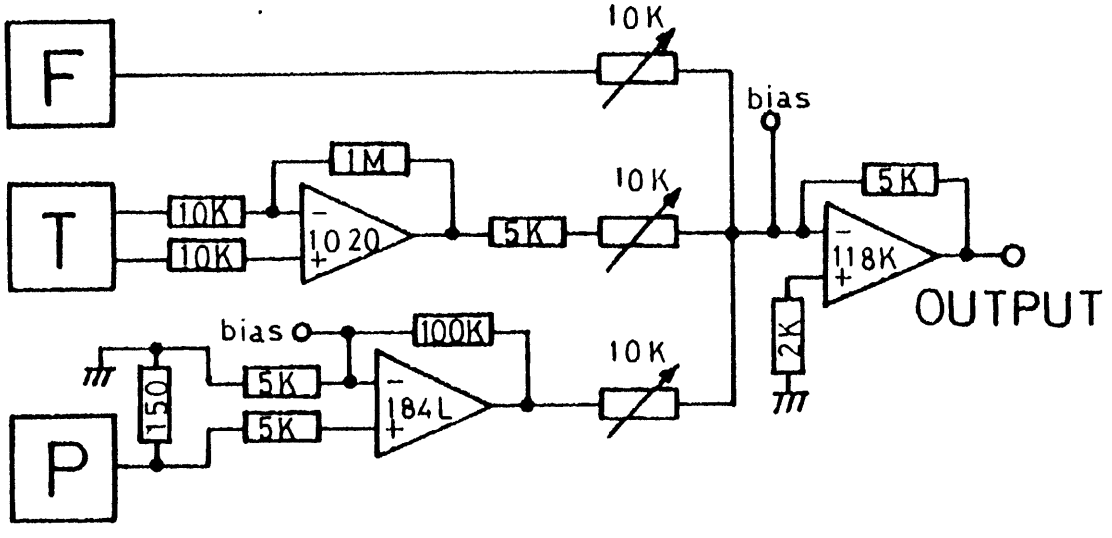

Fig.3 Circuit of operational amplifier:
F is fringe signal voltage; P is atmospheric pressure signal voltage; and T is atmospheric temperature signal voltage.

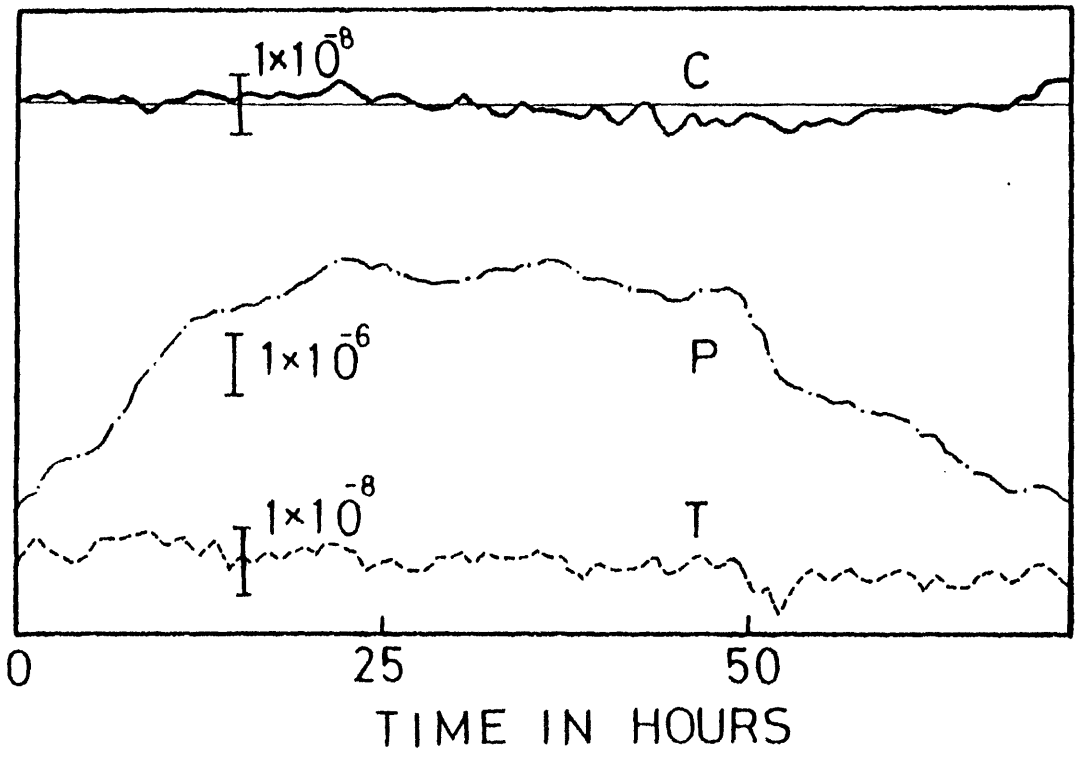

Fig.4 Record of residual of the compensator in the strainmeter: C is the residual of the compensator; P is the atmospheric pressure change; and T is the atmospheric temperature change.

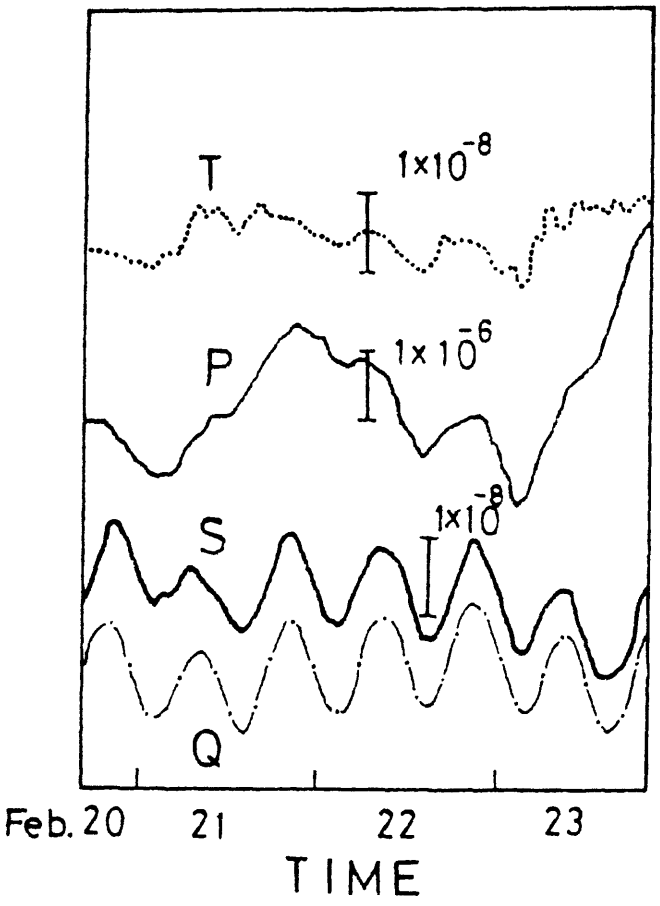

Fig.5 Earth tides recorded using vacuum pipeless strainmeter (S) and that of a quartz strainmeter (Q).

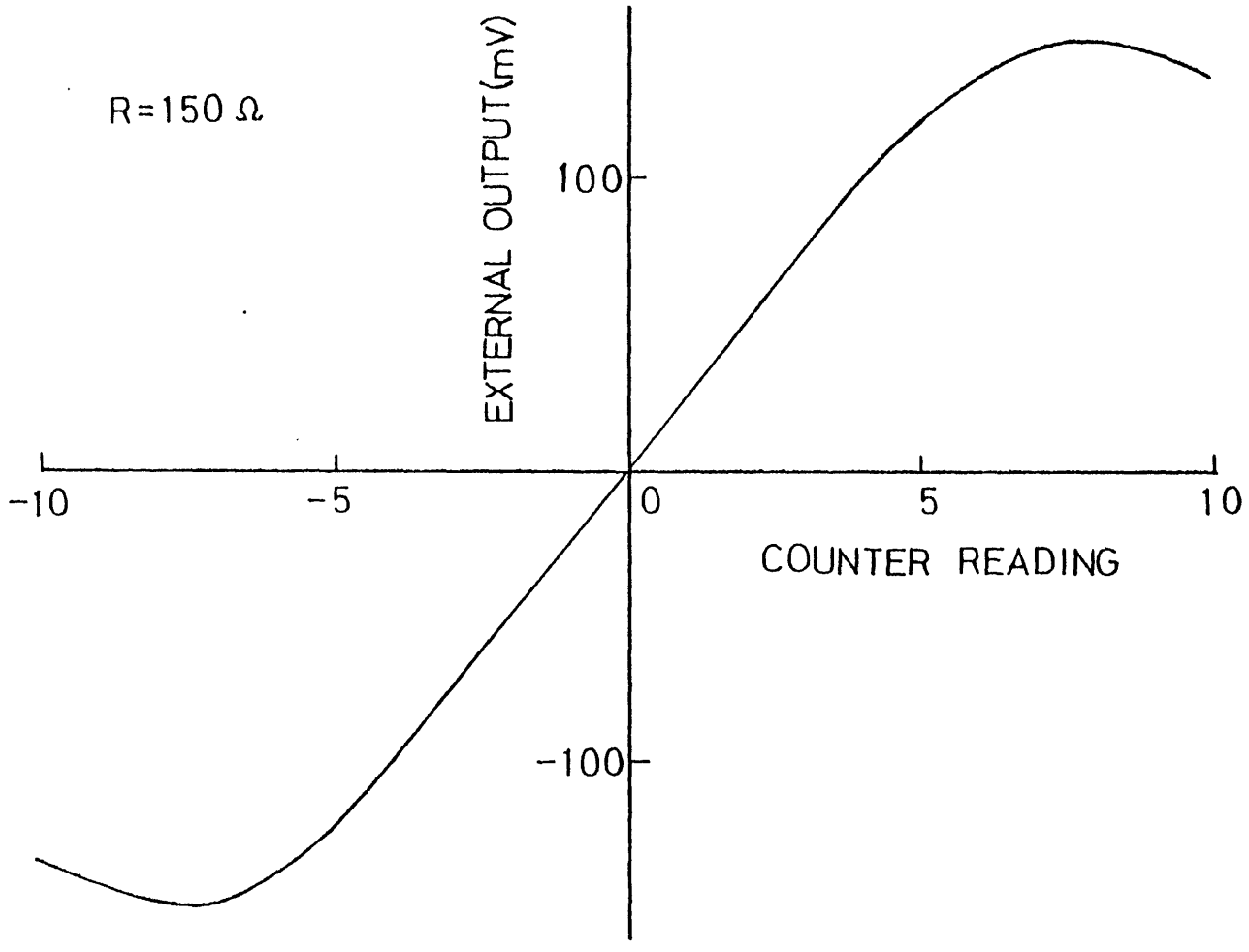

Fig.6 Output characteristics of the pressure gauge.

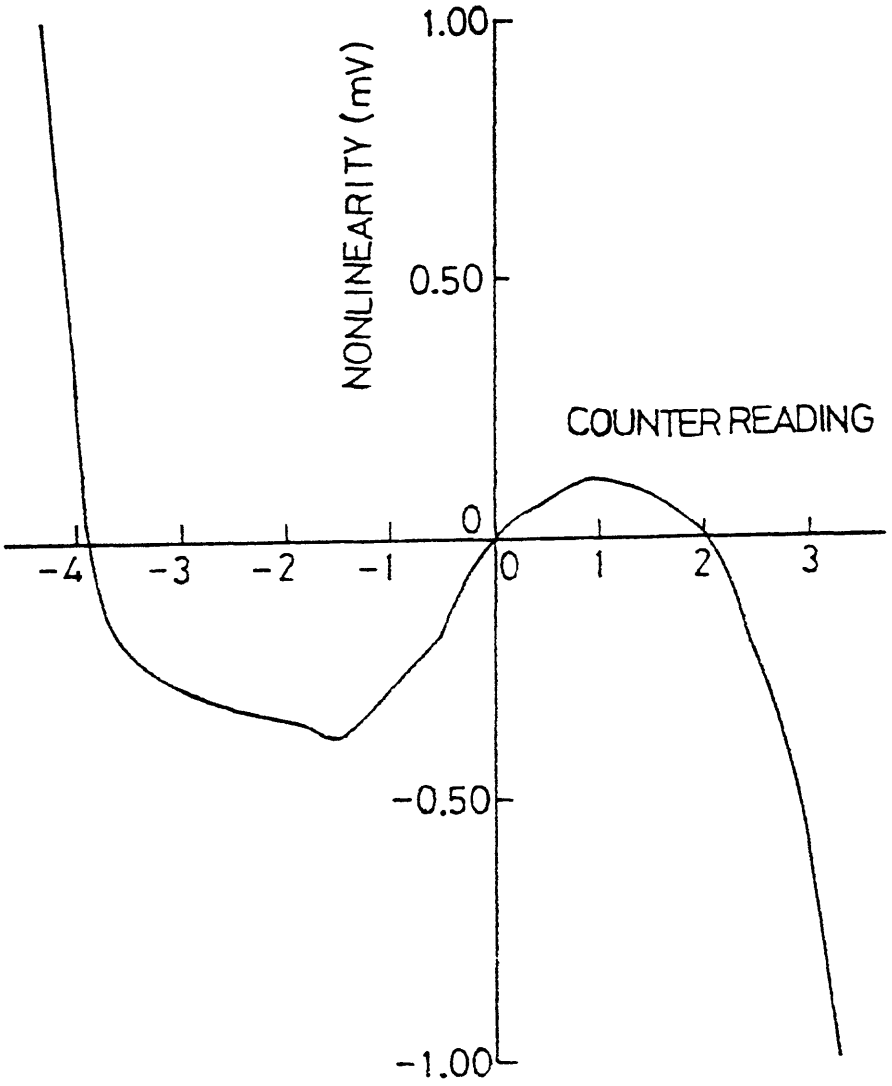

Fig.7 Nonlinearity in the output characteristics of the pressure gauge.

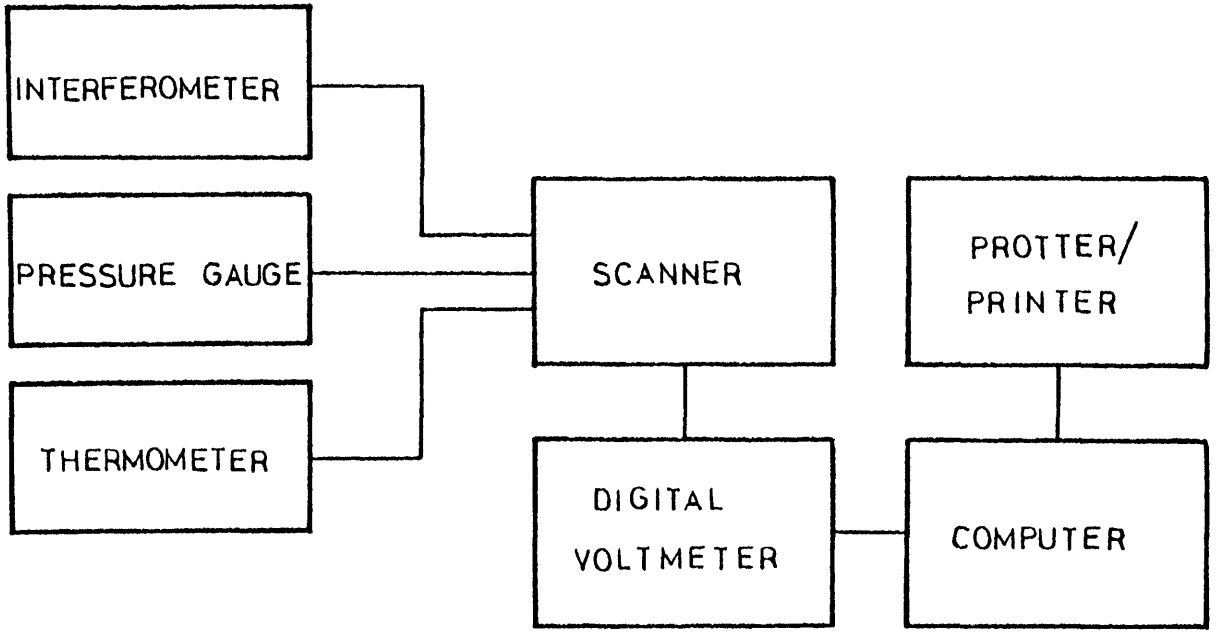

Fig.8 Block diagram of digital compensator for changes of the refractive index of air.

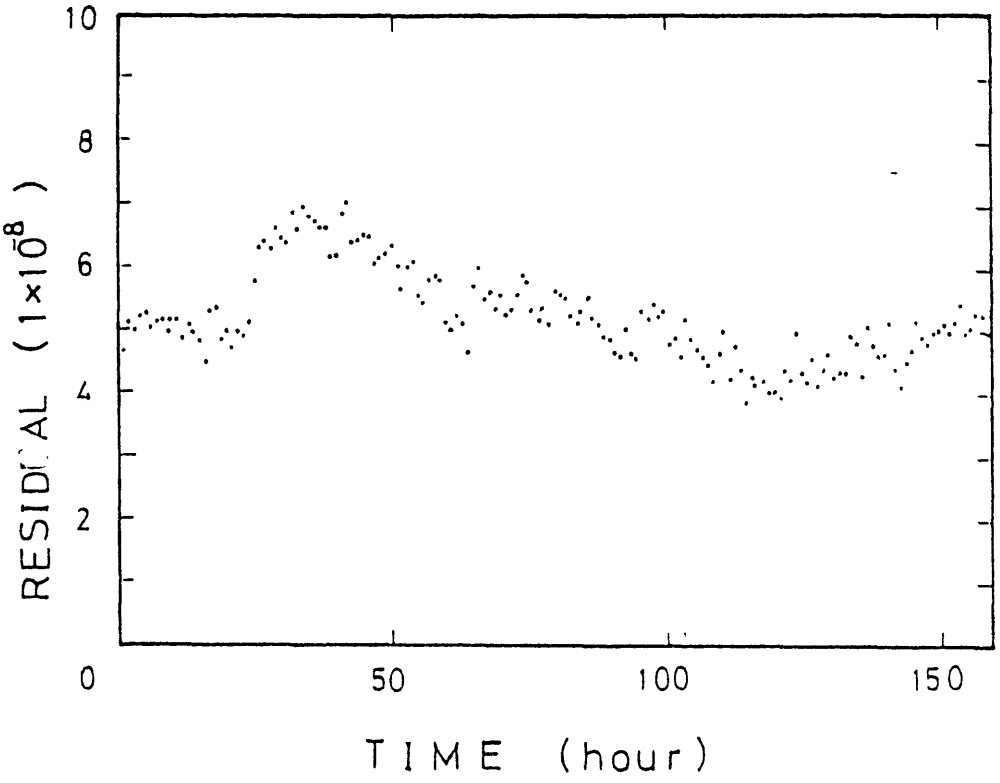

Fig.9 Residual of the compensator.

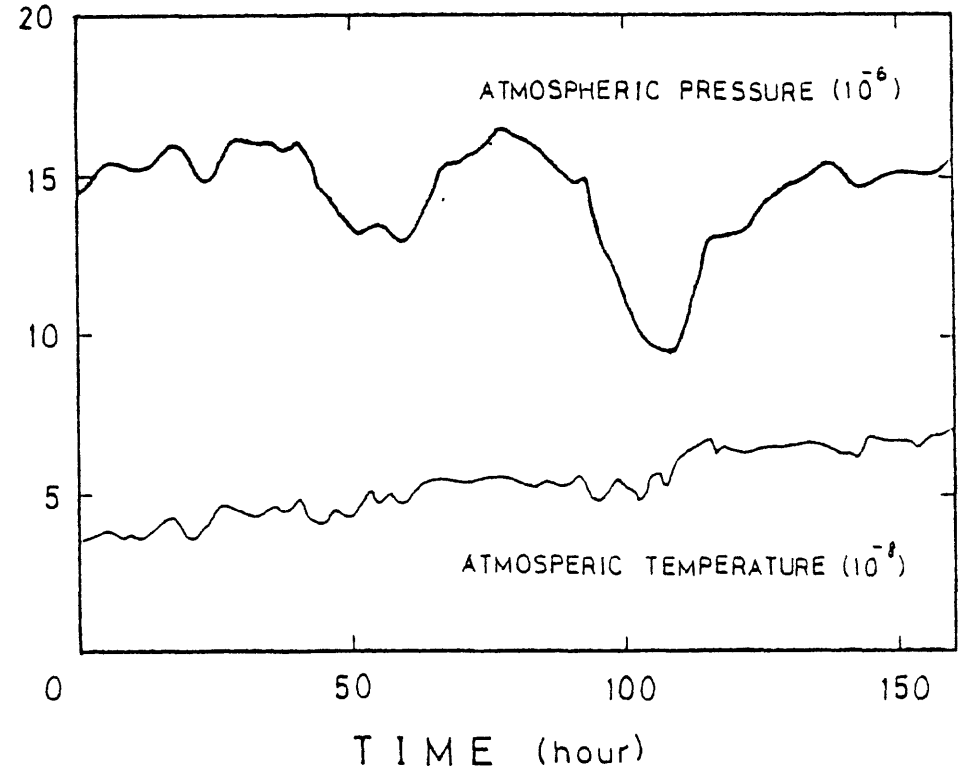

Fig.10 Changes in air consitions.

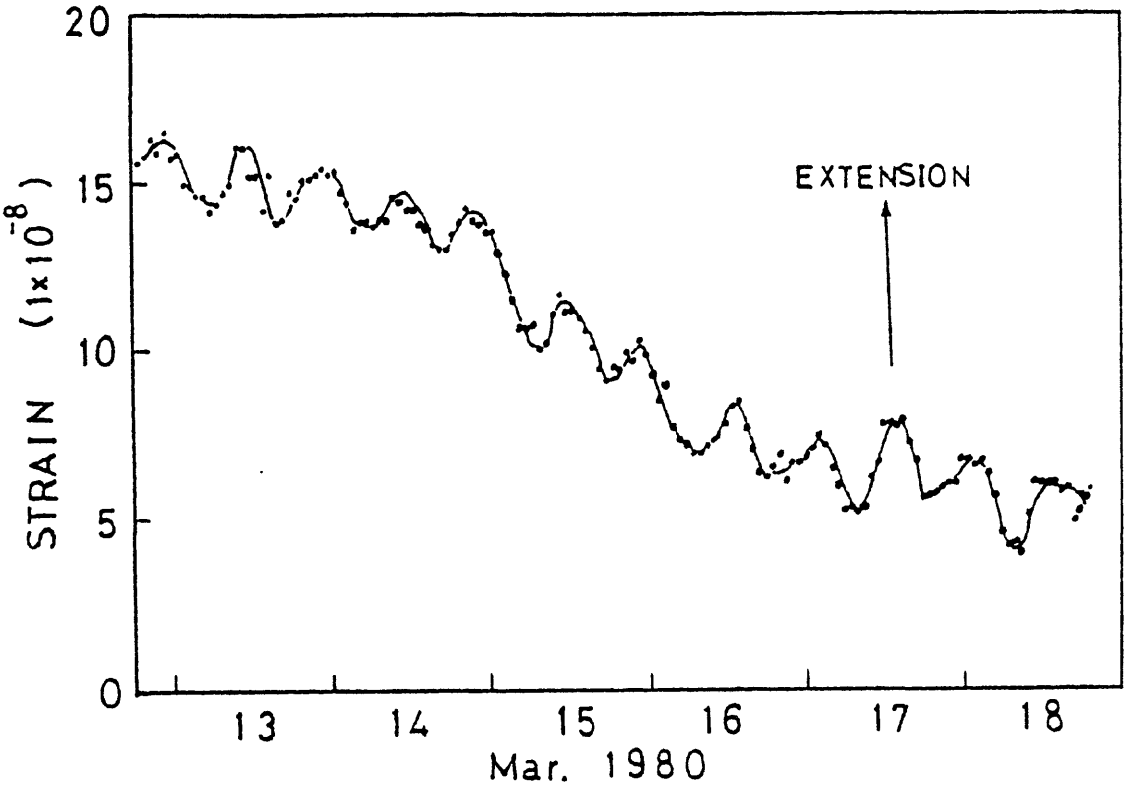

Fig.11 Earth strain recorded with the 25 m vacuum-pipeless laser strainmeter.

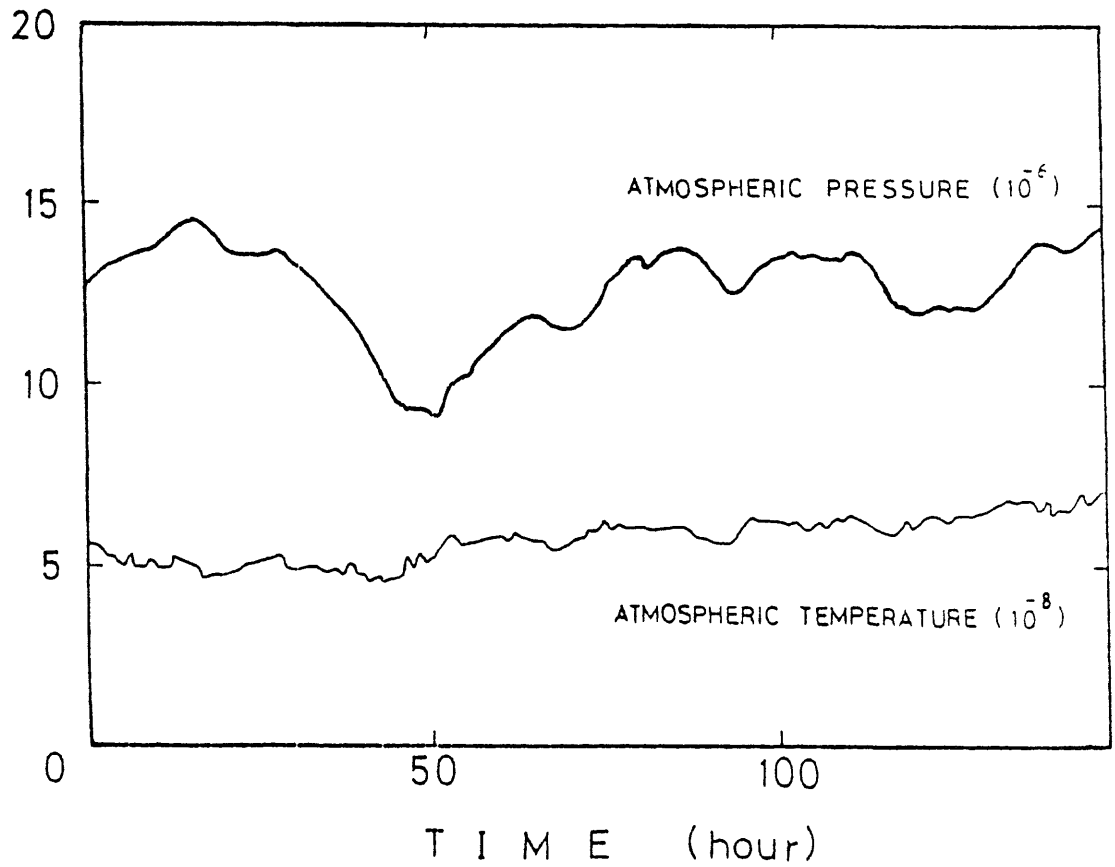

Fig.12 Records of atmospheric pressure and atmospheric temperature.

Development of New-type Three-component Borehole Strainmeters

Shoji SAKATA, Seiichi SHIMADA and Shin'ichi NOGUCHI

National Research Center for Disaster Prevention,
3 Tennōdai, Sakura, Niihari, Ibaraki 305, JAPAN

ABSTRACT

A new-type three-component borehole strainmeter has been developed to detect the three components of the horizontal strain change of the earth's crust for the purpose of earthquake prediction in plain field areas and study of crustal dynamics in triple junction areas.

The main part of this instrument is a dual cylinder, the inside of which is equally divided into three blocks. When the crustal strain field around the strainmeter changes, the volumes of these three blocks change differently from each other. Three components of the strain change can be calculated using the observed three independent values of the volumetric changes.

Two instruments were installed in 160m depth boreholes near Mt. Tsukuba in the Kanto District, a triple junction area where the Asian Plate, Philippine Sea Plate and Pacific Plate meet.

Recently they detected evident strain steps caused by an earthquake ($M = 7.0$). Those data proved the reliability of the strainmeters of this type.

1. Introduction

Continuous observation of crustal deformation is one of the major means of detecting earthquake precursors. In this field horizontal strain observation is very important, since most of the earthquakes

are caused by horizontal compressional stress. In an area where the tectonics is controlled by three or more plates, the direction of principal stress is a good indicator to show which combination of two plates is dominantly acting at present. For that reason observation of three components of horizontal strain is very important, for the purpose of earthquake prediction and study of tectonics, in the plain area of the Kanto District, a triple junction area where the Asian Plate is affected by both the Pacific Plate and Philippine Sea Plate (Fig. 4).

In mountain areas three components of the crustal strain are observed mainly by silica extension meters in tunnel type observatories. In plain areas the Japan Meteorological Agency is operating a number of borehole strainmeters [1]. But these instruments can detect only volumetric strain which is proportional to the sum of the maximum and the minimum stresses. Thus the necessity for a new type of borehole three-component strainmeter arises.

Sakata (1981) invented four types of borehole three-component strainmeters as shown in Fig. 1. Each of them is composed of three same section cylindrical cavities in an infinite elastic medium. When this elastic medium is submitted to a horizontal stress field, the three section areas will change independently from each other, depending on the direction to the principal stress. These three independent observed values are used to obtain three components of the stress or strain.

We made a new type borehole three-component strainmeter of the third type: the rigid partition wall three-part dual cylinder type.

2. Principle of the instrument

Fig. 2 shows the concept of the instrument. The most important

part of this instrument is a dual cylinder as the detection part, the inside of which is equally divided into three independent blocks by rigid partition walls. Each block is filled with silicon oil and is connected to its bellows with a pipe. When the crustal stress field around the strainmeter changes, the displacement of a bellows, which is proportional to the volumetric change of the corresponding block, is detected by the differential transformer. When the bellows displacement reaches the limit, the ejection valve opens to let excessive silicon oil escape into the oil reservoir and to avoid bellows fracture. This system for converting the volumetric change of a cavity to an electrical signal is the same as the one adopted in the JMA type borehole strainmeter.

The cylinder is so slender that the deformation is considered to be two-dimensional. The volumetric change of a block is proportional to the change of the section area (Fig.3). These three observed values, ΔS_1, ΔS_2, ΔS_3, of section area change are independent from each other and compose the following simultaneous equations;

$$\Delta S_1 = A(P_1+P_2)+B(P_1-P_2)\cos(2\beta-120°),$$

$$\Delta S_2 = A(P_1+P_2)+B(P_1-P_2)\cos 2\beta,$$

$$\Delta S_3 = A(P_1+P_2)+B(P_1-P_2)\cos(2\beta+120°),$$

where P_1, P_2 are the principal stresses and β is the direction of P_1 referring to the first wall, the partition wall between the block No 1 and the block No 3. A and B are the constants determined by elastic constants (E_1, ν_1 of the detection cylinder metal, E_2, ν_2 of the expansive mortar and E_3, ν_3 of the surrounding rock) and the geometry (the inner and the outer radii of the detection cylinder;

a and b, the radius of the borehole; c) and are shown as follows (Sakata, 1981),

$$A=(\pi a^2/3)(1-\nu_3^2)f(2-(1+\nu_3)C)/E_3,$$

$$B=\sqrt{3}\, a^2(1-\nu_3^2)g/E_3.$$

Here, f, C and g are constants.

We obtain the solutions as

$$P_1+P_2=(\Delta S_1+\Delta S_2+\Delta S_3)/3A,$$

$$P_1-P_2=\sqrt{2}\,\sqrt{(\Delta S_1-\Delta S_2)^2+(\Delta S_2-\Delta S_3)^2+(\Delta S_3-\Delta S_1)^2}/3B,$$

$$\tan 2\beta=\sqrt{3}\,(\Delta S_1-\Delta S_3)/(2\Delta S_2-\Delta S1-\Delta S_3).$$

The following transforming equations are used to get the solutions in strain forms;

$$\varepsilon_1=(1+\nu_3)((1-\nu_3)P_1-\nu_3 P_2)/E_3,$$

$$\varepsilon_2=(1+\nu_3)(-\nu_3 P_1+(1-\nu_3)P_2)/E3.$$

Then we get

$$\varepsilon_1+\varepsilon_2=(1+\nu_3)(1-2\nu_3)(P_1+P_2)/E_3$$

$$=(\Delta S_1+\Delta S_2+\Delta S_3)/3A',$$

$$\varepsilon_1-\varepsilon_2=(1+\nu_3)(P_1-P_2)/E_3$$

$$=\sqrt{2}\,\sqrt{(\Delta S_1-\Delta S_2)^2+(\Delta S_2-\Delta S_3)^2+(\Delta S_3-\Delta S_1)^2}/3B',$$

$$A'=(\pi a^2/3)(1-\nu_3)f(2-(1+\nu_3)C)/(1-2\nu_3),$$

$$B'=\sqrt{3}\, a^2(1-\nu_3)g.$$

3. Installation and observation

In January, 1982 the first instrument was installed in a 165m borehole at Yasato-machi near Mt. Tsukuba and in March the second was installed in a 160m borehole located 60m apart from the first. The surrounding rock is massive granite. Special care was taken to make the instruments concentric to the boreholes. The direction of the first wall (Fig. 3) is N60°E for each instrument. Each system includes a precision thermometer. This thermometer is also a new type one using the system of silicon oil expansion and bellows displacement. The resolution is expected to be to the 10^{-4} degree. Adoption of the thermometer will be useful for eliminating the thermal effect and for detecting the real crustal change.

All the data including temperature, atmospheric pressure, precipitation are telemetered to the Tsukuba office of the National Research Center for Disaster Prevention.

In Table 1 major factors of the system are summarized.

In Fig. 5 the result of short time observation is shown. It is clearly observed that section area changes due to earth tide are superposed on the big drift changes due to the effect of installation. The fact that the three phases are different from each other shows that the instrument is working well.

Recently these two instruments detected the strain steps caused by the earthquake (M = 7.0) which occurred off Ibaraki, 180km east of the observation point on July 23, 1982. The original data of step changes of section areas are shown in Fig. 6 and Table 2. Computed three components of the strain changes are shown in Table 3.

Two sets of three components of the strain change are in good agreement with each other. This fact clearly shows the reliability of the strainmeters of this type. The direction of the maximum

extention is in harmony with the focal mechanism solution, a reverse and pure dip-slip faulting whose dip direction and dip angle are ϕ = N70°W and δ = 45°, determined by initial motions of P waves detected at NRCDP seismic observation stations (Okada et al., 1982).

References

[1] Sacks, I., S. Suyehiro, D. W. Evertson and Y. Yamagishi: Sacks-Evertson strainmeter, its installation in Japan and some preliminary results concerning strain steps. Pap. Meteorol. Geophys., 22, (1971), 195-208.

[2] Sakata, S.: On the Concepts of Some Newly-invented Borehole Three-component Strainmeters. Report of the National Research center for Disaster Prevention, 25, (1981), 95-126.

[3] Okada, Y., S. Noguchi, M. Ukawa and M. Ohtake: Report on the Earthquake Eastern off the Ibaraki Prefecture, Japan of July 23, 1982. Research Notes of the National Research Center for Disaster Prevention, No 46, (1982).

Figure Captions

Fig. 1 Schematic illustrations of the four types of three-component borehole strainmeters and relations between them:
(a) elliptic cylinder type,
(b) diameter-constrained cylinder type,
(c) rigid partition wall three-part dual cylinder type, and
(d) slide partition wall three-part dual cylinder type.

Fig. 2 Schematic illustration of the borehole three-component strainmeter of rigid partition wall three-part dual cylinder type.

Fig. 3 Section of the detection part of the strainmeter in an infinite elastic medium submitted to two-dimensional stress field.

Fig. 4 Kanto District as a triple junction area and the location of installed strainmeters.

Fig. 5 Example of one week's observation data of the No 2 instrument (west well).

Fig. 6 Pen-recorded data of step changes of section areas.

Table 1. Major factors of the system.

Total length of the instrument including setting apparatus	8.5m
Detection cylinder	
outer diameter	114mm
thickness of the plate	3mm
inner diameter	106mm
width of the partition wall	12mm
effective length	3m60cm
Signal transducer	
effective section area of bellows	$1.98cm^2$
sensitivity of the differential transformer	1.4V/mm
range of bellows displacement	±1mm
Elastic constants	
metal(stainless steel)	$E_1=2\times10^6 kgf/cm^2$, $\nu_1=0.30$
mortar	$E_2=2\times10^5 kgf/cm^2$, $\nu_2=0.35$
rock(granite)	$E_3=4\sim5\times10^5 kgf/cm^2$, $\nu_3=0.35$
A'≈ 70	
B'≈ 50	

Table 2. Step changes of section areas detected by two strainmeters. Changes are referred to five minutes before and after the occurrence time of the earthquake. Decrease is taken as positive.

name of instrument	name of block and section area changes ($\times 10^{-8}$ cm^2)	
No 1 instrument (east well)	block No 1 (E0)	ΔS_1 = 59
	block No 2 (E120)	ΔS_2 = -628
	block No 3 (E240)	ΔS_3 = -469
		ΔS = -1038
No 2 instrument (west well)	block No 1 (W0)	ΔS_1 = 103
	block No 2 (W120)	ΔS_2 = -469
	block No 3 (W240)	ΔS_3 = -369
		ΔS = -735

Table 3. Three components of the strain change computed from the data in Table 2. Contraction is taken as positive.

	Three components	direction of maximum extension
No 1 instrument (east well)	ε_1 = 1.7 × 10^{-8} ε_2 = -6.6 × 10^{-8} β = 66°	N84°E
No 2 instrument (west well)	ε_1 = 1.8 × 10^{-8} ε_2 = -5.3 × 10^{-8} β = 65°	N85°E

(d)
(c)
(a)
(b)

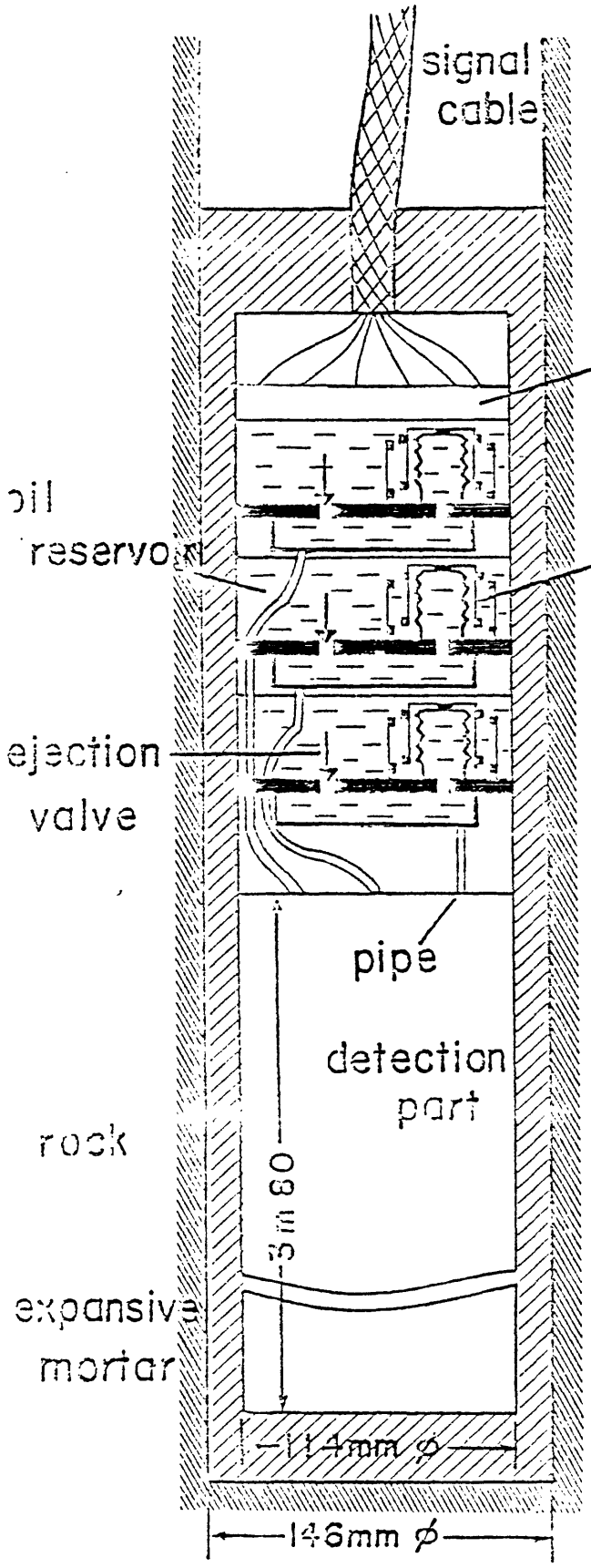

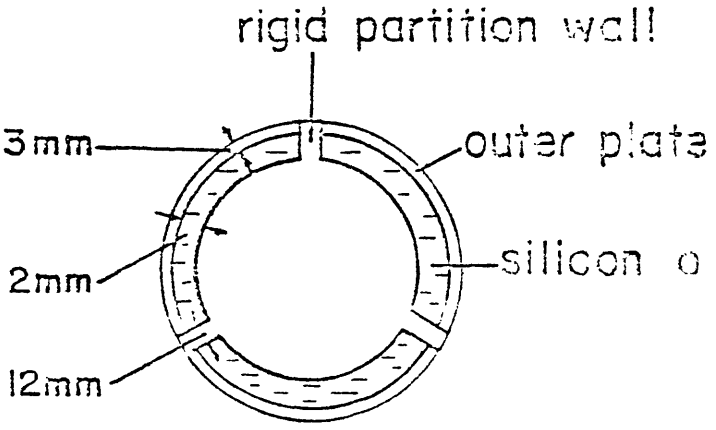

section of detection part

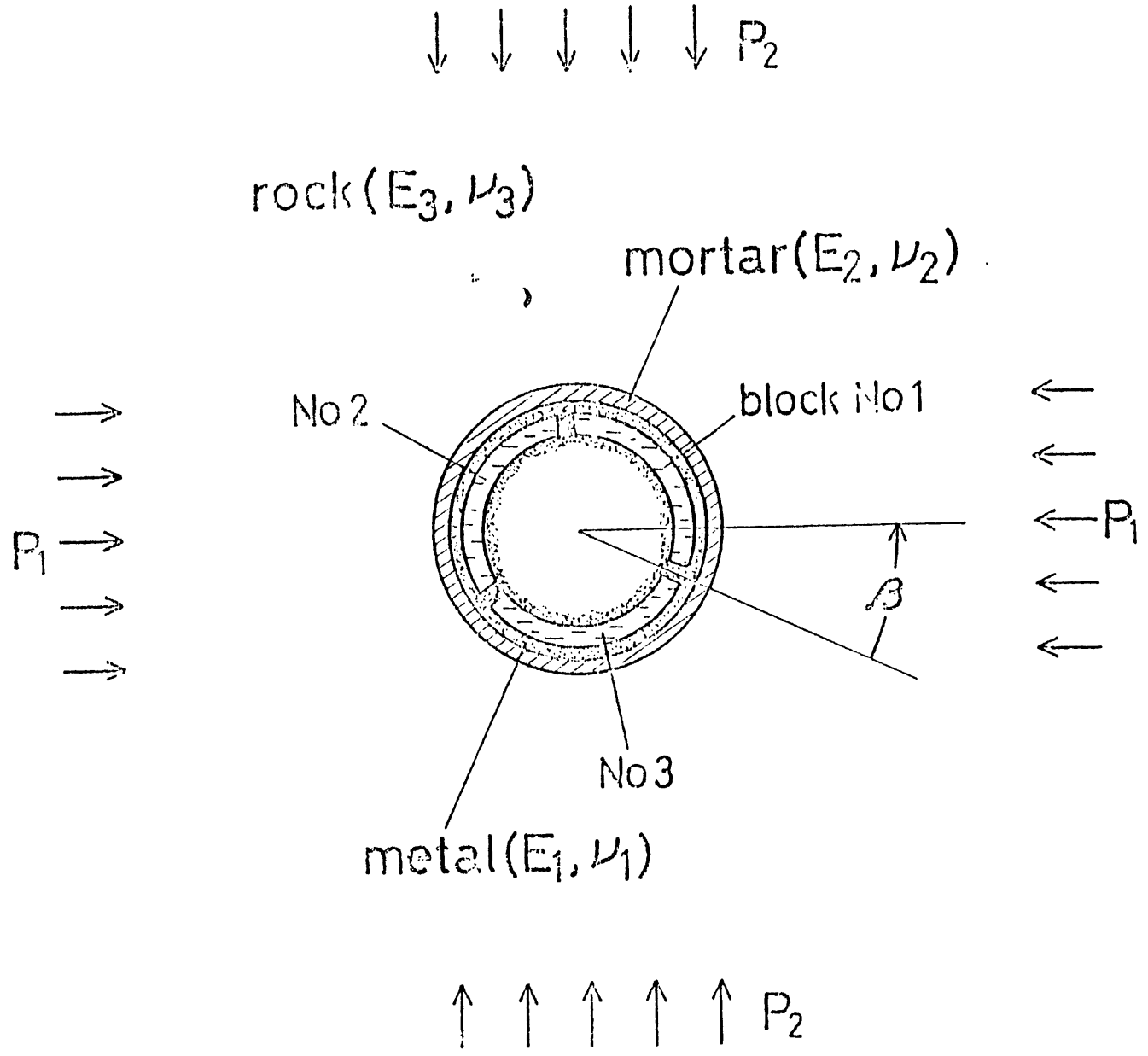
P2
rock (E3, ν3)
mortar(E2, ν2)
No 2
block No 1
P1
P1
β
No 3
metal(E1, ν1)
P2

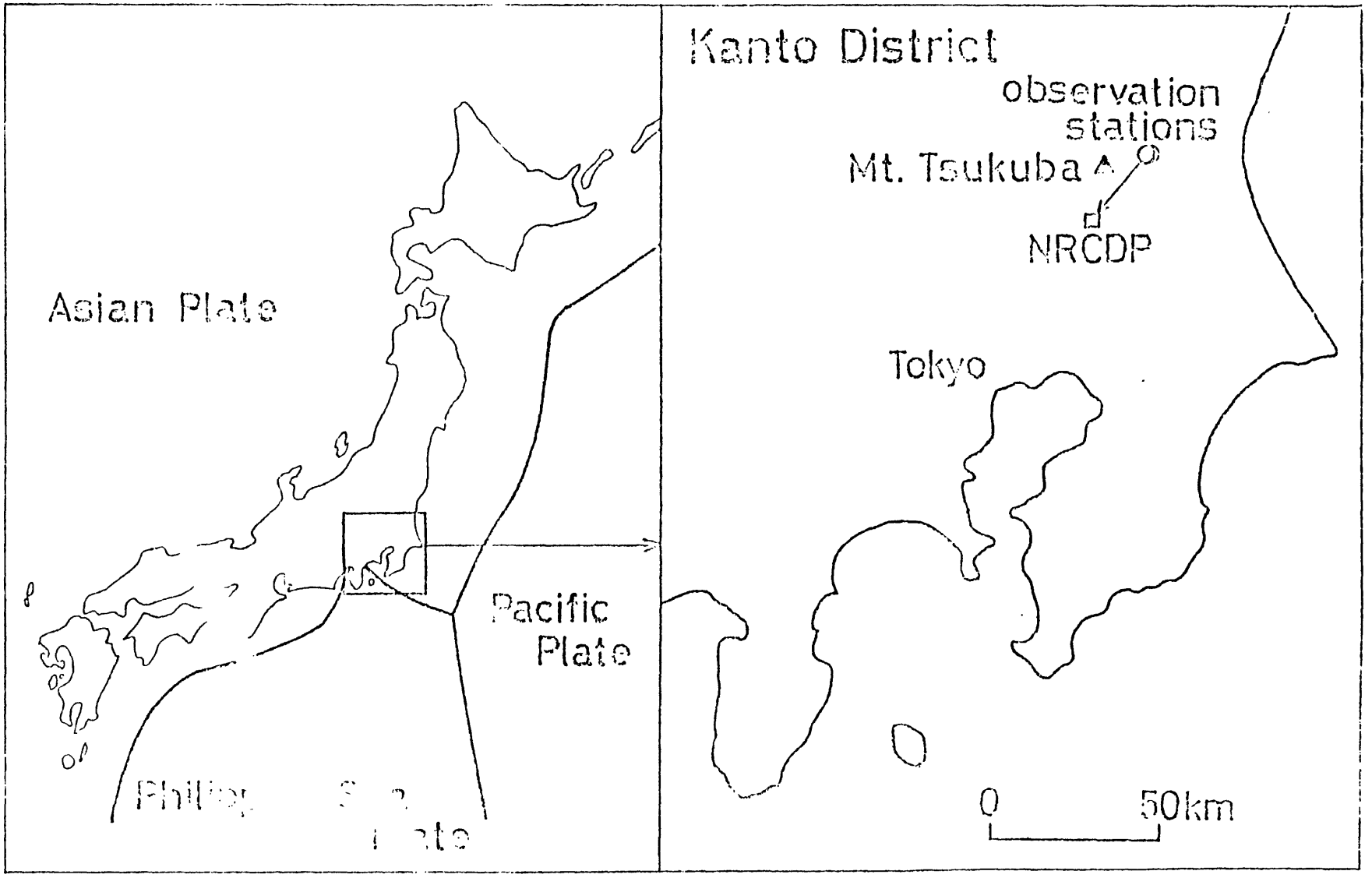
Kanto District
observation
stations
Mt. Tsukuba
NRCDP
Tokyo
Asian Plate
Pacific
Plate
0
50km

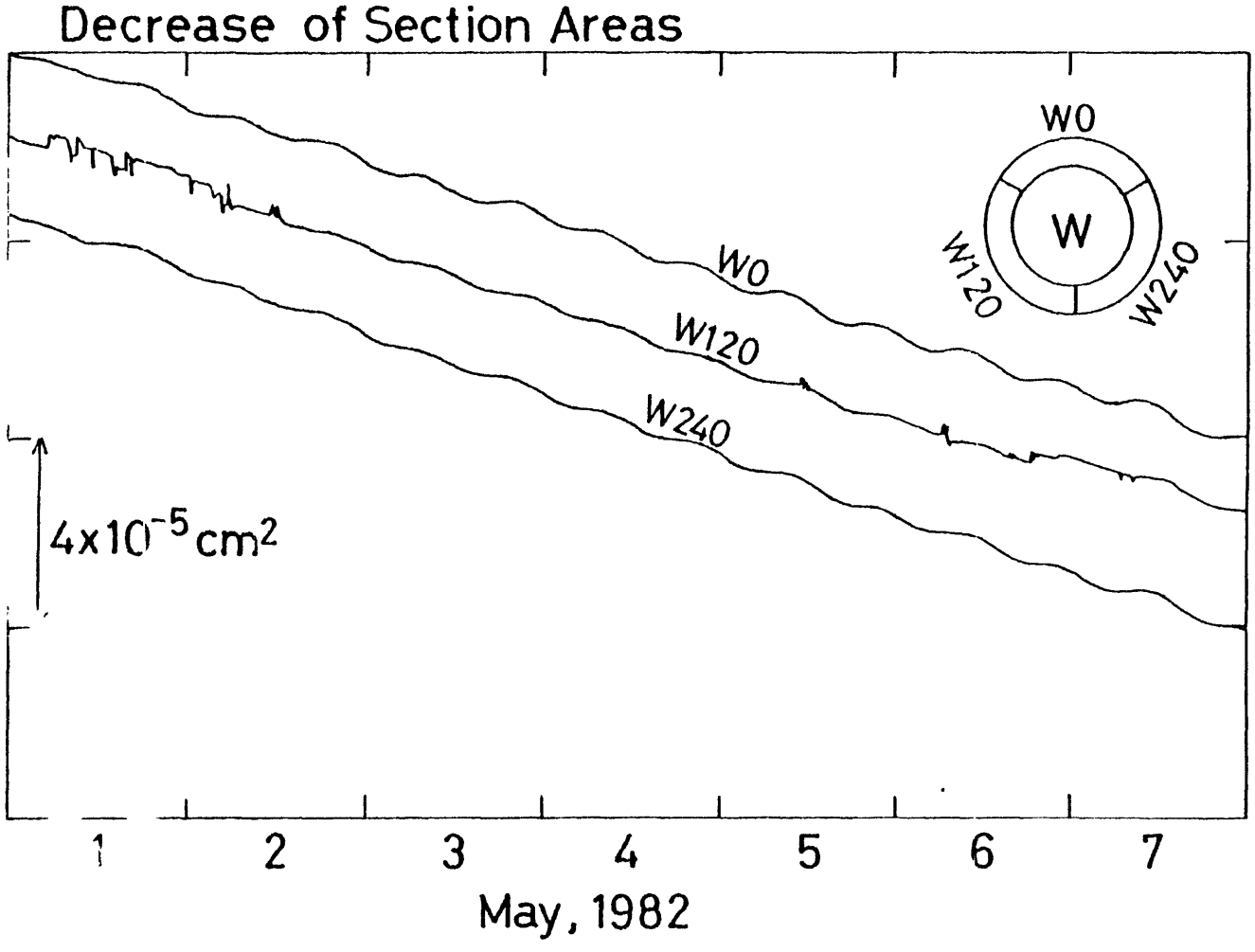
Decrease of Section Areas
W0
W120
W240
W
W0
W120
W240
4x10⁻⁵cm²
1
2
3
4
5
6
7
May, 1982

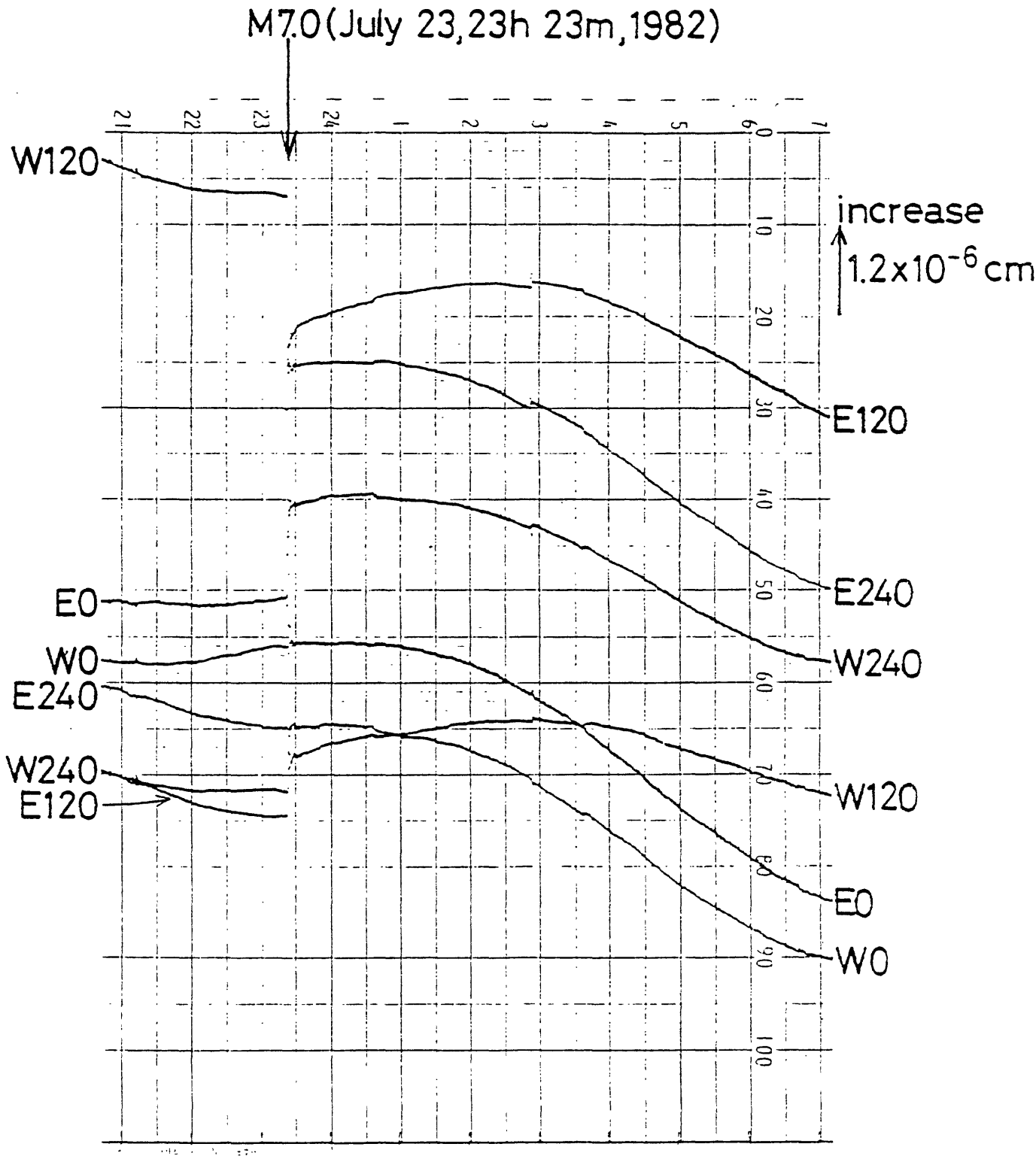
M7.0(July 23,23h 23m,1982)
W120
increase
1.2x10⁻⁶cm
E120
E240
E0
W0
E240
W240
E120
W240
W120
E0
W0

PROGRESS IN AUTOMATED DATA PROCESSING FOR DENSE SEISMIC NETWORKS

The management of data, including both derived data such as arrival times and event locations, as well as operational parameters, including such things as station histories and various kinds of calibration information, has presented severe problems regarding the efficient operation of moderate and large scale, local seismic networks. Manual methods that work well enough for small arrays of a few ten's of sensor do not scale well to networks of hundreds of instruments; the efficient management of larger, dense networks demands a more rigorous approach based on modern concepts in data management technology and computer technology. The CUSP (Caltech-USGS Seismic Processing) system, presently being used to manage the southern California seismic network at Caltech, represents such an approach and will be the principle theme of this discourse.

Dense seismic networks are primarily constituted to serve both the needs of the research community (completeness, convenience, and accuracy) as well as the rather pressing demands of a real-time, monitoring effort (efficiency and reliability) as is required for earthquake forecasting and short-term hazard accessment. In many ways these goals are incompatible, such as the trade-offs associated with accuracy and processing speed. The CUSP system attempts to resolve these conflicts by means of a system architecture centered on a relational data base system designed for efficient operation with the specific needs of seismic data processing in mind. This approach also provides the flexibility required to implement routine processing before all aspects of the problem can be completely defined. Further, since all references to data are by symbolic name and thereby do not require a knowledge of data structure, the implementation and integration of applications in response to evolving needs is greatly simplified. Because of specific decisions made with respect to data base architecture these advantages are obtained without a significant degradation of interractive response.

Minimization of manual operations or manually guided operations is requisite in managing large, dense networks with minimal staffing. A unique, data-driven, operation sequencing approach is used in the CUSP design to permit the evolution of the data from point of origin through the processing stages required to produce whatever products are deemed necessary. Human intervention is primairly by exception. A set of stages and transition rules is made part of the actual data base so that most aspects of routine network analysis can be fully automated.

System reliability is derived from design criteria requiring distributed processing and hardware isolation. The flow of data within the CUSP system is predicated on the requirements of a Local Area Network (LAN) for exchange of data between data acquisition hardware, graphics work stations, and archival facilities. Archiving of seismic data is designed assuming the requirements of high density, write-only optical storage. An evaluation of our experiences with this approach to the present as well as some projection for taking advantage of emerging technology will be presented in the discussion.

CJ:lr

PERFORMANCES AND DATA PROCESSING of K-3 VLBI SYSTEM for GEODESY

YUJI SUGIMOTO and NORIYUKI KAWAGUCHI

Kashima Branch, The Radio Research Laboratories
Ministry of Posts and Telecommunications
Kashima, Ibaraki 314, Japan

ABSTRACT

The K-3 VLBI hardware system, compatible with Mark III system has been developed since 1979. This will be used for the joint experiments between NASA and RRL from 1984.

Concerning a geodetic application of K-3 VLBI system, this paper presents a summary of the K-3 data acquisition system and a delay error due to the hardware is estimated to be 70 psec (2 cm in path length) on the joint experiments. It takes a quarter of recording time for processing, and about 1 % of the reproduced data are lost. K-3 correlation processor condenses recorded data into processed data, the ratio of which is 10^{-5}.

1. INTRODUCTION

The K-3 VLBI hardware system (Kawaguchi et al, 1982) has been developed since 1979. This system, compatible with Mark III system

developed in USA, will be used for the joint experiments between Japan and USA from 1984.

In this paper, we introduce the K-3 VLBI data acquisition hardware system. Concerning a geodetic application of K-3 VLBI system, one of the most important things is an error on delay observations. After considering performances of each device in the system, we give this error in following section.

In the data processing system, a primary consideration will be paid on long integration capability, which condense a large quantity of raw data to small cross correlation data without any loss of delay information. The K-3 correlation processing system can integrate the cross correlation data in a long period and produces cross correlated data with a small loss of coherence.

The secondary concern is on processing speed. The K-3 processing system can reproduce and process the raw data four times faster than the usual recording speed.

The last matter to be taken into account is a method of synchronizing two data recorders to minimize tape loss. In the section 3, we present this method using data recorders, correlation processor and the host computers.

2. DATA ACQUISITION

In this section, we present performances of the K-3 hardware system and estimation of delay error caused by this system.

2.1 A summary of the K-3 VLBI hardware system

A block diagram of the K-3 hardware system is shown in Fig. 1. A 26 m diameter antenna receives S-band (2 GHz) and X-band (8 GHz) signals. Both signals are amplified and down-converted to IF (100-520 MHz) signals respectively. The bandwidth of X-band is 420 MHz and that of S-band is 100 MHz.

In the K-3 acquisition terminal, 14 video converters convert the IF signals to corresponding 14 sets of upper and lower video signals, those usually having 2 MHz bandwidth each. The video converters can convert any frequencies of the IF signals to video signals. The frequencies are selected to maximize an effect of a bandwidth synthesis. The formatter samples the 28 video signals in one bit and formats them according to the Mark III data format. A wideband data recorder records these 28-channel signals at the usual speed of 135 ips with bit error rate of 10^{-6}. Two or more recorders are also used for data processing with the correlation processor mentioned later.

A hydrogen maser oscillator has short term stability of 7×10^{-15}, and is used as the frequency standard of the whole K-3 system. A delay calibrator calibrates the variation of cable delay in the data acquisition system. The resolution is 0.5 psec and the instability is less than 5 psec. Water vapor radiometer measures sky noise temperatures with 1 K error or better. These noises are emitted by water vapor. The wet component of the tropospheric delay is estimated from this sky temperature. And the dry

component of tropospheric delay is corrected using measured pressure with the accuracy of 0.1 mbar.

The whole system is controlled by HP-1000/10L computer according to the observation schedule (Takahashi et al, 1982).

2.2 Estimation of delay error

We estimate delay observation error caused by the K-3 hardware system. In this estimation, we suppose VLBI experiments between OVRO (Owens Valley Radio Observatory) station with 40 m antenna and Kashima station with 26 m antenna.

Table 1 shows errors due to the system noise in the receiving system. A coherence loss factor in this table consists of loss due to system imperfectness (43 %) and loss in correlation processing (7.4 %). The loss due to one bit sampling (36 %) is most dominant.

If we assume an observation time is 300 seconds and source flux density is 1 Jy, an error will be 13.6 nsec (S-band) and 19.9 nsec (X-band) in each channel, because a bandwidth of each channel is only 2 MHz. The error is improved to 111 psec and 50 psec by a bandwidth synthesis technique on 2 channels in S-band and 5 channels in X-band, span bandwidth of which is 100 MHz and 420 MHz respectively.

Then we reject an ionospheric effect by combining S-band and X-band data together, so a final error will become 54 psec.

Table 2 shows an estimated error due to the whole K-3 VLBI hardware system, and total observation error is expected to be 70 psec, equivalent to 2 cm in length. As mentioned above, we

recognize 7 channels observation is accurate enough for geodesy and crustal dynamics purpose, so the K-3 processor is designed 7 channels for one crate as follows.

3. DATA PROCESSING

After data acquisition, a large quantity of data should be processed. A method of recorder synchronization, data loss caused by this method and performances of the K-3 processor are presented in this section.

3.1 K-3 VLBI Correlation Processor

K-3 correlation processor will be accomplished by March 1983. A trial model, that can process one channel, has been assembled in August 1982. Now we are testing it for a 28 channels-full-system.

Fig.2 shows a block diagram of the correlation processing system, and Table 3 shows performances of the K-3 correlation processor. The processor consists of four crates, and each crate consists of one controller, seven correlation units and one reserve unit.

We present the performances of the K-3 processor as following.

1) Expandability

Each crate is operated independently, so that we can easily add more crate modules for the multi-baseline processing. When we use another data recorder, 4-crate processor processes two baselines simultaneously.

2) High speed processing

The processor can process at any reproduction data rate up to 8 Mbps. This means that reproducing speed can be twice as usual recording rate.

Data on a tape recorded by observation mode E (7-channel per one pass, i.e. twice forward and reverse recording) can be processed by reproducing only one forward and reverse pass.

These show that a processing time is reduced to a quarter of recording time.

3) Long integration time

Delay changes for a long integration time is compensated by 128-bit programmable delay. A fringe rotation, caused by the earth rotation, is stopped by using a sinusoidal function of three-level approximation. The resolution, minimum quantized fringe frequency, is high enough to integrate the correlation data for long period without loss due to a fringe phase error. Furthermore, fringe acceleration is also compensated and a fractional bit is corrected. These are made in time domain in order to simplify hardware.

These make possible long time integration of correlation data up to 8.38 seconds at 4 Mbps rate with low coherence loss (4 % by fringe rotation, 3.4 % by fractional bit compensation) at any inter-continental baseline. The raw data are condensed into processed data, the ratio of which is 10^{-5} without any loss of delay information.

4) Real time checking of correlation unit

The host computer alternately checks seven units during operation by comparing the correlation data from the operation unit with those from the reserve unit. Once the host computer finds a failure unit, it calls operator and changes the reserve unit in operation automatically. In this way, non-stop processing is achieved.

3.2 Synchronization of two data for correlation

Fig. 3 shows synchronous reproducing-system. There are two IEEE-488 bus interfaces in the processor. One is connected to the data analysis computer, HP-1000/45F, in order to send correlation data and to receive parameters. The other is connected to the system control computer, HP-1000/10L, in order to control data recorders (Takahashi et al, 1982). Although this figure shows a case of one-baseline processing, the same method can be used for multi-baseline processing.

1) Synchronization of recorders

The cross correlation is not valid until a synchronization between the reproduced data is achieved, so the fast synchronization is desired. We present an efficient method of the synchronization in Fig. 3.

-phase 1: The recorders are driven at very low speed, for example 8 and 7/16 inches per second, by a command from HP-1000/10L. HP-1000/45F calculates a priori delay between two data streams from the observation schedule and sends the information to the correlation processor.

-phase 2: The processor reads time code that express a time when the data are obtained, and calculates a synchronization error that is a time difference between a priori delay and time difference of two time codes.

-phase 3: The 10L receives this error from the processor, and controls speed-up timings of two recorders.

A parallellogram area in Fig. 3 indicates the synchronization error to be compensated.

-phase 4: After a while, when recorders reach at nominal speed independently, a coarse synchronization is achieved.

-phase 5: Then fine synchronization is achieved by finely changing speeds of two recorders.

-phase 6: When the difference is within a capacity of the buffer memory which consists in the processor, correlation data is available.

-phase 7: The 10L controls two recorders in order to set and keep the error at the middle of the buffer area.

It takes less than 10 seconds from tape starting to make correlation data available, and tape loss is less than 1 % of the tape length.

2) Perfect synchronization

At phase 2 as mentioned above, offset address of a 20,000bit buffer in the processor is set by controller of the processor using a priori bit difference between two data. Once a perfect

synchronization is achieved by this buffer, it is kept even when any wow or flatter occurs in the recorder transport system.

4. CONCLUSION

We present a summary of the K-3 acquisition system and an error estimation caused by the K-3 VLBI hardware system, performances of the K-3 correlation processor and a method of data synchronization for data processing.

We believe the K-3 VLBI hardware system has high performances and will be powerful tool for geodetic researches.

And we hope that the joint experiments will successfully start and those data will give new information to the fields of geodesy and crustal plate motion.

5. ACKNOWLEDGMENT

We would like to thank to Drs. A.E.E. Rogers, H. Hinteregger, G.M. Resch, A.R. Whiteny, J.I. Levine and many other VLBI hardware and software researchers for their kind suggestions and encouragements.

Finally, we express our gratitude to Drs. Y. Saburi, K. Yoshimura, F. Yamashita, N. Kawajiri, N. Kawano and other staff members of VLBI system developing group in RRL.

REFERENCES

Kawaguchi,N., Sugimoto,Y., Kuroiwa,H., Kondo,T., Hama,S., Amagai, J., Morikawa,T. and Imae,M.; "The K-3 hardware system being

developed in Japan and its capability", Proc. of IAG Symp. No.5, Tokyo (1982)

Takahashi,F., Yoshino,T., Murakami,H., Koike,K. and Kunimori,H.; "K-3 VLBI software development for international experiments", ibid. (1982)

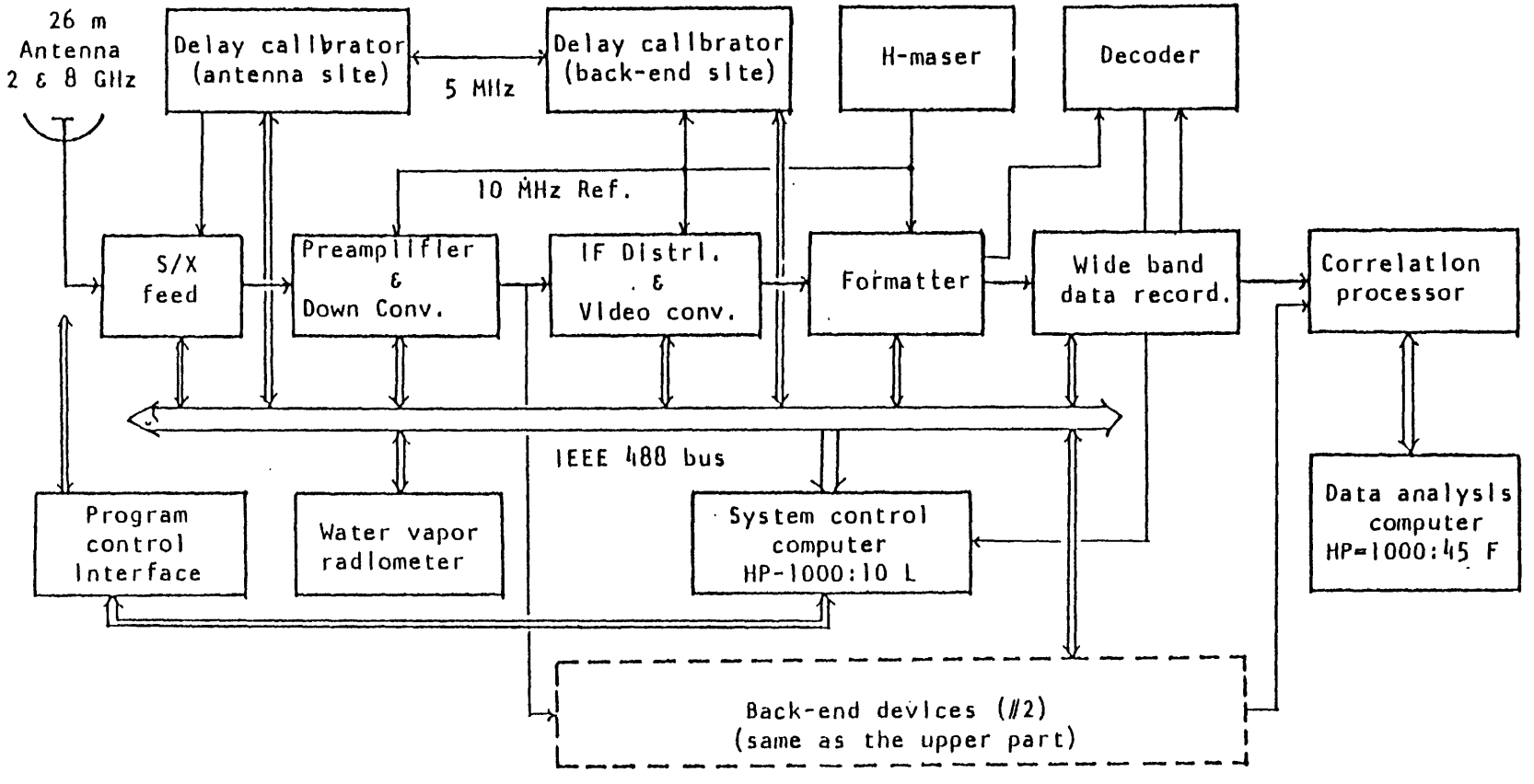

Fig. 1 Block diagram of K-3 VLBI hardware system

Table 1 Estimated delay error on experiments between OVRO 40 m and Kashima 26 m due to antenna and receiving system

band / items	S-band	X-band
G/T of Kashima stn	1.20×10^3	1.32×10^4
G/T of OVRO stn	4.47×10^3	3.55×10^4
averaged G/T	2.32×10^3	2.17×10^4
loss factor *1	0.5	0.5
integration time	300 sec	300 sec
flux density	1.0 Jy	1.0 Jy
error on one channel	13.6 nsec	19.9 nsec
error on each band using bandwidth synthesis	111 psec *2	50 psec *3
final error rejected ionospheric effect	54 psec	

*1 caused by the whole hardware system
*2 2.22 and 2.32 GHz
*3 8.24, 8.42, 8.44, 8.50 and 8.54 GHz

Table 2 The observation error estimation of the VLBI experiment between OVRO 40m and Kashima 26m

Error source	error	comment
Antenna and Receiving System	54 psec	1 Jy, 300 sec, Mode E
Hydrogen Maser Oscillator	18 psec	clock instability
Delay Calibrator	5 psec	time interval counter error of 1 micro-sec at 25 Hz
Wet Component Path Delay	38 psec	radiometer error of 1 K
Dry Component Path Delay	11 psec	pressure gauge error of 0.1 mbar
Phase Scintillation	6 psec	integration time of 300 sec
Total RSS	70 psec	about 2 cm

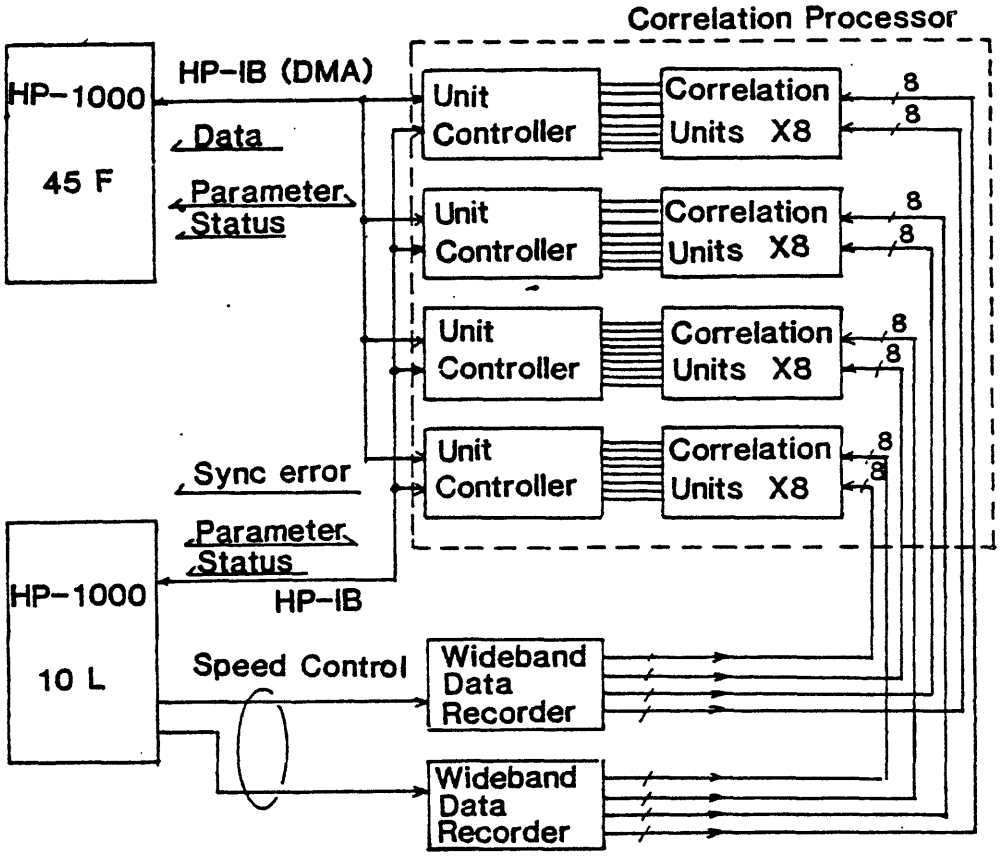

Fig. 2 Block diagram of K-3 Correlation processing system

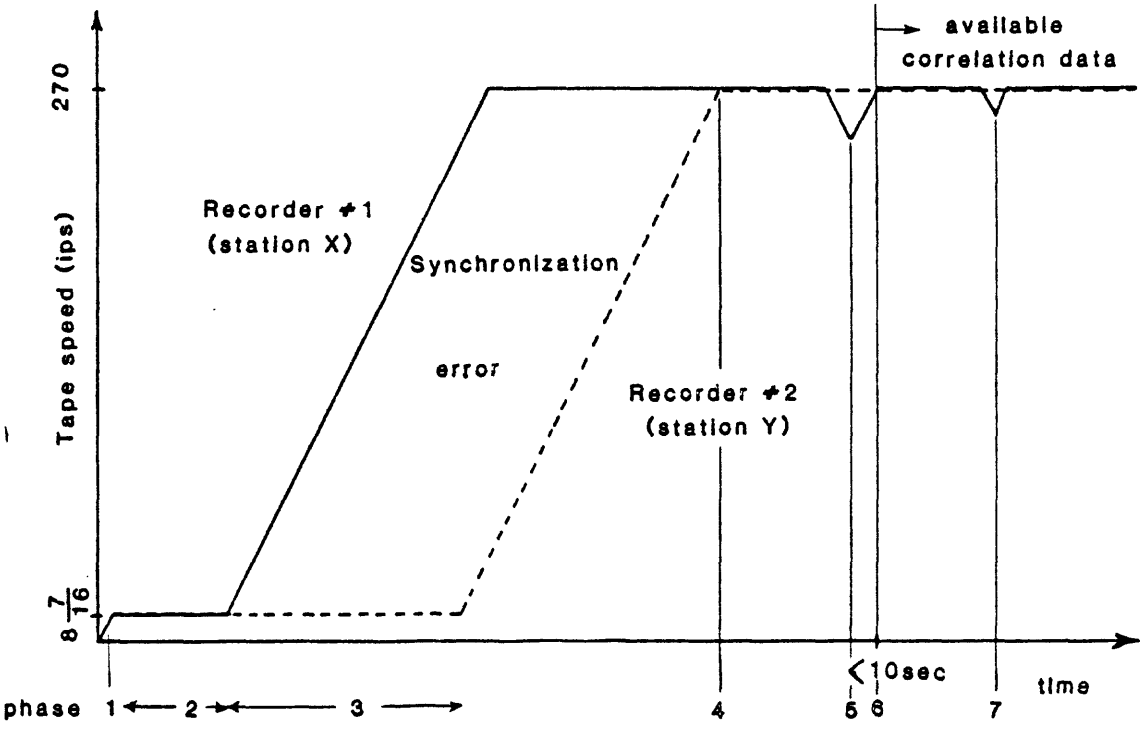

Fig. 3 Synchronization of Data recorders

Table 3 Performances of K-3 Correlation processor

Structure	8 channels x 4 crates
Maximum channel	32
Maximum processing speed	over 8 Mbps
Programable delay	128 bits
Correlation lags	complex 8-bit lags
Integration period	5 ms to 8.38 sec at 4 Mbps
Buffer memory	20 kbits
Phase calibrator	complex 24 bits
Host computers	HP-1000 /45F and /10L
Bus	IEEE-488 Bus, 800 kbyte/sec

Fringe rotator

Phase resolution	0.02 micro-radian
Phase rate resolution	0.93 mHz (selectable)
Phase acceleration	enable
Fringe pattern	3-level
Fractional bit correction	90 deg. jump of fringe rotation

GEOLOGICAL FEATURES OF KASHIMA VLBI STATION

T.YOSHINO, F.TAKAHASHI AND N.KAWAJIRI

Kashima Branch, Radio Research Laboratories
Ministry of Posts and Telecommunications
Kashima-Machi, Ibaraki-ken 314 Japan

ABSTRACT

New measurement of intercontinental baseline length between Kashima in Japan and US-operated observatories in North America, Alaska and Hawaii for geodesy, will be performed with use of the K-3 (being developed in Japan, and compatible with Mark III) and Mark III (developed in U.S.A.), starting in Jan. 1984. This experiment will provide us with the information of plate motion between the stations, which is very useful to Japan because it is greatly concerned with the study of generation mechanism of big earthquakes.

Before starting this experiment, we investigated the movement of antenna reference point from geological features, the structure of 26m antenna and the position of Kashima VLBI station. By analyzing the various components of movement of antenna structure, it is supposed that no big local movement has occurred except in

horizontal plane. We are planning to measure short baseline by Laser Ranging and VLBI to monitor the local crustal motion.

THE LOCATION OF KASHIMA VLBI STATION

In the beginning, Fig.1(Head 1981 Ref(1)) shows the world wide plates map. This figure also shows the location of VLBI stations and the baseline including Kashima station. There are very long baselines between Kashima and other VLBI stations, Haystack Observatory, Owens Valley Radio Observatory, and so on. Kashima VLBI station locates on nearly the same latitude as these in U.S.A. We can realize that Kashima locates near the plate boundary. By looking this picture, you can realize that the position of Kashima station is very important to investigate the plate motion. If Kashima station is excluded in this figure, the information taken by VLBI experiment will decrease considerably.

The magnified map of Fig.1 is shown in Fig.2. This map shows Japan main islands. Kashima locates near the center of these islands. Although this is a small area , we can see three plates together in this map, i.e. Pacific Plate, Phillipine Sea Plate, and Eurasian Plate. Kashima station seems to lie on the Eurasian Plate, but we can not entirely say that Japan islands and Eurasian Plate are connected completely. By using more VLBI stations in Asia, it will become clear in the future. And Kashima is only 150km apart from Japan Trench. Japan Trench means the subduction of Pacific Plate. It is believed that this motion triggers off the

big earthquakes.

In order to see the land and the sea together, bathymetric chart is used in Fig.3. Kashima is about 90km east by north-east from Tokyo. One more characteristic thing is that Kashima station is very near the seashore, only 1.5km apart. As the ocean loading effects are expected in Kashima, we intend to use the tidal data of the tide station at the port of Kashima to correct the VLBI data. The expected value of ocean loading effect is reduced to be a few centi-meters in distance error. Instead of theoretical estimation of tidal data, wewill use this real data in Kashima station.

THE FOUNDATION OF KASHIMA VLBI STATION

Geodesy is one of the main purposes of our VLBI experiments. As the position of each VLBI station is considered to become a global geodetic reference point in the near future, the position of antenna had better be stable to keep that point. But, Japan lies on the circum-Pacific seismic belt. About 10% earthquakes in the world has been occurred near Japan. Fig.4(a)(Ref.2) shows the vertical cross section of earthquake distribution, and Fig.4(b) shows the earthquakes map. We can understand from these maps that the Pacific Plate reaches to 50-100 km under the ground of Kashima. The rocks under Japanese islands have generally many clefts caused by the pressure of plates.

We had better treat the movement of reference point from 3

viewpoints.

1) Plate Motion

2) Local Crustal Motion (inside Japan)

3) Local Motion (just under the antenna site)

At the intercontinental VLBI experiment, the information we want to get is the item 1). At the domestic VLBI experiment, the one we want to get is the item 2). We must consider the items 2) and 3) at the intercontinental experiment.

As relative movement inside Japan had better be monitored to confirm the data of plate motion, we are now planning to measure the baseline between Kashima and GSI(Geographical Survey Institute) in Tsukuba(see Fig.3) by Laser Ranging. It is 50km apart. And it will also be measured by the VLBI method (antenna diameter; Kashima:26m, Tsukuba:5m). Furthermore, the local geological features must be investigated on each site. Next, we considered the move ment of antenna structure.

It is known that degrees of freedom of rigid body is 6. The movement of antenna structure can be reduced to 4 type as shown in Fig.5 by simplifying the shape. Most of these effects cause the shift of reference point. We call them Type 1 to 4 motion as shown in Fig.5. Generally these motion will occur simultaneously.

The sources of these effects are as follows:

1) Earthquakes

2) Strong wind

3) Settlement (Type 2)

4) Lack of uniformity of geological features (Type 3)

5) Plate motion (Type 1)

6) Other crustal movements

The soil profile including N-values under the 26m antenna is shown in Fig.6, and it was surveyed by boring before antenna construction. The structure of Kashima 26m antenna (cross section) including bottom view is shown in Fig.7. Table 1 shows the weight of antenna, and Table 2 shows the azimuth axis inclination effect on various condition.

Because the seashore is near in Kashima, the surface of the ground is covered with sand. But, sandy and loose stratum is not so thick. And since there is a discontinuity in the soil under 3 to 4 m depth, about 5m portion of foundation is put into the ground to increase the bearing capacity. There is a loose stratum of clay under 14m. If we constructed the 26m antenna without piles, it would be expected to settle 9 cm. So we made use of 30 pile groups. Each pile is 26 m long , and reaches 31m depth. We can understand from Fig.6 that piles reach very hard stratum. So the weight of antenna is considered to be dispersed to this stratum. The length of each pile is shortened only 0.4cm.

Consequently, we can describe about each type of antenna movement, as follows.

Type 1: Both plate motion and local crustal motion is included. This is the value we want to know.

Type 2: Settling is negligible by the pile groups in small area.

Type 3: Though we had many earthquakes and typhoons, we can say that azimuth axis did not inclined 10 arc min.(at 4GHz) at least during several years, according to our experience of radio star program tracking.

Type 4: It seems to be rare.
The antenna reference point does not move by this motion.

CONCLUSION

Firstly, we described the location of Kashima VLBI station. Secondly,three viewpoints on reference point is consicered. Thirdly, four types of movement of antenna structure is proposed from the conception of the degrees of freedom. From the facts we discussed before, it is supposed that no big local movements, which is much bigger than the plate motion, have occurred at Kashima VLBI station. We, however, think it is preferable to monitor the local crustal motion inside Japan. So the monitoring plan between Kashima and Tsukuba is now going on.

ACKNOWLEDGEMENT

The authors wish to thank Mr.Kaneko, PRL, for helping us to draw the figures.

REFERENCES

(1) Head,J. and Solomon,S.,1981: Tectonic Evolution of the Terrestrial Planets, SCIENCE, Vol.213,pp.62-76

(2) Earthquake Research Institute, University of Tokyo, 1982: Microearthquake Activity in and around the Kanto district (May, 1981-October, 1981), Report of the coordinating committee for earthquake prediction, Vol.27, pp.51-62, Edited by Geographical Survey Institute, Ministry of Construction, Japan

Table 1. Weight of antenna structure

Weight (above the ground)		1221 ton
	(antenna: 517 ton)	
(under the ground)		1278 ton
Total		2499 ton

Table 2. 26m antenna azimuth axis inclination effect on varicus conditions

Wind Velocity	15 m/s (on working)	1.3/1000 deg
	25 m/s (on working)	3.5/1000 deg
	60 m/s (at rest)	5.3/1000 deg
Earthquake	k=0.3	22.7/1000 deg

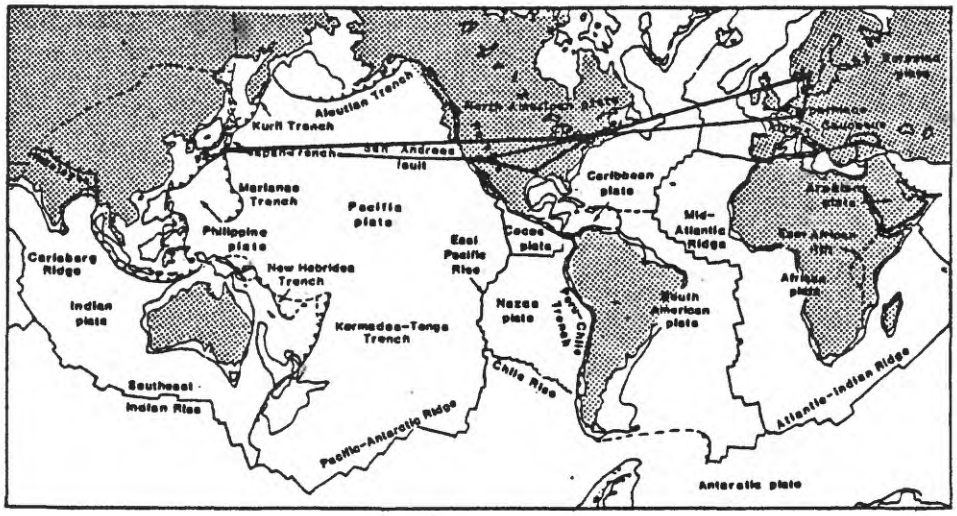

Fig.1 World Plates Map (some of baselines are drawn)

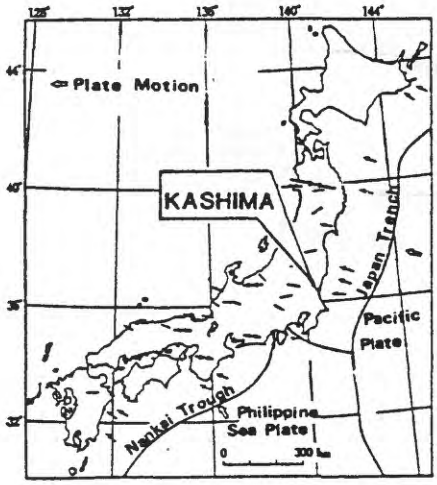

Fig.2 Japan Islands and the Plate Boundary

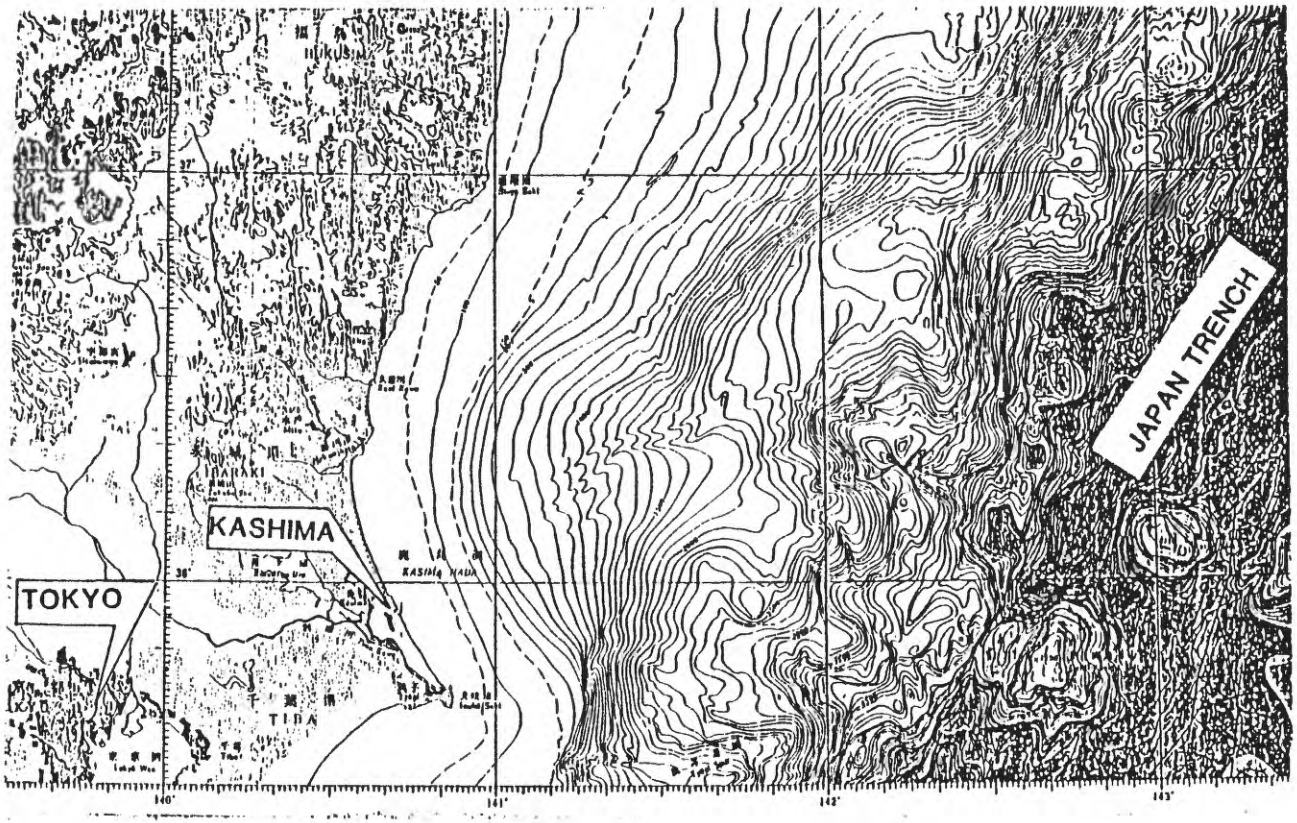

Fig.3 Bathymetric Chart